Brain Plasticity and Aerobic Fitness

Adam G. Thomas

A thesis submitted for the degree of Doctor of Philosophy

Linacre College

University of Oxford

Submitted: January 2014, Revised: June 2014

Contents

List of Figures

Acknowledgements

This work could not have been been completed without the help of many people. I would like to extend my sincere thanks to:

- My supervisors, Heidi Johansen-Berg and Peter Bandettini for providing excellent guidance and support
- My collaborators Andrea Dennis, Nancy Rawlings, Sinead Brady, Charlie Stagg, Claire Sexton, Jill Betts, Stuart Clare, Shannon Kolind, Martyn Morris, Helen Dawes, James Bateman, Cassandra Sampaio-Baptista, Allison Nugent, Mark Jenkinson, Tom Nichols, and Jesper Andersson for all of their help with collecting the data, doing the the analyses, and making the science happen
- Cameron Holloway, Lucy Matthews, and Charlie Stagg for excellent medical assistance with gadolinium injections and other issues
- All of our participants for their hard work and patience
- Dave Flitney, Duncan Mortimer, Michael Sanders, Jon Campbell, and Kenny Kan for technical and scanner support
- The staff of the Biowulf at NIH for the best computer clusters anyone could ask for (http://biowulf.nih.gov).
- Sean Marrett, the fMRI Facility and the Section on Functional Imaging at NIH for invaluable support and endless patience
- Alan Koretsky and the Intramural Research Program of the NIMH for providing encouragement and support
- Shane T. Mueller for custom code and the Psychology Experiment Building Language (PEBL, http://pebl.sf.net)
- Jim, Allison, and Nancy for patient proof reading
- My parents, Darla and R.J., and my family for love and support
- And Emily for making it all worthwhile

Abstract

Regular aerobic exercise has a wide range of positive effects on health and cognition. Exercise has been demonstrated to provide a particularly powerful and replicable method of triggering a wide range of structural changes within both human and animal brains. However, the details and mechanisms of these changes remain poorly understood. This thesis undertakes a comprehensive examination of the relationship between brain plasticity and aerobic exercise.

A large, longitudinal experiment was conducted in which healthy but sedentary participants were scanned before and after six-weeks of monitored aerobic exercise. Increases in the volume of the anterior hippocampus were observed, as previously reported in an older cohort after a longer exercise intervention. Multimodal imaging methods allowed an in-depth exploration of the mechanisms underlying this volume change, which proved to be dominated by white matter changes rather than the vascular changes that have been previously reported. A surprising global change in the balance of CSF, blood, and brain tissue within the cranial cavity was also observed.

Cross-sectional differences in memory and brain structure associated with fitness were also observed. The volume of the anterior hippocampus was shown to correlate with a measure of working memory. Higher cerebral blood volume throughout the brain was found to correlate with greater fitness and better working memory. Focal associations between fitness and magnetic susceptibility, a measure of iron content, were also observed in the basal ganglia. These findings demonstrate that aerobic fitness is associated with improved cognition and brain structure throughout the lifespan rather than simply acting to mitigate age related brain atrophy or accelerate brain development.

Finally, a new pipeline was developed for analysing hippocampal morphometry using high-resolution, 7 Tesla scans. Striking variability in the convolution of the hippocampal surface is reported. This technique shows promise for imaging the precise nature of the change in hippocampal volume associated with aerobic exercise.

This thesis adds to the evidence that aerobic exercise is a potent catalyst for behavioural and brain plasticity while also demonstrating that the mechanisms for those plastic changes are likely different than previously supposed. Future work will refine these measurement techniques, perhaps to a point where brain changes can be monitored on a single subject level. This work will provide an important tool to understand how best to utilize aerobic exercise to facilitate adaptive behavioural changes, mitigate the negative effects of ageing and disease on the brain, and maximize the benefits of active lifestyles.

Chapter 1

Introduction

1.1 Abstract

This chapter provides a literature review and background on the effects of aerobic exercise on structural plasticity. I review the literature documenting these structural changes and explore exactly where in the brain these changes occur as well as the potential underlying substrates of the changes including neural, glial, and vasculature components. Aerobic activity has been shown to produce different types of changes in the brain. The presence of novel experiences or learning is an especially important component in how these changes manifest. I discuss the distinct time courses of structural brain changes with both aerobic activity and learning as well as how these effects might differ in diseased and elderly groups. The majority of this chapter has been published in review form (Thomas et al., 2012).

1.2 What is exercise?

Physical activity is defined as bodily activity that results in energy expenditure above resting levels (US Department of Health and Human Services, 1998). Exercise refers to physical activity that is structured to meet specific fitness gains (Caspersen et al., 1985). Maintaining a physically active lifestyle has been associated with a vast range

of positive health outcomes that include benefits to cognitive function (Cancela Carral & Ayán Pérez, 2007; Kramer & Erickson, 2007; Smiley-Oyen et al., 2008; Ruscheweyh et al., 2011; Smith et al., 2010; Cassilhas et al., 2007). The American College of Sports Medicine recommends that most adults engage in a regular exercise regime in order to maintain health and well-being, suggesting that higher activity levels are associated with greater health outcomes (Haskell et al., 2007). The current UK guidelines for optimal health and fitness recommend that adults should be active daily. Over the course of one week, activity should add up to at least 150 total minutes of moderate activity in bouts of 10 minutes or more, or 75 total minutes of vigorous-intensity activity, or a combination of moderate- and vigorous-intensity activity. In addition, it is also recommended that individuals undertake resistance or strength training at least two days a week. Finally, adults should minimize time spent being sedentary (sitting) for extended periods (United Kingdom Department of Health, 2011).

Moderate-intensity exercise refers to exercising at sub-maximal workloads, during which energy is supplied by the aerobic energy system. Exercising within this zone results in a host of physiological responses to the increased metabolic demand for oxygen by the skeletal muscle, skin and brain. Prolonged training at moderate aerobic intensities results in physiological adaptations, including increased blood volume, capillary density, mitochondrial size and density, improved fat mobilization, and thermoregulation. Collectively these adaptations represent improved cardio-respiratory fitness. This fitness can be quantified by measuring the maximum rate at which an individual can take up and utilize oxygen, known as the "$\dot{V}O_2$ max" (Åstrand et al., 2003). $\dot{V}O_2$ max can be increased with aerobic training, but this effect is modulated by several factors, including age, the initial level of aerobic fitness, and the intensity, frequency and duration of training. The greatest increases in $\dot{V}O_2$ max are generally observed in previously sedentary individuals. Aerobic training for improved cardiorespiratory fitness is typically performed between 65-85% of an individual's $\dot{V}O_2$ max.

Vigorous-intensity exercise involves training above 85% of $\dot{V}O_2$ max, during which energy is supplied by the anaerobic energy system. Such high-intensity exercise requires

rapid re-synthesis of Adenosine Triphosphate (ATP) to provide energy for muscular contraction. The demand for this energy exceeds the rate at which oxygen delivery and consumption can support it. As a result, this type of exercise is limited by a finite capacity for energy production. Once this limit is reached, fatigue results and the exercise must either cease or be reduced in intensity. Training at this intensity, as with resistance training, results mainly in peripheral adaptations to the muscles being stressed as well as a strengthening of the neuromuscular mechanisms for movement. The effects of anaerobic (Winter et al., 2007), resistance (Lachman et al., 2006; Cassilhas et al., 2007; Busse et al., 2008), and flexibility training (Erickson et al., 2011) on brain structure have been explored, yet the results remain equivocal. The majority of studies on the effects of physical activity on brain structure have focused on aerobic or moderate-intensity exercise (Colcombe et al., 2006; Voss et al., 2010). The frequency and the duration of the training intervention required for brain plasticity remains vague. Similarly, it is not clear whether an increase in aerobic fitness (as indicated by increased $\dot{V}O_2$ max) is necessary to effect changes to the brain's morphology or cognitive processes. For example, it may be possible that the simple stimulus of increased cerebral blood volume during exercise is enough to drive the changes.

1.3 What is structural brain change?

This thesis is focused on structural brain changes; however, the difference between structural and functional brain measures is not always straightforward. Neuroimaging provides many different tools for measuring different aspects of the human brain, but ultimately all imaging modalities are providing information about the composition or motion of physical particles in a given voxel of tissue. Nevertheless, it is natural to separate the modalities into those that measure relatively rapidly changing aspects of the brain (functional) from those that measure more static features (structural). The two most common examples of rapidly changing measures are functional MRI (fMRI), which measures relative amounts of blood oxygenation, and Magnetic Resonance Spectroscopy (MRS), which measures the absolute amount of various molecules such as Gamma-

Aminobutyric Acid (GABA) and glutamate in a given voxel. These measures have been demonstrated to detect changes on time scales of 100 ms and five seconds, respectively (Lin et al., 2012; Gussew et al., 2010).

The most familiar structural measure of the brain is the T1-weighted MRI scan. T1-weighted images appear very similar to how a brain looks visually when it is removed, fixed, and sliced. Thus, it provides a familiar and comfortable basis for measuring gross structure. It also provides an image that is relatively static from day to day in the absence of disease, insult, or changes in hydration (Leow et al., 2006). There are a multitude of other modalities that can provide measures of static brain structure including T2, susceptibility, mean diffusivity, fractional anisotropy, and cerebral blood volume. These measures will be discussed in more detail in chapter 2. For some measures there is some question on how static they truly are. Diffusivity measures have recently been shown to change on a time scale of hours (Sagi et al., 2012) and may provide clues to neural activity (Le Bihan & Johansen-Berg, 2012), whereas maps of the correlation between the fMRI signals during rest have been shown to be remarkably stable (Shehzad et al., 2009).

1.4 Where in the brain do structural changes occur?

Environmental enrichment in rodents has been shown to produce structural changes assessed by histological methods in several distinct regions of cerebellar and cerebral cortex (Markham & Greenough, 2004). To date, however, these methods have only demonstrated exercise-related structural change in motor areas, such as the cerebellum and motor cortex, and in specific regions within the hippocampus, which plays a prominent role in learning, memory, and navigation. Human imaging studies have at times complemented these findings in specific regions, while in other cases they have found global changes in brain structure.

1.4.1 Cerebellum and Motor Cortex

In a rodent study, Black et al. (1990) contrasted effects of aerobic exercise and motor learning. Specifically, while 30 days of wheel running produced an increase in capillary density, 30 days of traversing an acrobatic maze produced an increase in the number of synapses per Purkinje cell (a very large nerve cell found in the cerebellum). Subsequent studies have demonstrated similar changes in blood vessel density in motor cortex using both histological (Kleim et al., 2002) and magnetic resonance imaging (MRI) techniques (Swain et al., 2003).

1.4.2 Hippocampus

Some of the most compelling evidence of exercise-mediated brain changes has been found in the hippocampus, a brain structure involved with memory as well as stress regulation (Kim & Diamond, 2002; Small et al., 2011). As early as 1999 it was demonstrated in mice that wheel running dramatically increased the number of new neurons in the hippocampus (van Praag et al., 1999b,a). (Pereira et al., 2007) replicated this finding and went on to demonstrate that the number of new neurons correlated with increases in cerebral blood volume (CBV), measured using contrast-enhanced MRI. The same paper showed a similar increase in CBV in a small group of middle-aged human subjects after 12 weeks of exercise training.

Chaddock et al. (2010) showed that preadolescent children with higher $\dot{V}O_2$ max scores had larger hippocampal volumes (as determined by MRI scans) than those with lower $\dot{V}O_2$ max scores. Erickson et al. (2009) showed a correlation between the volume of the hippocampus and cardiovascular fitness ($\dot{V}O_2$ peak) in a cohort of 165 older adults. A follow-up study by the same authors (Erickson et al., 2011) demonstrated that one year of aerobic exercise increased the volume of hippocampus by 2% in elderly adults, while controls who underwent one year of stretching exercises exhibited a 1.4% decrease in hippocampal volume. Similarly, (Pajonk et al., 2010) reported a 12-16% increase in hippocampal size in a small group of exercising schizophrenic patients as well as in matched controls.

In summary, aerobic activity reliably induces structural change in hippocampal volume and vasculature. This high degree of plasticity evident in this particular brain structure is perhaps not surprising given the purported role of the hippocampus in rapid encoding of episodic memory (McClelland et al., 1995). It is also notable that the hippocampus displays dramatic volume changes in disease states such as Alzheimer's disease and depression (Steffens et al., 2000; Butters et al., 2008).

1.4.3 Global effects?

All of the afore-mentioned studies, including the neuroimaging studies, limited their investigations to specific regions of interest. However, it is possible that some effects of aerobic exercise on brain structure occur via a diffuse mechanism (such as globally altered blood volume) that would not produce localized effects. Some whole-brain, voxel-based morphometry (VBM) studies have reported an association between physical activity levels (Flöel et al., 2010) or an exercise intervention (Colcombe et al., 2006) and large clusters of increased grey matter density in frontal, temporal, and cingulate areas of the brain. Prefrontal cortex volume has also been shown to mediate the relationship between fitness and cognitive measures of executive function (Weinstein et al., 2012). Another recent study has shown that aerobic activity levels in elderly human subjects correlate with both the number and tortuosity of blood vessels throughout the brain using the relatively novel technique of magnetic resonance angiography (Bullitt et al., 2009). These studies suggest that while some regions of the brain may show localized volume changes in response to aerobic exercise, there may also be more global changes.

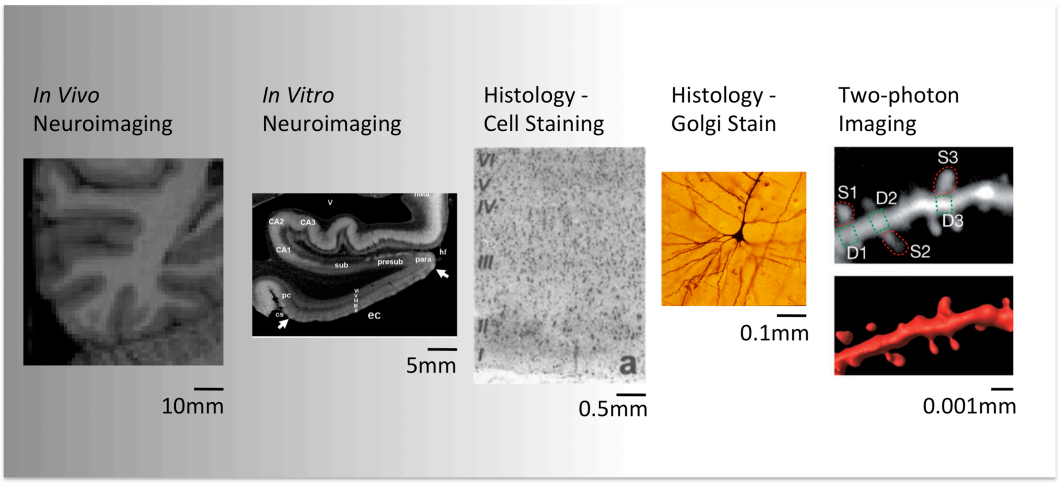

Figure 1.1: Illustration of different spatial scales provided by different imaging techniques (Arnold & Rioux, 2001; Cheng, 2011, Wikimedia Commons).

1.5 What is changing? Components of plasticity

1.5.1 Grey Matter

The study of structural brain change in humans is currently limited to the relatively macroscopic measurements that are possible using neuroimaging techniques. These techniques contrast sharply with histological studies in animals that can measure cell number, density of dendrites, or even the size and shape of dendritic spines (See Figure 1.1). Many neuroimaging studies report changes in "grey matter density" or the overall volume of a given structure. These measures are commonly derived from segmenting T1-weighted MR images using the relative intensities of different voxels. Although these image intensities depend on the underlying tissue structure, they do not relate in a straightforward way to specific tissue components (e.g., cell density). The magnitude of these changes are typically in the range of 1 to 8 percent (Draganski et al., 2004; Scholz et al., 2009; Erickson et al., 2011), but it is not possible to draw conclusions on which microscopic structures within grey matter are exhibiting an increase in volume.

Some insight into this question can be gleaned from animal studies. Figure 1.2 provides an approximate breakdown of the components of cerebral grey matter by volume

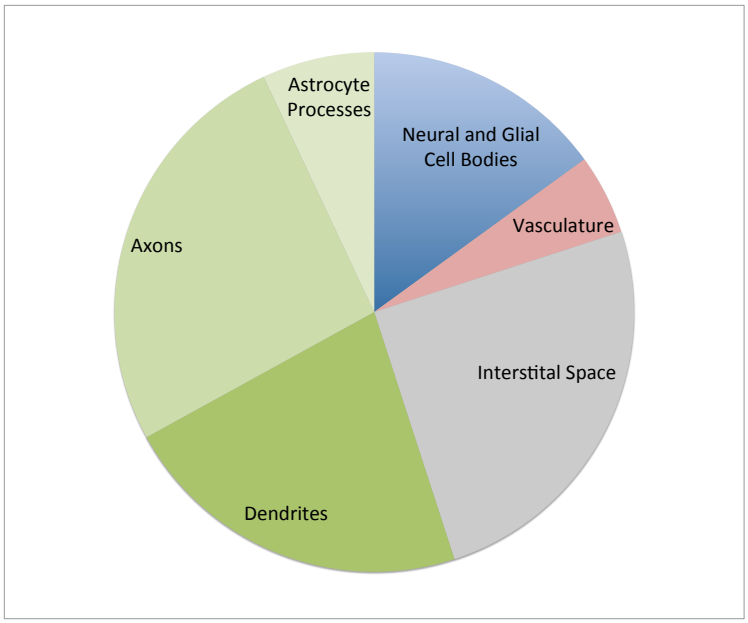

Figure 1.2: Approximate percentage of the components of cerebral gray matter by volume, based on estimates from several histological studies. The three green wedges are all components of the neuropil (Cherniak, 1990; Syková, 1997; Braitenberg & Schüz, 1998; Chklovskii et al., 2002; Kleim et al., 2007).

based on several histologic studies (Cherniak, 1990; Syková, 1997; Braitenberg & Schüz, 1998; Chklovskii et al., 2002; Kleim et al., 2007). Note that these ratios should be taken only as a rough guide. The composition of cortical grey matter can vary considerably between brain areas (Chklovskii et al., 2002) and species (Herculano-Houzel et al., 2007; Sarko et al., 2009). However, it has been consistently shown that well over 50% of grey matter is composed of the tangle of axonal, dendritic, and glial processes known as the neuropil, while vasculature accounts for no more than 5% of grey matter volume. Cell bodies account for less than 20% and the interstitial space between cells, synapses, and vessels accounts for over 20%.

These ratios give us some feel for the magnitude each compartment would need to change to produce the volume changes reported in recent imaging. For example a 20% increase in the neuropil volume would be sufficient to produce the 8% global grey matter changes that have been reported. However, if the change were limited to vasculature, a near doubling would be required to produce an 8% change in grey matter volume.

1.5.2 Vasculature

Angiogenesis in response to exercise is well studied in muscle tissue (Prior et al., 2004). Angiogenesis can occur via a splitting process known as intusseception or by a sprouting process in which a new branch sprouts from one capillary and merges onto another (Makanya et al., 2009). Studies on changes in the capillary density in rat brains were some of the first to distinguish between the effects of exercise versus learning or exposure to complex environments (Black et al., 1990). A replication and elaboration is provided in a follow-up study that dissociates increases in capillary number from increases in capillary density (Isaacs et al., 1992). Exposure to a complex environment produces an expansion of the volume of the molecular layer in the cerebellum, while the density of blood vessels remains constant. This necessarily involves an increase in the number of capillaries. However, the voluntary exercise condition results in an increase in the density of capillaries, while the volume of the molecular layer remains constant. Thus the ratio of blood vessel volume to other components of the layer has increased.

This dissociation between the effects of exercise and enrichment on angiogenesis was subsequently replicated in the rat motor cortex (Kleim et al., 1996, 2002). The basic result of increased vasculature with exercise has also been replicated many times in motor cortex as well as striatum with both histological and imaging techniques (Swain et al., 2003; Ding et al., 2005, 2006). The magnitude of increased blood vessel density reported in the original Black et al. (1990) study was approximately 20%, but the subsequent studies using different quantification methods have reported increases from 50% to over 1000%. If these measures are accurate they could account for the grey matter changes discussed above entirely within the vascular compartment.

A recent study using a small sample of macaques replicated the increase in vascular volume fraction in motor cortex with five months of daily treadmill exercise. Interestingly, this effect was found only in older animals (15-17 years old) while middle-aged animals (10-12 years old) showed no change in vascular volume fraction (Rhyu et al., 2010).

The mechanism by which aerobic exercise results in increased angiogenesis in the

brain is not fully understood. It is believed that mechanical sheer stress on the walls of the capillaries as well as a reduction in the degree of blood oxygenation (hypoxia) may play a role (Makanya et al., 2009). Independent of exercise, hypoxia itself is a potent stimulant of angiogenesis in the brain; Patt et al. (1997) demonstrated that rats exposed to progressive amounts of hypoxia over 130 days showed angiogenesis in a wide variety of brain areas including cerebral cortex, striatum, and hippocampus. Differences in capillary density in cerebellum and the medulla oblongata failed to reach significance due to the high variability in baseline vascular density in control animals. Contrary to Isaacs et al. (1992), Patt and colleagues also found increases in capillary diameter in cerebral cortex and cerebellum. Such changes could potentially also occur in association with the mild hypoxia that can occur during aerobic activity. Differences in vessel diameter associated with aerobic activity have also been shown in a magnetic resonance angiography study of elderly human individuals (Bullitt et al., 2009).

A considerable amount of work has evaluated angiogenesis in the hippocampus; however, these studies have focused on the tight relationship between angiogenesis and the growth of new neurons. This work will be discussed in more detail in section 1.5.4.

1.5.3 Glia

As revealed in the graph above, astrocytes, oligodendrocytes, and other glial cells consume a significant proportion of neuropil volume. Recent evidence suggests that glial cells may play a previously overlooked role in learning and plasticity (Fields et al., 2013; Fields, 2013). For example, in addition to their well established role in immune responses, microglia participate in remodeling of synapses (Tremblay et al., 2010). Remodelling of oligodendrocytes may allow for activity-dependent changes in myelination (see section 1.5.5 below). While astrocytes are similar to the vasculature compartment in that they play an important role in the metabolic support of neurons, they also have an active role in regulating the efficacy of synapses and even directly communicating with neurons via calcium signaling (see Zhang & Haydon, 2005, for review). Given these dual roles,

it might be expected that astrocytes would behave like neural processes and expand their volume only in response to learning. Alternatively, they might behave more like vasculature and respond to both exercise and learning. Anderson et al. (1994) addressed this question in rat cerebellar cortex by measuring the volume of astrocytes after a period of motor learning or voluntary exercise. The study showed that while the overall density of glial processes did not differ between groups, the glial volume per Purkinje cell in rats exposed to the motor learning condition was significantly greater than that of rats exposed to voluntary exercise alone. The motor learning group also showed an overall increase in the volume of the molecular layer. This finding suggests that the astroglia are more similar to the synaptic and neural structure than they are to vasculature in their pattern of growth.

1.5.4 Neurogenesis

New neurons are generated in the vertebrate brain throughout the organism's life span (see Colucci-D'Amato & di Porzio, 2008, for an account of the rise and fall of the "no new neurons" dogma over the course of the 20th century). There is general agreement that neurogenesis occurs in two areas of the mammalian brain: the sub-granular zone of the dentate gyrus within the hippocampus and the subventricular zone located in the lateral ventricles. Neurogenesis in the hippocampus, like angiogenesis, has been shown to increase with physical activity (van Praag et al., 1999a,b), but the creation of new neurons in the hippocampus is a delicate process. A large fraction of the new neurons created do not survive (see Kempermann et al., 2010, for review and discussion). Kronenberg et al. (2003) showed that while exercise increases the rate of neurogenesis, environmental enrichment increases the ratio of new neurons that survive and get incorporated into the lattice of the existing neural network.

Some studies have suggested that both new neural cells and new endothelial cells (used to build new capillaries) derive from the same pool of stem cells (Palmer et al., 2000). Pereira et al. (2007) demonstrated a correlation between the number of new neurons generated in mouse dentate gyrus and the degree of increase in regional cerebral

blood volume as measured by contrast-enhanced MRI. In a small sample of human subjects, they demonstrated a significant increase in regional cerebral blood volume (rCBV) after three months of aerobic exercise. Changes in rCBV were shown to correlate with increases in $\dot{V}O_2$ Max scores as well as post-exercise performance on a verbal learning task. The authors argue that these data suggest that rCBV can be used as a proxy for measuring neurogenesis in mice as well as humans. This exciting possibility must be reconciled with the fact that there are several regions of the brain in which angiogenesis has been observed, such as the cerebral cortex and cerebellum, which most researchers believe are not capable of neurogenesis. Some authors have argued that neurogenesis does occur in the cerebral cortex (Gould et al., 1999) and in the cerebellum (Carletti & Rossi, 2008). This would provide a possible resolution to this apparent contradiction in Periera and colleagues' theory. But the idea of neurogenesis outside of the hippocampus and the subventricular zone remains very controversial (Rakic, 2002; Ming & Song, 2005, 2011).

1.5.5 White Matter and Connectivity

The majority of the literature on structural change with aerobic activity has focused on the region of the brain that contains the majority of cell bodies, synaptic connections and vasculature, i.e., the "grey matter". The effects of exercise on "white matter", the large mass of mostly myelinated axons below the surface of the brain, have been overlooked until very recently. An early attempt to look at white matter volume was conducted by Colcombe et al. (2004) using VBM techniques on segmented white matter images. They reported an anterior cluster of increased white matter after six months of exercise in a group of elderly adults. However, the use and interpretation of VBM on white matter volumes are somewhat controversial (Draganski et al., 2006; Smith et al., 2006).

The past five to ten years have witnessed significant advancements in our ability to study the connectivity between brain areas embodied by the white matter. The advent and popularization of diffusion tensor imaging (DTI) have allowed researchers to study

the structural integrity of white matter directly (see Johansen-Berg, 2010, for review). Concurrently, another area of study has grown in popularity and sophistication: that of "functional connectivity", in which functional MRI data is acquired while the subject lies at rest and is used to explore temporal correlations between brain areas (see Smith et al., 2011, for review). The strength of these correlations is thought to provide a measure of the degree to which different regions of the brain are working in concert as a "functional network".

DTI changes associated with aerobic activity have recently been examined in a one-year fitness training study on elderly adults. Voss et al. (2012) show a correlation between white matter integrity and changes in $\dot{V}O_2$ max scores in frontal and temporal white matter tracts. Interestingly, the change in white matter integrity for the aerobic training group did not significantly differ from a control group that participated in one year of non-aerobic exercise, suggesting that aspects other than aerobic exercise contributed to the observed change. Another recent cross-sectional study showed a correlation between cardiorespiratory fitness and Fractional Anisotropy (FA) in the corpus callosum in a group of older adults (Johnson et al., 2012). Tract tracing suggested the regions of correlated FA were connected to premotor cortex.

Differences in resting functional connectivity associated with fitness level were reported in a recent study by Voss et al. (2010). Aging has been shown to result in a decrease of functional connectivity in the so-called "default mode network" (DMN, Andrews-Hanna et al., 2007). The DMN is a well-studied set of brain regions that shows a decrease in activity when external processing demands are increased. Voss and colleagues demonstrate that some of the functional connections within the DMN (particularly the connection between the posterior cingulate gyrus and the middle frontal gyrus) exhibit a positive correlation with $\dot{V}O_2$ max score, controlling for age. They also demonstrated several positive correlations between functional connectivity and cognitive measures of executive function and spatial memory.

1.6 Biochemical Mechanisms

Complex biochemical cascades are responsible for building new vascular and neural structure in the brain. Detailed discussion of these cascades is beyond the scope of this chapter (see Olson et al., 2006; Zhao et al., 2008; Erickson et al., 2012, for review), however two important and well-studied growth factors bear a brief discussion. Brain Derived Neurotrophic Factor (BDNF) and Vascular Endothelial Growth Factor (VEGF) are both up regulated with exercise. BDNF synthesis is triggered by a local increase in neural activity while VEGF production is triggered by hypoxia (Shweiki et al., 1992; Goodman et al., 1996). BDNF triggers an intracellular biochemical cascade that expands the neural structure such as dendritic spines and axonal buttons (McAllister et al., 1999). VEGF acts on the endothelial cells lining the wall of the blood vessels triggering them to divide and produce new blood vessels (Bloor, 2005). Both BDNF and VEGF play important but different roles in neurogenesis. While VEGF promotes the proliferation of new neural progenitor cells inside the neurogenic niche, BDNF promotes their survival and incorporation into the neural architecture. Both VEGF and BDNF genetic polymorphisms are associated with depression (Neves-Pereira et al., 2002; Sklar et al., 2002; Strauss et al., 2005; Viikki et al., 2010). The BDNF polymorphism has been shown to moderate the effect of exercise on mood, heart rate and perceived exertion (Bryan et al., 2007). Antidepressant medications also cause an increase in BDNF expression (Martinowich & Lu, 2008; Ventriglia et al., 2009). Changes in BDNF and VEGF serum levels have been shown to correlate with changes in functional connectivity between parahippocampal gyrus and middle temporal gyrus (Voss et al., 2013a).

1.7 Time course

Each of the components of brain plasticity has a unique function and therefore also has a unique temporal profile with respect to the onset and offset of increased aerobic activity. Studies have shown that the primary component of change associated with exercise, i.e., increased capillary density, has a very rapid time course. A recent study in

rat hippocampus demonstrates that an increase in capillary density occurs within three days of the onset of increased aerobic activity (Van der Borght et al., 2009). Perhaps even more surprisingly, rats removed from the exercise condition returned to baseline levels of capillary density after just 24 hours of sedentary behavior. As discussed above, the creation of new neurons seems to be tightly coupled with angiogenic growth and therefore also follows a time course that rapidly responds to changes in aerobic activity. However, new neurons created over the course of increases in aerobic activity will quickly die off if adequate learning opportunities or novel experiences do not accompany the increased aerobic activity (Kempermann et al., 1997). Astrocytes are also sensitive to the presence of environmental enrichment and will only exhibit volume increases when these stimuli exist (Kleim et al., 2007). However, they differ from neurogenic growth in that they return to baseline volume as soon as the animal is removed from the stimulating environment. Synaptic growth in the neuropil is also dependent on learning or novel experiences, but unlike astrocytes, increases in synaptic density and neuropil volume are relatively persistent. Kleim et al. (1997) demonstrated that increases in synaptic density in cerebellum lasted for at least four weeks after animals were removed from an enriched environment.

These studies provide us with a rough idea of the time course of plasticity in the different components of brain architecture as well as the necessary and sufficient conditions for plasticity in each (Figure 1.3). Vasculature plasticity has a rapid onset, is reliable in both exercise and enrichment conditions, and is quick to return to baseline after the intervention. Neurogenesis is also present across both exercise and enrichment paradigms, but long-lasting only when learning is present. Both astrocyte and neuropil plasticity are only responsive to enrichment, but only astrocyte volume returns to baseline post-intervention.

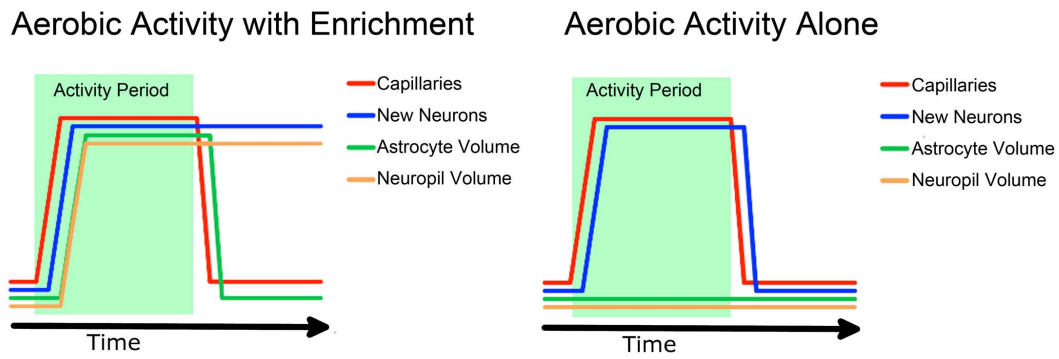

Figure 1.3: A schematic summary of the time courses of the different components of structural change associated with exercise and environmental enrichment, based on several studies discussed in this chapter (Black et al., 1990; Kleim et al., 2007; Van der Borght et al., 2009; Kempermann et al., 2010).

1.8 Group Specificity and Ceiling effects

There is a long-standing debate in the literature regarding whether environmental enrichment manipulations can be truly considered "enrichment," or whether they simply represent a modest reprieve from the extremely impoverished environment of a typical laboratory animal (Grossman et al., 2002). This issue raises the question as to whether reported brain changes can be thought of as enhancements from a typical baseline or a recovery from atrophy. Similarly, in the human literature, the majority of the published work on the effects of exercise on the brain is in participants who may have also experienced brain atrophy due to either age (Erickson et al., 2011) or other mental illness (Pajonk et al., 2010; de Lange et al., 2008). Podewils et al. (2005) provide a counter-example of one at-risk population that does not seem to benefit from exercise. In a large epidemiological study of older participants, they show that while level of fitness is protective against the onset of dementia and Alzheimer's Disease (AD) across the entire population, carriers of the Apolipoprotein E (APOE) genotype e4 allele, which is associated with increased dementia risk, show no association between fitness level and dementia risk. This finding suggests that aerobic activity cannot rescue individuals from the increased risk incurred by this genotype.

Although relatively few studies exist on the effects of aerobic activity on the brain structure of healthy, younger individuals, there are a wealth of data demonstrating the cognitive benefits of frequent aerobic exercise throughout the lifespan – perhaps none more convincing as a recent study of 1.2 million Swedish military conscripts that showed a strong correlation between fitness and intelligence (Aberg et al., 2009). Much work remains to be done to determine what level of aerobic activity is required for cognitive and brain health to be maximized, but it seems likely this level is well above that of the average individual.

1.9 Conclusion and Objectives

The study of the effects of exercise on brain structure and cognition is still in its infancy. The research reviewed here by and large simply demonstrates that aerobic activity is indeed a powerful modulator of structural brain plasticity. The precise components and time-course of exercise-mediated changes in brain structure are beginning to be delineated, but many unanswered questions remain.

In this thesis I have investigated the underlying basis of exercise-mediate plasticity in humans using standardized fitness testing and physiological monitoring, multifaceted cognitive testing, and multimodal neuroimaging. These techniques have allowed me to address several specific objectives.

My first objective was to better understand the relationship between fitness, cognition, and the volume and structure of the hippocampus. Specifically, I aimed to determine if the previously reported volume change in the hippocampus was dominated by specific aspects of brain structure such as myelination or vasculature. I also aimed to explore if exercise-related hippocampal growth occurs in the absence of age-related hippocampal atrophy in younger adults.

My second objective was to elucidate the relationship between Cerebral Blood Volume (CBV) and fitness. I aimed to determine if fitness related to CBV in specific regions of the brain, or if this relationship might be more global. I also aimed to determine

if higher levels of brain vascularization might contribute to improved cognition observed with greater fitness levels.

My third objective was to explore the relationship between fitness, cognition, ageing, and brain iron content. The accumulation of iron in the basal ganglia with age is well documented but poorly understood (Connor & Menzies, 1996; Guizzetti, 1915). I aimed to explore if this iron accumulation relates to fitness levels over and above it's correlation with age. In addition I aimed to determine if a relationship between iron content and cognitive measures exists, as the potential role of iron in cognitive decline remain equivocal.

For my final objective, I returned to the hippocampus using high resolution, susceptibility weighted imaging techniques and a novel analysis pipeline. I aimed to determine if the highly variable convolution observed in the hippocampus might correlate with fitness or cognitive measures.

In the following chapters I will address each of these specific aims and provide important new details regarding the mechanisms and time courses of known exercise-mediated brain plasticity, as well as describe entirely new aspects of brain plasticity not previously reported.

Chapter 2

Methods

2.1 Abstract

One of the central goals of this thesis is to determine the biological substrates of volume changes frequently reported in traditional T1-weighted Magnetic Resonance Imaging (MRI) imaging as well as their relationship to changes in fitness and behaviour. In order to do so I have used several different standard measures of fitness and cognitive assessments. I have also utilized a wide array of imaging modalities and techniques, each of which provides unique and complimentary information about the underlying neural tissue. In this chapter I will describe each of the measures I have employed as well as some of the rationale as to why they were chosen. I will provide a brief introduction to MRI and discuss each of the imaging modalities and analysis techniques that I have employed. I will also provide some background on the unique methodological considerations involved in within-subject neuroimaging analyses.

2.2 Fitness assessments

There are many different approaches to assessing physical activity and physical fitness (Tudor-Locke & Myers, 2001; Ainsworth et al., 2000). Fitness and activity reflect different but correlated aspects of an individual's profile (Siconolfi et al., 1985). Activity

can be assessed through a number of validated questionnaires, or using more objective measurements such as accelerometry. Here, I have used two validated questionnaires to measure activity, which are described in detail below. To assess fitness, I used a standard $\dot{V}O_2$ max protocol, which is also described below.

2.2.1 Baecke questionnaire

The original Baecke Habitual Physical Activity Questionnaire (Baecke et al., 1982) was designed to assess to day-to-day physical activity of a young Dutch population between the ages of 20 and 32. It consisted of prompts such as "At work I sit:" and "During leisure time I sweat:". Possible answers were never, seldom, sometimes, often, and very often. The Baecke questionnaire has the advantage of being short and easy to complete and has been tested for validity and repeatability in different populations (Ono et al., 2007; Bigard et al., 1992). The original Baecke questionnaire was later modified to be more appropriate to a wider age group (Blair et al., 1992; Riboli, 1992). This version has also been validated (Pols et al., 1995). The modified version of the Baecke was used throughout this thesis.

2.2.2 International Physical Activity Questionnaire (IPAQ)

The International Physical Activity Questionnaire (IPAQ) was carefully developed to provide a standard, cross-national instrument for physical activity monitoring (Ainsworth et al., 2000; Craig et al., 2003). It is freely available via the internet in 20 different languages and has been extensively tested for validity and repeatability (Kurtze et al., 2008; Gauthier et al., 2009, http://www.ipaq.ki.se/). Unlike the Baecke questionnaire, the IPAQ asks specific questions regarding activity over the past seven days rather than asking participants to report on their physical activity in general. Some studies have shown that participants are more accurate at reporting on their actual activity over a recent period than they are at estimating their average activity levels in general (Ainsworth et al., 2000). Therefore, the IPAQ was used in this thesis, in addition to the modified Baecke questionnaire.

2.2.3 $\dot{V}O_2$ max test

The gold standard measure of physical fitness is $\dot{V}O_2$ max, which is the rate of oxygen volume utilized by the body at the peak of physical exertion. While this quantity is indeed an excellent measure of overall fitness, the practical methods by which it is measured are not entirely standardized. In practice, it may be impossible to obtain an accurate measure of $\dot{V}O_2$ max in participants who lack the ability or resolve to reach their peak of physical exertion. I will first provide a detailed description of our $\dot{V}O_2$ max testing procedure followed by an example and a discussion of other means of characterizing the $\dot{V}O_2$ max test.

Our $\dot{V}O_2$ max testing procedure was conducted on an electromagnetically braked cycle ergometer (Lode Excaliber, Groningen, Netherlands). The continuous, incremental test started with a warm-up phase of 3 mins at 0 W and then increased to 50 W for 2 minutes. Thereafter resistance was increased by 25 W every 2 minutes. The participants were instructed to maintain a cadence of 60 Revolutions Per Minute (RPM) throughout. The test was ended when volitional exhaustion was reached or the participant was no longer able to maintain a pedal rate of 60 RPM.

The rate of oxygen consumption ($\dot{V}O_2$) and Heart Rate (HR) were measured throughout the test and Rating of Perceived Exertion (RPE) was recorded after every 2-minute increment using the Borg 0-10 scale (Borg, 1970). HR was measured using a Polar Heart Rate Monitor (Polar, Finland) and oxygen consumption rate was assessed using a fully automated indirect calorimetry system (Metalyser, Cortex), sampling expired air collected through a face mask with every breath. The calorimetry system was calibrated prior to each test using standard calibration gas (15% O_2 and 5% CO_2, balance N_2) and atmospheric pressure and volume according the manufacturer's instructions. The point of maximal exertion was defined as the point at which two of the following criteria were met: (a) a plateau in $\dot{V}O_2$ uptake/exercise intensity relationship, (b) a Respiratory Exchange Ratio (RER) of 1.13 or above (c) final HR within 10 beats per minute of the age-predicted maximum or (d) subjective fatigue and volitional exhaustion. Once

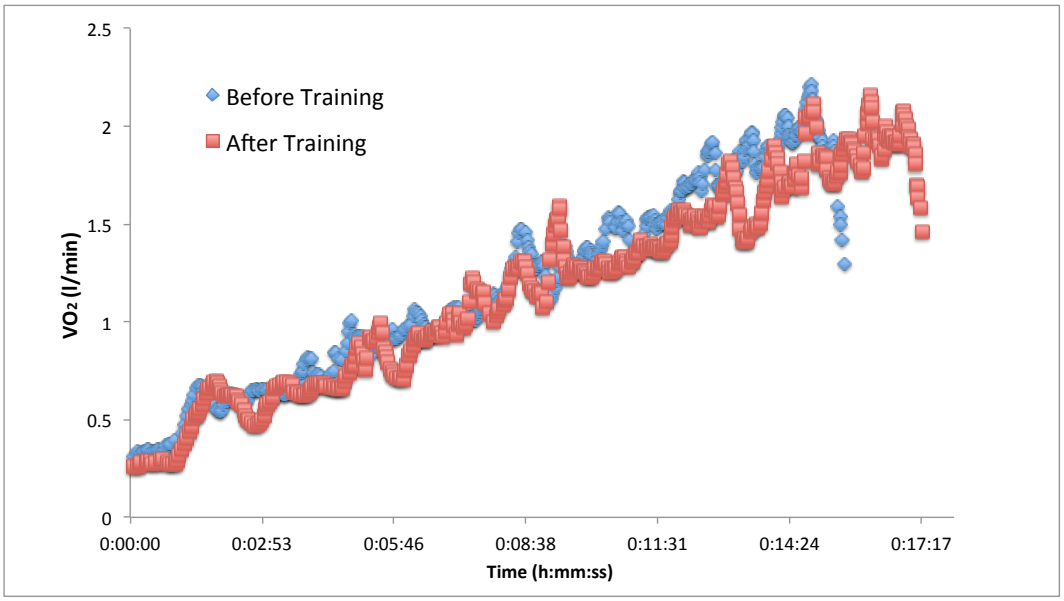

Figure 2.1: Comparison of different $\dot{V}O_2$ change curves on different visit. The blue curve is before exercise training and the red curve is after exercise training. Note that although the exhaustion happens later on the red curve, the blue line reaches a higher $\dot{V}O_2$ level.

these criteria were met, $\dot{V}O_2$ max was taken as the highest 30-second average value for $\dot{V}O_2$.

Following the $\dot{V}O_2$ max test, participants were encouraged to cool-down by gently cycling with no resistance until their HR had fallen by approximately 20 BPM. Following this, subjects were monitored for 15-20 minutes before leaving the laboratory to ensure that their resting blood pressure had returned to pre-testing baseline levels. Figure 2.1 illustrates two $\dot{V}O_2$ max tests for one participant before (blue) and after (red) six weeks of training.

After the six-weeks of exercise training, the participant was able to continue pedalling on the stationary bike for almost 2.5 minutes longer than she did before the training, reaching a higher level of resistance. The post training $\dot{V}O_2$ max score, however, is actually lower than the pre-training value (1.9 l/min vs. 2.0 l/min averaged over a 15 second window). By examination of the participant's heart rate during the test, we can determine that she had not reached her true peak level of exertion on the post-training test, but was

unable to maintain 60 RPM at the higher level of resistance, likely due to a limitation of her leg strength. This example illustrates the problems inherent in measurement of $\dot{V}O_2$ max.

As an alternative to the $\dot{V}O_2$ max measure, we have adopted a different metric of fitness, particularly useful when comparing between sessions in the same participant. What we will refer to as Time To Exhaustion (TTE) is defined as the total time of the $\dot{V}O_2$ max test, from the beginning until the participant fails to maintain 60 RPM. In the example above, TTE is 14:23 pre training and 17:10 post training. Although this measure does not have a direct physiological interpretation, we have found it to provide a superior measure of increases in fitness that is more robust to differences in participant leg strength.

2.3 Cognitive and mood assessments

Aerobic exercise has been associated with a broad array of behavioural changes including changes in working memory, executive function, spatial memory, and symptoms of depression (see Kramer & Erickson, 2007; Kempermann et al., 2010; Angevaren et al., 2008; Aberg et al., 2009, for review). For this study I include a battery of tests that will be sensitive to effects across a number of cognitive domains. All tests used are well represented and validated in the cognitive literature and were amenable to three, repeated administrations either by using different versions or by other forms of randomization.

2.3.1 Rey Osterrieth Complex Figure Test

The Rey-Osterrieth Complex Figure Test (ROCF) Test, first devised in 1941, is a simple and common measure of visuo-spatial reasoning, spatial memory, and planning (Rey, 1941; Corwin & Bylsma, 1993). In addition to the original ROCF, we used four other figures developed to have an equivalent level of difficulty so that participants could be tested on multiple occasions (Meador et al., 1991) (Figure 2.2). All figures have been tested for validity and reproducibility (Meador et al., 1993).

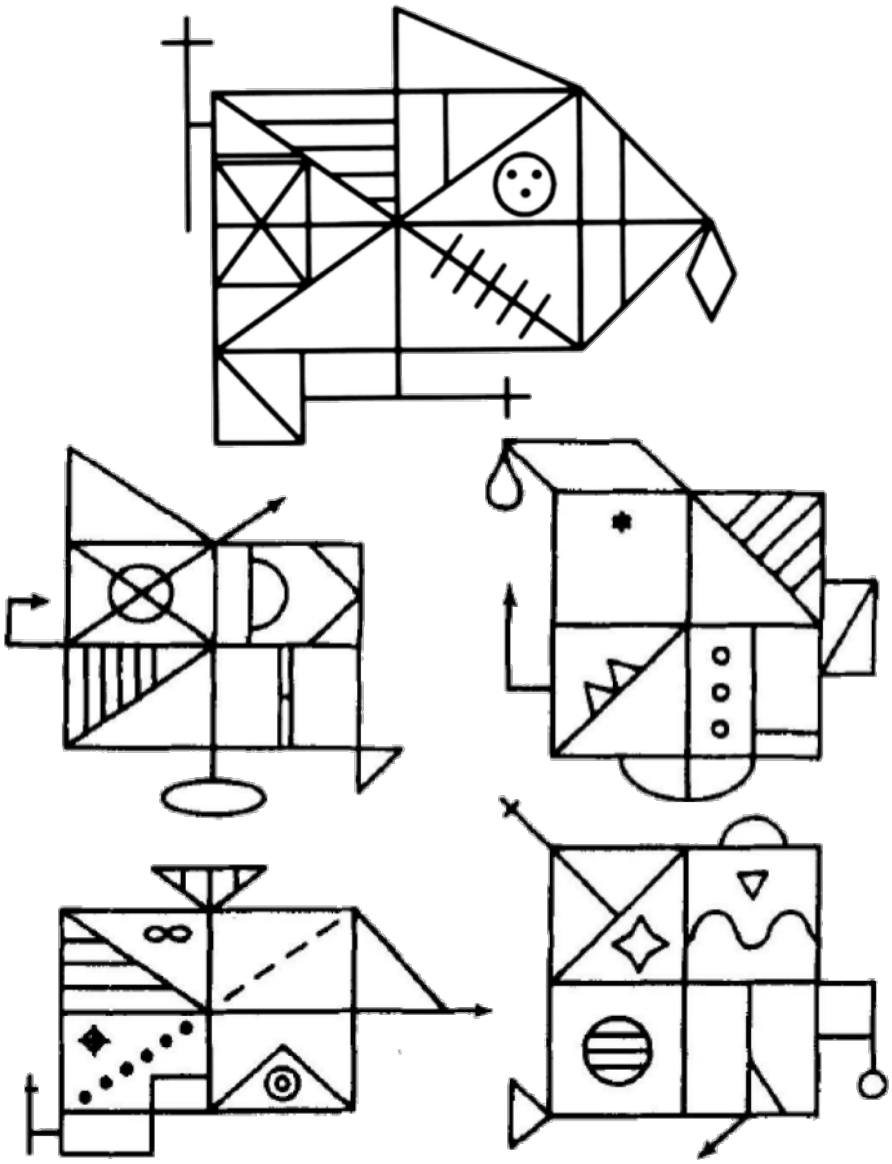

Figure 2.2: The original Rey-Osterrieth Complex Figure is depicted at top. The four variant Medical College of Georgia complex figures are depicted below. (Rey, 1941; Corwin & Bylsma, 1993; Meador et al., 1993).

2.3.2 Hopkins/Rey Verbal Learning Test

Three alternative forms of the Rey Verbal Learning Task (RVLT) were used as measures of short-term verbal memory (Rey, 1941; Hawkins et al., 2004). The test consists of a list of 15 words that are read to the participant five times. After each reading, the participant is asked to list all words remembered. The participant is then read a distractor list of words, after which participants are asked to recall as many of the distractor words as possible. After the distractor list, the participant is again asked to recall as many words as possible from the original list. Approximately 15 minutes later the participant is asked to recall the original list of words. Finally, a list of written words is presented to the subject including words on both the primary and the distractor lists plus additional distractor words that were not on either list. The participant is scored on their ability to recall the list on each occasion as well as the performance on the final written recognition test. For the experiments in this thesis, we also calculated the participants' learning rate, which was defined as the sum of the number of words recalled on each of the first five recall trials minus the first recall trial multiplied by 5:

$$LearningRate = \sum_{i=1}^{5} Recalled_i - 5 * Recalled_1$$

This measure reflects the degree to which recall improves over the course of 5 recall trials.

2.3.3 Forward and backward digit span

The forward and backward digit span test is one of the oldest and simplest measures of short-term and working memory (Richardson, 2007). It involves reading a list of random digits of varying length to a participant and then asking the participant to repeat the digits back either in the same or reverse order. Although the two measures tend to be correlated, it has been shown that they measure different mental constructs with forward digit span being more associated with the "phonological loop" and backward digit span being more related to working memory (Reynolds, 1997). For our study we used a laptop

to administer varying lengths of digits that increased and decreased based on a stair-step method proposed by Woods et al. (2010). Fourteen different digit lists were presented for each test. If the participant answered correctly, the length was increased by one item. If the participant gave two consecutive incorrect answers, the length of the list was decreased by one. The mean digit span score was determined by summing the hit rate (0.0 to 1.0) for each digit plus the initial number of digits (3 for forward, 2 for backward) minus 0.5 as per Woods et al. (2010).

2.3.4 Verbal Fluency

Verbal fluency tests are a simple and common test of executive function. We conducted two versions of the test: semantic fluency and letter fluency. In the semantic fluency version, the participant was given a category (e.g. animals) and was asked to list as many examples of that category as possible in a one-minute period. In the letter fluency version, the participant was given a letter of the alphabet and asked to generate as many words beginning with that letter as possible in a one-minute period. We used letters and categories that have been previously demonstrated to have a similar level of difficulty (T, B, P; Animals, Cities, Fruits; Basso et al., 1999; Cauthen, 1978; Borkowski & Benton, 1967).

2.3.5 Depression Scale

A strong relationship between exercise, brain structure, and depression has been repeatedly demonstrated (Erickson et al., 2012), thus we also included the Center for Epidemiological Studies standard 20 question depression index in our study (Radloff, 1977). The Center for Epidemiological Studies Depression Inventory (CES-D) questionnaire provides a quick and accurate means of measuring depression and has been validated for sensitivity and reproducibility (Weissman et al., 1977).

2.4 Neuroimaging Assessments

The aim of this thesis was to assess how the brain changes with exercise. For this we chose to use MRI due to its unique ability to provide information on brain structure in human subjects *in vivo*. This section provides some background on MRI physics as well as an overview of each of the MRI modalities and analysis methods we employed.

2.4.1 Introduction to MRI

Nuclear magnetic resonance is, at its core, the measurement of electromagnetic radiation absorbed and re-emitted by atomic nuclei inside a magnetic field. The basic principles of magnetic resonance were discovered and described over 70 years ago and are the subject of several encyclopaedic works (Haacke, 1999; Harris & Wasylishen, 2012; Becker, 1993). The fundamental parameters relevant for this thesis will be briefly summarized, and greatly simplified, here.

The nuclei of atoms with an odd number of protons or neutrons have a positive and a negative pole. When placed inside an external magnetic field, these poles will tend to align themselves with the poles of the external magnetic field. The crucial discovery that led to the field of Nuclear Magnetic Resonance was the observation that when a pulse of Radio Frequency (RF) energy is delivered at a given nuclei's characteristic resonance frequency, the atoms inside the field will simultaneously a) synchronize their precession, b) absorb the energy and c) tilt their magnetic axis away from that of the external magnetic field. Once this energy is absorbed, the atoms will then simultaneously release this RF energy and return their axes back to that of the external magnetic field. This RF energy will be released at a specific rate that can reveal information about the atom and its environment (Rabi et al., 1939; Bloch et al., 1946). Three parameters that describe the release of this energy are particularly relevant for the work presented in this thesis. These are the time constants T1, T2, and T2*, which are described below. T1, also known as the spin-lattice relaxation time or the longitudinal relaxation time, is a parameter that describes the time constant for the tilt of the atom's magnetic axis to

come back in line with the axis of the external magnetic field.

T2, also known as the spin-spin relaxation time or the transverse relaxation time, is a parameter that describes the time constant at which the atomic spins de-phase or lose their spin coherence. As mentioned above, when the RF pulse is applied, the nuclei will precess synchronously, i.e., they will be in phase. But this synchrony is lost relatively quickly due to random magnetic field fluctuations caused by the presence of neighbouring nuclei. T2 is the time constant that describes the rate at which this synchrony is lost.

But not all de-phasing is due to random fluctuations. De-phasing can also be caused by magnetic inhomogeneity that is characteristic of the tissue and does not change with time. As this de-phasing is not random, but predictable and reproducible, coherence lost due to these factors can be recovered using what is known as a spin echo sequence (for description, see Haacke, 1999). The time constant that describes the rate of de-phasing that is due to predictable magnetic inhomogeneity is known as T2' (pronounced "Tee-two-prime"), but this is not easily or frequently measured directly. It is far more common to measure the combination of both predictable and unpredictable sources of dephasing. The time constant describing this rate is known as T2*.

T1, T2, and T2* all provide unique information about the underlying tissue. Different scan sequences vary as to which of these parameters they are most sensitive to. Scans which are most sensitive to variation in T1 are referred to as T1-weighted scan, and are particularly useful for differentiating tissues with differing amounts of fat. Hence these scans provide high contrast between grey and white matter as well as different amounts of myelination within grey matter. T2-weighted scans tend to be very sensitive to fluid content, hence they are very useful for detecting oedema and other sources of fluid accumulation. T2*-weighted scans are most sensitive to areas of magnetic susceptibility. In the brain, the most common sources of magnetic susceptibility are venous blood, ferritin, (which is particularly prevalent in deep brain nuclei such as the putamen, pallidum, and red nuclei) and myelin (more visible at higher magnetic fields). T2*-weighting is also

essential for functional MRI (Moonen et al., 1999; Huettel et al., 2008).

Several parameters of the scan acquisition can affect which of the above relaxation parameters a given image will be most sensitive to. Among the most important are how and when we choose to apply the RF pulse and when to read out the signal. The order and timing of these parameters is referred to as the "pulse sequence". The time between the RF pulse and the center of the echo is referred to as the "echo time" or TE. A longer TE will make the scan more sensitive to T2. The time between consecutive repetitions of the RF pulse is referred to as the "repetition time" or TR. A shorter TR tends to increase the T1-weighting while a longer TR tends increase the T2-weighting.

Note that these are generalizations. These relationships are all highly dependent on both the type of sequence and the value of the other parameters. A full exploration of this parameter space is beyond the scope of this thesis. A discussion of each of the specific sequences used in this thesis follows below.

2.4.2 Assessing Brain Morphology

Measurement of brain morphology in MRI typically refers to volumetric quantification of anatomical structures, Voxel-Based Morphometry (VBM) or Deformation-Based Morphometry (DBM). These techniques are almost always conducted on T1-weighted scans due to their high Contrast-to-Noise Ratio (CNR) but there is no theoretical reason the techniques can't be applied to other types of scans. In this thesis I have applied morphometric techniques to whole brain T1-weighted images acquired at 3T with a multi-echo 3D MPRAGE sequence as well as to limited field of view, T2* weighted images of the hippocampus acquired at 7T with a 3D gradient echo sequence. In this section I will discuss the parameters of both of these MRI sequences as well as the three types of morphometric analyses: anatomical volumetry, VBM, and DBM.

2.4.2.1 The Multi-echo 3D MPRAGE Sequence

The 3D MPRAGE (3-**D**imensional **M**agnetization-**P**repared 180-degrees radio-frequency pulses and **Ra**pid **G**radient-**E**cho) sequence was first proposed by Mugler & Brookeman

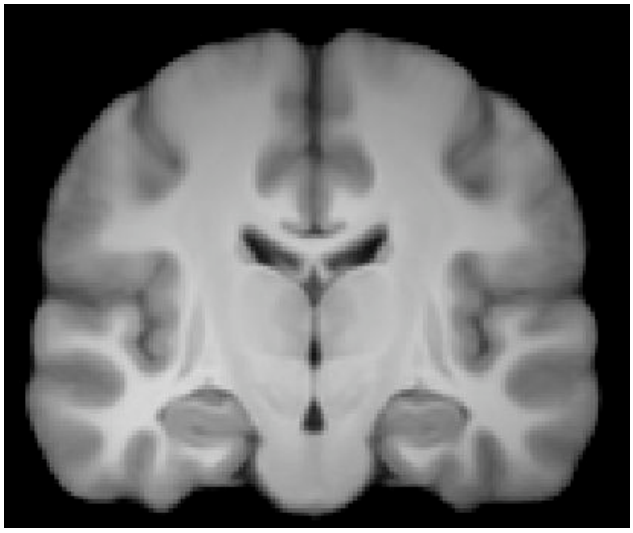

Figure 2.3: Mean ME-MPRAGE image across 62 participants.

(1990) and quickly became the preferred MRI sequence for structural brain imaging. This sequence provides excellent contrast between white and grey matter tissues that make it ideal for visualization and segmentation of the cortical ribbon as well as many (but not all) sub-cortical structures (Figure 2.3).

One limitation of the traditional MPRAGE sequence is that it typically has a relatively low bandwidth, which is critical for its high Signal-to-Noise Ratio (SNR), but it also increases the geometric distortions. van der Kouwe et al. (2008) implemented a modification to the traditional MPRAGE sequence with a shorter bandwidth but multiple echoes. The shorter bandwidth decreases the geometric distortions while the multiple echoes maintain the high SNR. This sequence also has the added advantage that multiple echoes can be used to calculate a rough estimated T2* map. This map can then be used to differentiate regions that have near identical T1 values, but very different T2* values, such as abutting regions of cortex and dura. The root mean square of all four echoes from this multi-echo MPRAGE sequence was used for all 3T, T1-weighted structural scans in this thesis, as well as for the cerebral blood volume quantification discussed below. Scans were collected at a resolution of 1 x 1 x 1 mm, TR = 2530 ms, Inversion Time (TI) = 1200 ms, TE = 1.69, 3.55, 5.41 and 7.27 ms, matrix size = 256

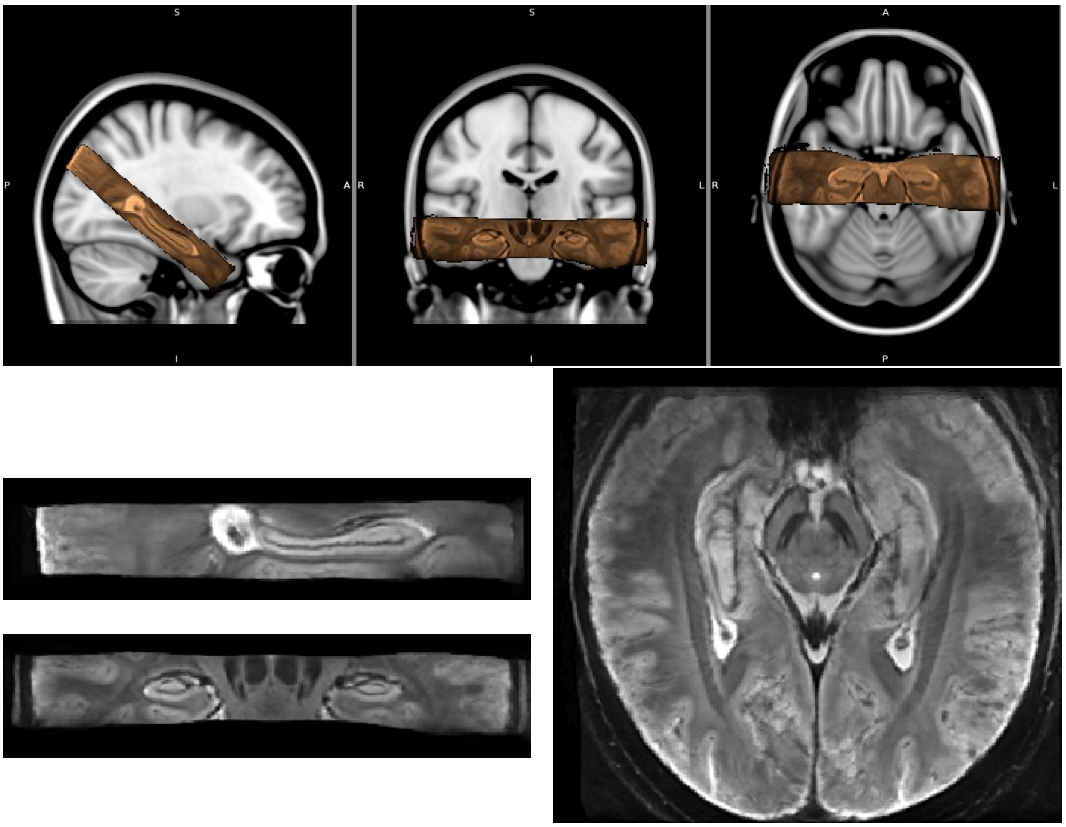

Figure 2.4: Illustration of the T2*-weighted gradient echo sequence at 7T. Top: Illustration of the location and orientation of oblique slice plane for the limited field of view hippocampal scans. Bottom: The average non-linearly aligned template across 24 participants.

x 256 x 176, and Generalized Autocalibrating Partially Parallel Acquisition (GRAPPA) factor = 2. The scanner's pre-scan normalization feature was used to correct for B1 bias fields.

2.4.2.2 The T2*-weighted gradient echo sequence

As discussed above, T1-weighted sequences have been the work horse of MRI morphometry since the field began (Ashburner & Friston, 2000; Woods et al., 1998; Caviness et al., 1989). No other contrast provided comparable anatomical detail until the introduction of 7T where susceptibility or T2*-weighted images were shown to exhibit structural details previously unseen at 1.5 or 3 Tesla (Duyn et al., 2007). For imaging the

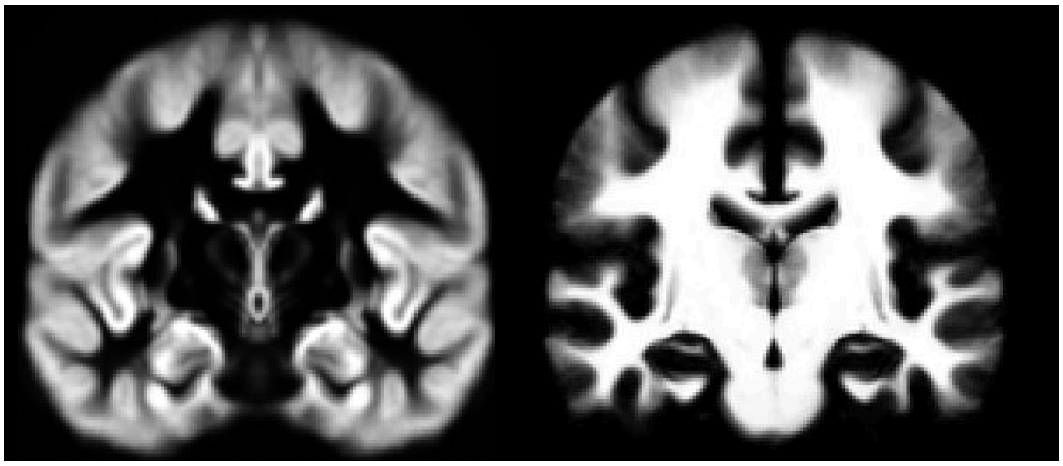

Figure 2.5: Mean segmented white matter and grey matter images used from the VBM pipeline.

human hippocampus at 7T, we use a slightly modified version of a recently published T2* weighted sequence (Cho et al., 2010). Modifications include a slight increase in voxel size (0.4mm isotropic to 0.5mm), the addition of flow compensation, and a change in the phase encode direction (Anterior-Posterior to Left-Right). With these modifications we were able to produce very high quality hippocampal images suitable for deformation-based morphometric analysis described below (see Figure 2.4).

2.4.2.3 Voxel-Based Morphometry

The human brain is composed of hundreds of different functional regions as well as hundreds of different types of neural, glial, and vascular cells (Zeng et al., 2012; Masland, 2004). However on a T1-weighted MRI scan, just three different types of tissue are readily apparent: 1) white matter, which contains mostly fat-laden, myelinated axons; 2) grey matter, which contains mostly neural cell bodies, dendritic processes, synapses, astrocytes, and small vasculature; and 3) Cerbrospinal Fluid (CSF), which in addition to actual cerebral spinal fluid also includes larger vasculature such as the sagittal sinus, since venous vasculature and CSF are both very dark on T1-weighted scans (arterial vessels can be bright depending on orientation and flow). The relative volume and distribution of these three tissue classes varies considerably across age, sex, and disease. But in the early

days of MRI the only way of quantifying this variability was to draw a region of interest and count the voxels within it that fell into one of the three classes. VBM was proposed to provide an automated, systematic, whole-brain method of quantifying the variability in these three tissue classes (Ashburner & Friston, 2000; Good et al., 2001).

VBM can be broken down into several steps.

1. For each participant, all non-brain tissue is removed with a skull-stripping algorithm (see Fennema-Notestine et al., 2006, for a review of different approaches).
2. Each brain is then segmented into the three tissue classes: grey, white, and CSF using a program such as FMRIB's Automated Segmentation Tool (FAST) or Statistical Parametric Mapping (SPM) (Zhang et al., 2001; Friston et al., 2004).
3. One of the tissue classes, assume it is grey for the purposes of this example, is then spatially registered to a standard grey matter template. The template published by the Montreal Neurological Institute and the International Consortium on for Brain Mapping is the one most commonly used (Mazziotta et al., 1995).
4. All registered grey matter images are then averaged to create a new template specific to the participants in the study.
5. Step three is then repeated using the study-specific template as a registration target. If the initial template is very different from the study population, as is the case in severe neurological disorders, ageing, or early in development, step three can be repeated multiple times, refining the template on each iteration.
6. Non-linearly registering each grey matter image to the template generates two outputs: 1) the registered image and 2) the warp field which contains a three dimensional vector for each voxel that describes how that voxel in the original image needed to be shifted and contorted in the X, Y, and Z directions in order to map it onto the template image. This three dimensional vector can be reduced to single scalar value, known as the Jacobian determinant.
7. The Jacobian determinant is then used to scale the registered grey matter image.

This scaling ensures that the net amount of grey matter across the whole brain is conserved. The scaled grey matter image is then smoothed with a Gaussian smoothing kernel with a sigma value typically between 1 and 4. This smoothed image is then run through a non-parametric, permutation-based statistical inference process such as the one provided by randomise or SnPM (Nichols & Holmes, 2002).

2.4.2.4 Deformation-Based Morphometry

The non-linear registration of one brain to another or to a standard template results in a warp field that describes this registration. Performing statistics on this warp field directly is know as DBM or Tensor-Based Morphometry (TBM) depending on the exact techniques used (Ashburner & Friston, 2004). For the purpose of this thesis, I will use the term DBM exclusively. Non-linear warping algorithms have improved considerably in the past decade (Klein et al., 2009), and as a result there has been increasing interest in use of DBM for structural brain analysis. The details of different implementations of non-linear warping are beyond the scope of this thesis. All non-linear deformations presented here have employed either FMRIB's Non-linear Image Registration Tool (FNIRT) from the FMRIB's Software Library (FSL) or Advanced Normalization Tools (ANTS) (Andersson, 2007a,b; Avants et al., 2011, 2010).

The simplest and most popular version of DBM can be performed on the whole brain following very similar steps to those used for VBM outlined above. The only differences are 1) all registration can be conducted on the skull-stripped brain without further segmentation and 2) the final inference step is performed on the Jacobian determinant (or the log of the Jacobian determinant) directly, as opposed to the aligned and modulated grey matter images.

In the case of our limited field of view 7T data, the process is slightly more complex as no standard template is available to align to. It is possible to create a template from any dataset provided that a rough initial alignment can be achieved, which can then be iteratively improved. This process was used for the high resolution, 7T hippocampal images acquired in this thesis. A detailed description of the pipeline is included in

Chapter 7. Briefly, each scanning session included a whole brain T1-weighted image, two T2*-weighted images of the hippocampus with opposite frequency directions, and a whole-brain T2*-weighted scan for registration purposes. When possible, the two, limited field of view hippocampal scans with opposite distortion directions were combined using the FSL tool topup (Smith et al., 2004; Andersson et al., 2003). The distortion-corrected hippocampus image was then linearly aligned to the T2*-weighted whole brain image which in turn was aligned to the whole brain T1-weighted scan using boundary-based registration (Jenkinson et al., 2002a; Jenkinson & Smith, 2001; Greve & Fischl, 2009). The T1-weighted whole brain image was aligned to Montreal Neurological Institute's template based on 152 scans (MNI152). The proceeding registrations were then concatenated together to register each participant's hippocampus scan into standard space. These scans are then used to bootstrap iterative non-linear registration to create a study-specific template using ANTS (Avants et al., 2011, 2010). Once a template exists, a standard DBM analysis is conducted as outlined above.

2.4.2.5 Anatomical Volumetry

VBM and DBM are typically applied voxelwise after the images have been registered into a standard template such as the MNI 152 template, or to a template defined by the participants in the study. An alternative approach is to simply segment the brain in its native space into different anatomical regions then determine the approximate volume of the regions. Segmentation typically is done on a T1-weighted image which allows for easy segmentation of grey and white matter in cortex as well as several subcortical structures including the thalamus, amygdala, hippocampus, caudate, putamen, globus pallidus, nucelus accumbens, and brain stem (Patenaude et al., 2011; Fischl et al., 2002). Cortical areas can also be segmented based on the location of sulci and gyri or even using the degree of myelination visible on the T1-weighted scan (Fischl et al., 2004; Eickhoff et al., 2005). Although less common, T2*-weighted images allow the segmentation of substantia nigra, red nucleus, and subthalamic nucleus (Xiao et al., 2012). More advanced segmentation algorithms also handle voxels that lie on the border between

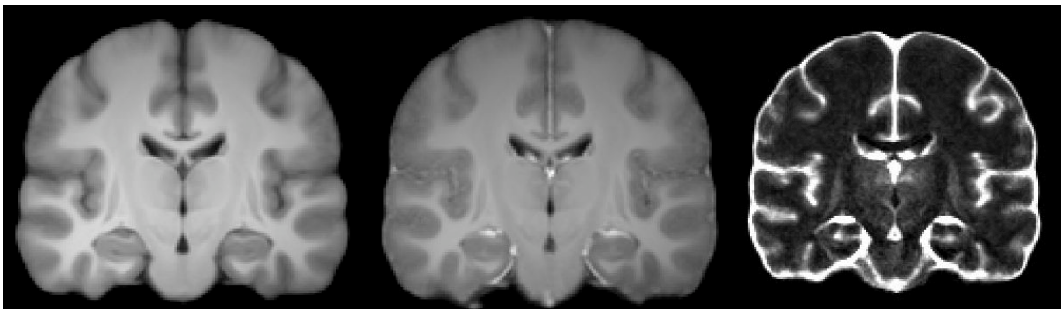

Figure 2.6: Mean ME-MPRAGE images with (left) and without (middle) contrast agent and the mean cerebral blood volume image (right) which is produced by subtracting and normalizing the two image to the left.

regions using partial volume estimation techniques (Van Leemput et al., 2009; Patenaude et al., 2011).

2.4.3 Assessing Cerebral Blood Volume (CBV)

Cerebral Blood Volume (CBV) is a measure of the percentage of blood (both arterial and venous) in a given voxel or region of interest. There are two prevalent techniques of measuring CBV using MRI, one known as the "dynamic" or "bolus-tracking" method and the other as the "static" or "steady-state" technique (Lin et al., 1999; Speck et al., 1999; Barbier et al., 2001). Both involve the injection of a gadolinium-based contrast agent. In the dynamic method, echo-planar images are acquired continuously during the injection of gadolinium and the passage of the contrast agent through the brain is modelled. This technique has the advantage of enabling the simultaneous measurement of cerebral blood flow, but has the disadvantage of lower resolution due to the necessity of acquiring whole brain images in rapid succession. In the static method, a T1-weighted MRI scan is collected before and after a bolus of contrast agent is injected.

For our study we opted to use the static method in order to maximize our resolution and to maintain similar methods to previous studies investigating exercise and angiogenesis (Pereira et al., 2007). At the end of our scanning session an ME-MPRAGE scan was collected with the parameters discussed above. The participant then received an injection of contrast agent (Dotorem, 0.1 mg per kg) via a previously inserted venous

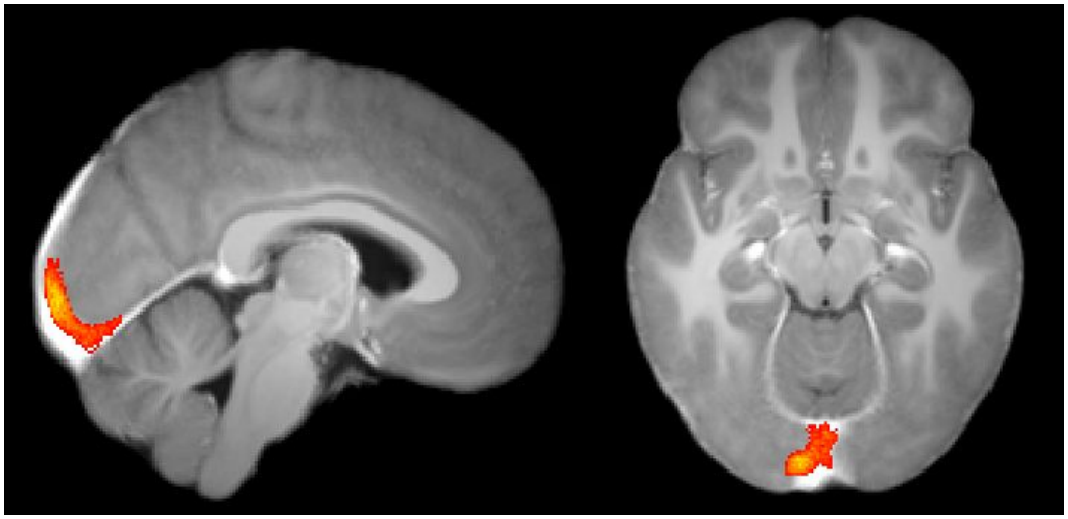

Figure 2.7: The average location of the blood mask in standard space overlaid on the average MPRAGE image with contrast agent for all 56 participants that received contrast injection.

catheter in the arm. A second ME-MPRAGE scan was then conducted with identical parameters. These two images are used to produce an image of cerebral blood volume using the static method (Figure 2.6). Specifically, the pre- and post contrast scans were aligned and subtracted. A Region of Interest (ROI) containing only blood was automatically identified by selecting the 1000 brightest voxels on the post contrast agent scan within the sagittal sinus near the center of the brain immediately above the cerebellum. The mean difference between the post-contrast and pre-contrast signal intensity inside this region was used to normalize the subtracted image:

$$rCBV = \frac{Brain_{post} - Brain_{Pre}}{\overline{Bloodmask_{post}} - \overline{Bloodmask_{pre}}}$$

2.4.4 Assessing relaxation parameters: T1, T2, and T2*

In order to assess the nature of structural plasticity, we endeavoured to collect several low-level relaxation parameters from the brain including T1, T2, and Susceptibility or T2*. The sequences used to collect these parameters are discussed in the following sections along with the details on how these parameter maps were aligned for non-

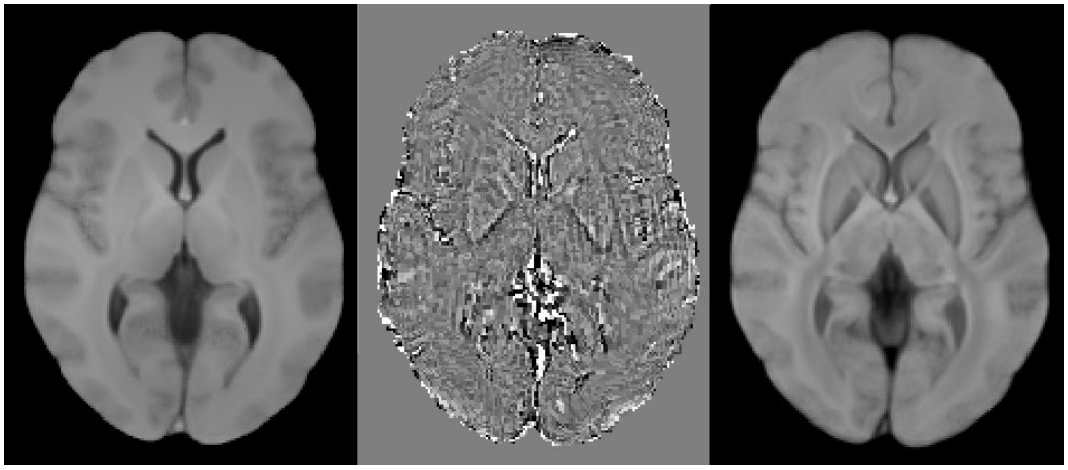

Figure 2.8: Mean magnitude (left), phase (middle), and susceptibility-weighted (center) images across all 62 participants.

parametric statistical analysis.

2.4.4.1 Susceptibility weighted imaging (SWI)

Susceptibility Weighted Imaging (SWI) came into wide use in the late 1990s and was originally used to map venous blood (Reichenbach et al., 1997). However, as larger field strengths became more widespread, SWI imaging has been increasingly used as a powerful tool to measure anatomical structure not visible in traditional T1-weighted scans (Figure 2.8). The most obvious examples are the iron-rich regions of the mid brain including the putamen, caudate, and red nucleus. At ultra-high field strengths (7T and above) susceptibility weighting can be used to detect the fine structure of myelination (Wharton & Bowtell, 2012; Duyn, 2013). In our study we use a standard multi-echo 3D gradient echo sequence with 1.3 mm isotropic voxels, TE=6.72 ms & 24.60 ms, TR=30 ms, matrix size = 192 x 192, and GRAPPA factor = 2. Combining the phase and frequency images to produce susceptibility weighted image is performed on the scanner console using a published method (Haacke et al., 2004).

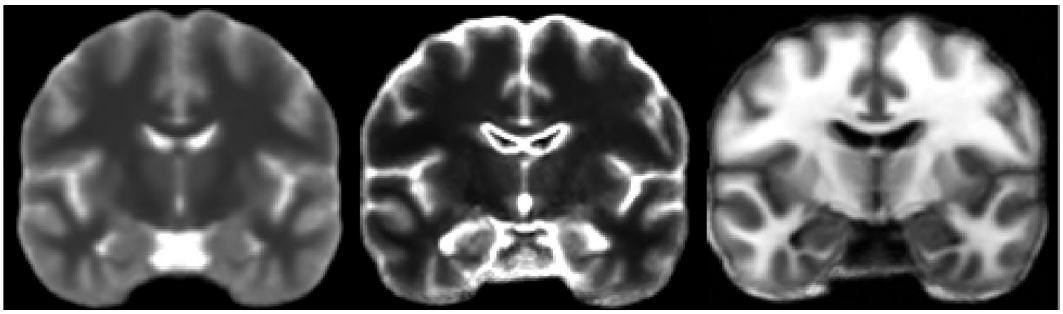

Figure 2.9: Mean T1, T2, and Fast Volume Fraction maps from the DESPOT1 and DESPOT2 pipeline.

2.4.4.2 DESPOT1/2 sequences

The DESPOT1/2 (Driven Equilibrium Single Pulse Observation of T1/T2) family of sequences was first developed and proposed by Sean Deoni and collaborators nine years ago and has been under active development ever since (Deoni, 2007; Deoni et al., 2004, 2005, 2008, 2013). It provides quantitative maps of T1 and T2 as well as estimation of the water trapped in myelin bilayers (myelin water fraction); however, this quantification of myelin has been the subject of controversy in the literature (Lankford & Does, 2013).

In our study we used the DESPOT1-HIFI sequence, which consists of one multi-echo Spoiled Gradient Echo (SPGR) sequence and one inversion recovery SPGR (IR-SPGR) sequence. We also used DESPOT2-FM, which consists of two Steady-State Free Precession (SSFP) sequences with opposite phases (0 and 180). T1 and T2 maps were calculated using DESPOT1-HIFI (Deoni, 2007) and DESPOT2-FM (Deoni, 2009). Briefly, the acquired signal at multiple flip angles was fit to the signal equations for the steady state images, with corrections for flip angle inhomogeneity and off-resonance effects (Figure 2.9).

2.4.4.3 Voxel-Based Quantification

For many of the imaging measures discussed above we are able to estimate a true quantitative value such as Mean Diffusivity or Cerebral Blood Volume. In other cases,

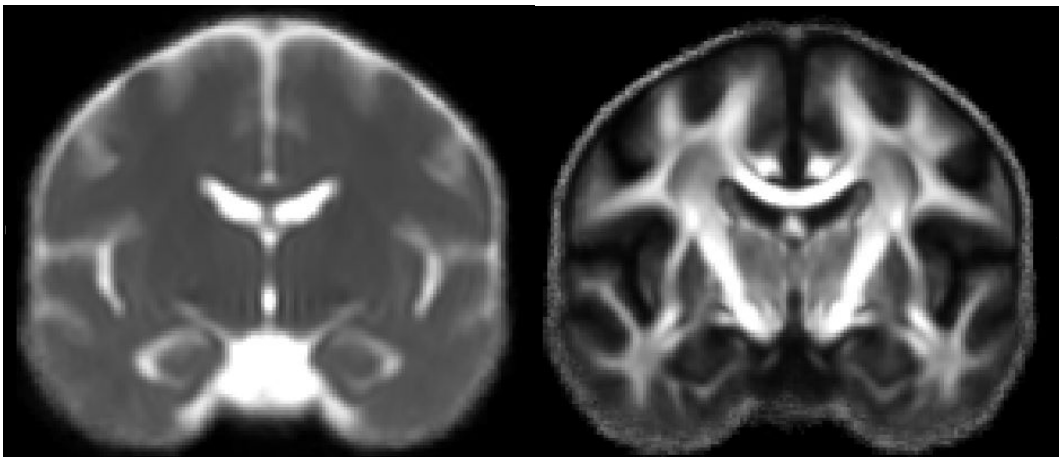

Figure 2.10: Mean MD and FA images from the diffusion tensor sequences.

we conducted statistics on the raw signal intensity of a given sequence, such as with our susceptibility weighted scans. In these instances the processing pipeline was as follows. The image is first normalized by the global median signal to remove large differences in the overall brightness of the image, which are typically due to scanner calibration issues. The image is then linearly registered to the high-resolution structural image from the same session. This registration is then combined with the registration from the VBM pipeline to register the image into standard MNI space. Statistical inference can then be performed using the non-parametric tool, randomise (Nichols & Holmes, 2002).

2.4.5 Assessing Diffusion: Mean Diffusivity and Fractional Anisotropy

The ability to measure the diffusion of water molecules using magnetic resonance was demonstrated a decade after the discovery of MRI itself (Carr, 1958; Stejskal & Tanner, 1965). The application of diffusion-weighting in medical imaging was first demonstrated in the mid 1980s (Le Bihan et al., 1986). It was not until the invention of the diffusion tensor model in 1994 that it became possible to build detailed maps of the brain's white matter structure using only microscopic differences in the diffusion of water molecules trapped inside axons (Basser et al., 1994; Pierpaoli et al., 1996). The diffusion tensor model estimates a number of parameters. The most commonly used are mean diffusivity MD and FA (Figure 2.10). While measuring the integrity and tracking the di-

rection of axons has recently become one of the more popular uses of diffusion imaging, diffusion imaging also seems to be one of the most sensitive measures of neural structure possible with MR. Diffusion-weighted scans have become a routine diagnostic scan to detect ischemic stroke in its earliest stages when all other imaging modalities show apparently healthy tissue (Le Bihan & Johansen-Berg, 2012). Similarly, there have been recent reports that rapid changes in mean diffusivity can be measured after a learning tasks in the absence of detectable changes on other MR modalities (Sagi et al., 2012). This sensitivity may be due to the fact that the diffusion signal is a measure of molecular movements occurring on a micrometer scale, far smaller than the millimetre resolution of typical structural MRI scans.

There are many methods and approaches for analysing diffusion data (Johansen-Berg, 2012). The most sophisticated of which are targeted at determining how different areas' connectivity changes (tract tracing) or determining differences in the integrity of white matter bundles using Tract-Based Spatial Statistics (TBSS) (Smith et al., 2006; Behrens et al., 2003; and Sotiropoulos et al., 2012). However, these techniques are used to analyse white matter connectivity, and most of the work presented in this thesis is focused on changes within grey matter where these methods do not apply. Except where noted, analysis of diffusion data (FA and MD) has used the voxel-based quantification approach discussed in section 2.4.4.3.

2.5 Conducting Within-Subject Analyses

A central goal of this thesis is to gain a better understanding of within-subject plasticity. Many researchers approach within-subjects designs in much the same way they would approach a between subjects design. They simply add an additional regressor for the subject's identity. This approach leads to at best a loss of statistical power and at worst spurious and biased results. Much has been written in recent years discussing the unique issues facing within-subject neuroimaging analyses such as properly accounting for variance and establishing unbiased templates (Bernal-Rusiel et al., 2013b,a; Reuter et al., 2012; Fox et al., 2011; Aarts et al., 2014). This section will summarize some of

these concerns and techniques and discuss the approach taken in this thesis.

2.5.1 The Perils of Removing Inter-subject Variance

A crucial challenge in all empirical scientific research is maximizing signal to noise ratio or statistical power. The researcher tries to maximize to signal – the variance that is correlated with the variable of interest, while minimizing the noise – the variance that does not correlate with the variable of interest. There are many different strategies to achieve this goal. One of the most obvious and most common strategies is to increase the sample size. Adding more participants to an MRI study will continually increase the variance of interest while the variance of no interest will eventually asymptote.

Another approach is to attempt to decrease the noise. There are many sources of noise in any given experiment, from instrument fluctuations, to time of day, to experimenter error. But the largest source of noise is almost always due to the variance between participants. Each participant brings their own unique anatomy and physiology and the difference between the participants typically dwarfs all other differences. Within-subject designs attempt to remove this source of variance from the experiment by collecting multiple data points from each participant and looking only at the relationship between those data points.

This approach at first seems very appealing as it suggests that we can achieve much greater statistical power with a smaller number of participants. However it should be recognized that longitudinal designs are far less forgiving than cross sectional designs. It is surprisingly easy for small amounts of bias to creep into an experiment. For example a minor upgrade in the scanner software might subtly change the contrast in participants scanned after the upgrade. In a cross sectional design, this difference is tiny compared to the differences between participants. However, in a longitudinal design the inter-subject variance is subtracted or regressed away. So even a minor bias in the number of scans conducted before versus after the upgrade could have dramatic affects on the statistical results. Potential sources of bias in longitudinal designs as well as rigorous statistical methods to detect these biases are discussed in the following sections.

2.5.2 Creating an Unbiased template in Longitudinal Image Processing

Some longitudinal imaging processing pipelines completely ignore the identity of the participant in the processing stream. That is to say that different time points for a given participant are processed equivalently to different subjects. This approach does not introduce any bias into the processing pipeline and may be entirely appropriate when there is a robust process for mapping each participant into a standard analysis space. For example, this method is the current recommended approach in FSL's TBSS pipeline where there is not (yet) evidence that the skeleton creation process would benefit from a participant-specific initialization process.

However, in most within-subject analysis pipelines, the first step is the creation of a template for each participant. This step requires aligning each time point into a common space and ensuring that that space is not biased toward any specific time point in any way. I have written previously on this problem, as have others (Thomas et al., 2009; Smith et al., 2002). In these publications, we discussed the problems of interpolating one image in a longitudinal pipeline differently from others. This leads to one time point being slightly smoother than others. This subtle difference might be washed out in a cross-sectional analysis, but with the extreme sensitivity of a within-subject design it can lead to false positives. However, interpolation is only one of many issues that must be considered in longitudinal neuroimaging analysis. Other issues included differences in global signal intensity, different distortions due to head position in the field, different coil profile intensities, and even different jaw positions from scan to scan. These issues have been the subject of several recent publications and are now carefully addressed in the Freesurfer pipeline (Reuter et al., 2010, 2012). The Freesurfer longitudinal pipeline has been used for cortical and subcortical segmentation throughout the work in this thesis.

2.5.3 Statistical Approaches to Longitudinal Analysis

Traditionally, within-subject statistical analysis in neuroimaging has employed a repeated measures ANOVA or simple paired t-tests approach. However, these methods fail to appropriately model the within-subject and between-subject variance pools and can be shown to be less powerful than alternative methods using a linear-mixed effects (LME) approach (Bernal-Rusiel et al., 2013a). LME models explicitly model both the trajectory of the mean measurement over time and the correlation structure among serial measurements. LME also accounts for the interdependence between these two models. Another advantage is that LME models distinguish between within- and between-subject sources of variance and allow the independent analysis of both.

Until very recently, the tools to perform these tests voxelwise throughout the brain were not available. However, several groups have recently made these tools available (Chen et al., 2013a; Bernal-Rusiel et al., 2013b). Unfortunately the linear-mixed effects approach is iterative. Therefore it can be prohibitively slow or can fail to converge completely. Another alternative approach is the use of sandwich estimators which aim to provide the speed of ordinary least squares approaches such as repeated-measures ANOVA while increasing power and validity (Guillaume et al., 2013). However, these tools are not yet widely available. In this thesis, I have made use of linear-mixed effects analyses with univariate data when evaluating three data points. These analyses were used to guide whole-brain, voxelwise T-tests of hypotheses involving only two data points.

Chapter 3

Volume, vascular, and white matter changes in the anterior hippocampus associated with aerobic exercise

3.1 Abstract

The hippocampus is believed to be among the most plastic structures in the brain. The size of the human hippocampus has been shown to increase in response to relatively long periods (6 months or greater) of aerobic exercise in older adults. It is currently unknown whether this growth reflects a recovery from age related atrophy or a more general plastic response independent of age. It is also unknown how long-lasting this plasticity is and exactly what aspect of the neural tissue is changing. In this chapter I show that anterior hippocampal growth can be observed in young to middle-aged, sedentary adults after just six weeks of aerobic exercise. Hippocampal growth was not maintained in the absence of continued aerobic exercise, returning to baseline six weeks after cessation of exercise training. Anterior hippocampal volume is also shown to correlate with backward

digit span – a measure of working memory. Finally, multimodal neuroimaging revealed that, within the anterior hippocampus, measures associated with expanded neuropil or myelination showed a significant increase with exercise while measures associated with vasculature, which is thought to accompany neurogenesis, did not. These results provide novel insights into the contingencies, mechanism, and time course of structural change after exercise in the human hippocampus.

3.2 Introduction

Habitual aerobic exercise has been widely associated with greater cognitive performance in older adults as well as adolescents (Kramer & Erickson, 2007; Anderson-Hanley et al., 2012; Benedict et al., 2012; Aberg et al., 2009). Epidemiological studies have also shown that lifestyle during middle age has significant consequences for cognitive performance decades later (Wilson et al., 2002; Karp et al., 2006). Thus, determining the effects of exercise interventions on the middle-aged brain has relevance to lifelong cognitive health. A recent longitudinal study has demonstrated that aerobic exercise has a direct causal role in increasing the volume of the hippocampus in sedentary older adults (Erickson et al., 2011). It has also been shown that aerobic exercise increases the rate of neurogenesis in the dentate gyrus region of the rodent hippocampus and increases the cerebral blood volume in the same region in humans (Pereira et al., 2007; van Praag et al., 1999a,b). In rats, some efforts have been made to relate the morphometric measurements commonly used in neuroimaging to underlying changes in the neural tissue elicited by other behavioural training paradigms (Lerch et al., 2011), but little is known about what drives these changes in humans. And while a great deal of work has focused on older adults, relatively little research has explored exercise-mediated plasticity in the middle of the lifespan. Finally, it is not yet known to what degree exercise-mediated brain plasticity persists in the absence of continued aerobic exercise, an important question for designing effective interventions and informing exercise guidelines.

In this study we show that just six weeks of aerobic exercise is sufficient to induce growth in the volume of the anterior hippocampus in a young to middle-aged cohort

of sedentary adults. This volume growth does not occur in a control period without exercise and is demonstrated to be relatively transient, returning to baseline six-weeks after the cessation of the exercise intervention. In addition to showing volume growth using traditional morphometric techniques, we also investigate changes in a wide range of complementary imaging modalities (including T1, T2, MD, FA, SWI, and CBV) to further characterize the nature of the underlying change. Interrogation of these multimodal changes does not support a change in vasculature, but instead suggests an expansion of neuropil or myelination.

3.3 Methods

3.3.1 Participants & Design

We acquired 151 MRI scans from sixty-two sedentary adult subjects (35 women, mean age 33.7, S.D. 11.9). All participants were recruited from the Oxford community using flyers, online forums, and word of mouth. Inclusion criteria included right-handedness and no history of psychiatric or neurological disease. Recruitment information requests participants who engaged in less that 30 minutes per week. Participants found to have above average fitness were used as baseline controls only (see below). Informed written consent was obtained from all subjects in accordance with ethical approval from the Central Office for Research Ethics Committees. Using a standard crossover design, the participants were pseudo-randomly assigned to one of two groups: "rest first" or "exercise first" (Figure 3.1). At baseline, all participants were given a battery of cognitive tests, a fitness assessment ($\dot{V}O_2$ max test) and an MRI scan. Participants in the rest first group were then asked to maintain their normal level of physical activity for six weeks, after which they returned for a second behavioural and fitness assessment and MRI scan. They then began a six-week exercise program consisting of 30 minutes of supervised aerobic exercise on a stationary bicycle, five days per week. At the end of the six-weeks they were given a final behavioural and fitness assessment and MRI scan. Participants in the exercise first group started the same exercise program immediately after their baseline assessment. At the end of the exercise program they were scanned and assessed then al-

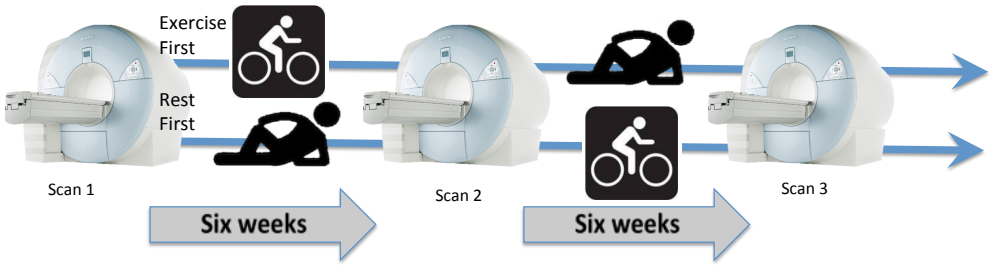

Figure 3.1: Top: Forty-nine participants were recruited, scanned, and pseudo-randomly assigned to one of two conditions. In the "exercise first" condition (top) participants completed six weeks of aerobic exercise (five times per week, 30 minutes per day) and were scanned again. These participants were then allowed to return to their baseline activity levels for six weeks and then scanned again. For participants in the "rest first" condition (bottom), the order of the exercise and rest periods was reversed.

low to return to their normal level of physical activity. After six weeks they were scanned and assessed again.

Twenty-six participants were assigned to the exercise-first condition with one completing only the first two scans (pre- and post-training). Twenty-three participants were assigned to the rest-first condition with 7 completing only the first two scans (pre- and post-rest). A total of 41 participants completed the exercise intervention across both groups. In addition, 13 participants were recruited for baseline assessment and a single scan only. These data were only used in cross sectional analyses. (Figure 3.2).

3.3.2 Behavioural and physiological measures

Full details of all behavioural and physiological measures are provided in sections 2.3 and 2.2. Briefly, a battery of behavioural tests was administered to each participant at each time point. Of interest for the results presented in the chapter, the battery included a computerized, verbal, forward and backward digit span test administered in a stepwise fashion by computer (Woods et al., 2010). Physiological tests included a standard $\dot{V}O_2$ max test administered on a stationary exercise bike. Ventilatory Oxygen consumption ($\dot{V}O_2$) was measured while the resistance on the bike was increased every two minutes. TTE was also measured.

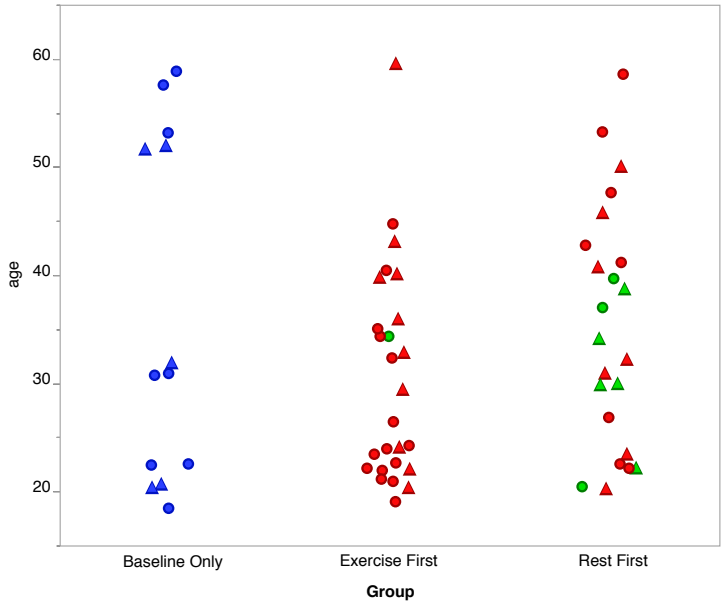

Figure 3.2: Age and group of all 62 participants. Triangles indicate males, circles indicate females. Red markers indicate the participant completed all three scans, green indicates two scans, and blue indicates a single scan.

3.3.3 Exercise training

Participants were required to attend monitored training sessions 5 days a week, for 6 consecutive weeks. The training consisted of 30 minutes continuous cycling at a cadence between 60-70 RPM, on an upright exercise bike, and to maintain a heart rate consistent with their aerobic training zone of between 55%-85% of their maximum heart rate (HR max). Training zones were calculated using age-predicted heart rate maximum (220-age), and were monitored by an experimenter every 5 minutes using digital heart rate monitoring hand sensors. Participants were started at the lower end of the aerobic zone for the first few sessions and were encouraged to progress by increasing the heart rate range as the weeks progressed.

3.3.4 Imaging methods

Each MRI scanning session was conducted on 3T Siemens Verio scanner (Erlangen, Germany). A battery of different imaging sequences were collected including Multi-echo

MPRAGE (before and after contrast agent injection), DTI, SWI, DESPOT1-HIFI and DESPOT2-FM (Deoni, 2007, 2009; van der Kouwe et al., 2008). Further details on each of these sequences are included in chapter 2 section 2.4. Additional details on the calculation of CBV are included in section 2.4.3.

Segmentation of the hippocampus for each time point was performed on individual subject MPRAGE images (without contrast) in native space using the Freesurfer hippocampal subfield segmentation pipeline (Van Leemput et al., 2009). This pipeline produces a probabilistic map of each subfield in each subject. In order to create an ROI for the whole hippocampus in each subject, the probability distributions of all hippocampal subfields were first thresholded at 50%, binarized, and combined. Thus a mask was created in which voxels with a 50% likelihood of being contained within the hippocampus were included. As previous studies have shown that hippocampal plasticity tends to be focused in the anterior head portion (Erickson et al., 2011; Sagi et al., 2012; Maguire et al., 2000), we focused our analysis on the anterior quarter of the hippocampus. The posterior-most 75% of the full hippocampal mask was removed, leaving just the anterior-most 25% of the hippocampus (based on the y coordinated of the center of gravity as per Erickson et al., 2011) on which volume and ROI measures were based. The volume of this ROI was calculated for each subject and each timepoint. For ROI measurements, whole brain voxel-wise maps of T1, T2, MD, FA, T1/T2 Ratio, CBV, and SWI were rigidly aligned to the MPRAGE scan collected on the same subject in the same session. Spline interpolation was used to minimize blurring. For each measure, the average across all voxels within the anterior hippocampus ROI was then determined in the subject's native space. For voxelwise analyses, all scans were aligned to standard space via unbiased subject-specific templates. This procedure is described in detail in section 2.5.2.

3.3.5 Statistical Analyses

Anterior hippocampal volume changes were analysed using a longitudinal Linear Mixed Effects (LME) approach implemented in the nlme package of the R statistical programming language.(Bernal-Rusiel et al., 2013a; R Core Team, 2013; Pinheiro et al.,

2013; Verbeke & Molenberghs, 2009; Fitzmaurice et al., 2011). Inference on multi-modal imaging parameters were conducted using a non-parametric, permutation-based version of Stouffer's method implemented in MATLAB (MATLAB, 2013; Stouffer et al., 1949).

Stouffer's Method is a meta-analytic method for combining a set of Z-scores when the consistency of the sign of the effect is important. (Compare to Fisher's method Mosteller & Fisher (1948), where significance can be obtained even if the signs are inconsistent). If there are K independent Z-scores to combine, the the method simply consists of computing the average Z-score and scaling by $\sqrt{K}$; the scaling is necessary so that the Stouffer's measure is once again a Z-score under the null hypothesis. Here, as we don't have independent studies but $K = 4$ dependent tests, it is essential that we use a non-parametric permutation procedure to obtain P-values for this measure. The permutation method randomly flips the signs of each subject's data, but does so synchronously over subjects to preserve the dependence.

3.4 Results

3.4.1 Exercise training and fitness change

Out of 30 possible aerobic exercise training sessions, the average attendance was 29.05 sessions (SD 1.05). Change in fitness was evaluated using a longitudinal linear mixed effects (LME) approach (Bernal-Rusiel et al., 2013a). Longitudinal LME modelling is similar to hierarchical linear regression in that explanatory variables are sequentially added and tested to determine if they explain a statistically significant amount of the variance to warrant their inclusion in the final model. There are two important differences between the hierarchical linear regression approach and longitudinal LME. The first is that LME separately and effectively models variance due to within and between subject factors (Fitzmaurice et al., 2011; Verbeke & Molenberghs, 2009). Second, the baseline model or the null hypothesis in longitudinal LME is often a linear change with time. Many incidental factors, such as practice, ageing, and instrument drift, can cause the

dependent variable to change with time. Longitudinal LME allows one to ask if some other variable, exercise in this case, is associated with a change that is different than in the control condition.

I constructed a model to explain variation in the TTE on the fitness test across all subjects and all sessions using three explanatory variables: subject ID, time (visit number, 1-3), and a binary variable indicating whether the subject had just completed the six week exercise training program (postEx, 1 or 0). This model provided a significantly better fit for the variance in TTE than the baseline model which included only subject ID and time alone (log likelihood Ratio=49.56, $P<0.0001$). In order to determine if TTE remained elevated six weeks after the completion of training I added an additional binary within-subject explanatory variable to the model indicating if the participant had completed exercise training six weeks earlier (6wksPostEx, 1 or 0). Although the TTE score tended to be slightly elevated on the six week follow up scan, the model fell short of being significantly different from the previous simpler model containing subject ID, time, and the postEx variable (log likelihood=3.62,$P=0.057$). Thus, TTE is not statistically different from baseline six weeks after the end of the exercise training program. Figure 3.3 summarizes these results.

3.4.2 Anterior Hippocampal Volume Growth

To test whether the six-week exercise intervention had a significant effect on the volume of the anterior hippocampus, I again used a longitudinal LME approach and constructed a model to explain the variance in anterior hippocampal volume across all time points and subjects. Explanatory variables were subject ID, visit number (1-3), and a binary variable indicating whether the subject has just completed the six-week training regime (postEx, 1 or 0). This model provided a significantly better fit for the anterior hippocampal volume as compared to a model containing just subject ID and time (Log Likelihood Ratio=6.95, $P=0.0084$), demonstrating that the exercise intervention significantly changes anterior hippocampal volume. Inspection of the time course of volume change (Figure 3.4) reveals that hippocampal volume is increased immediately

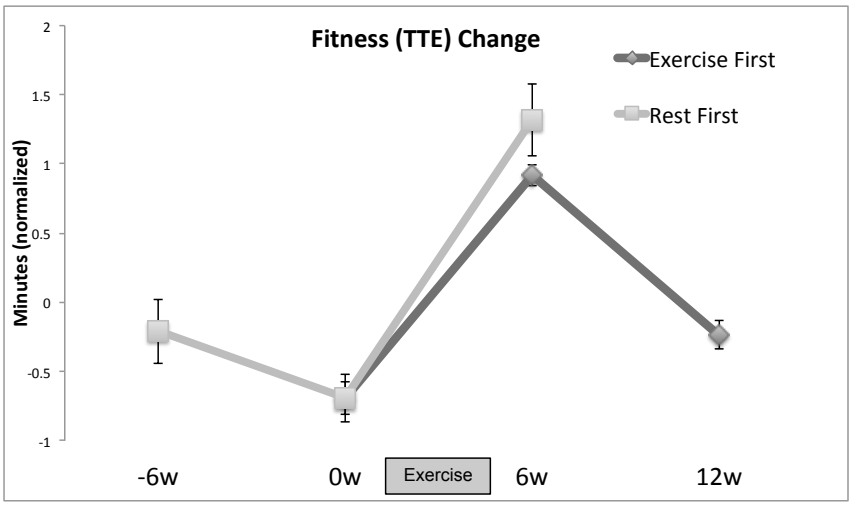

Figure 3.3: Mean-normalized time to exhaustion (TTE) for both the "Exercise First" group (dark grey) and the "Rest First" group (light grey) before and after the six-week exercise intervention. The two groups have been aligned based on the time they underwent the exercise intervention. Linear-mixed effects analysis demonstrates a significant increase in TTE immediately after exercise that falls back to near baseline after six weeks without training.

post-training. I then asked whether hippocampal volume remain elevated in the six-week post-training scan. I again addressed this question by adding an additional within-subject explanatory variable for the scan six weeks after the end of the exercise training program (6wkPostEx, 1 or 0) to the model. This variable provided no significant additional power to the model (Log Likelihood Ratio=0.381, P=0.54), suggesting that six weeks after the completion of the exercise training program, anterior hippocampal volume was not statistically different from baseline. These data are summarized in Figure 3.4.

3.4.3 Correlation between anterior hippocampal volume, fitness, and working memory

LME analyses of behavioural measures showed no significant effects of exercise over and above effects of time. However, it has been previously noted that studies containing a larger number of female participants show a more pronounced effect of exercise on cognition than those with more men (Colcombe & Kramer, 2003; Kramer & Erickson, 2007). We noticed a similar dissociation on the backwards digit span task. Women

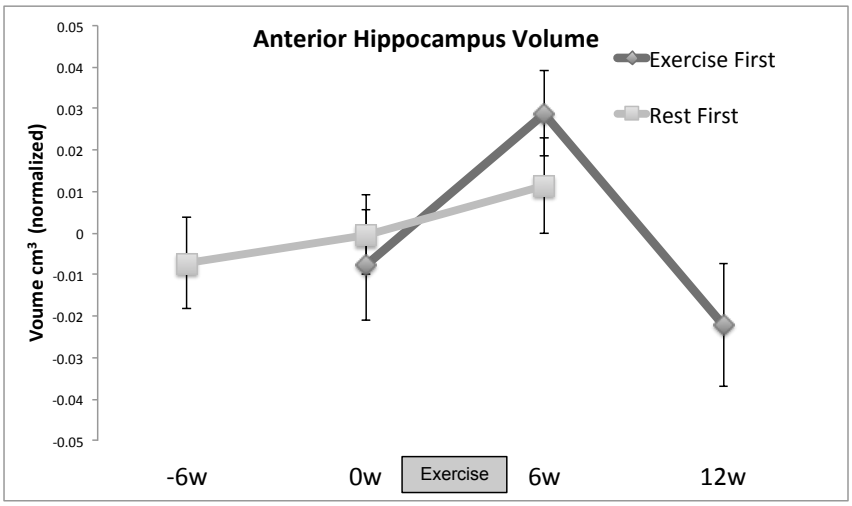

Figure 3.4: Mean-normalized volume of anterior hippocampus volume for both groups before and after the six-week exercise intervention. Linear-mixed effects analysis demonstrates a significant growth in volume immediately after exercise that does not persist in a follow up scan six weeks later.

showed a significant increase in performance after exercise that increased further on the six-week follow-up scan; however, the LME analysis failed to demonstrate that a model containing explanatory variables for post exercise and six-week post exercise provided a significant better fit than time (or practice alone) (Figure 3.5).

Cross-sectionally, there was a positive correlation between baseline backwards digit span score and anterior hippocampal volume at baseline (R=0.3, P=0.02, Figure 3.6), such that a larger anterior hippocampal volume was associated with a higher backwards digit span after accounting for age, sex, and total brain volume.

3.4.4 Multimodal measurements of change within anterior hippocampus

After having demonstrated an aerobic exercise-mediated volume growth in anterior hippocampus I sought to use alternative imaging modalities and measures to elucidate the underlying causes of the volume change. Two potential substrates for exercise-mediated volume growth have been discussed in the literature that are relatively accessible with neuroimaging methods: increased vasculature (i.e. angiogenesis), possibly accompanied

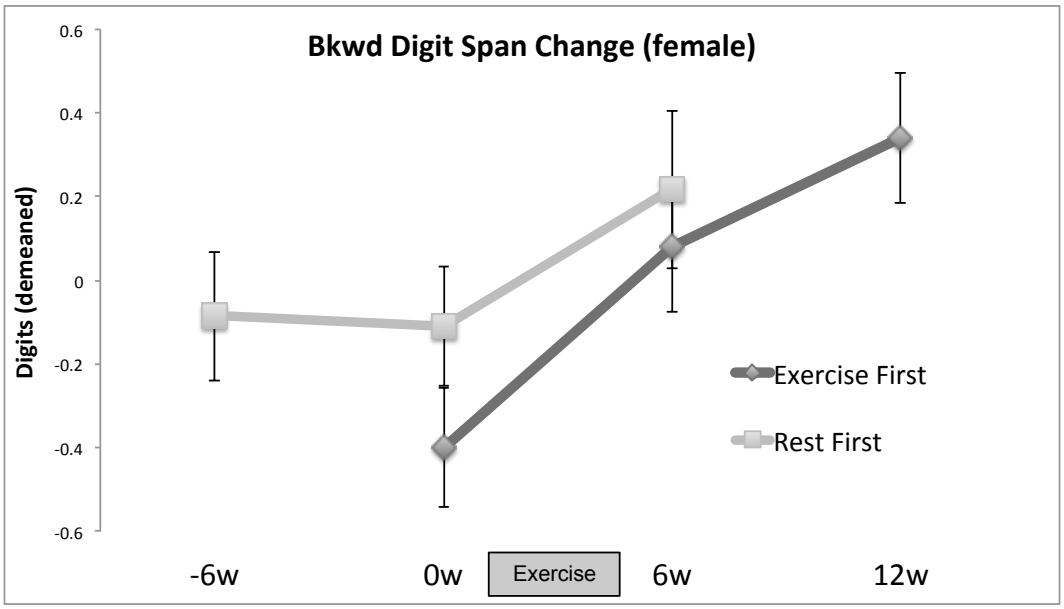

Figure 3.5: Women showed an increase in the backwards digit span after aerobic exercise that continued to increase on the six-week follow up test. Demeaned digit span is on the y-axis and time point is on the X-axis. Statistically it was not possible to dissociate an exercise-mediated increase in digit span from a practice effect. (P=0.35).

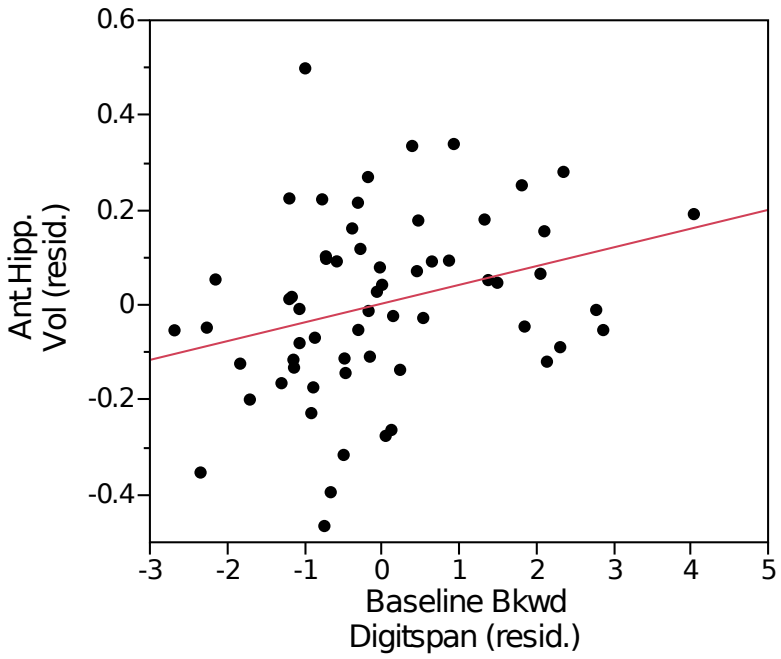

Figure 3.6: Baseline backward digit span significantly correlates with the volume of anterior hippocampus after accounting for age, sex, and total brain volume (R=0.3,P=0.02).

by neurogenesis (Black et al., 1990; Pereira et al., 2007), and increased myelination, possibly accompanied by other related changes within the neuropil such as axonal or dendritic branching and glial expansion. I hypothesized that these two underlying mechanisms would produce predictable but distinct changes in T1, T2, SWI, and CBV, due to the different sensitivities of these MR measures to different tissue components. Specifically, I predicted that an increase in vasculature would be reflected by an increase in T1, T2, and CBV and a decrease in SWI. Similarly, I predicted an increase in myelination would be reflected by a decrease in T1 and T2 with an increase in both the segmented "white matter" in the standard VBM pipeline and in the T1/T2 ratio (Glasser & Van Essen, 2011).

These predictions were tested using a non-parametric version of Stouffer's method to assess changes in relevant measures within the anterior hippocampal ROI (Stouffer et al., 1949). Similar to Fisher's method (Mosteller & Fisher, 1948), Stouffer's method allows several tests to be combined into a single Z-score. The permutation-based version employed here addresses potential interdependence between the tests. Testing the vascular change hypothesis failed to reach significance on the Stouffer's test (Z=-0.65, P=0.69), while the myelin change hypothesis was significant (Z=2.66, P=0.02). Some measures showed greater change than others. The top of Figure 3.7 shows all of the paired T-statistics (before vs. after training) for every measure collected. It is apparent from this graph that WM, T2, and T1/T2 ratio are all showing relatively large shifts consistent with a myelin increase, while T1 and CBV show little change at all (Figure 3.7).

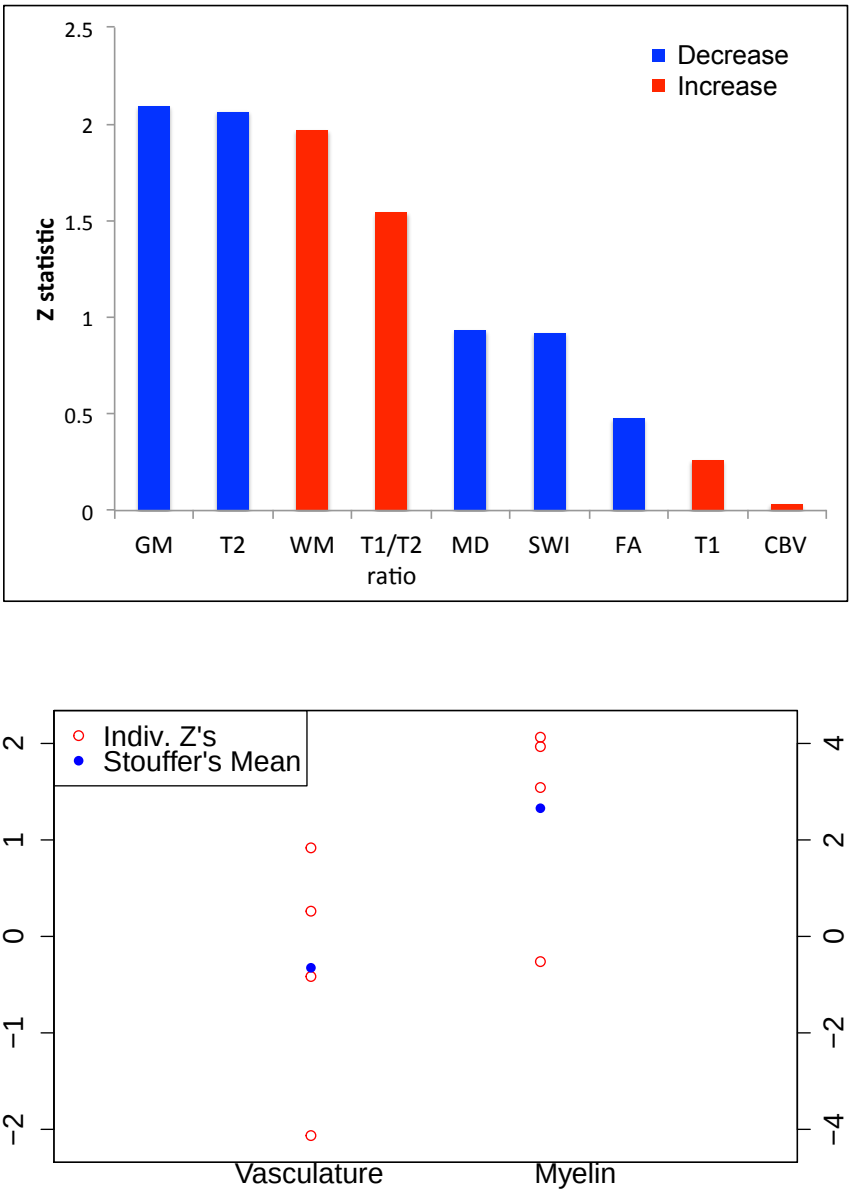

Figure 3.7: Top: Z-scores of change in each MRI measure from before to after exercise. Decreases in blue and increases in red. Bottom: Plot of Z-scores from individual tests (red circles) predicted in the case of an increase of vasculature vs. a predicted increase in myelination (scale for both is shown on left Y-axis). These values are equivalent to those plotted in the top, but the sign of the score depends on whether an increase or decrease was predicted and observed (i.e., a positive Z-score is assigned when the observed change is in the predicted direction). For each prediction, the combined Stouffer's Z-score is plotted in blue (scale shown on the right Y-axis). This is significant for the myelin test (Z=2.66) but not for the vasculature test (Z=0.65).

3.5 Homeostatic changes in CSF and brain volume

One potential confound for studying brain volume changes is hydration levels. Acutely, intense bouts of aerobic exercise with restricted access to liquids results in a decrease in whole body water content. In contrast, extended periods of exercise with unrestricted access to fluids quickly results in a sustained increase in whole body water content (Convertino, 1991, 2007). Dehydration has been shown to produce changes in brain structure including growth in ventricular volume and contraction of grey matter, while hyperhydration has shown the opposite effect (Kempton et al., 2011, 2009; Dickson et al., 2005; Streitburger et al., 2012). In our study we looked at both ventricle volume and grey matter as potential indicators of dehydration. Surprisingly, we found significant growth in ventricular volume and a significant contraction in grey matter density after exercise that did not persist in the follow up scan (Figures 3.8 and 3.9).

In order to evaluate if the change in ventricle volume might be a temporary effect due to dehydration caused by recent aerobic exercise, we plotted the time between the final aerobic exercise session and the scan time. We found no correlation, suggesting that ventricle shrinkage is unlikely due to acute dehydration from the most recent exercise session (Figure 3.10).

Finally, we asked if these global brain changes could account for the growth in anterior hippocampal volume. Plotting the change in ventricle size against the change in anterior hippocampal volume showed no correlation, suggesting that ventricle growth and exercise-related hippocampal growth reflect separate processes (Figure 3.11).

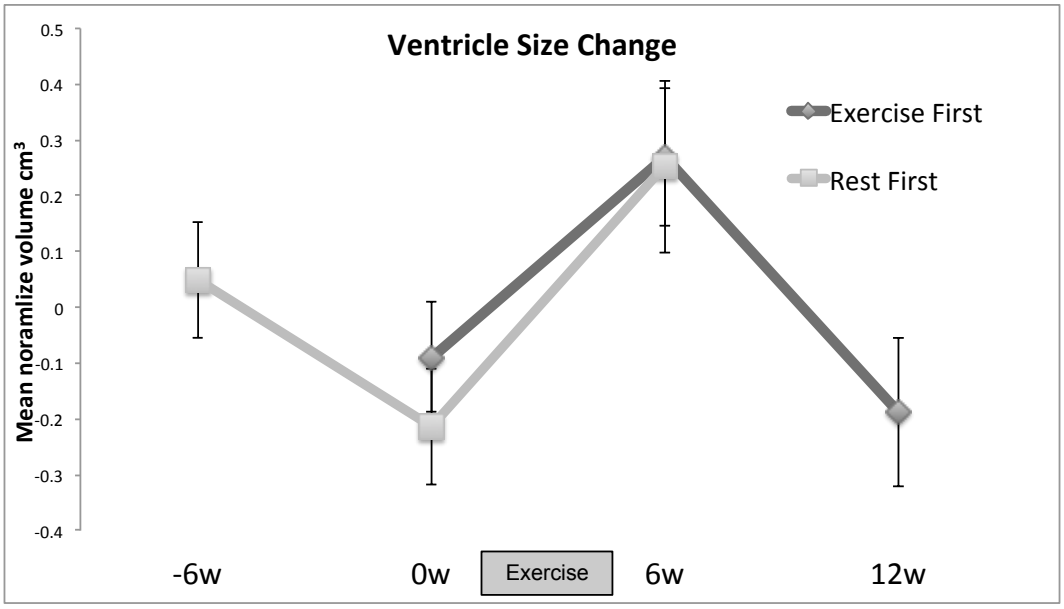

Figure 3.8: Plot of mean normalized ventricle volume across the aerobic exercise intervention. Ventricle volume is significantly increased after aerobic exercise and returns to baseline on a six week follow up.

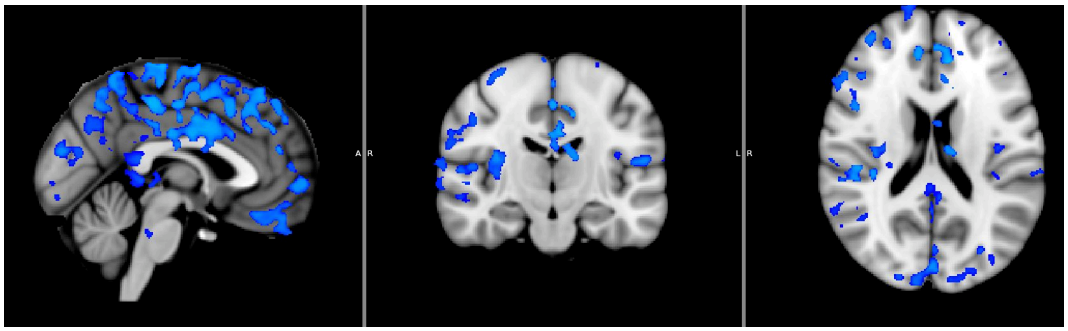

Figure 3.9: A whole brain analysis of change in grey matter density (Post < Pre) using a standard VBM pipeline (see methods) reveals a contraction of grey matter with aerobic exercise that is widely distributed over the cortex (P<0.05, TFCE corrected).

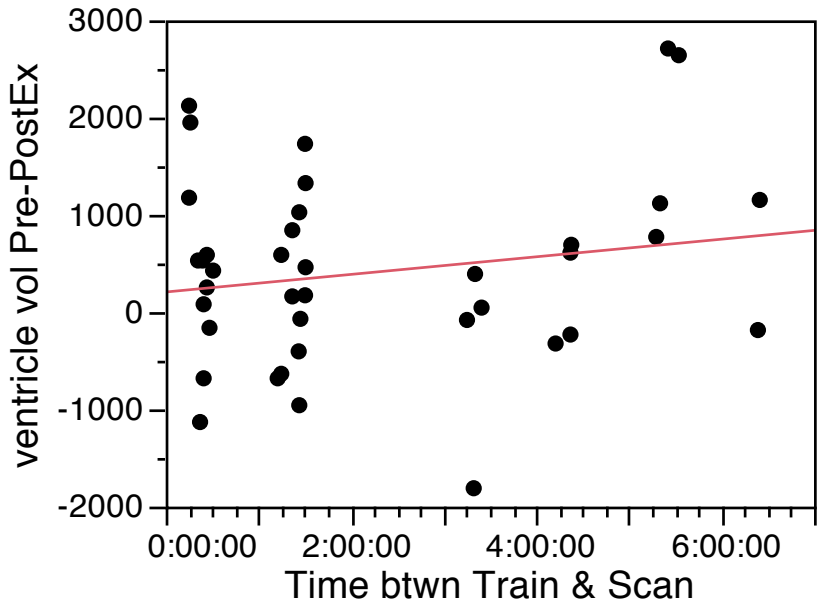

Figure 3.10: No correlation was found between the growth in ventricle volume (cm^3) and time (D:HH:MM) between final training session and MRI scan (R=0.18) suggesting the ventricle growth is not due to acute dehydration.

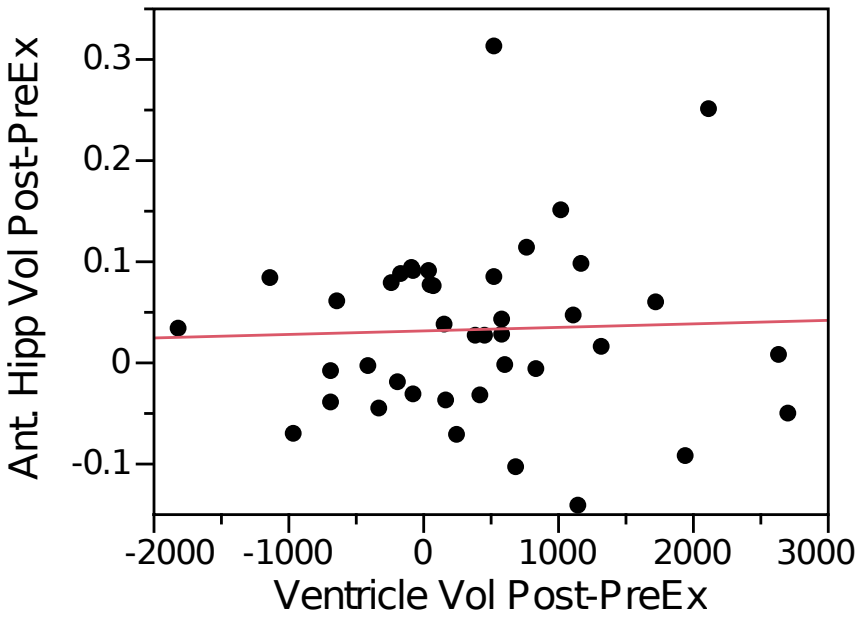

Figure 3.11: Change in ventricle volume plotted against change in anterior hippocampus volume with aerobic exercise (both in cm^3). The lack of correlation suggests these changes are separate processes.

3.6 Discussion

In this study we have demonstrated that volume growth in the anterior hippocampus occurs in young to middle-aged adults after just six weeks of aerobic exercise. This growth is not permanent, returning to baseline after six further weeks without regular aerobic exercise. Baseline anterior hippocampal volume was shown to correlate with backwards digit span score, confirming the results from many other studies that hippocampal volume is directly related to cognitive performance (Kramer & Erickson, 2007; Erickson et al., 2009; Chaddock et al., 2010). Using multi-modal neuroimaging to quantify tissue properties within this region, we have shown that changes in GM, WM, T1, T2, T1/T2 ratio, CBV, and SWI are more consistent with an increase in myelin and the neuropil than an increase in vasculature.

Previous studies have reported increases in hippocampal volume with exercise interventions of six months or more in older adults (Erickson et al., 2011). In the current study we have shown that just six weeks of regular exercise causes significant brain growth in sedentary, middle-aged adults. Furthermore, while previous studies have considered only volume measurements derived from structural MRI, by employing a multi-modal imaging battery we are able to provide insight into potentially underlying mechanisms. Our findings suggest that the exercise-mediated plasticity in the hippocampus may in part reflect myelin changes. In a T1-weighted MRI scan, myelin is most apparent in the white matter, however there are also a considerable number of myelinated fibers within hippocampal grey matter that have been shown in human histological studies (Benes et al., 1994). Neuronal activity-dependent changes in myelination have been observed in cell culture (Wake et al., 2011; Fields, 2010), and it is possible that such mechanisms explain the changes in white matter structure associated with experience that have been reported in several recent imaging studies (Blumenfeld-Katzir et al., 2011; Zatorre et al., 2012; Sampaio-Baptista et al., 2013). Cross-sectionally, an association between physical activity and white matter integrity has been shown in older adults (Tseng et al., 2013), however longitudinal studies have shown mixed results (Heo et al., 2011). Growth of

mossy fibers in the rat hippocampus with physical exercise has been observed, but these fibers are not myelinated (Toscano-Silva et al., 2010). Increased motor activity in rats has also been associated with increased myelination in the peripheral nervous system (Canu et al., 2009).

It is interesting to note that our results differ from previously published studies in rodents that have shown a robust vascular change within the hippocampus after a prolonged period of exercise (Pereira et al., 2007; Van der Borght et al., 2009; van Praag et al., 2005). In contrast, we found no evidence of an increase in vasculature in the anterior hippocampus. There are several possible reasons for this difference. Human neuroimaging and animal histology are very different measurement techniques. In imaging we must rely on the average signal from 1 mm^3 voxels, which will contain thousands of capillaries. Histological techniques allow these capillaries to be counted and the density of capillaries in an area of tissue can be determined directly. It is therefore possible that the histological technique is far more sensitive to subtle effects than the imaging technique. The disadvantage of histology is that only a small portion of a given region is sampled, whereas imaging allows the signal to be averaged across the entire region of issue. Histology also requires fixation which, depending on the precise procedure used, can cause shrinkage and dehydration, potentially distorting volume measurements (Overgaard & Meden, 2000).

A previous human study reported a significant increase in CBV specifically in the dentate gyrus region of the hippocampus after three months of regular aerobic exercise in a group of eleven healthy adults (Pereira et al., 2007). We were unable to replicate this result in our study even when our CBV analysis was restricted to the dentate gyrus region of the hippocampus. There are several differences between the present study and that of Pereira and collegues. While this study had more participants completing the exercise intervention (44 vs. 11), the intervention in Pereira et al. (2007). is twice as long (6 weeks vs. 3 months). The present study used automated calculation of hippocampal subfields whereas the subfields in Pereira et al. (2007) were manually drawn on a limited number of slices. CBV changes and correlations throughout the brain will be discussed

in chapter 4 and detailed choices that affect how CBV is calculated will be discussed section 7.5.3.

A number of rodent studies have focused on how exercise alone vs. exercise with environmental enrichment produces different structural modifications in the brain. In the hippocampus, exercise alone leads to increased production of new neurons while exercise paired with environmental enrichment leads to greater survival of new neurons (van Praag et al., 2000, 2005). Similarly, in cerebellum, exercise alone has been shown to increase capillary density while exercise paired with environmental enrichment leads to an increase in synaptic density (Black et al., 1990). It is difficult to address this dichotomy in a human study, as the daily lives of humans are constantly enriched compared to that of a rodent housed in a laboratory setting. Although this study was designed to assess the effects of cardiovascular exercise, we can not rule out the possibility that other features of the intervention, such as social interaction and experience of a novel environment, could contribute to the effects we observed.

We have shown a significant increase in backward digit span scores over time among female participants. Female participants were analysed separately as previous studies have shown that studies containing more females tend to show stronger effects, possibly due to an interaction between estrogen and aerobic exercise (see Kramer & Erickson, 2007; Erickson et al., 2007). Casual inspection of Figure 3.5 suggests a persistent effect of exercise on backward digit span. A model with explanatory variables for both immediate and persistent effects of exercise, however, was not statistically different from a simple increase in performance with time, potentially due to practice. Although we did show a cross-sectional relationship between anterior hippocampal volume and backwards digit span, we did not observe a correlation between the change in anterior hippocampus volume and the change in backward digit span score. Previous studies have shown longitudinal change in performance on a spatial memory task in older adults that correlates with change in hippocampal volume (Erickson et al., 2011). It is possible that spatial tasks are more closely linked to hippocampal volume. It is also possible that older adults have more capacity for recovering performance degraded by cognitive decline.

We have also shown that aerobic exercise is associated with a contraction of grey matter and an expansion of ventricle size that suggests a shift in the homeostatic balance of blood, CSF, and brain tissue. This volume change is not correlated with the growth in anterior hippocampal volume, suggesting they are separate processes. Ventricle volume returned to baseline after six weeks without exercise but showed no correlation with time since last exercise session, suggesting it cannot be explained by acute dehydration but is rather a more persistent change in homeostatic balance. Changes in ventricle size have not previously been reported in the exercise literature, however it is unlikely they have been directly examined. Future studies should bear this effect in mind as it may confound experiments targeted at measuring focal changes in neural tissues. Additional studies are also needed to understand the functional role of this shift CSF and brain volume.

In response to the recent critical reviews of longitudinal neuroimaging approaches (Bernal-Rusiel et al., 2013a; Thomas & Baker, 2012; Thomas et al., 2009), all longitudinal analyses in this study have used unbiased longitudinal averaging techniques and well established Linear Mixed Effects models for statistical inference. These approaches remove the possibility of spurious results due to biased alignments, properly model both between and within subject sources of variance, and always control for potential time-related confounds such as scanner drift and practice.

In conclusion, this study has provided important insight into the time course and mechanism of exercise-mediated plasticity in the anterior hippocampus, but further work is needed. Animal studies are needed to determine if proposed changes in hippocampal myelination with physical exercise can be confirmed with histological techniques. Future imaging studies might employ higher resolution imaging of the hippocampus to explore the laminar specificity of changes in volume and myelination. Finally, additional analyses are needed to determine the biochemical mechanism by which increased aerobic exercise triggers structural expansion in specific brain regions such as the hippocampus.

Chapter 4

Cerebral blood volume correlates with fitness and working memory

4.1 Abstract

In this chapter I will explore the relationship between CBV, aerobic fitness, and cognition. Our data show that greater CBV in grey matter is correlated with greater performance on a working memory task. Grey matter CBV is also correlated with fitness throughout the brain. This relationship with fitness is stronger than the relationship with age in middle adulthood (18-59 years), suggesting that physical activity may play an important role in mitigating age related changes in brain vasculature. Contrary to many histological studies conducted in animals, we did not observe focal increases in CBV associated with a six-week aerobic exercise intervention. Rather, we report a diffuse decrease in measured CBV throughout the brain. Correlations with changes in ventricle volume suggest this decrease may reflect a decrease in hydration. Implications of these results are discussed.

4.2 Introduction

Increased aerobic fitness is associated with improved cognitive function, particularly measures of working memory and executive function (Kramer & Erickson, 2007; Aberg et al., 2009; Hillman et al., 2008). However, the mechanisms of this relationship are poorly understood. Changes in brain vasculature provides one attractive hypothesis. The cardiovascular system provides for the delivery of all of the energy necessary for brain function as well as the removal of metabolic waste via the CSF (Dwyer, 2002). It has long been known that the circulatory system is subject to change in the face of age, exercise, and perhaps enriched environment or learning (Diamond et al., 1964). The relationship between vascular plasticity and neural function, however, remains poorly understood (Thomas et al., 2012; Markham & Greenough, 2004; Zhao et al., 2008). Two related but largely separate bodies of literature have developed around how vasculature changes in the brain in response to experience. The first is focused on changes throughout the cortex and especially in motor areas. The second is specifically concerned with the tightly coupled relationship between angiogenesis and neurogenesis in what is known as the "vascular niche" of the Subgranular Zone (SGZ) in the dentate gyrus and the Subventricular Zone (SVZ) of the lateral ventricles (Zhao et al., 2008).

The first body of literature has largely focused on the motor cortex and cerebellum in rats (Black et al., 1990; Isaacs et al., 1992; Kleim et al., 2002), though there are studies that have looked at visual cortex (Sirevaag et al., 1988), striatum (Ding et al., 2006), and also primate motor cortex (Rhyu et al., 2010). Much of this work has focused on separating the effect of simple aerobic exercise from that of learning or environmental enrichment. The general consensus from this work is that while exercise alone induces angiogenesis, learning induces both angiogenesis and neural plasticity. Several of these studies have also concluded that the angiogenic effects of exercise are relatively short-lived, returning to baseline if increased physical activity doesn't continue. In contrast, neural plasticity appears to persist well beyond the exercise period (Kleim et al., 1997).

The second body of literature has also explored the difference between exercise alone compared to exercise paired with environmental enrichment (Kempermann et al., 2010; van Praag et al., 1999a,b). In these studies, it has been shown that both the creation of new neurons and new vasculature is enhanced by aerobic exercise; however, without novel experience, the majority of the new neurons are destined to die off. It is only with environmental enrichment that these new neurons survive and are incorporated into the circuitry of the hippocampus. The up-regulation of vasculature has also been shown to quickly fall back to baseline when exercise is discontinued (Van der Borght et al., 2009). So in both bodies of literature, angiogenesis plays the role of a metaphorical "scaffolding" that temporarily provides enhanced energy and nutrients during the process of neural plasticity.

As most of these studies have employed histological techniques, it has not been practical to conduct whole brain analyses. Therefore, it remains unclear to what degree exercise-mediated angiogenesis is localized to motor and limbic structures or whether it is a whole brain effect. The role of CBV on cognitive measures, such as working memory and executive function, has also not been examined. Finally, although the relationship between whole brain CBV and age has been examined (Leenders et al., 1990; Wenz et al., 1996; Small, 2004), these studies have not explored how fitness interacts with the effects of ageing on brain vasculature.

This study aims to fill these gaps in the literature by looking at the relationship between fitness, age, working memory, and CBV across the entire brain using both cross-sectional and longitudinal analyses. Rather than focusing on older participants (as many studies have), this experiment focuses on middle age, including a broad range of ages (18-59) incorporating the entirety of middle adulthood. Using this approach we show correlations between whole brain, grey matter CBV, and working memory as well as fitness. We show that fitness is a better predictor of grey matter CBV than age. We also show that the effects of exercise are distributed throughout the brain and are not obviously focused in motor or limbic areas.

4.3 Methods

4.3.1 Participants and procedures

A total of 134 of the 151 MRI scans discussed in chapter 3 include the administration of a contrast agent and the calculation of regional CBV. These scans were conducted on 56 different participants (33 women, mean age 32.1, S.D. 10.8). All subjects were right-handed, with no history of psychiatric or neurological disease. Informed written consent was obtained from all subjects in accordance with ethical approval from the Central Office for Research Ethics Committees. Using a standard crossover design, the participants were pseudo-randomly assigned to one of two groups: "rest first" or "exercise first" as discussed in chapter 3.

Among the participants who received the contrast injection, 25 were assigned to the exercise-first condition with one completing only the first two scans (pre- and post-training). 22 participants were assigned to the rest-first condition with eight completing only the first two scans (pre- and post-rest). A total of 36 participants receiving the contrast injection completed the exercise intervention across both groups. Nine participants were recruited for baseline assessment and a single scan with contrast agent. These data were only used in cross sectional analyses.

4.3.2 Behavioural and Physiological Measures

Full details of all behavioural and physiological measures are provided in sections 2.3 and 2.2. Briefly, a battery of behavioural tests was administered to each participant at each time point. Of interest for the results presented in this chapter, the battery included a computerized, verbal, backward digit span test administered in a stepwise fashion by computer (Woods et al., 2010). Details of this test are discussed in section 2.3.3. Physiological tests included a standard $\dot{V}O_2$ max test administered on a stationary exercise bike. Ventilatory Oxygen consumption ($\dot{V}O_2$) was measured while the resistance on the bike was increased every two minutes. Total Time to Exhaustion (TTE) was also measured.

4.3.3 Imaging methods

Each MRI scanning session was conducted on 3T Siemens Verio scanner (Erlangen, Germany). As discussed in section 2.3, a battery of different imaging sequences were collected – only two of which are relevant for this chapter. A multi-echo MPRAGE sequence (1 x 1 x 1 mm, TR = 2530 ms, TI = 1200 ms, TE = 1.69, 3.55, 5.41 and 7.27 ms, matrix size = 256 x 256 x 176, and GRAPPA factor = 2) was used for anatomical analysis and segmentation (van der Kouwe et al., 2008). Segmentation of cortical and subcortical regions of interest were conducted using FreeSurfer version 5.2 (Fischl et al., 2004, 2002). Hippocampal subfields were segmented using a toolbox available for FreeSurfer that applies Bayesian prior probability maps to the hippocampus constructed from manually labeled high resolution in vivo scans (Van Leemput et al., 2009). Segmentation of grey matter was conducted using FAST (Zhang et al., 2001; Smith et al., 2004).

CBV was measured using the "static" method in order to maximize spatial resolution and to maintain comparability to previous studies investigating exercise and angiogenesis (Pereira et al., 2007; Lin et al., 1997, 1999; Small, 2004). At the end of each scanning session, an ME-MPRAGE scan was collected with the parameters discussed above. The participant then received an injection of contrast agent (Dotorem, 0.1 mg per kg) via a previously inserted venous catheter in the arm. A second ME-MPRAGE scan was then conducted with identical parameters. The pre- and post-contrast scans were aligned in post processing and subtracted. A ROI containing only blood was automatically identified by selecting the 1000 brightest voxels on the post contrast agent scan within the sagittal sinus near the center of the crux of the cerebellum. The mean difference between the post-contrast and pre-contrast signal intensity inside this region was used to normalize the subtracted image:

$$rCBV = \frac{Brain_{post} - Brain_{Pre}}{\overline{Bloodmask_{post}} - \overline{Bloodmask_{pre}}}$$

Grey matter masks were determined by segmenting the structural images in native

space using FAST (Zhang et al., 2001). CBV values for each voxel within the mask were averaged. Voxelwise analyses were conducted by spatially normalizing the CBV images into standard MNI space and applying a Gaussian smoothing kernel ($\sigma = 3$). Statistical inference was performed non-parametrically using randomise and Threshold-Free Cluster Enhancement (TFCE) to correct for multiple comparisons (Nichols & Holmes, 2002; Hayasaka et al., 2004; Smith & Nichols, 2009).

4.4 Results

To validate the accuracy of our CBV measure we calculated the average CBV within the 53 different grey matter regions segmented by Freesurfer (including 8 hippocampal subfields) across all 56 participants at baseline (Figure 4.1). The relative values of CBV in each region are similar but tend to be slightly higher than those reported by Kuppusamy et al. (1996). This may be due to partial voluming along the edges of the Freesurfer segmentations. Twenty-two participants in the rest-first condition underwent two separate CBV scans with a six-week interval between and no intervention. Using these two scans we calculated a mean coefficient of variation ($C.V. = \frac{StdDev}{Mean}$) of CBV within grey matter of 6.1% (Figure 4.2).

Using an ordinary least squares regression we constructed a model including sex, age, and fitness as independent variables and mean grey matter CBV as the dependent variable. The model explained a significant amount of the variance in CBV (R^2=0.35, P<0.0001). Sex was not found to be a significant predictor of total grey matter CBV (P=0.67). As has been previously reported (Wenz et al., 1996; Leenders et al., 1990), CBV in grey matter showed a negative relationship with age, but only at a trend level in our data (P=0.055). In our middle-aged group, the strongest predictor of whole grey matter CBV was fitness as measured by TTE (P=0.001, Figure 4.3).

Running a voxelwise regression on CBV maps, including regressors of age, sex and fitness in the model, revealed significant clusters of correlation with sex and fitness, but none for age. Clusters showing a positive correlation between CBV and fitness were found

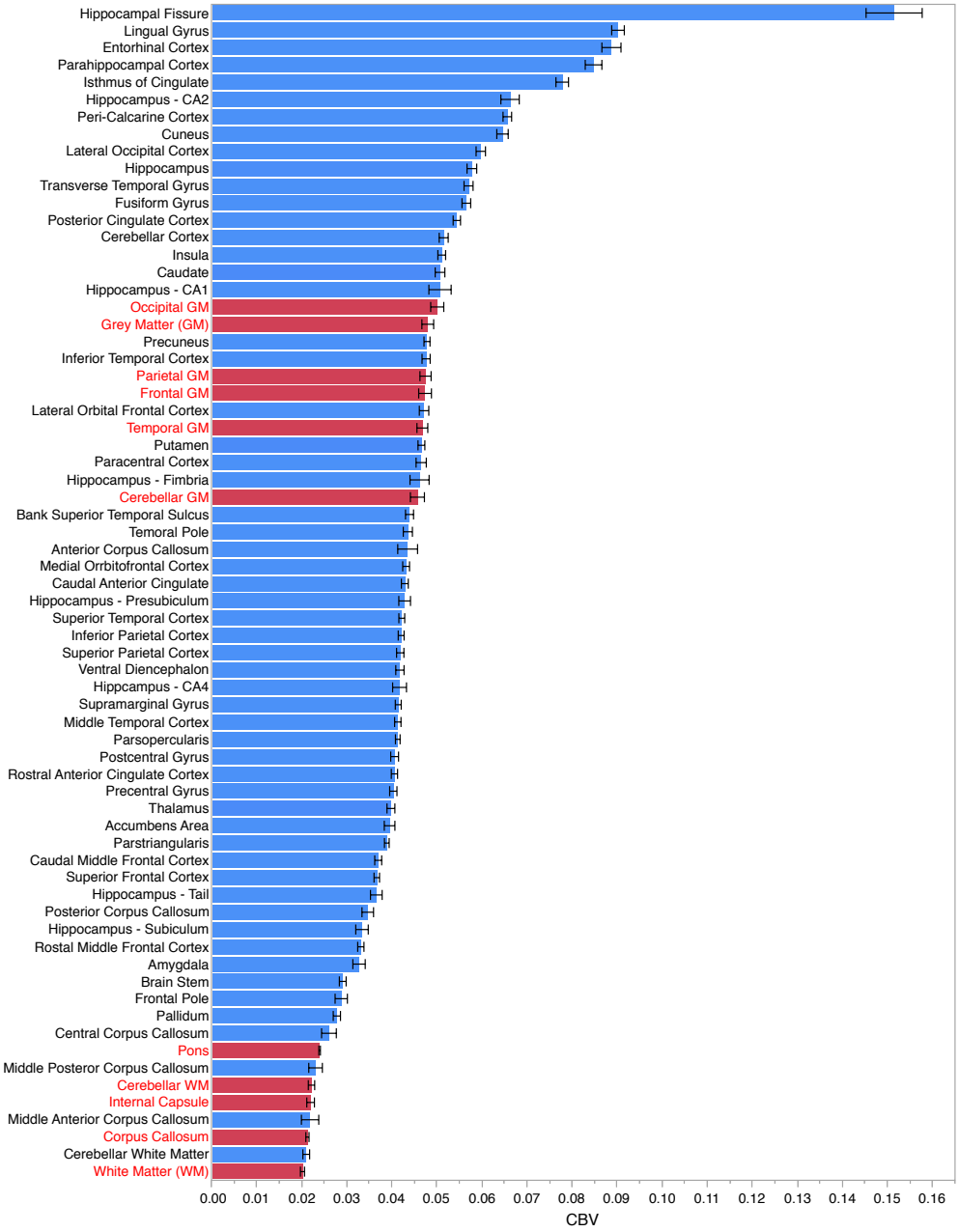

Figure 4.1: The mean CBV of each anatomical region of interest within grey matter (as segmented by Freesurfer) across all 56 subjects at baseline (blue bars). CBV values for eleven regions reported in (Kuppusamy et al., 1996) are also included for comparison (red bars).

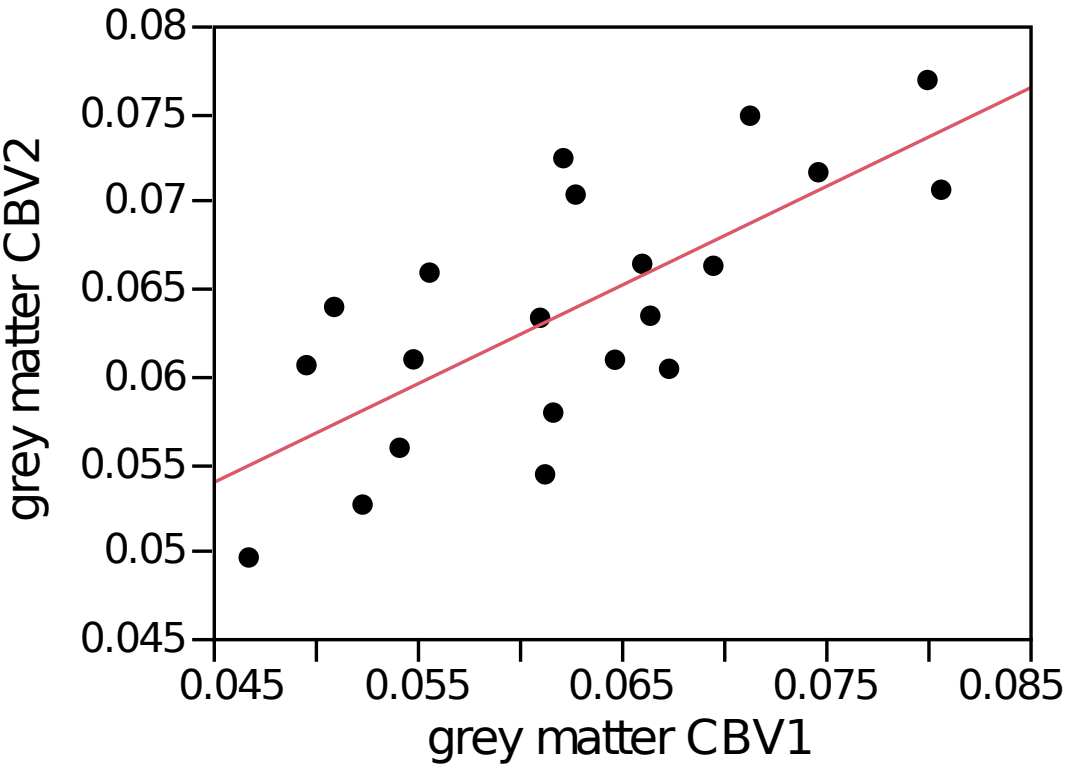

Figure 4.2: The mean grey matter CBV of the first scan correlated well with that of the second scan for those participants in the "rest first" group who had two CBV scans at a six week interval with no intervention (21 participants, one outlier removed, based on Grubb's test, P< 0.05). R=0.77 and the average coefficient of variation was 6.1%.

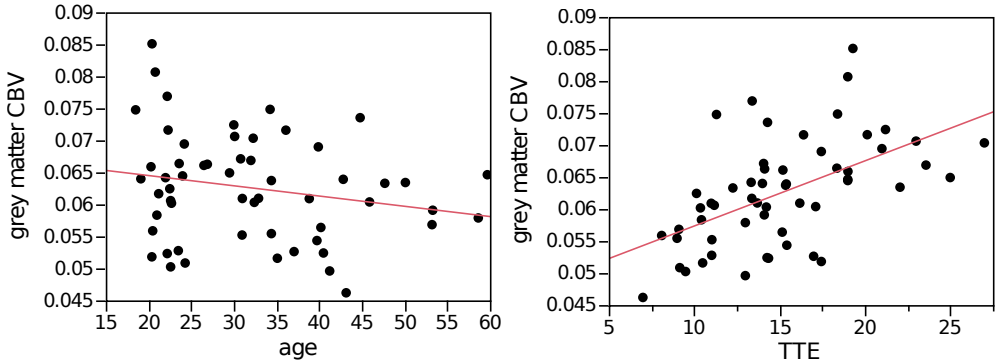

Figure 4.3: Raw correlation between age and grey matter CBV (left), and fitness (TTE) and grey matter CBV (right). While age show a weak negative trend, fitness shows a strong positive correlation.

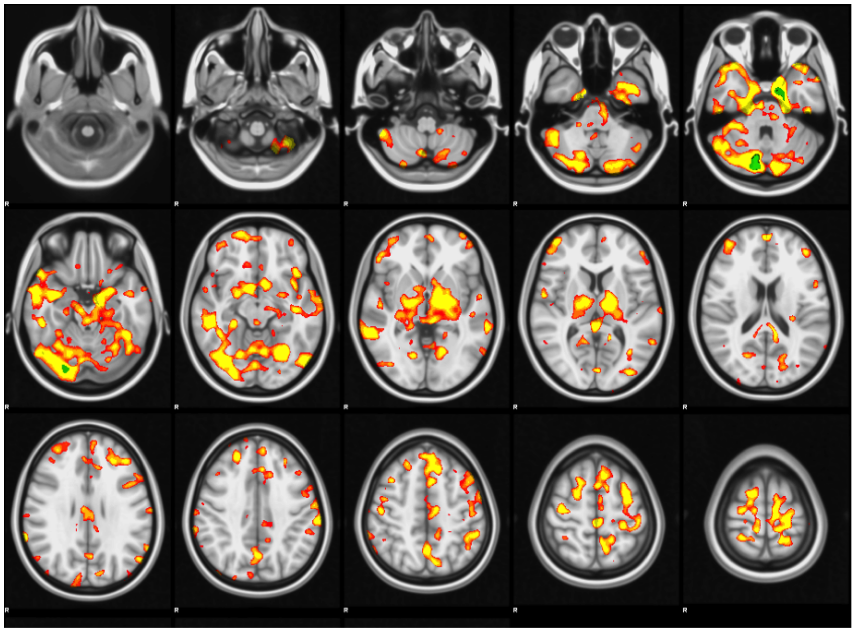

Figure 4.4: Voxelwise positive correlation between CBV and fitness (TTE). ($p<0.05$ TFCE corrected in green, $p<0.01$ uncorrected in yellow-red).

in right cerebellum and left parahippocampal gyrus. Lowering the threshold to $p=0.05$ (uncorrected) revealed that the positive correlation existed at lower levels throughout grey matter (Figure 4.4). Surprisingly, no significant clusters were found showing a greater CBV for males compared to females. Rather, several clusters were found showing a greater CBV for females compared to males, in bilateral thalamus, cerebellum, and brainstem areas (Figure 4.5).

We next asked if grey matter CBV impacted cognitive ability. We ran a linear regression between grey matter CBV at baseline and participants' score on a backward digit span task. This regression showed a significant positive correlation ($R=0.39$, $P=0.0028$, Figure 4.6) suggesting that greater grey matter CBV is associated with improved working memory and executive function. This correlation remained significant when age and sex were included as covariates ($P=0.0138$).

To test whether grey matter CBV changed with the six-week aerobic exercise intervention, we first plotted the mean-normalized grey matter CBV for each group across

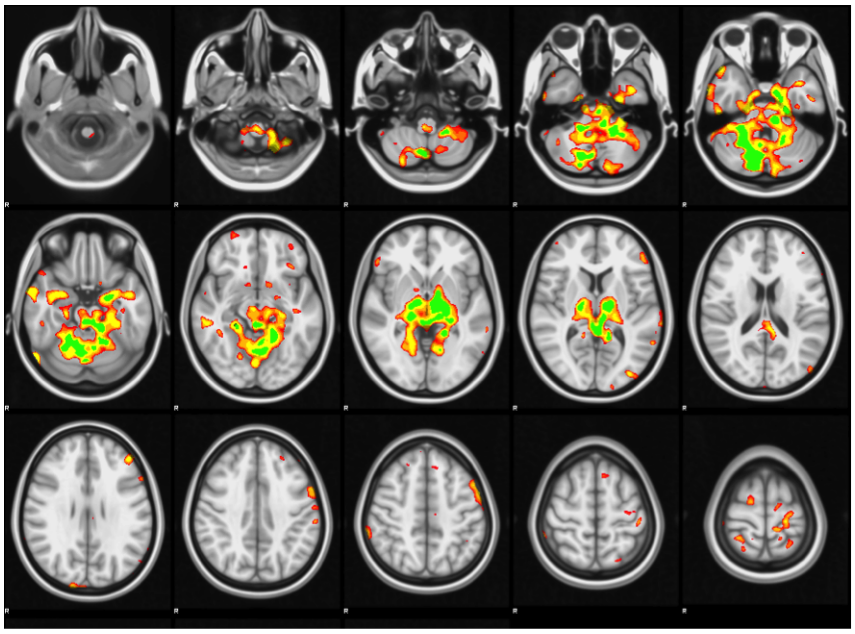

Figure 4.5: Voxelwise test showing areas of significantly higher CBV in females compared to males. ($p<0.05$, TFCE corrected in green, $p<0.01$ uncorrected in yellow-red).

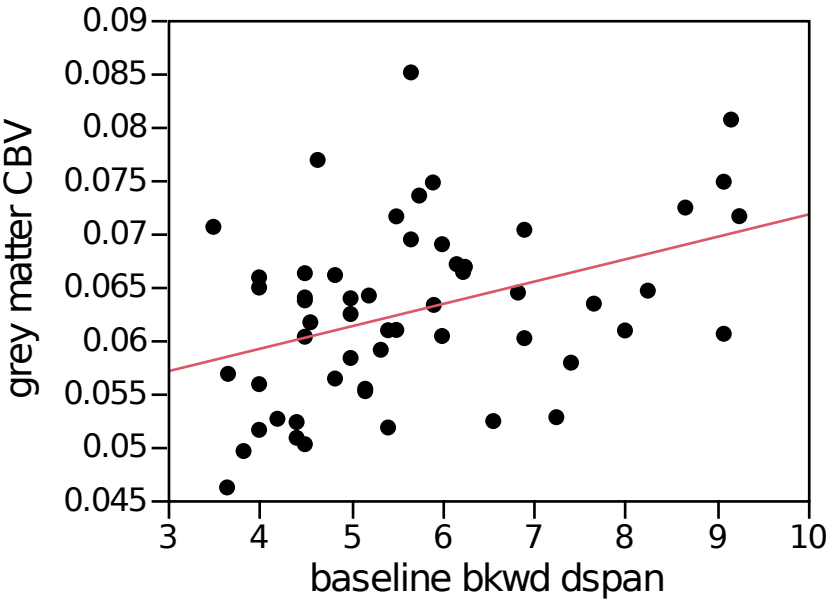

Figure 4.6: Grey matter CBV showed a significant correlation with backward digit span (R=0.39, P=0.0029).

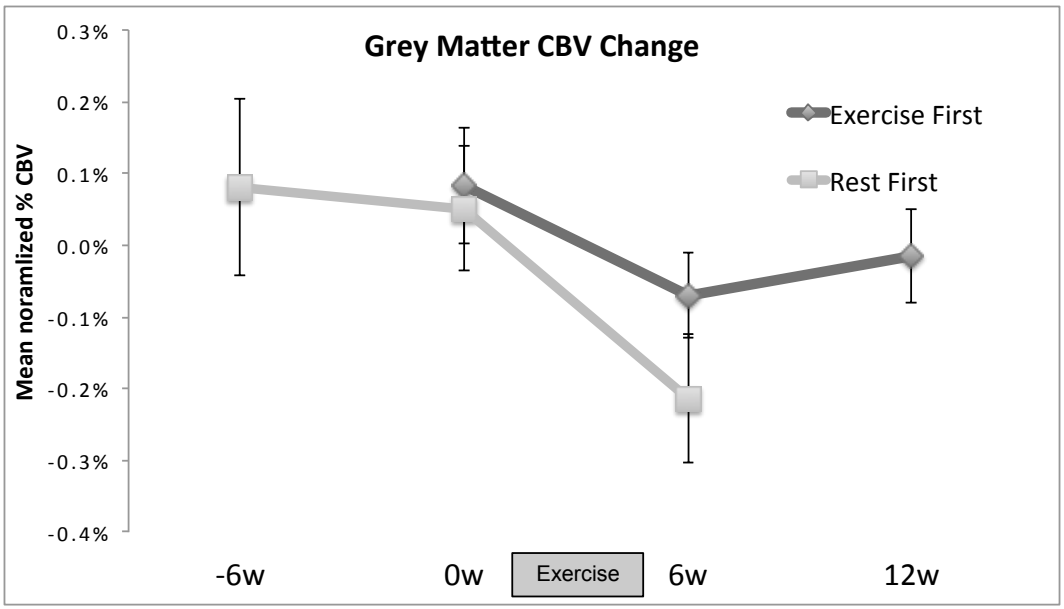

Figure 4.7: Change in grey matter CBV across time and group. Aerobic exercise did not provide a significantly better fit than time alone.

each condition (Figure 4.7). Visual inspection of this plot suggested that rather than increasing grey matter CBV, aerobic exercise in fact resulted in a decrease in CBV. In order to explore this change statistically, we employed the same longitudinal linear mixed effects approach used in chapter 3. We constructed a model including subject ID, visit number (1-3), and a binary variable indicating whether the participant had just completed the six weeks of aerobic exercise training (postEx, 0 or 1). This model did not provide a significantly better fit than subject ID and visit number (time) alone (Log Likelihood Ratio=2.55, P=0.11).

4.5 Discussion

In this study, we have provided the first evidence that physical fitness correlates with grey matter CBV and that higher grey matter CBV is associated with greater working memory, as measured using the backwards digit span test. In our sample of participants between the ages of 18 and 59, fitness was a much stronger predictor of CBV than age. It has long been known that greater fitness is associated with reduction in age related

cognitive decline and dementia (Kramer & Erickson, 2007; Rovio et al., 2005). It has also been shown that higher levels of physical activity at younger ages is associated with better cognitive outcomes later in life (Podewils et al., 2005; Schuit et al., 2001; Yaffe et al., 2001) These results suggest one potential mechanism for these findings.

Previous studies have shown that CBV also decreases with age (Leenders et al., 1990; Wenz et al., 1996). In the greater population, physical activity levels and fitness level tend to decrease with age (Jackson et al., 2009). In this study, we have demonstrated that decreases in fitness may play a larger role in decreased CBV than ageing itself for the 18-59 age range.

As the cardiovascular system is the mechanism by which oxygen and glucose are delivered to the brain, as well as how metabolic waste is removed (via the CSF), the size and extent of the capillary bed within the grey matter provide attractive candidates for the primary mechanisms for delaying the brain atrophy and cognitive decline associated with ageing. The mechanism by which heightened physical activity results in angiogenesis is outside the scope of this work, but has been extensively studied in muscle tissues (Bloor, 2005; Prior et al., 2004).

Correlations of CBV with fitness were widely distributed throughout the brain with significant clusters found in cerebellum and para-hippocampal areas. We interpret these maps to suggest that the effect of fitness on CBV occurs throughout the brain, but more so in limbic and motor areas. Longitudinally, we did not find focal changes in CBV after a six-week exercise intervention, as other studies have reported in both animals and humans in hippocampus and motor cortex (Pereira et al., 2007; Swain et al., 2003). In contrast, we showed a global decrease in grey matter CBV after exercise. The degree of CBV decrease correlated with the increase in ventricle size observed with exercise. As discussed in chapter 3, we believe the most likely explanation for the increase in ventricle size is change in the homeostatic balance between blood, CSF, and brain within the cerebral cavity. The fact that CBV decreased with the grey matter contraction suggests an acute increase in the amount of CSF within the skull immediately following

the exercise training program. The functional role of this CSF increase demands further study, however, several recent studies have suggested that CSF flow has a more important role in brain metabolism and function that previously supposed (Iliff et al., 2012; Lehtinen et al., 2011; Xie et al., 2013).

Another study of CBV change with exercise reported a focal increase of CBV in the Dentate Gyrus (DG) of the hippocampus (Pereira et al., 2007). In our study, none of the nine hippocampal subfields (as segmented by Freesurfer) showed an increase in CBV with exercise. There are several possible explanations for this discrepancy. In Pereira et al. (2007), subjects participated in 12 weeks of exercise, four times per week, and 40 minutes per session. The subjects in the present study participated in 6 weeks of exercise, five times per week, and 30 minutes per session. It is possible a longer period of aerobic activity is required to observe the CBV effects in the dentate gyrus. The hippocampal subfield regions in Pereira et al. (2007) were manually drawn on coronal slices with 0.86 mm x 0.86 mm resolution in plane and 4 mm thickness. The ROIs were also limited to a subset of slices in which the subfields could be clearly determined. In the present study the subfield ROIs were automatically generated on 1 mm^3 isotropic voxels, and covered the length of the hippocampus. Pereira et al. (2007) do not report changes in ventricle size or grey matter volume. However, if there were an expansion of the hippocampal fissure that encroached into the dentate gyrus ROI, it could erroneously be interpreted as an increase in CBV as the hippocampal fissure is filled with CSF and vasculature. Freesurfer generates a separate segmentation for the hippocampal fissure, and in our data this had an average CBV value that was considerably higher than the DG/CA4 region (15.1% vs. 4.0% at baseline).

In summary, these results provide strong support that, in middle-aged adults, higher levels of physical fitness are associated with greater cerebral blood volume throughout the brain. Greater CBV is also associated with better working memory performance regardless of age. Many studies have demonstrated the benefits of physical activity during development and in the face of age-related cognitive decline. This study provides one of the few demonstrations that fitness is beneficial throughout the life span. Further

research is necessary to explore the possibility that increased vascular volume has a primary, causal role in preventing cortical atrophy and cognitive decline.

Chapter 5

Age associated iron deposition in basal ganglia increases with physical fitness

5.1 Abstract

It is well known that the amount of iron in several basal ganglia structures increases with age and is a feature of neurodegenerative disease. The significance of this iron accumulation is not well understood. Using susceptibility weighted MRI scans, I estimated brain iron content on 56 participants between the ages of 18 and 59. The data show a linear increase in magnetic susceptibility with increasing age in the basal ganglia, with the strongest correlation in the putamen. We also show that putamen susceptibility is positively correlated with fitness level. This correlation is not explained by differences in vasculature as measured by cerebral blood volume (CBV). We also found a robust regional sex difference in estimates of iron content. Males showed higher iron estimates in superior cortical grey and white matter while females showed higher iron in cerebellum and subcortical structures including hippocampus. Unlike reported associations in older adults, no correlations were found between iron estimates and several measures of

cognitive function in our sample.

5.2 Introduction

Iron is essential for normal brain function and myelin formation but has also been associated with oxidative damage to neural tissue, particularly in the ageing brain (Moos et al., 2007; Moos & Morgan, 2004; Connor & Menzies, 1996). Little to no iron is found in the brain before birth and its accumulation is an asymptotic process, increasing sharply in the first two decades of life as part of the myelination process (Connor & Menzies, 1996; Guizzetti, 1915). Classic histological studies demonstrated that iron levels near their peak in the 5th or 6th decade of life in putamen and even earlier in other regions of the brain (Hallgren & Sourander, 1958; Guizzetti, 1915; Koeppen, 1995).

The advent of MRI has allowed measurement of this iron accumulation *in vivo* using sequences designed to measure magnetic susceptibility such as SWI and T2*-weighted gradient echo sequences (Haacke et al., 2005; Haacke & Ye, 2012). Iron exists in several different molecules within the brain, but ferritin (and to a lesser extent, hemosiderin) are the only forms of non-haemoglobin iron present in the brain in quantities sufficient to alter MRI signal (Schenck, 2003). Nonetheless, MRI techniques have been used to replicate the finding of an increase in iron accumulation with age suggesting MRI technique are also measuring a change in ferritin (Thomas et al., 1993; Drayer et al., 1986).

Whether the accumulation of iron in the brain has cognitive implications is still unclear. Clinical studies have detected an increase in iron in neurodegenerative diseases such as Alzheimer's, Parkinson's and Huntington's Disease, while other studies have suggested that the magnitude of iron accumulation is associated with an impairment in cognitive ability and may play a causal role in cognitive decline (Haacke et al., 2005; Bartzokis et al., 2007; Schröder et al., 2013).

An early study by Pujol et al. (1992) reported a correlation between T2 signal intensity in globus pallidus and measures of dual tasking and word learning in 25 healthy adults between the ages of 65 and 76. Sullivan et al. (2009) reported a correlation

between iron estimates in putamen and caudate with scores on the mini-mental health state exam in a group of 10 healthy, elderly participants. In a large cohort of 113 healthy adults (age 19-83 years), Rodrigue et al. (2013) report that age-related differences in memory performance can be partially explained by differences in hippocampal volume, and that these volume changes can in turn be explained by differences in hippocampal iron concentration. Additional animal studies suggesting a relationship between iron and cognitive performance are reviewed in Schröder et al. (2013). Bartzokis et al. (2007) reported that women have less iron content (measured by Field-Dependent R2 Increases (FDRI)), suggesting that this may account for the observation that males are more likely to develop early onset Alzheimer's and Parkinson's disease. Another variable that has been shown to modulate risk of age-related cognitive decline and neurodegenerative disease is physical fitness (Kramer & Erickson, 2007; Rovio et al., 2005). However, the relationship between iron levels, fitness, and age has not been examined directly.

Although iron accumulation in later life is well described, there is little available whole brain data on the time course of iron accumulation during young to middle adulthood. In this study, we aim to characterize age-related iron accumulation in a group of healthy adults between 18 and 59 years of age. We also explore the relationship between susceptibility, fitness, cerebral blood volume, and several measures of cognitive function. Rather that the commonly-used region of interest approach, all of the analyses in this study are conducted on voxelwise basis across the entire brain while using cerebral blood volume (measured using a contrast agent injection) as a voxelwise confound. This method allows us to measure susceptibility due to non-heme iron separately from the iron found in the vasculature.

5.3 Methods

5.3.1 Participants and procedures

Full details regarding the participants can be found in chapter 3. The analyses presented in this chapter are restricted to the 56 participants who received a gadolinium

injection at baseline, as cerebral blood volume (CBV) has proven to be an important confound in measuring brain susceptibility. These participants (33 women, mean age 32.1, S.D. 10.8) were all right-handed, with no history of psychiatric or neurological disease. Informed written consent was obtained from all subjects in accordance with ethical approval from the Central Office for Research Ethics Committees. Although these participants were assigned to different groups and received interventions at different stages, only cross-sectional analyses will be presented in this chapter, using baseline scans acquired before any interventions were administered.

5.3.2 Behavioural and fitness assessment

Full details of all behavioural and physiological measures are provided in sections 2.3 and 2.2. Briefly, a battery of behavioural tests was administered to each participant including forward and backward digit span, the Rey-Osterrieth Complex Figure Drawing task (ROCF) task, semantic and verbal fluency, Rey Verbal Learning Test (RVLT), and the CES depression index. Physiological tests included a standard ($\dot{V}O_2$ max test administered on a stationary exercise bike. Ventilatory oxygen consumption ($\dot{V}O_2$) was measured while the resistance on the bike was increased every two minutes. Total Time to Exhaustion (TTE) was also measured. These procedures are described in full in section 2.3.

5.3.3 Imaging methods

Each MRI scanning session was conducted on 3T Siemens Verio scanner (Erlangen, Germany). As discussed in section 2.4, a battery of different imaging sequences were collected – only three of which are relevant for this chapter. A multi-echo MPRAGE sequence (1 x 1 x 1 mm, TR = 2530 ms, TI = 1200 ms, TE = 1.69, 3.55, 5.41 and 7.27 ms, matrix size = 256 x 256 x 176, and GRAPPA factor = 2) was used for alignment and registration to standard space (van der Kouwe et al., 2008). CBV was measures using the "static" method discussed in chapter 4. Susceptibility phase and magnitude images were collected using a standard multiecho SWI sequence distributed by Siemens with 1.3

mm isotropic voxels, TE = 6.72 ms & 24.60 ms, TR = 30 ms, matrix size = 192 x 192, and GRAPPA factor = 2. Susceptibility weighted images were calculated on the scanner console using a published method (Haacke et al., 2004). All of the analyses presented here were conducted on the first echo (6.72 ms).

Note that on a susceptibility-weighted scan, greater magnetic susceptibility results in less signal intensity in the image. For the purposes of clarity, we will always use the term "susceptibility" to refer to the inverse of the signal intensity in the susceptibility-weighted scans. Thus, when we refer to a positive correlation between age and susceptibility, this is equivalent to a negative correlation between age and signal intensity on the susceptibility-weighted scan.

5.3.4 Post processing, registration, and statistical methods

ME-MPRAGE images were non-linearly registered to MNI152 standard space using the FSL tools FMRIB's Linear image Registration Tool (FLIRT) and FNIRT (Smith et al., 2004; Jenkinson et al., 2002b). The magnitude image of the SWI sequence was linearly aligned to the corresponding ME-MPRAGE image. These registrations were then concatenated and applied to the SWI images with spline interpolation to transform them into standard MNI152 space. A Gaussian smoothing kernel ($\sigma = 2$) was applied to both SWI and CBV images. Statistical inference was conducted using permutation based techniques implemented in the FSL program randomise (Nichols et al., 2008; Nichols & Holmes, 2002; Hayasaka et al., 2004). All of the maps presented in this chapter were obtained from a single non-parametric regression with voxelwise SWI signal intensity as the dependent variable, that included age, sex, and TTE as explanatory variables (with each variable having one entry per subject), plus CBV as a voxelwise explanatory variable (with one CBV entry per voxel per subject). Additional regressions were performed, including individual behavioural measures in addition to the four explanatory variables above. We avoided selecting an arbitrary threshold for cluster formation by utilizing Threshold Free Cluster Enhancement (TFCE) for all inferences (Smith & Nichols, 2009).

5.4 Results

5.4.1 Susceptibility correlation with age

Whole brain, voxelwise regression revealed clusters of significant positive correlation between susceptibility and age bilaterally in the putamen and in a region on the ventromedial edge of the right pallidum ($P<0.05$, correct for multiple comparisons using TFCE, Figure 5.1). No clusters of negative correlation with age cleared the corrected threshold.

5.4.2 Susceptibility correlation with CBV

Whole brain, voxelwise regression revealed large expanses of significant positive correlation between voxelwise CBV and voxelwise susceptibility (Figure 5.2). These clusters tended to be focused in regions containing large amounts of blood such as the superior and inferior sagittal sinus, the transverse sinus superior to the cerebellum, and the subarachnoid space along the surface of the cortex. No significant clusters of negative correlation with CBV were found.

5.4.3 Susceptibility correlation with fitness

Whole brain, voxelwise regression revealed two clusters of significant positive correlation between fitness and voxelwise susceptibility in the right putamen and medial frontal cortex (Figure 5.3, $P<0.05$, TFCE corrected). Lowering the threshold to $P < 0.01$ (uncorrected) revealed the bilateral putamen clusters and a large region of positive correlation primarily in frontal white and grey matter with the largest and most significant clusters found on the right side.

5.4.4 Susceptibility correlation with cognitive measures

Whole brain, voxelwise correlations were conducted on seven different cognitive measures while also including age, sex, TTE, and CBV as confounds. Cognitive measures included forward and backward digit span, complex figure recall, semantic and verbal

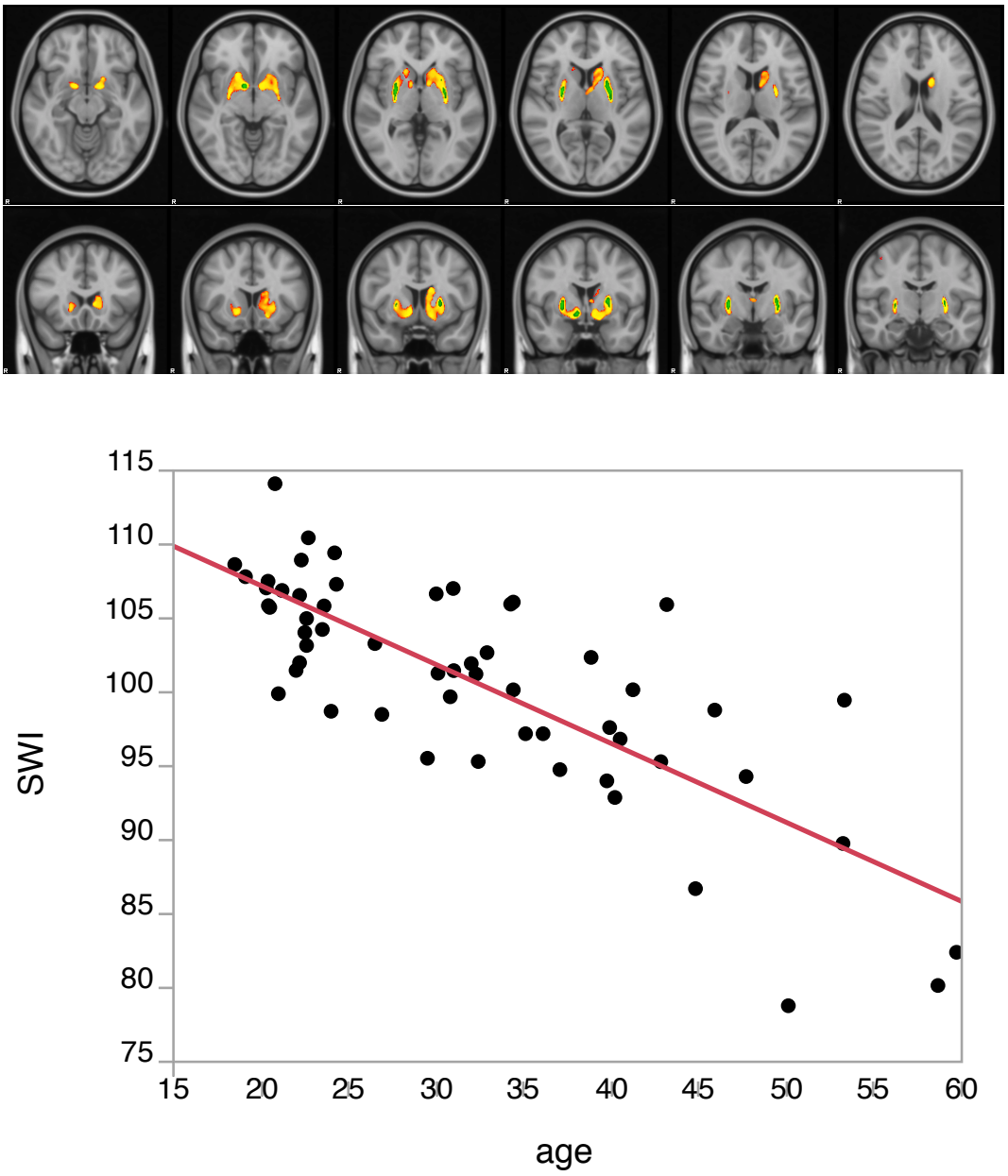

Figure 5.1: Top: Green clusters show regions of positive correlation between age and susceptibility (P<0.05, TFCE corrected). Yellow shows sub-threshold regions of positive correlation (P<0.01, uncorrected). Bottom: Scatter plot shows susceptibility values for the green regions vs. age, to visualize the distribution of values.

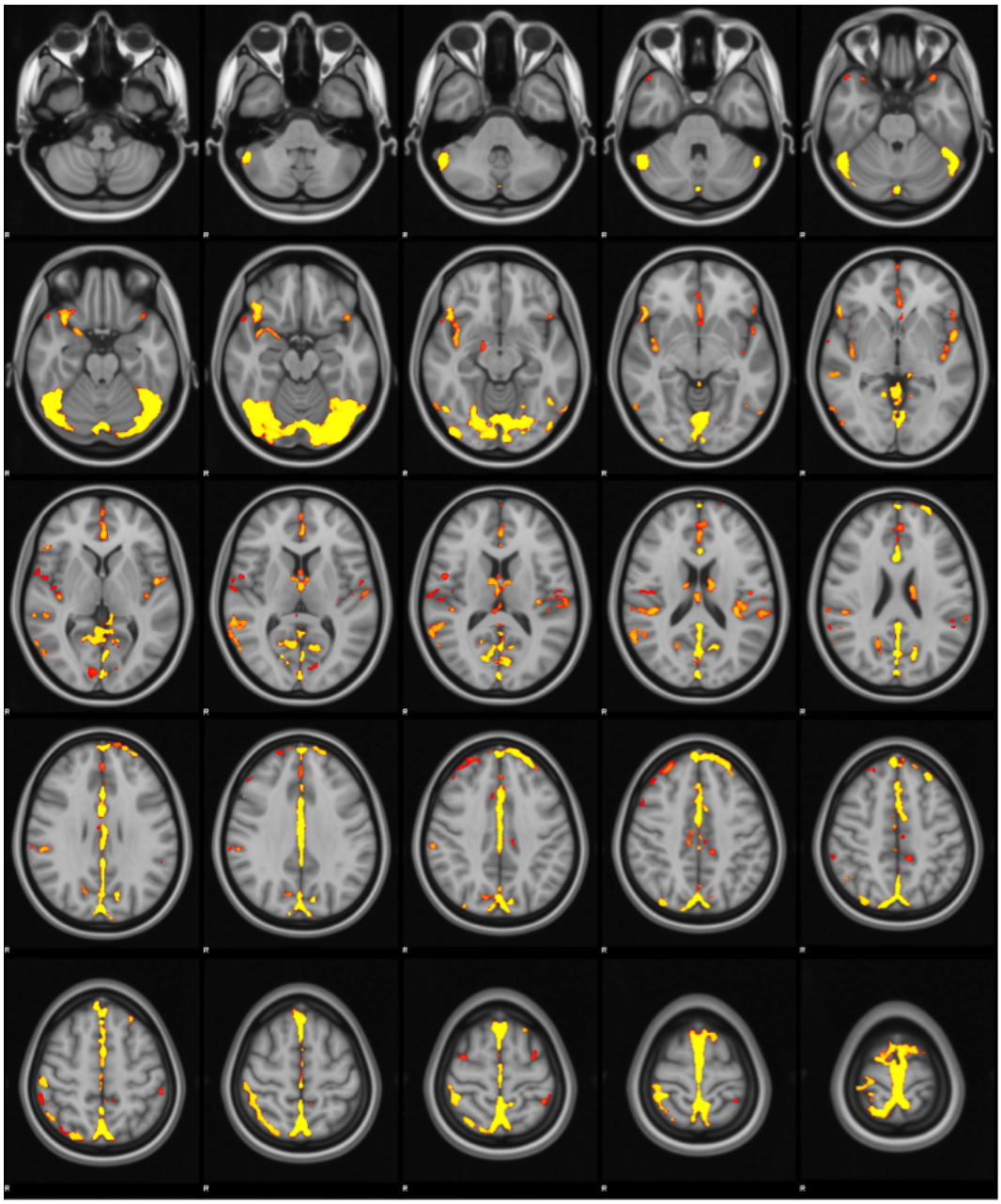

Figure 5.2: Yellow clusters show regions of positive correlation between CBV and susceptibility (P<0.05, TFCE corrected).

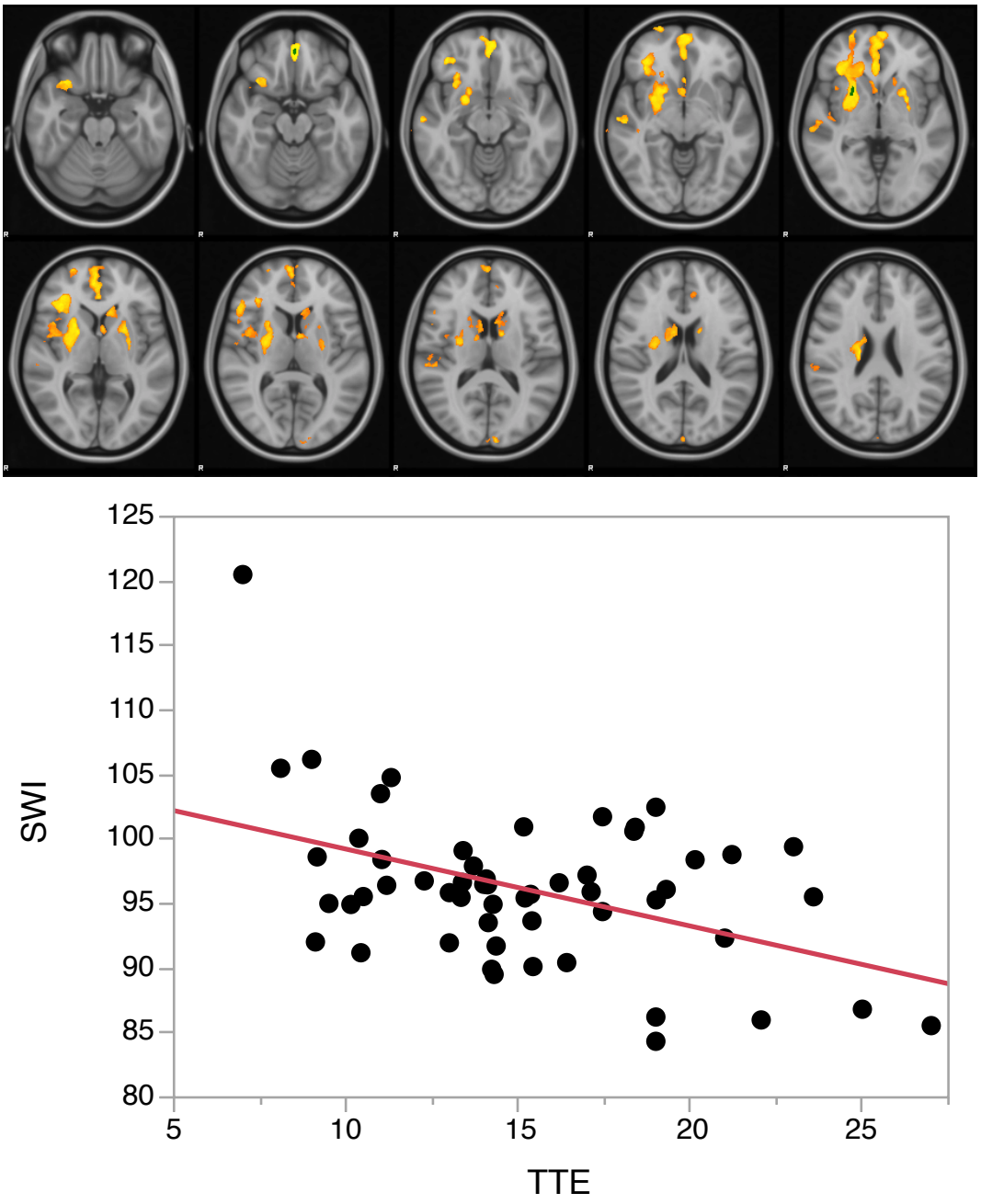

Figure 5.3: Top:Two green clusters in the right putamen and medial frontal cortex show regions of positive correlation between fitness and susceptibility ($P<0.05$, TFCE corrected). Yellow shows sub-threshold regions of positive correlation ($P<0.01$, uncorrected). Bottom: Scatter plot shows susceptibility values for the green regions vs. TTE, to visualize the distribution of values.

fluency, verbal learning, and depression index. None of these measures revealed regions of significant correlation when corrected for multiple comparisons across the whole brain. As the putamen was found to show maximal differences with respect to age and fitness, we also ran a regression with the mean susceptibility value in the putamen as the dependent variable and also found no significant correlations.

5.4.5 Susceptibility difference with sex

Whole brain, voxelwise regression revealed large regions of significant differences based on sex. Females tended to show higher susceptibility in inferior subcortical regions such as cerebellum, brain stem, and hippocampus while males show great susceptibility in superior cortical areas including frontal, temporal and parietal cortex (Figure 5.4, $P<0.05$, TFCE corrected).

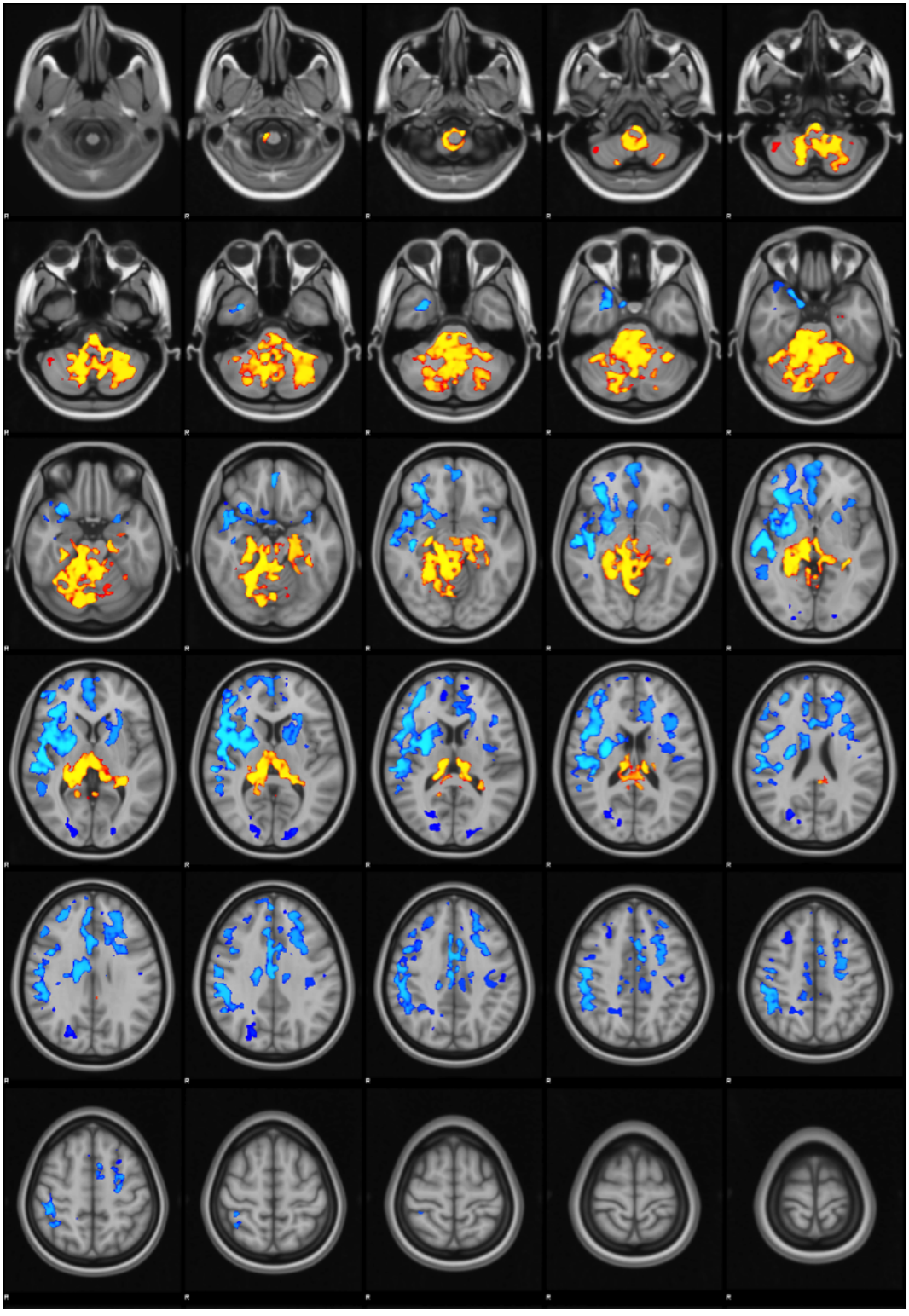

Figure 5.4: Blue regions show cluster where males showed significantly higher susceptibility and yellow regions show clusters where females showed significantly higher susceptibility ($P<0.05$, TFCE corrected).

5.5 Discussion

In this study, we have shown that susceptibility increases linearly between the ages of 18-59 in the bilateral putamen as well as a region near the medial edge of right pallidum. We also show that higher levels of fitness are associated with an increase in susceptibility in the right putamen and medial frontal cortex. Contrary to findings reported for older adults, we found no association in young to middle aged adults between susceptibility and any of several cognitive measures. Finally, contrary to the existing literature, we found a unique pattern of strong gender difference in susceptibility, with cortical grey and white matter regions higher in males, and cerebellar, brain stem and hippocampal areas higher in females.

Many existing studies of iron and susceptibility in the brain have focused on older participants and/or the potential role of iron accumulation in cognitive decline (Pujol et al., 1992; Schroeder et al., 2012; Sullivan et al., 2009). The current study is unique in that it focuses on a younger age group at a point when the slope of change in iron content, as measured in postmortem tissue, is significantly higher (Hallgren & Sourander, 1958). Our findings do not suggest any cognitive impact of the age-related accumulation of iron in the basal ganglia during middle age.

We also found a previously unreported positive correlation between physical fitness and susceptibility in the basal ganglia. Despite the intensive study of iron and susceptibility in the brain, the full picture of its functional role remains poorly understood (Moos et al., 2007). It is clear that iron has a role in basic cell metabolism as well as in the creation of myelination in development. However, it is not clear whether the continued accumulation of iron throughout adulthood is advantageous, detrimental, or inconsequential to optimal brain health and function. The uncertainty of the functional role of iron in middle adulthood makes the finding that susceptibility increases with higher fitness levels difficult to interpret. A functional role of iron accumulation in myelin production has been demonstrated in development (see Todorich et al., 2009, for review). If the susceptibility increase we see here is related to myelin formation, the higher susceptibility

levels with fitness may reflect the expansion of neural circuitry that has been associated with higher levels of fitness and physical activity (Markham & Greenough, 2004; Kempermann et al., 2010; Thomas et al., 2012). However, if the susceptibility is associated with iron outside the neural circuity, the higher levels associated with higher fitness may reflect a process by which higher levels of activity results in accelerated deposits of iron in the tissue from the vasculature with unknown effects on cognitive function. As with any correlational finding, it is possible that the relationship between fitness and susceptibility is mediated by a third factor, such as vascular health or diet, for example.

Previous studies have reported that increased iron content in older age is associated with poorer performance in a range of cognitive tasks (Pujol et al., 1992; Schroeder et al., 2012; Sullivan et al., 2009). In contrast, we did not find any significant relationships between cognitive performance and susceptibility. There are a number of possible reasons for this discrepancy. It is possible that our sample size was inadequate to detect these effects, or that our cognitive tests were not sufficiently sensitive to certain types of cognitive decline. It is also possible that these cognitive changes are not manifest in this younger age group.

Gender differences in brain iron content have received considerable attention in the literature in recent years. Bartzokis et al. (2007) reported higher estimated iron content (using FDRI) for males in five different regions of interest in 165 older adults (mean age 53.2, SD=18 years). They suggest that this additional iron may be responsible for the higher rates of early onset Parkinson's and Alzheimer's disease in men. More recently, (Xu et al., 2008) reported finding no gender differences in estimated iron content (using susceptibility weighting) in seven different regions of interest in a smaller and younger cohort of 78 adults (mean age 43. 3, SD=14.1). Our voxelwise results show large and significant regions of gender difference in our even younger group of subjects. Our results are consistent with three of the five regions of gender difference reported by Bartzokis et al. (2007). Significant clusters of higher iron estimates for males were found in the frontal white matter, the genu of the corpus callosum, and the caudate. However, contrary to Bartzokis et al. (2007) the thalamus and splenium of the corpus

callosum contained clusters that showed significantly higher iron estimates for females. This difference may be related to the different sensitivities of FDRI for susceptibility based iron estimations (see below).

There is currently no consensus on the optimal method for measuring iron content *in vivo*. Many different imaging measures have been employed to measure iron content, including FDRI and quantitative susceptibility mapping with several different approaches to phase regularization (Haacke et al., 2005; Wharton & Bowtell, 2010; Wharton et al., 2010). Some studies have suggested that FDRI methods are less sensitive to myelin than susceptibility quantifying methods and that susceptibility based methods are therefore more sensitive to age effects (Bilgic et al., 2012). In this study, we use susceptibility weighted imaging in which the phase images are high-pass-filtered and then transformed to a special phase mask. This mask is then multiplied into the original magnitude image to create enhanced contrast between tissues with different susceptibilities. As both phase and frequency data were collected at two different echo times, there are many additional post-processing options to attempt to obtain a more precise and quantitative measure of iron content. These analyses will be the subject of future work. However, the current SWI measure has some precedence in the literature (Haacke et al., 2005) and produces meaningful correlation with demographic variables as well as blood volume.

Contrary to the anatomical region of interest approach that has been commonly used, in this study we used a whole-brain voxelwise analysis that refrains from imposing borders on how susceptibility varies across the brain in its relationship to demographic variables. Using this approach, we show that the well-studied relationship between age and susceptibility exhibits a pair of striking bilateral focus points that do not fall within any well-defined anatomical area. These clusters lie between the between the ventromedial edge of the pallidum and the caudal posterior edge of the nucleus accumbens in a region that appears unremarkable on a T1-weighted scan (Figure 5.5). The significance of this location is a topic for future study.

In summary, we show that susceptibility increases with age in the putamen and

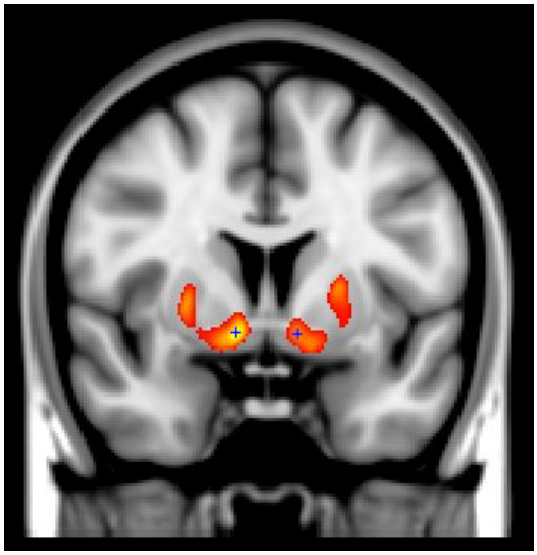

Figure 5.5: Clusters of positive correlation between age and susceptibility ($p<0.001$, uncorrected). In addition to clusters in the putamen and caudate, this figure show two clusters centered at MNI coordinates 11, 3, -8 and -11, 3, -9, marked with blue cross hairs on the right and left, respectively, that do not fall clearly within any known anatomical boundaries.

pallidum through young and middle adulthood. Unlike susceptibility in the brain's sinuses, susceptibility differences in these regions are not driven by blood borne iron within the vasculature. We have also shown that fitness further modulates susceptibility in the putamen, suggesting fitness may increase myelination or some other form of deposition of iron. Finally, we have shown substantial gender difference in susceptibility with a previously unreported pattern of higher susceptibility in anterior cortical areas for males and a higher susceptibility in subcortical regions as well as the cerebellum for women. These data provide additional clues on the role of iron and iron accumulation in the brain and how it relates to healthy ageing. Future studies will help determine if iron does indeed provide an early biomarker of degenerative brain processes and if the iron cycle provides a target for interventions aimed at mitigating age-related cognitive decline.

Chapter 6

Detailed hippocampal morphometry analysis at 7 Tesla

6.1 Abstract

A major aim of this thesis has been to test for subtle effects of experience, exercise, and age on brain structure, with a particular focus on the hippocampus. High field imaging offers great potential for improved sensitivity of hippocampal structure. In this chapter I will present initial work on imaging hippocampal morphometry using susceptibility-weighted imaging at 7 Tesla. Using this novel method, we document a high degree of variability in the convolution of the dentate gyrus across different participants. We show a focal cluster of contraction that correlates with age using deformation-based morphometry. In agreement with other published studies, this cluster was found in anterior ventromedial hippocampus. Furthermore, the cluster is within the dentate gyrus, one of two loci of neurogenesis within the adult mammalian brain, and may be related to the age related decrease previously observed in adult neurogenesis. Techniques are discussed regarding how to improve the analysis of the convolution structure and to enhance the

quality of the 7T hippocampal scans.

6.2 Introduction

The hippocampus is a critical region of the brain for learning and memory. It has also been shown to be the site of a remarkable degree of structural plasticity in tasks such as spatial navigation (Maguire et al., 2000), aerobic fitness (Erickson et al., 2009), and both the onset and drug-mediated remediation of depression (Boldrini et al., 2009; MacQueen et al., 2003; Sheline, 2000). Also, the dentate gyrus region of the hippocampus is one of only two regions in the mammalian brain capable of adult neurogenesis (see Zhao et al., 2008, for review).

The hippocampus is an important target structure for neuroimaging, however it has a complex and detailed substructure that is difficult to resolve at the typical 1 mm isotropic resolution of structural MRI scans at 1.5T and 3T (Duvernoy, 2005; Van Leemput et al., 2009). Recently, there has been significant progress in imaging this complex structure using higher field strengths. Thomas et al. (2008) provides one of the early examples using a T1-weighted "turbo field echo" sequence in which the authors were able to manually identify several hippocampal subfields. Subsequently, Kerchner et al. (2010) used a T2*-weighted sequence at 7T on both AD patients and controls. They report that AD subjects showed a thinner hypointense region on oblique cross section slices that they identify as the CA1 apical neuropil. Cho et al. (2010), also using a T2*-weighted sequence, provided the first high-resolution hippocampal images at 7T using isotropic voxels of just 0.4 mm. The sagittal slices of these scans reveal the unique, undulating structure along the longitudinal axis of the human hippocampus not previously shown *in vivo* (Duvernoy, 2005). Several subsequent *in vivo* 7T human hippocampal studies have been conducted on both patients and humans using similar sequences (Wisse et al., 2012; Kirov et al., 2013; Prudent et al., 2010). *Ex vivo* 7T and 9.4T studies have also been recently conducted, revealing unprecedented levels of anatomical detail (Augustinack et al., 2013; Adler et al., 2014). Finally, there has also been progress in automating the analysis of hippocampal morphometry both cross-sectionally and longitudinally, using

deformation-based methods (Das et al., 2012).

For the purposes of this thesis, 7T hippocampal morphometry provides an ideal tool to better understand the changes in hippocampal volume associated with changes in aerobic fitness. We used T2*-weighted 7T scans to reveal substantial variability in hippocampal morphometry across subjects – particularly in the undulating surface of the dentate gyrus. We employed DBM techniques to explore demographic and physiological (e.g. fitness) correlates to this variation. DBM is a particularly valuable technique with these scans as traditional VBM and volumetric techniques are not available for T2*-weighted images. DBM allows the expansion or contraction of a given region to be measured directly regardless of image contrast. We also have begun developing a pipeline to measure the curvature of this surface more directly.

6.3 Methods

6.3.1 Participants

Four participants from the study discussed in the previous chapters also received baseline 7T scans for this study. An additional 23 participants were recruited from the Oxford community, one of which was excluded due to an incidental finding and another two due to excessive motion artefacts. A total of 24 subjects were therefore included in the analyses presented in this chapter (15 female, mean age 34.4, SD 16.6). All subjects gave their informed consent to participate in the study in accordance with local ethics committee approval (REC B 10/H0605/48). All participants were right handed, English speaking, and had no history of neurological or psychiatric conditions. In addition, all participants were screened for and excluded if they had high blood pressure, a history of diabetes or any heart, mobility or other problems that might have prevented them from engaging in aerobic exercise.

6.3.2 Imaging methods

Each subject was scanned using a Siemens 7 Tesla MRI Scanner (Erlangen, Germany). Pulse sequences included a T1-weighted MPRAGE (0.7 mm isotropic resolution, TR = 2200 ms, TI = 1050 ms, TE = 2.96 ms, flip angle= 7 degrees, matrix size = 320 x 320, 256 sagittal slices, and GRAPPA factor = 2). This scan was then used to prescribe an oblique, 3D fast low angle shot (FLASH) sequence just covering both hippocampi, similar to that of Cho et al. (2010) (0.5 mm isotropic resolution, TR = 50 ms, TE = 25.7 ms, flip angle= 10 degrees, matrix size = 384 x 384, partial Fourier 6/8, 48 slices, 7 min 17 seconds acquisition time, see Figure 6.1 for slice prescription). This scan was acquired twice to increase SNR. Finally, a whole brain sequence with similar contrasts to the hippocampal sequence was acquired to aid in registering the hippocampal sequence to the T1-weighted whole brain scan in post-processing (1.3 mm isotropic resolution, TR = 50 ms, TE = 25.7 ms, flip angle= 10 degrees, matrix size = 192 x 192, partial Fourier 6/8, 104 slices).

6.3.3 Fitness test

Full details of the fitness test are provided in chapter 2 section 2.2.3. Briefly, aerobic fitness ($\dot{V}O_2$ max) was assessed by a maximal graded exercise test performed on an electromagnetically braked cycle ergometer (Lode Excaliber, Groningen, Netherlands). Resistance was increased every two minutes and participants cycled until volitional exhaustion. Peak $\dot{V}O_2$, TTE, and maximum heart rate were recorded.

6.3.4 Image analysis

6.3.4.1 Calculation of subfields in standard space

Each T1-weighted MPRAGE scan was processed with Freesurfer and the associated hippocampal subfield segmentation package (Fischl et al., 1999; Dale et al., 1999; Van Leemput et al., 2009). The hippocampal subfield maps were then nonlinearly warped to standard MNI space using FSL tools (Smith et al., 2004). The segmentations were

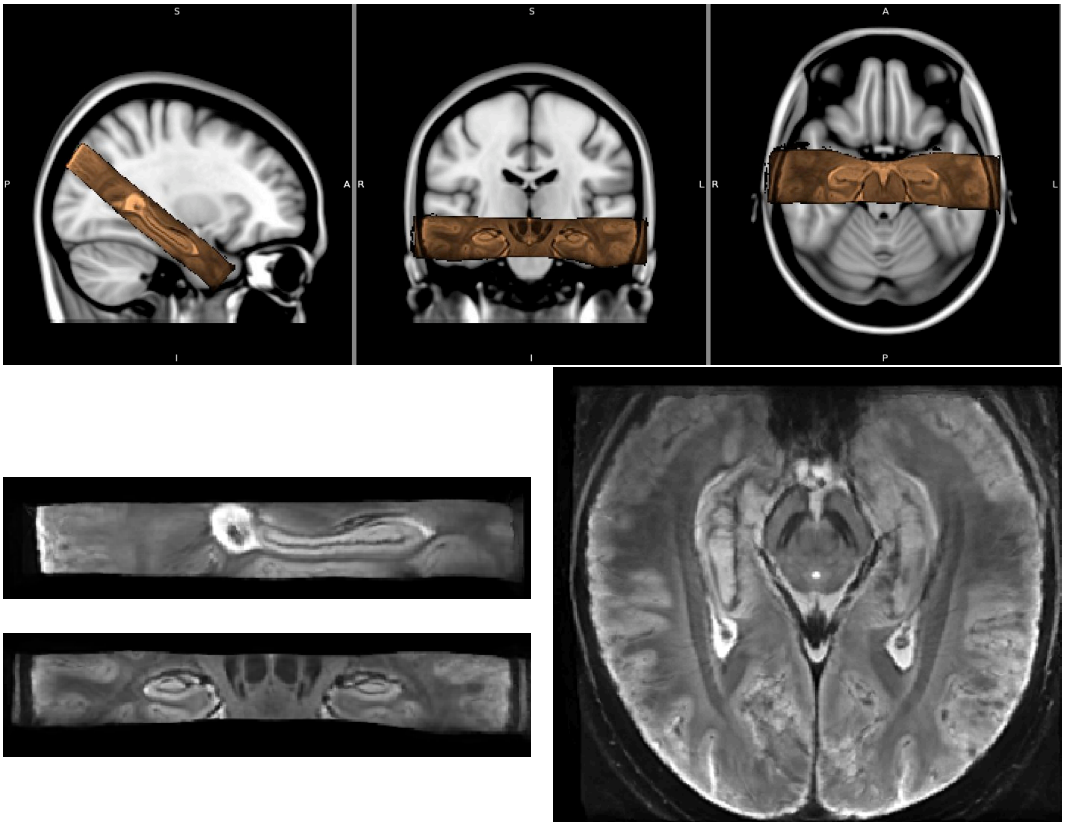

Figure 6.1: Top: Illustration of the location and orientation of oblique slice plane for the limited field of view hippocampal scans. Bottom: The average non-linearly aligned template across 24 participants.

averaged, voxelwise, and each voxel was assigned to a subfield based on the maximum mean probability (Van Leemput et al., 2009).

6.3.4.2 Building a template in standard space

Each limited field of view hippocampal scan was visually inspected for quality and motion artefacts. 7 out of 52 individual scans had to be excluded due to motion artefacts (including the scans from two excluded subjects). When two scans were available they were rigidly aligned and averaged (N = 21). If only one scan was available (N = 3), that scan was used for subsequent processing.

For each participant, the averaged hippocampus image was then linearly aligned to the T2*-weighted whole brain image which in turn was aligned to the whole brain T1-weighted scan using boundary-based registration (Greve & Fischl, 2009; Jenkinson et al., 2002a; Jenkinson & Smith, 2001). The T1-weighted whole brain image was bias-corrected, skull-stripped, and non-linearly aligned to standard MNI152 space using fsl_anat from the FSL software package (Jenkinson et al., 2011). The proceeding registrations were then concatenated together to register each participant's hippocampus scan into standard space. The mean of all participants' hippocampus scans is used to boot strap iterative non-linear registration to a study-specific template using Advanced Neuroimaging Tools (ANTS) (Avants et al., 2011, 2010). Four iterations were sufficient to produce a high quality template (see Figure 6.1).

6.3.4.3 Statistical Analysis

DBM techniques were used to evaluate morphometric change (Chung et al., 2001; Ashburner et al., 1998). The Jacobian determinants of each subject's three dimensional nonlinear warp to the final template was used to determine how the relative expansion and contraction related to the variables of interest. We conducted a voxelwise, non-parametric, permutation based analysis using randomise (Nichols & Holmes, 2002; Salimi-Khorshidi et al., 2011; Hayasaka et al., 2004) with a design matrix containing variables for age, sex, and peak $\dot{V}O_2$ score within a voxel mask that included the entirety of both left

and right hippocampus. Multiple comparison correction was performed using a cluster mass threshold value of $p < 0.05$, uncorrected.

6.4 Results

6.4.1 Visibility and variability of the dentate gyrus surface

Visual inspection of hippocampal high resolution scans revealed an undulating hypointense line through the center of the hippocampus (see Figure 6.2). This line had a location and shape similar to the dentate gyrus visualized *ex vivo* in Duverynoy's hippocampal atlas (Duvernoy, 2005). We also noted the degree of convolution of this surface varied considerably from subject to subject. Two extreme examples are depicted in Figure 6.2. We also aligned 14 subjects into standard space and created a movie cycling through the participants. This movie is available at `https://sites.google.com/site/adamthomas/dphil`

Several attempts have been made to quantify the convolution of the dentate gyrus. We manually labelled the hypointense surface on several of the hippocampal scans (see Figure 6.2), and degree of convolution was scored on a scale of 1 to 5 by two different raters independently. However, inter-rater reliability was poor. The degree of convolution varies considerably along the longitudinal axis and raters tended to focus on different aspects of the surface. It should be possible to quantify the degree of curvature along the dentate gyrus surface in an automated fashion by determining the surface normal vector at each voxel and then calculating the derivative of this vector along the surface. This technique is currently being implemented but was not functional at the time of writing. We expect this technique to provide an objective and robust measure of dentate gyrus convolution.

6.4.2 Voxelwise deformation-based morphometry

Voxelwise analysis on the magnitude of the deformations failed to show a significant correlation with sex or measures of fitness. However, we did find a significant positive

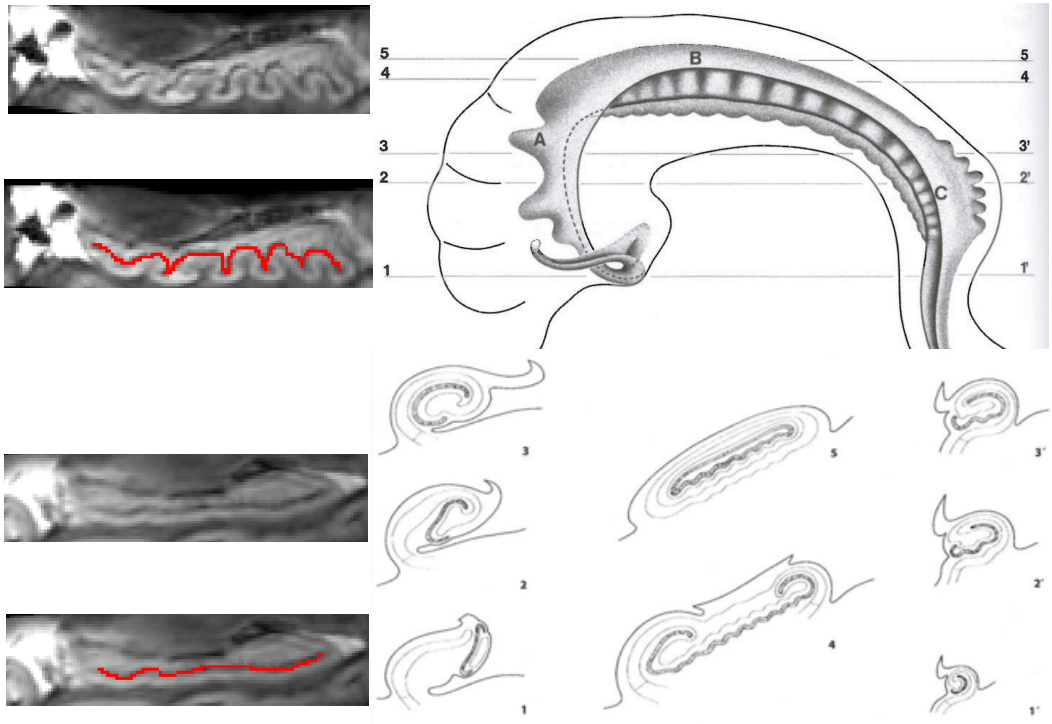

Figure 6.2: Left: Sagittal slices through high-resolution hippocampal scans of two different participants with varying degrees of convolution. Dentate gyrus surface traced in red. Right: schematic drawing of the dentate gyrus surface from Duvernoy (2005).

correlation between the magnitude of the Jacobian and age in a cluster of voxels located in anterior ventromedial hippocampus, suggesting this region shows a focal contraction with age ($P < 0.05$ corrected, see Figure 6.3). At a lower threshold ($P<0.01$ uncorrected) this cluster could be seen bilaterally.

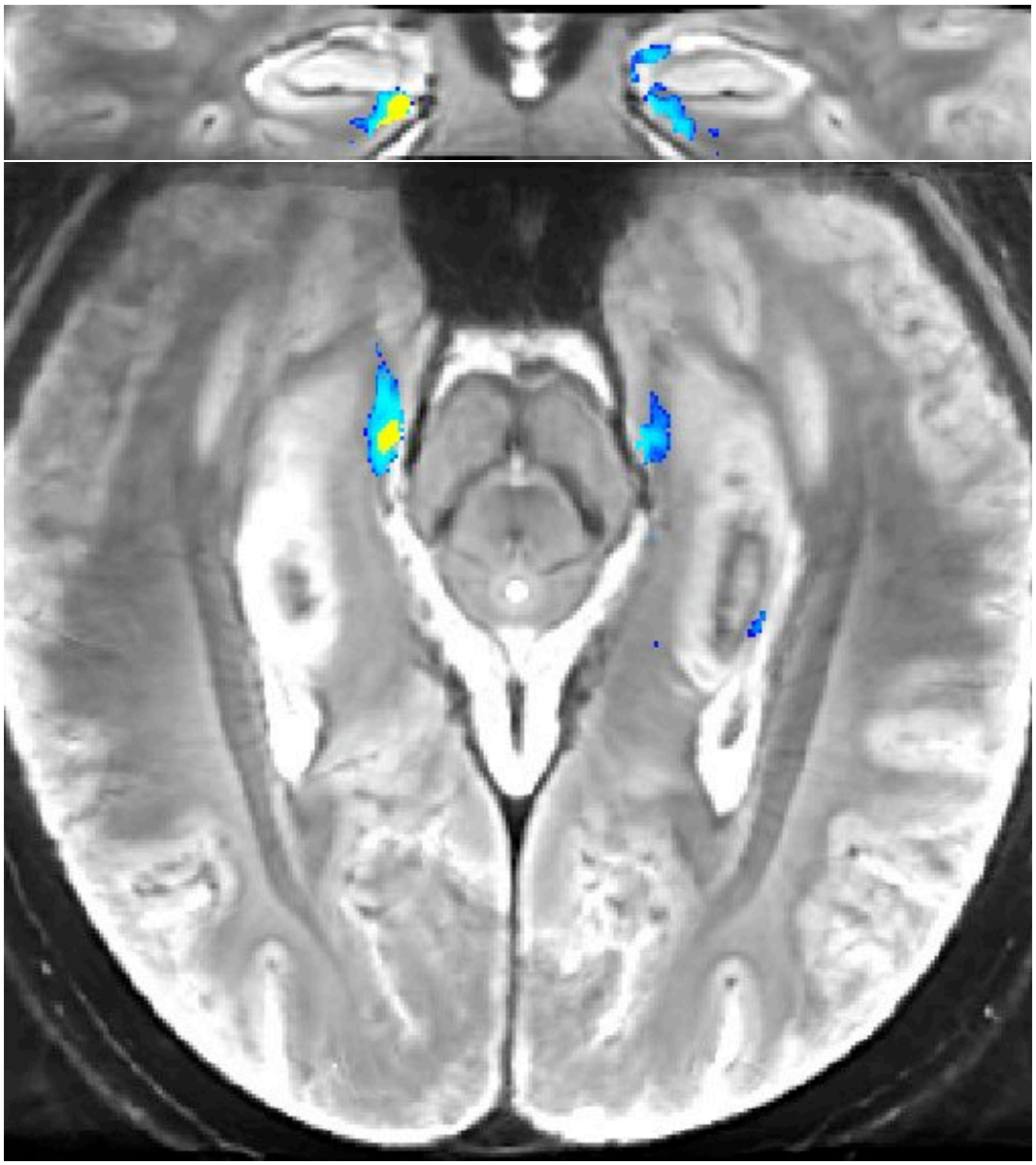

Figure 6.3: Regions showing positive correlation between Jacobian and age. Top image shows an oblique coronal slice, bottom image show an oblique axial slice. Yellow cluster: $P < 0.05$ corrected, blue clusters: $P < 0.01$ uncorrected.

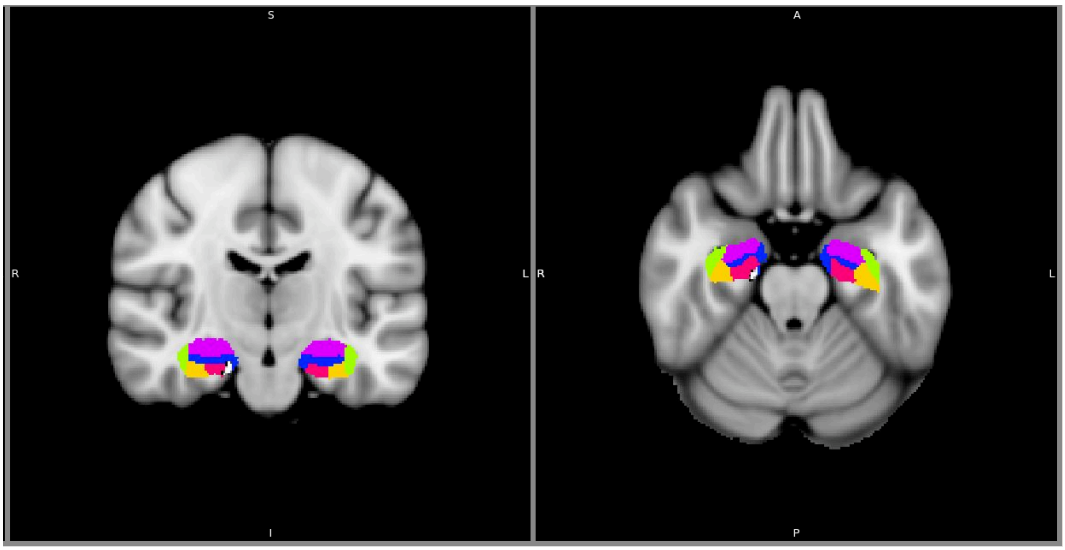

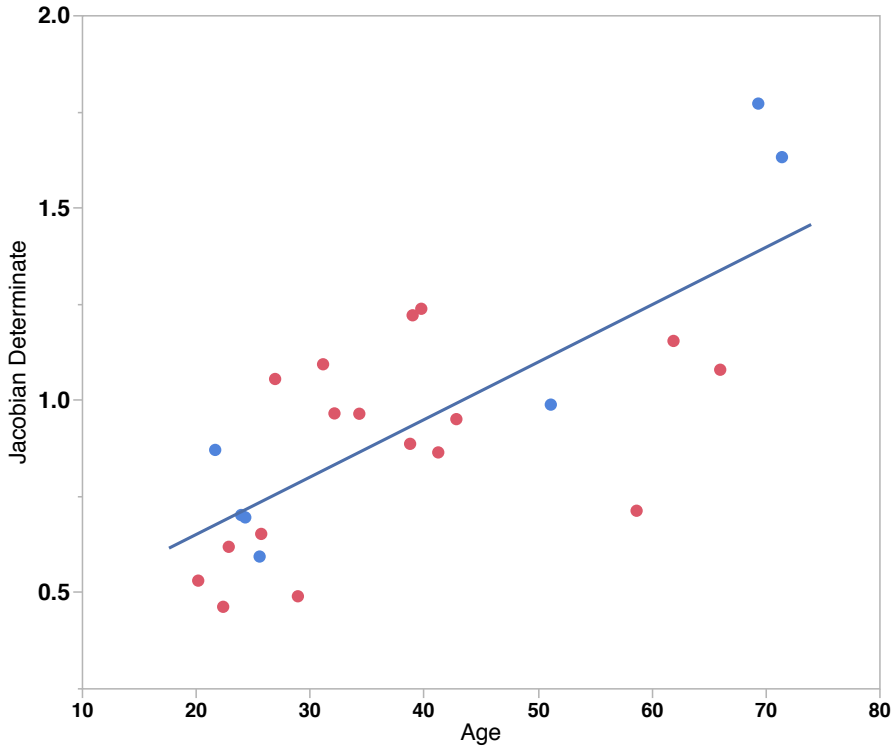

Figure 6.4: Top: Registering the cluster (white) to standard space and overlaying it on the maximum probability map revealed that it was located within dentate gyrus (blue), centred at MNI coordinate 18, -17, -23. Hippocampal subfields as segmented by Freesurfer shown in colors (blue = DG/CA4, purple = CA2/3, light green = CA1, orange = subiculum, pink = presubiculum). Bottom: Plot of correlation of the average Jacobian determinate within cluster. Males in blue, females in red.

6.5 Discussion

In this chapter, we have used high resolution, T2*-weighted hippocampal imaging at 7 Tesla to show a high degree of variability in the convolution of the dentate gyrus, and indeed the entire hippocampal surface, across different participants. We have employed deformation based morphometry to show a focal cluster of contraction correlated with age. Contraction detected by DBM is typically interpreted as evidence for atrophy or reduced volume (Chung et al., 2001; Ashburner et al., 1998). This cluster was found in anterior ventromedial hippocampus, in line with other studies that have shown an anterior focus of age-related hippocampal atrophy (Erickson et al., 2011). Furthermore, the cluster is within the anterior portion of the dentate gyrus, one of two loci of neurogenesis within the adult mammalian brain. Like many aspect of physiological and cognitive function, neurogenesis has been shown to decrease with age (Kuhn et al., 1996).

6.5.1 The relevance of hippocampal convolution and the neurogenic niche

As is evident from the elaborate degree of folding in the cerebral cortex of higher mammals, surface area is an important variable in the central nervous system on which there is significant evolutionary pressure (Rakic, 1995; Kappers et al., 1936). The convolution of the hippocampus has received less attention in the literature, presumably due to the prevalence of rodents as a model system, which have a relatively mild degree of hippocampal folding compared to humans. In humans, this complex folding structure is seldom observed directly due to limitations in standard neuroimaging techniques and is difficult to quantify in post mortem tissue.

Human hippocampal morphometry has typically focused on differences between the subfields (Small et al., 2011), which extend along the entirety of the longitudinal axis of the hippocampus, although they are difficult to parcellate in the most posterior region of the hippocampal tail (Van Leemput et al., 2009). The degree of hippocampal folding or convolution as a possible mediator of cognitive or physiological function has, to our

knowledge, received virtually no attention in the literature. By contrast, there is evidence on the relevance of cerebral cortical sulcal folding patterns to individual differences and disease state (Van Essen et al., 2006; Harris et al., 2004; Whittle et al., 2009). As with the cerebral cortex, the degree of folding in the hippocampus is likely to be directly related to the total amount of surface area. Surface area may be a particularly functionally relevant feature in the hippocampus as the subgranular zone of the dentate gyrus likely tracks these convolutions. Thus more surface area may allow for a greater volume in which neurogenesis can occur.

6.5.2 Limitations and future direction

Deformation-based morphometry is a helpful first step in analysing the complex structure of the hippocampus, but it does not allow for quantitative measurement of convolution or surface area. A more complete reconstruction of the hippocampal surface will be necessary to fully realize these measures.

Several of the high-resolution hippocampal scans we acquired had to be discarded due to poor image quality, including two entire subjects that could not be used. In other pilot scans on older participants, the rate of scan loss due to motion is higher. These motion artefacts are likely due to slight motion of the subject's head in the scanner during the seven-minute acquisition. It is also possible that variation in cardiac and respiratory motion may have compromised some of the scans. These problems illustrate the endemic problem of subject motion in the scanner that is even more challenging at high field and high resolution. Various techniques are currently under development to combat motion-related scan artefacts, including optically monitoring motion to dynamically adjust the gradients to compensate (Schulz et al., 2014). Another technique involves detecting motion using the images themselves and compensating in real time (Tisdall et al., 2012; White et al., 2010). We are currently exploring implementing these techniques for this sequence, which should increase both the number of acceptable scans and the quality of the scans accepted.

In future 7T studies, we will employ the same longitudinal design with an exercise

intervention discussed in the first several chapters of this thesis. This study will allow us to explore how physical activity alters hippocampal structure. Observation from rodent studies would lead to the prediction that physical activity would induce a slight expansion of the dentate gyrus, whereas ageing would be associated with a decrease. High field hippocampal spectroscopy will also be employed to measure GABA levels as newborn neurons have been shown to be tonically activated by GABA in the early stages of their incorporation into hippocampal circuits (see Ming & Song, 2011, for review). These and other measures that examine changes in the subventricular zone, which will be discussed in the final chapter of this thesis, should bring us closer to directly measuring the relationship between exercise and human neurogenesis (see Couillard-Despres & Aigner, 2011, for review).

Chapter 7

Discussion

7.1 Introduction

At the outset of my D.Phil work I aimed to address several gaps and contradictions in the literature regarding the nature of exercise-mediated plasticity in specific limbic and motor structures such as the hippocampus, cerebellum, striatum and motor cortex, as well as in the brain overall. The previous four chapters of this thesis presented specific experimental investigations in this field. In this final chapter I will attempt to synthesize both the positive and negative findings from these studies and explain what bearing they have on the gaps and contradictions I identified at the outset. I will also address some of the more surprising results and possible underlying mechanisms. Finally, I will address some of limitations, unanswered questions, and future directions for further studies of exercise mediated plasticity.

7.2 Focal vs. global changes with aerobic exercise

One primary limitation of the existing exercise plasticity literature is that studies tend to focus on either a specific region of interest or they consider global effects across the entire brain. This level of focus is sometimes due to the nature of the technique (e.g. histology). In other cases, it is due to a specific hypothesis addressed by the paper

in question. This has been the case with multiple papers focusing on exercise-mediated plasticity in the hippocampus (Erickson et al., 2009, 2011; Pereira et al., 2007). We specifically designed our longitudinal exercise intervention study with high resolution, whole brain scans that would allow us to investigate both local and global changes. In this section I review which changes we found to be local versus those that appeared to occur throughout the brain.

7.2.1 Global changes

Aerobic exercise training, even for relatively short periods of time, has many profound global effects on the vascular system including lowering of resting heart rate, lowering of both systolic and diastolic blood pressure, increasing cardiac stroke volume, and increasing total blood volume (Convertino, 1991; Sandercock et al., 2005; Jones & Carter, 2000; El-Sayed et al., 2005). Despite these changes, investigation of the effects of exercise training on the vasculature within the central nervous system has largely been targeted at specific regions. As discussed in section 1.5.2, a number of these studies have examined capillary density using histological methods, where it is necessary to limit investigation to specific regions (Rhyu et al., 2010; Black et al., 1990; Kleim et al., 2002). Other studies have focused on the tight link between angiogenesis and neurogenesis, and have thus focused on the dentate gyrus region of the hippocampus, where neurogenesis is known to occur (van Praag et al., 2005; Van der Borght et al., 2009; Pereira et al., 2007).

In the work reported in this thesis, I was able to identify a number of global effects of exercise and fitness on brain structure. Similar to the higher vessel number in fitter individuals reported by Bullitt et al. (2009), we found a positive correlation across subjects between cerebral blood volume and fitness level throughout grey matter, with particularly high correlations found in cerebellum and parahippocampal gyrus. However, we did not observe a within-subject increase in CBV following an exercise intervention that increased fitness. Instead, although they did not reach significance, our data are suggestive of a decrease in CBV throughout grey matter following an exercise intervention. This change

in CBV with exercise showed a voxelwise correlation with change in ventricular volume. One interpretation of this finding is that cerebral blood volume was influenced by systemic changes of the homeostatic mechanisms maintaining brain and CSF volume. These changes will be discussed in more detail below.

7.2.2 Local changes

The hippocampus has been repeatedly shown to be a specific target of exercise-mediated plasticity, with larger hippocampal volume being observed following an exercise intervention, or correlated with higher fitness levels (Erickson et al., 2009, 2011; Chaddock et al., 2010). We replicated this finding in the anterior portion of the hippocampus, showing a volume increase associated with exercise training that subsided several week after the termination of exercise training. However, contrary to other studies (Pereira et al., 2007), we did not find an increase in cerebral blood volume in the dentate gyrus (the locus of neurogenesis) nor in any other region of the hippocampus. Whereas most previous studies have focused on a single neuroimaging modality, we used a multimodal battery of measures, in the hope that, in combination, these complementary measures would allow us to narrow down the underlying drivers of the observed effects on volume. Our multimodal results were more consistent with a change in neuropil than in vasculature.

As noted above, we also observed that CBV in the cerebellum exhibits a particularly strong positive correlation with fitness, though we also found this correlation when all of grey matter was considered. The strength of the correlation in cerebellum may reflect its role in motor function, or perhaps its physical relationship to the large vascular network that surrounds it.

Finally, we noted that fitness specifically modulated the susceptibility-weighting within the basal ganglia that is typically associated with age-related accumulation of iron. Specifically, we found that greater levels of fitness were associated with increased susceptibility in this region. This may reflect additional iron deposited by higher levels of blood flow associated with fitness, or alternatively may reflect additional neural circuitry,

and associated iron-laden myelination, facilitated by higher fitness levels.

7.3 The relationship between hippocampal growth and neurogenesis

Within the past 20 years of brain plasticity research, the recognition and wider acceptance of adult neurogenesis has been a major paradigm shift (Kuhn et al., 1996; Altman & Das, 1965; Ming & Song, 2011). The additional observation that exercise accelerates neurogenesis has also generated considerable enthusiasm (van Praag et al., 1999b). However, it is difficult to study neurogenesis in human participants, as the identification of new neurons requires cell labelling and post-mortem histology. Therefore, there has been a strong effort to identify other markers associated with neurogenesis that can be measured *in vivo* in humans. One candidate is hippocampal volume, which can be measured on a standard structural MRI scan (Erickson et al., 2011). Another is angiogenesis, which has been shown to be tightly coupled with neurogenesis in animal studies and can be measured with various imaging techniques (Pereira et al., 2007). One of the primary goals of this study was to attempt to evaluate this link.

As discussed above, we replicated the finding that hippocampal volume, particularly in the anterior head, increases with exercise. This volume increase did not show any specificity to the dentate gyrus. This is perhaps not surprising, as volume increase of the dentate gyrus has also not been shown in rats, where the neurogenesis can be confirmed (van Praag et al., 2005). We also did not find an increase in cerebral blood volume in the dentate gyrus and no correlation between CBV and volume changes. Thus, although our results do support the existence of some form of exercise-mediated hippocampal plasticity, they do not support the use of hippocampal volume or CBV as proxy measures for adult neurogenesis in human. Finding additional measures which might correlate with adult neurogenesis remains an important goal for future studies. Higher resolution scans performed at higher field strength and alternative imaging modalities provide promising avenues for this work.

7.4 Brain Volume Changes

We observed an expansion of ventricular space, and a contraction of cortical grey matter throughout the brain following a six-week exercise intervention. The biological changes underlying this effect are uncertain, but potential interpretations are discussed in this section.

One potential explanation is that the observed global volume change relates to hydration levels. As an organism becomes less hydrated, water molecules diffuse from intracellular spaces to extracellular compartments (Gullans & Verbalis, 1993). This is due to the fact that cellular membranes are relatively more permeable to water than they are to electrolytes and other molecules. In the brain, the net effect is a shrinkage of brain tissue and an expansion of cerebral spinal fluid chambers, such as the ventricles and the subarachnoid space. Additional CSF flows from the spinal dural sack which, unlike the skull, can expand and contract to accommodate changes in CSF volume and intracranial pressure. This shift is an illustration of the Monro-Kellie hypothesis, which states that since the cranial volume is fixed its constituents (brain, blood, and CSF) must remain in equilibrium – an increase in one must result in a decrease in one or both of the others (Mokri, 2001).

In our study, the six-week exercise intervention produced a shift in the brain-blood-CSF equilibrium that mimics what has been observed under conditions of experimentally-imposed dehydration via excessive sweating without liquid replenishment (Kempton et al., 2011, 2009; Dickson et al., 2005; Streitburger et al., 2012). This finding is surprising, as although aerobic exercise is associated with acute dehydration, longer periods of aerobic training is typically associated with an increase in blood volume and total body water content (Convertino, 2007, 1991). Substantial increases in plasma volume are observed within hours of a single training session assuming unrestricted access to fluids. This increase in body water content is believed to contribute to increases in aerobic efficiency by enhancing thermoregulation (Sawka et al., 2000).

Determining which component of the brain-blood-CSF equilibrium is causal in this

balance shift is not obviously possible with our current dataset. Measurement of total blood volume is a time consuming and involved procedure that was not feasible for the current study (Ertl et al., 2007). Traditional, gold standard dilution methods using heavy water to measure total body water are also challenging (Schoeller et al., 1980). Recent advances in bioelectrical impedance analysis provide a promising alternative to measuring total body water; however, these tools were not available at the time of this study (Schoeller et al., 1980; Kyle et al., 2004). Without these measurements, I can not completely rule out the possibility that our participants experienced some degree of decreased hydration following the exercise intervention. However, given the highly replicated finding that total body hydration *increases* with periods of aerobic training lasting more than a day, I find it much more likely that the expansion of the ventricles and contraction of grey matter reflects some other aspect of the complex homeostatic process regulating blood volume, heart rate, blood pressure, CSF, and brain volume. One possible hypothesis is that the exercise-mediated decreases in resting heart rate and blood pressure are not offset by a corresponding decrease in intracranial pressure (partially regulated by the production and absorption of CSF), leading to a shift in the balance between CSF and blood in the brain at rest (Pollay, 2010). Future studies could test this hypothesis by conducting a similar intervention study while also measuring total blood volume and CSF flow rates (Battal et al., 2011). Importantly, the flow of CSF has been linked to the migration of newly born neurons in the subventricular zone in rats (Sawamoto et al., 2006). As exercise is known to up-regulate the creation of new neurons, it is plausible to consider the possibility that exercise might also up-regulate CSF pressure and flow. To my knowledge, this hypothesis has not been explored.

It is also an open question as to what the functional implications of brain contraction are. At either extreme of hypohydration or hyperhydration, the result is the death of the organism (Gullans & Verbalis, 1993). However, it appears that the human brain can occupy several different levels expansion or contraction that are within the range of normal function. It is also possible that the degree of contraction is dynamically regulated to achieve specific physiological goals related to brain function. For example, a

relatively diffuse brain allows more room for neurotransmitter to spill out of the synapse and influence nearby structures. It also allows for greater diffusion of hormones and waste products through the interstitial space. On the other hand, a relatively contracted brain is more likely to keep neurotransmitters at the point of synaptic release (Syková & Nicholson, 2008; Kinney et al., 2013).

All of these questions are topics for future studies. But it is clear that neuroimaging studies of volume change need to pay close attention to not just the expansion of synapses, dendrites, myelin, and neurogenesis but also to the expansion of the space between these structures, as this has repeatedly been shown to be a very dynamic variable in changes in brain structure (Johansen-Berg et al., 2012; Sagi et al., 2012).

7.5 Limitations and Future Directions

7.5.1 Physiological Measures

For the first three data chapters in this thesis I used time to exhaustion or TTE as the primary measure of fitness. This use contrasts with other studies that tend to use $\dot{V}O_2$ max as the measure of fitness. This choice was discussed in section 2.2.3. Briefly, we found that some participants achieved a lower $\dot{V}O_2$ max after training even though they spent more time in the graded exercise test, which, suggests that they did not reach their true max and quit cycling for another reason, such as muscle fatigue. I found TTE provided a more robust measure of fitness. However, it is also not a perfect measure as it also relies on the participant's willingness to continue cycling to the point of exhaustion. Two other measures are possible which are less reliant on volitional factors. The first method is estimated $\dot{V}O_2$ max, in which $\dot{V}O_2$ is plotted against heart rate to obtain a linear fit. Then the theoretical maximum $\dot{V}O_2$ is determined using the age-predicted or the observed maximum heart rate. Another method is to simply determine the participant's average heart rate at a relatively low work rate such as 50 watts, which has been shown to provide a good measure of fitness and be subject to training (Bouchard & Rankinen, 2001; Skinner et al., 2001). Both of these methods rely on the fact that

while maximum heart rate is highly age dependent, sub-maximal heart rate is highly variable based on individual fitness level.

Due to technical problems, the heart rate of our participants was not recorded digitally thus we had to rely on paper based recording. At the time of writing, these paper based records were being manually entered and matched with the corresponding $\dot{V}O_2$ measures. Thus, the estimated $\dot{V}O_2$ max and HR at 50 W were not available. These alternative metrics of fitness may provide additional insight into the correlations we have observed.

7.5.2 Cognitive Measures

A wide battery of well established cognitive tests was used to assess baseline cognitive function as well as longitudinal change in cognitive function. In order to use long-standing, paper-based tests (e.g. RVLT, ROCF, semantic and verbal fluency) multiple times on the same participants, it is necessary to use multiple versions of the tests. In most cases it was possible to obtain additional test versions that had been previously determined to be of similar difficulty. However when analysing for longitudinal change it was necessary to include regressors for both test version and general practice effect, in addition to the exercise training effect of interest. Given our sample size, we were not able to detect significant changes due to exercise training in any of the tests in which multiple test versions were used. Also, contrary to the literature, we did at times find that difficulty varied between versions for our participants. For this reason we largely relied on the computerized backward digit span test for longitudinal assessments. In the backward digit span test, the computerized administration allowed the digit lists to be selected at random on each trial, thus there was no concern of multiple versions. We were also able to easily implement a stair step test design further enhancing the sensitivity of the measurement.

In future studies, computerized administration of cognitive tests will be favoured over paper based versions in order to allow us to more effectively utilize randomisation and stair step designs in other cognitive domains.

7.5.3 Measurement of Cerebral Blood Volume

Several papers in the literature have discussed the various methodologies used for measuring cerebral blood volume with a contrast agent (Lin et al., 1999; Speck et al., 1999; Barbier et al., 2001). Specifically, these papers have discussed the difference between the static method using a bolus injection of contrast agent with two T1-weighted scans before and after and the dynamic method, in which T2*-weighted scans are continuously collected while the contrast agent is injected and passed through the blood stream. In this thesis, we have employed the static method in order to maximize spatial resolution and maintain consistency with other research that has explored CBV associated with ageing and fitness (Small, 2004; Pereira et al., 2007). However, we have also discovered important choices that can dramatically affect CBV results that have received relatively little treatment in the literature. Two of these choices are discussed below.

7.5.3.1 Normalization of Cerebral Blood Volume

The calculation of CBV using either the static or the dynamic method requires normalization by the signal located in a voxel or group of voxels that contain only blood. In the static method, where there is no concern whether the voxel lies in arterial or venous blood, the typical choice is the sagittal sinus. The exact location and number of voxels included varies widely from study to study, and is in some cases not clearly specified (Speck et al., 1999; Lin et al., 1997; Small, 2004; Pereira et al., 2007; Lin et al., 1999).

We found the selection of this voxel mask had dramatic effects on the calculated CBV values. We found that a larger voxel mask tended to lead to more reproducible CBV values from session to session, but the correlations with age and sex that have been reported in the literature were weak or absent. Smaller voxel masks (e.g. consisting of 1-3 of the brightest voxels in the sagittal sinus) had lower reproducibility from session to session, but showed stronger correlation with age and sex. All of our masks were generated automatically by specifying size and approximate location in standard space. Our final mask of 1000 voxels on the midline above the cerebellum was selected based

on reasonably strong reproducibility, as well as correlations that were consistent with those reported in the literature. Future studies should be cognizant of the importance of this variable and provide a thorough explanation of exactly how the mask is created. Additional analyses might also be conducted to provide a theoretical justification as to exactly how the blood mask should be determined.

7.5.3.2 Large vs. Small Vessels

When creating a CBV image, a subset of voxels will fall either completely or partially within large vascular structures resulting in very large CBV values for these voxels. Some authors have found that these voxels introduce considerable noise, such that correlations were not observed with early results collected using Positron Emission Tomography (Lin et al., 1999; Kuppusamy et al., 1996; Lin et al., 1997; Leenders et al., 1990). In order to obtain these correlations it was necessary to attempt to eliminate these large vessels by thresholding the maps at 10% CBV. In more recent studies, it appears that this threshold has not been applied (Pereira et al., 2007). For this reason, we used unthresholded CBV maps in our work. We did note significant differences between thresholded and unthresholded maps in their relationship to demographic variables. Future analyses might explore these differences in more detail.

7.5.4 Genetic phenotypes and exercise mediated plasticity

There is substantial evidence that genetics influences how the body responds to exercise. In a large, longitudinal study, researchers showed that the physiological response to exercise training (as measured by submaximal heart rate) was highly heritable and that heritability could be largely explained by just nine single-nucleotide polymorphisms (SNPs) (Bouchard et al., 2010; Rankinen et al., 2012). The evidence for how genetics influences the interaction between exercise and the brain is more limited. The APOE gene is the best established risk factor for Alzheimer's disease (Farrer et al., 1997). A number of large longitudinal and cross sectional studies have been conducted attempting to test if different APOE genotypes respond to physical exercise differently with respect to their

progression to dementia. The results are surprisingly mixed, with some studies suggesting e4 alleles show greater benefit from exercise while other suggest the more common e2 and e3 alleles show more benefit (see (Voss et al., 2013b) for a review of these and other studies). Other candidate genes include BDNF, Catechol-O-methyltransferase (COMT), 5-hydroxytryptamine (5HT), and Kidney and Brain Expressed Protein (KIBRA) which have shown to be related to learning, mental disorders, and other cognitive variables (Goldberg & Weinberger, 2004; Green et al., 2008). There is also some evidence that BDNF and COMT modulate the relationship between exercise and cognition (Stroth et al., 2010; Mata et al., 2010).

Although we did not prospectively genotype our participants to obtain a balanced sampling of any particular genotype, we did collect saliva samples in order to genotype all of our participants for nine relevant SNPs coding for different variation of APOE, COMT, BDNF, 5HT, and KIBRA. Unfortunately, at the time of this writing these genotypes have not been received back from the third-party genotyping service. Once these data are available, future analyses will explore whether these genotypes have any predictive value on the exercise-mediated plasticity we have shown, though we expect the sensitivity of these analyses to be limited given the subject numbers and expected distribution of polymorphisms.

7.5.5 Hippocampal plasticity

As discussed above, we found little evidence to support the hypothesis that hippocampal volume growth is caused by neurogenesis. However, we have shown that exercise-mediated hippocampal volume growth does occur in younger adults over relatively short interventions and is dependent on the maintenance of continued aerobic activity. The precise mechanism and nature of this volume change remains unclear. Future longitudinal studies on a similar population, conducted on a high field scanner could help answer this question. Considerable advances in quantifying myelin at high field have been made in recent years (Deistung et al., 2013; Wharton & Bowtell, 2010; Chen et al., 2013b) and could be employed to determine what contribution myelin makes to this

volume change. The technique employed cross-sectionally in chapter 5 could also be employed to better visualize the precise changes to the surface of the dentate gyrus. Finally, recent advances in high field spectroscopy techniques offer the potential of measuring specific neurotransmitter changes in the hippocampus associated with aerobic exercise training and increases in fitness (Emir et al., 2012).

7.5.6 Conclusion

In this thesis, considerable progress has been made in directly measuring structural brain plasticity associated with increased aerobic fitness, and the associated improvements in cognitive function. The work presented here provides insight into how the brain changes with exercise in healthy, middle aged adults – a cohort that has been infrequently studied in the literature. This work is also one of few studies to simultaneously employ a wide range of different imaging measures to investigate these structural changes. I have also proposed a novel method of combining these measures in order to test specific hypotheses regarding the nature of underlying structural changes. I have also shown that fitness appears to modulate the well reported, age-related increase in magnetic susceptibility in basal ganglia, possibly reflecting an alteration in the deposition of iron or myelin. In addition to these localized affects, I have shown that changes in aerobic fitness result in systemic changes in the homeostatic balance of tissue and fluid volume and pressure inside the cranial cavity, such that the entire brain shape is altered. Cross-sectionally, I have shown whole brain cerebral blood volume correlates with fitness and is predictive of working memory, a measure closely related to fluid intelligence. Finally, I have provided the first steps toward a valuable analysis pipeline that will allow investigation of the detailed structural morphology of the hippocampus using high field MRI and advanced image processing methods.

This thesis provides a novel addition to the wealth of evidence that aerobic exercise is a potent catalyst for behavioural and brain plasticity. Understanding how these changes occur will help clinicians and individuals better utilize aerobic exercise to facilitate adaptive behaviour changes, mitigate the negative affects of aging and disease on

the brain, and maximize the benefits of active lifestyles.

Appendix A

Questionnaires

The following questionnaires were administered in the first longitudinal experiment discussed in this thesis (see chapters 3, 4, and 5) and are included here for reference. They are discussed in more detail in chapter 2.

1. Edinburgh Handedness Inventory
2. Modified Baecke Questionnaire
3. International Physical Activity Questionnaire (IPAQ)
4. Rey Verbal Learning Test (RVLT)
5. Center for Epidemiologic Studies Depression Scale (CES-D)

Edinburgh Handedness Inventory

Your Initials:_____

Please indicate with a check (✓) your preference in using your left or right hand in the following tasks.

Where the preference is so strong you would never use the other hand, unless absolutely forced to, put two checks (✓✓).

If you are indifferent, put one check in each column (✓ | ✓).

Some of the activities require both hands. In these cases, the part of the task or object for which hand preference is wanted is indicated in parentheses.

Task / Object	Left Hand	Right Hand
1. Writing		
2. Drawing		
3. Throwing		
4. Scissors		
5. Toothbrush		
6. Knife (without fork)		
7. Spoon		
8. Broom (upper hand)		
9. Striking a Match (match)		
10. Opening a Box (lid)		
Total checks:	LH =	RH =
Cumulative Total	CT = LH + RH =	
Difference	D = RH – LH =	
Result	R = (D / CT) × 100 =	
Interpretation: (Left Handed: R < -40) (Ambidextrous: -40 ≤ R ≤ +40) (Right Handed: R > +40)		

APPENDIX

Modified Baecke Questionnaire

1.	What is your main occupation? ...		1 - 3 - 5
2.	At work I sit ...		
	never/seldom/sometimes/often/always		5 - 4 - 3 - 2 - 1
3.	At work I stand ...		
	never/seldom/sometimes/often/always		1 - 2 - 3 - 4 - 5
4.	At work I walk ...		
	never/seldom/sometimes/often/always		1 - 2 - 3 - 4 - 5
5.	At work I lift heavy loads ...		
	never/seldom/sometimes/often/very often		1 - 2 - 3 - 4 - 5
6.	After work I am tired ...		
	never/seldom/sometimes/often/very often		1 - 2 - 3 - 4 - 5
7.	At work I sweat ...		
	never/seldom/sometimes/often/very often		1 - 2 - 3 - 4 - 5
8.	In comparison with others of my own age I think my work is physically ...		
	much lighter/lighter/as heavy/heavier/much heavier		1 - 2 - 3 - 4 - 5
9.	Do you play sport? yes/no		
	If yes:		
	– which sport do you play most frequently? ...		1 - 3 - 5
	– how many hours a week?	<1/1–2/2–3/3–4/>4	1 - 2 - 3 - 4 - 5
	– how many months a year:	>1/1–3/4–6/7–9/>9	1 - 2 - 3 - 4 - 5
	If you play a second sport·		
	– which sport is it? ...		1 - 3 - 5
	– how many hours a week?	<1/1–2/2–3/3–4/>4	1 - 2 - 3 - 4 - 5
	– how many months a year?	<1/1–3/4–6/7–9/>9	1 - 2 - 3 - 4 - 5
10.	In comparison with others of my own age I think my physical activity during leisure time is ...		
	much less/less/the same/more/much more		1 - 2 - 3 - 4 - 5
11	During leisure time I sweat ...		
	never/seldom/sometimes/often/very often		1 - 2 - 3 - 4 - 5
12.	During leisure time I play sport ..		
	never/seldom/sometimes/often/very often		1 - 2 - 3 - 4 - 5
13.	During leisure time I watch television ...		
	never/seldom/sometimes/often/very often		5 - 4 - 3 - 2 - 1
14.	During leisure time I walk ...		
	never/seldom/sometimes/often/very often		1 - 2 - 3 - 4 - 5
15.	During leisure time I cycle ...		
	never/seldom/sometimes/often/very often		1 - 2 - 3 - 4 - 5
16.	How many minutes per day do you walk and/or		
	cycle to and from work, school and shopping?	<5/5–15/15–30/30–45/>45	1 - 2 - 3 - 4 - 5
*17.	During leisure time I do do-it-yourself activities ...		
	never/seldom/sometimes/often/very often		1 - 2 - 3 - 4 - 5
*18.	During leisure time I work in the garden ...		
	never/seldom/sometimes/often/very often		1 - 2 - 3 - 4 - 5
*19.	How many hours per day do you sleep on average?	≤5/6/7/8/≥9	5 - 4 - 3 - 2 - 1

* Questions 17–19 were added to the original questionnaire.

Calculation of the score for question 9

If type of sport = 1 then Intensity = 0.76
3 1.26
5 1.76

If number of hours a week = <1 then Time = 0.5
1–2 1.5
2–3 2.5
3–4 3.5
>4 4.5

If number of months a year = <1 then Proportion = 0.04
1–3 0.17
4–6 0.42
7–9 0.67
>9 0.92

Question 9 = (Intensity$_1$*Time$_1$*Proportion$_1$) + (Intensity$_2$*Time$_2$*Proportion$_2$) = 0/0.01–<4/4–<8/8–<12/≥12* 1 - 2 - 3 - 4 - 5
* 0 is given to people who do not play sport.

Calculation of the indices of physical activity

WORK INDEX = (I1 + I2 + I3 + I4 + I5 + I6 + I7 + I8)/8

SPORTS INDEX = (I9 + I10 + I11 + I12)/4

LEISURE TIME INDEX = (I13 + I14 + I15 + I16 + I17 + I18 + I19)/7

TOTAL INDEX = work index + sports index + leisure time index

INTERNATIONAL PHYSICAL ACTIVITY QUESTIONNAIRE (October 2002)

LONG LAST 7 DAYS SELF-ADMINISTERED FORMAT

FOR USE WITH YOUNG AND MIDDLE-AGED ADULTS (15-69 years)

The International Physical Activity Questionnaires (IPAQ) comprises a set of 4 questionnaires. Long (5 activity domains asked independently) and short (4 generic items) versions for use by either telephone or self-administered methods are available. The purpose of the questionnaires is to provide common instruments that can be used to obtain internationally comparable data on health–related physical activity.

Background on IPAQ

The development of an international measure for physical activity commenced in Geneva in 1998 and was followed by extensive reliability and validity testing undertaken across 12 countries (14 sites) during 2000. The final results suggest that these measures have acceptable measurement properties for use in many settings and in different languages, and are suitable for national population-based prevalence studies of participation in physical activity.

Using IPAQ

Use of the IPAQ instruments for monitoring and research purposes is encouraged. It is recommended that no changes be made to the order or wording of the questions as this will affect the psychometric properties of the instruments.

Translation from English and Cultural Adaptation

Translation from English is encouraged to facilitate worldwide use of IPAQ. Information on the availability of IPAQ in different languages can be obtained at www.ipaq.ki.se. If a new translation is undertaken we highly recommend using the prescribed back translation methods available on the IPAQ website. If possible please consider making your translated version of IPAQ available to others by contributing it to the IPAQ website. Further details on translation and cultural adaptation can be downloaded from the website.

Further Developments of IPAQ

International collaboration on IPAQ is on-going and an ***International Physical Activity Prevalence Study*** is in progress. For further information see the IPAQ website.

More Information

More detailed information on the IPAQ process and the research methods used in the development of IPAQ instruments is available at www.ipaq.ki.se and Booth, M.L. (2000). *Assessment of Physical Activity: An International Perspective.* Research Quarterly for Exercise and Sport, 71 (2): s114-20. Other scientific publications and presentations on the use of IPAQ are summarized on the website.

INTERNATIONAL PHYSICAL ACTIVITY QUESTIONNAIRE

We are interested in finding out about the kinds of physical activities that people do as part of their everyday lives. The questions will ask you about the time you spent being physically active in the **last 7 days**. Please answer each question even if you do not consider yourself to be an active person. Please think about the activities you do at work, as part of your house and yard work, to get from place to place, and in your spare time for recreation, exercise or sport.

Think about all the **vigorous** and **moderate** activities that you did in the **last 7 days**. **Vigorous** physical activities refer to activities that take hard physical effort and make you breathe much harder than normal. **Moderate** activities refer to activities that take moderate physical effort and make you breathe somewhat harder than normal.

PART 1: JOB-RELATED PHYSICAL ACTIVITY

The first section is about your work. This includes paid jobs, farming, volunteer work, course work, and any other unpaid work that you did outside your home. Do not include unpaid work you might do around your home, like housework, yard work, general maintenance, and caring for your family. These are asked in Part 3.

1. Do you currently have a job or do any unpaid work outside your home?

   ☐ Yes

   ☐ No → ***Skip to PART 2: TRANSPORTATION***

The next questions are about all the physical activity you did in the **last 7 days** as part of your paid or unpaid work. This does not include traveling to and from work.

2. During the **last 7 days**, on how many days did you do **vigorous** physical activities like heavy lifting, digging, heavy construction, or climbing up stairs **as part of your work**? Think about only those physical activities that you did for at least 10 minutes at a time.

   _____ **days per week**

   ☐ No vigorous job-related physical activity → ***Skip to question 4***

3. How much time did you usually spend on one of those days doing **vigorous** physical activities as part of your work?

   _____ **hours per day**
   _____ **minutes per day**

4. Again, think about only those physical activities that you did for at least 10 minutes at a time. During the **last 7 days**, on how many days did you do **moderate** physical activities like carrying light loads **as part of your work**? Please do not include walking.

   _____ **days per week**

   ☐ No moderate job-related physical activity → ***Skip to question 6***

5. How much time did you usually spend on one of those days doing **moderate** physical activities as part of your work?

_____ **hours per day**
_____ **minutes per day**

6. During the **last 7 days**, on how many days did you **walk** for at least 10 minutes at a time **as part of your work**? Please do not count any walking you did to travel to or from work.

_____ **days per week**

☐ No job-related walking → ***Skip to PART 2: TRANSPORTATION***

7. How much time did you usually spend on one of those days **walking** as part of your work?

_____ **hours per day**
_____ **minutes per day**

PART 2: TRANSPORTATION PHYSICAL ACTIVITY

These questions are about how you traveled from place to place, including to places like work, stores, movies, and so on.

8. During the **last 7 days**, on how many days did you **travel in a motor vehicle** like a train, bus, car, or tram?

_____ **days per week**

☐ No traveling in a motor vehicle → ***Skip to question 10***

9. How much time did you usually spend on one of those days **traveling** in a train, bus, car, tram, or other kind of motor vehicle?

_____ **hours per day**
_____ **minutes per day**

Now think only about the **bicycling** and **walking** you might have done to travel to and from work, to do errands, or to go from place to place.

10. During the **last 7 days**, on how many days did you **bicycle** for at least 10 minutes at a time to go **from place to place**?

_____ **days per week**

☐ No bicycling from place to place → ***Skip to question 12***

11. How much time did you usually spend on one of those days to **bicycle** from place to place?

_____ **hours per day**
_____ **minutes per day**

12. During the **last 7 days**, on how many days did you **walk** for at least 10 minutes at a time to go **from place to place**?

_____ **days per week**

☐ No walking from place to place → ***Skip to PART 3: HOUSEWORK, HOUSE MAINTENANCE, AND CARING FOR FAMILY***

13. How much time did you usually spend on one of those days **walking** from place to place?

_____ **hours per day**
_____ **minutes per day**

PART 3: HOUSEWORK, HOUSE MAINTENANCE, AND CARING FOR FAMILY

This section is about some of the physical activities you might have done in the **last 7 days** in and around your home, like housework, gardening, yard work, general maintenance work, and caring for your family.

14. Think about only those physical activities that you did for at least 10 minutes at a time. During the **last 7 days**, on how many days did you do **vigorous** physical activities like heavy lifting, chopping wood, shoveling snow, or digging **in the garden or yard**?

_____ **days per week**

☐ No vigorous activity in garden or yard → ***Skip to question 16***

15. How much time did you usually spend on one of those days doing **vigorous** physical activities in the garden or yard?

_____ **hours per day**
_____ **minutes per day**

16. Again, think about only those physical activities that you did for at least 10 minutes at a time. During the **last 7 days**, on how many days did you do **moderate** activities like carrying light loads, sweeping, washing windows, and raking **in the garden or yard**?

_____ **days per week**

☐ No moderate activity in garden or yard → ***Skip to question 18***

17. How much time did you usually spend on one of those days doing **moderate** physical activities in the garden or yard?

_____ **hours per day**
_____ **minutes per day**

18. Once again, think about only those physical activities that you did for at least 10 minutes at a time. During the **last 7 days**, on how many days did you do **moderate** activities like carrying light loads, washing windows, scrubbing floors and sweeping **inside your home**?

_____ **days per week**

☐ No moderate activity inside home → ***Skip to PART 4: RECREATION, SPORT AND LEISURE-TIME PHYSICAL ACTIVITY***

19. How much time did you usually spend on one of those days doing **moderate** physical activities inside your home?

_____ **hours per day**
_____ **minutes per day**

PART 4: RECREATION, SPORT, AND LEISURE-TIME PHYSICAL ACTIVITY

This section is about all the physical activities that you did in the **last 7 days** solely for recreation, sport, exercise or leisure. Please do not include any activities you have already mentioned.

20. Not counting any walking you have already mentioned, during the **last 7 days**, on how many days did you **walk** for at least 10 minutes at a time **in your leisure time**?

_____ **days per week**

☐ No walking in leisure time → ***Skip to question 22***

21. How much time did you usually spend on one of those days **walking** in your leisure time?

_____ **hours per day**
_____ **minutes per day**

22. Think about only those physical activities that you did for at least 10 minutes at a time. During the **last 7 days**, on how many days did you do **vigorous** physical activities like aerobics, running, fast bicycling, or fast swimming **in your leisure time**?

_____ **days per week**

☐ No vigorous activity in leisure time → ***Skip to question 24***

23. How much time did you usually spend on one of those days doing **vigorous** physical activities in your leisure time?

_____ **hours per day**
_____ **minutes per day**

24. Again, think about only those physical activities that you did for at least 10 minutes at a time. During the **last 7 days**, on how many days did you do **moderate** physical activities like bicycling at a regular pace, swimming at a regular pace, and doubles tennis **in your leisure time**?

_____ **days per week**

☐ No moderate activity in leisure time → ***Skip to PART 5: TIME SPENT SITTING***

25. How much time did you usually spend on one of those days doing **moderate** physical activities in your leisure time?
_____ **hours per day**
_____ **minutes per day**

PART 5: TIME SPENT SITTING

The last questions are about the time you spend sitting while at work, at home, while doing course work and during leisure time. This may include time spent sitting at a desk, visiting friends, reading or sitting or lying down to watch television. Do not include any time spent sitting in a motor vehicle that you have already told me about.

26. During the **last 7 days**, how much time did you usually spend **sitting** on a **weekday**?

_____ **hours per day**
_____ **minutes per day**

27. During the **last 7 days**, how much time did you usually spend **sitting** on a **weekend day**?

_____ **hours per day**
_____ **minutes per day**

This is the end of the questionnaire, thank you for participating.

REY AUDITORY VERBAL LEARNING

Participant ID:_____

I am going to read a list of words. Listen carefully, when I stop repeat back as many words as you can remember. It doesn't matter what order you repeat them, just try to remember as many as possible.
Read the 15 words on list A with a 1-sec interval between words. Check off the words recalled and give no feedback regarding the number of correct responses.
After the participant has indicated they can remember no more words, reread the list and give the instruction "Now I am going to read the same list again, and once again when I stop I want you to tell me as many words as you can remember, including words you said the first time".
The list is reread for trial 3-5 using the same instruction as in trial 2.

LIST A	A1		A2		A3		A4		A5	LIST B	B1	A6		A7
Drum		Drum		Drum		Drum		Drum		Desk			Drum	
Curtain		Curtain		Curtain		Curtain		Curtain		Ranger			Curtain	
Bell		Bell		Bell		Bell		Bell		Bird			Bell	
Coffee		Coffee		Coffee		Coffee		Coffee		Shoe			Coffee	
School		School		School		School		School		Stove			School	
Parent		Parent		Parent		Parent		Parent		Mountain			Parent	
Moon		Moon		Moon		Moon		Moon		Glasses			Moon	
Garden		Garden		Garden		Garden		Garden		Towel			Garden	
Hat		Hat		Hat		Hat		Hat		Cloud			Hat	
Farmer		Farmer		Farmer		Farmer		Farmer		Boat			Farmer	
Nose		Nose		Nose		Nose		Nose		Lamb			Nose	
Turkey		Turkey		Turkey		Turkey		Turkey		Gun			Turkey	
Colour		Colour		Colour		Colour		Colour		Pencil			Colour	
House		House		House		House		House		Church			House	
River		River		River		River		River		Fist			River	
Total correct														

After trial 5, read list B with instructions "Now I am going to read a second list of words, listen carefully and repeat back as many words as you can remember. It doesn't matter what order you repeat the, just try and remember as many words as possible. Immediately after trial B, ask the participant to recall as many words from the first list as s/he can (Trail 6) without further presentation of those words. After a 20minute delay, the subject is again asked to recall the words from the first list: A while ago I read a list of words to you several times, and you had to repeat them back to me. Tell me the words from that list"

Total A1- A5_____
Trial A6-A7_____

On completion of the delay trial, the recognition test should be given. The recognition task requires the participant to identify as many words from the list as s/he can and if possible, the specific list of origin. If the participant has reading of at least grade 7 level, ask them to read the list and circle the correct words. If they have difficulty reading, read the list to them and as say “I am going to read some words, some of the words were on the list and some of them weren’t. Tell me each time a word was read to you and if possible whether the word was from the first or second list”.

Ball (A)	Home (SA)	Towel (B)	Boat (B)	Glasses (B)
Window (SA)	Fish (B)	Curtain (A)	Hot (PA)	Stocking (SB)
Hat (A)	Moon (A)	Flower (SA)	Parent (A)	Shoe (B)
Barn (SA)	Tree (PA)	Colour (A)	Water (SA)	Teacher (SA)
Ranger (B)	Balloon (PA)	Desk (B)	Farmer (A)	Stove (B)
Nose (A)	Bird (B)	Gun (B)	Rose (SPA)	Nest (SPB)
Weather (SB)	Mountain (B)	Crayon (SA)	Cloud (B)	Children (SA)
School (A)	Coffee (A)	Church (B)	House (A)	Drum (A)
Hand (PA)	Mouse (PA)	Turkey (A)	Stranger (PB)	Toffee (PA)
Pencil (B)	River (A)	Fountain (PB)	Garden (A)	Lamb (B)

Center for Epidemiologic Studies Depression Scale (CES-D), NIMH

Below is a list of the ways you might have felt or behaved. Please tell me how often you have felt this way during the past week.

	During the Past Week			
	Rarely or none of the time (less than 1 day)	Some or a little of the time (1-2 days)	Occasionally or a moderate amount of time (3-4 days)	Most or all of the time (5-7 days)
1. I was bothered by things that usually don't bother me.	☐	☐	☐	☐
2. I did not feel like eating; my appetite was poor.	☐	☐	☐	☐
3. I felt that I could not shake off the blues even with help from my family or friends.	☐	☐	☐	☐
4. I felt I was just as good as other people.	☐	☐	☐	☐
5. I had trouble keeping my mind on what I was doing.	☐	☐	☐	☐
6. I felt depressed.	☐	☐	☐	☐
7. I felt that everything I did was an effort.	☐	☐	☐	☐
8. I felt hopeful about the future.	☐	☐	☐	☐
9. I thought my life had been a failure.	☐	☐	☐	☐
10. I felt fearful.	☐	☐	☐	☐
11. My sleep was restless.	☐	☐	☐	☐
12. I was happy.	☐	☐	☐	☐
13. I talked less than usual.	☐	☐	☐	☐
14. I felt lonely.	☐	☐	☐	☐
15. People were unfriendly.	☐	☐	☐	☐
16. I enjoyed life.	☐	☐	☐	☐
17. I had crying spells.	☐	☐	☐	☐
18. I felt sad.	☐	☐	☐	☐
19. I felt that people dislike me.	☐	☐	☐	☐
20. I could not get "going."	☐	☐	☐	☐

SCORING: zero for answers in the first column, 1 for answers in the second column, 2 for answers in the third column, 3 for answers in the fourth column. The scoring of positive items is reversed. Possible range of scores is zero to 60, with the higher scores indicating the presence of more symptomatology.

Appendix B

Scanner Sequences

This appendix includes a full listing of the Siemens scanner protocols that describe all of the sequences for imaging data collected as part of this thesis. The details of these sequences are discussed in chapter 2.

B.1 3 Tesla Verio Sequences

1. Localiser
2. Auto align localizer
3. EPI BOLD (resting state)
4. Gradient echo field map
5. Susceptibility weighted imaging (SWI)
6. DESPOT1-HIFI (three sequences)
7. DESPOT2-FM (two sequences)
8. DTI (three sequence)
9. Multi-Echo MPRAGE (two acquisitions)

SIEMENS MAGNETOM Verio syngo MR B17

\\USER\FMRIB Limited Release\Adam Thomas\exercise_protocol\localizer_ALL TRUE AXIAL

TA: 0:13 PAT: Off Voxel size: 1.1×1.0×7.0 mm Rel. SNR: 1.00 SIEMENS: gre

Properties

Prio Recon	Off
Before measurement	
After measurement	
Load to viewer	On
Inline movie	Off
Auto store images	On
Load to stamp segments	Off
Load images to graphic segments	Off
Auto open inline display	Off
Start measurement without further preparation	Off
Wait for user to start	Off
Start measurements	single

Routine

Slice group 1	
Slices	1
Dist. factor	20 %
Position	L0.0 P20.0 H0.0
Orientation	Sagittal
Phase enc. dir.	A >> P
Rotation	0.00 deg
Slice group 2	
Slices	1
Dist. factor	20 %
Position	L0.0 P20.0 H0.0
Orientation	Transversal
Phase enc. dir.	A >> P
Rotation	0.00 deg
Slice group 3	
Slices	1
Dist. factor	20 %
Position	L0.0 P20.0 H0.0
Orientation	Coronal
Phase enc. dir.	R >> L
Rotation	0.00 deg
Phase oversampling	0 %
FoV read	250 mm
FoV phase	100.0 %
Slice thickness	7.0 mm
TR	8.6 ms
TE	4.00 ms
Averages	2
Concatenations	3
Filter	Prescan Normalize, Elliptical filter
Coil elements	HEA;HEP

Contrast

TD	0 ms
MTC	Off
Magn. preparation	None
Flip angle	20 deg
Fat suppr.	None
Water suppr.	None
SWI	Off
Averaging mode	Short term
Reconstruction	Magnitude
Measurements	1
Multiple series	Each measurement

Resolution

Base resolution	256
Phase resolution	90 %
Phase partial Fourier	Off
Interpolation	On
PAT mode	None
Matrix Coil Mode	Auto (CP)
Image Filter	Off
Distortion Corr.	Off
Unfiltered images	Off
Prescan Normalize	On
Normalize	Off
B1 filter	Off
Raw filter	Off
Elliptical filter	On
Mode	Inplane

Geometry

Multi-slice mode	Sequential
Series	Interleaved
Saturation mode	Standard
Special sat.	None
Tim CT mode	Off

System

Body	Off
HEP	On
HEA	On
Positioning mode	REF
Table position	H
Table position	0 mm
MSMA	S - C - T
Sagittal	R >> L
Coronal	A >> P
Transversal	F >> H
Save uncombined	Off
Coil Combine Mode	Adaptive Combine
AutoAlign	---
Auto Coil Select	Default
Shim mode	Tune up
Adjust with body coil	Off
Confirm freq. adjustment	Off
Assume Silicone	Off
? Ref. amplitude 1H	0.000 V
Adjustment Tolerance	Auto
Adjust volume	
Position	Isocenter
Orientation	Transversal
Rotation	0.00 deg
R >> L	350 mm
A >> P	263 mm
F >> H	350 mm

Physio

1st Signal/Mode	None
Segments	1
Dark blood	Off
Resp. control	Off

Inline

Subtract	Off
Liver registration	Off
Std-Dev-Sag	Off

Std-Dev-Cor	Off
Std-Dev-Tra	Off
Std-Dev-Time	Off
MIP-Sag	Off
MIP-Cor	Off
MIP-Tra	Off
MIP-Time	Off
Save original images	On
Wash - In	Off
Wash - Out	Off
TTP	Off
PEI	Off
MIP - time	Off

Sequence

Introduction	On
Dimension	2D
Phase stabilisation	Off
Asymmetric echo	Allowed
Contrasts	1
Bandwidth	320 Hz/Px
Flow comp.	No
Allowed delay	0 s
RF pulse type	Normal
Gradient mode	Normal
Excitation	Slice-sel.
RF spoiling	On

\\USER\FMRIB Limited Release\Adam Thomas\exercise_protocol\AAHScout

TA: 0:14 PAT: 3 Voxel size: 1.6×1.6×1.6 mm Rel. SNR: 1.00 SIEMENS: AALScout

Properties

Prio Recon	Off
Before measurement	
After measurement	
Load to viewer	On
Inline movie	Off
Auto store images	On
Load to stamp segments	On
Load images to graphic segments	On
Auto open inline display	Off
Start measurement without further preparation	Off
Wait for user to start	Off
Start measurements	single

Routine

Slab group 1	
Slabs	1
Dist. factor	20 %
Position	L0.0 P20.0 H0.0
Orientation	Sagittal
Phase enc. dir.	A >> P
Rotation	0 deg
AutoAlign	Head
Phase oversampling	0 %
Slice oversampling	0.0 %
Slices per slab	128
FoV read	260 mm
FoV phase	100.0 %
Slice thickness	1.6 mm
TR	3.15 ms
TE	1.37 ms
Averages	1
Concatenations	1
Filter	Prescan Normalize
Coil elements	HEA;HEP

Contrast

Flip angle	8 deg
Averaging mode	Short term
Reconstruction	Magnitude
Measurements	1

Resolution

Base resolution	160
Phase resolution	100 %
Slice resolution	69 %
Phase partial Fourier	6/8
Slice partial Fourier	6/8
PAT mode	GRAPPA
Accel. factor PE	3
Ref. lines PE	24
Accel. factor 3D	1
Matrix Coil Mode	Auto (Triple)
Reference scan mode	Integrated
Image Filter	Off
Distortion Corr.	Off
Unfiltered images	Off
Prescan Normalize	On
Normalize	Off
B1 filter	Off
Raw filter	Off
Elliptical filter	Off

Geometry

Multi-slice mode	Sequential
Series	Ascending

System

Body	Off
HEP	On
HEA	On
SP4	Off
SP2	Off
SP8	Off
SP6	Off
SP3	Off
SP1	Off
SP7	Off
SP5	Off
Positioning mode	REF
Table position	H
Table position	0 mm
MSMA	S - C - T
Sagittal	R >> L
Coronal	A >> P
Transversal	F >> H
Save uncombined	Off
Coil Combine Mode	Adaptive Combine
Auto Coil Select	Off
Shim mode	Tune up
Adjust with body coil	Off
Confirm freq. adjustment	Off
Assume Silicone	Off
? Ref. amplitude 1H	0.000 V
Adjustment Tolerance	Auto
Adjust volume	
Position	Isocenter
Orientation	Transversal
Rotation	0.00 deg
R >> L	350 mm
A >> P	263 mm
F >> H	350 mm

Inline

Time to center	6.2 s

Sequence

Introduction	On
Dimension	3D
Asymmetric echo	Weak
Contrasts	1
Bandwidth	550 Hz/Px
RF pulse type	Fast
Gradient mode	Normal
Excitation	Non-sel.
RF spoiling	On

SIEMENS MAGNETOM Verio syngo MR B17

\\USER\FMRIB Limited Release\Adam Thomas\exercise_protocol\ep2d_resting_P2

TA: 5:16 PAT: 2 Voxel size: 3.0×3.0×3.0 mm Rel. SNR: 1.00 SIEMENS: ep2d_bold

Properties

Prio Recon	Off
Before measurement	
After measurement	
Load to viewer	On
Inline movie	Off
Auto store images	On
Load to stamp segments	Off
Load images to graphic segments	Off
Auto open inline display	Off
Start measurement without further preparation	On
Wait for user to start	Off
Start measurements	single

Routine

Slice group 1	
Slices	44
Dist. factor	0 %
Position	L4.3 P10.2 H28.4
Orientation	T > S0.2
Phase enc. dir.	A >> P
Rotation	0.00 deg
Phase oversampling	0 %
FoV read	192 mm
FoV phase	100.0 %
Slice thickness	3.0 mm
TR	2410 ms
TE	30 ms
Averages	1
Concatenations	1
Filter	Raw filter
Coil elements	HEA;HEP

Contrast

MTC	Off
Flip angle	90 deg
Fat suppr.	Fat sat.
Averaging mode	Long term
Reconstruction	Magnitude
Measurements	128
Delay in TR	0 ms
Multiple series	Off

Resolution

Base resolution	64
Phase resolution	100 %
Phase partial Fourier	7/8
Interpolation	Off
PAT mode	GRAPPA
Accel. factor PE	2
Ref. lines PE	24
Matrix Coil Mode	Auto (Triple)
Reference scan mode	Separate
Distortion Corr.	Off
Prescan Normalize	Off
Raw filter	On
Intensity	Weak
Slope	25
Elliptical filter	Off
Hamming	Off

Geometry

Multi-slice mode	Interleaved
Series	Interleaved
Special sat.	None

System

Body	Off
HEP	On
HEA	On
SP4	Off
SP2	Off
SP8	Off
SP6	Off
SP3	Off
SP1	Off
SP7	Off
SP5	Off
Positioning mode	FIX
Table position	H
Table position	0 mm
MSMA	S - C - T
Sagittal	R >> L
Coronal	A >> P
Transversal	F >> H
Coil Combine Mode	Adaptive Combine
AutoAlign	---
Auto Coil Select	Default
Shim mode	Standard
Adjust with body coil	Off
Confirm freq. adjustment	Off
Assume Silicone	Off
? Ref. amplitude 1H	0.000 V
Adjustment Tolerance	Auto
Adjust volume	
Position	L4.3 P10.2 H28.4
Orientation	T > S0.2
Rotation	0.00 deg
R >> L	192 mm
A >> P	192 mm
F >> H	132 mm

Physio

1st Signal/Mode	None

BOLD

GLM Statistics	Off
Dynamic t-maps	Off
Starting ignore meas	0
Ignore after transition	0
Model transition states	On
Temp. highpass filter	On
Threshold	4.00
Paradigm size	20
Meas[1]	Baseline
Meas[2]	Baseline
Meas[3]	Baseline
Meas[4]	Baseline
Meas[5]	Baseline
Meas[6]	Baseline
Meas[7]	Baseline
Meas[8]	Baseline
Meas[9]	Baseline
Meas[10]	Baseline
Meas[11]	Active
Meas[12]	Active

Meas[13]	Active
Meas[14]	Active
Meas[15]	Active
Meas[16]	Active
Meas[17]	Active
Meas[18]	Active
Meas[19]	Active
Meas[20]	Active
Motion correction	Off
Spatial filter	Off

Sequence

Introduction	Off
Bandwidth	2368 Hz/Px
Free echo spacing	Off
Echo spacing	0.52 ms
EPI factor	64
RF pulse type	Normal
Gradient mode	Fast*

\\USER\FMRIB Limited Release\Adam Thomas\exercise_protocol\gre_field_mapping

TA: 0:54 Voxel size: 3.0×3.0×3.0 mm Rel. SNR: 1.00 SIEMENS: gre_field_mapping

Properties

Prio Recon	Off
Before measurement	
After measurement	
Load to viewer	On
Inline movie	Off
Auto store images	On
Load to stamp segments	Off
Load images to graphic segments	Off
Auto open inline display	Off
Start measurement without further preparation	On
Wait for user to start	Off
Start measurements	single

Routine

Slice group 1	
Slices	36
Dist. factor	25 %
Position	L4.3 P10.2 H28.4
Orientation	T > S0.2
Phase enc. dir.	R >> L
Rotation	90.00 deg
Phase oversampling	0 %
FoV read	192 mm
FoV phase	100.0 %
Slice thickness	3.0 mm
TR	400 ms
TE 1	5.19 ms
TE 2	7.65 ms
Averages	1
Concatenations	1
Filter	None
Coil elements	HEA;HEP

Contrast

MTC	Off
Flip angle	60 deg
Fat suppr.	None
Averaging mode	Long term
Reconstruction	Magn./Phase
Measurements	1
Multiple series	Off

Resolution

Base resolution	64
Phase resolution	100 %
Phase partial Fourier	Off
Interpolation	Off
Matrix Coil Mode	Auto (CP)
Image Filter	Off
Distortion Corr.	Off
Prescan Normalize	Off
Normalize	Off
B1 filter	Off
Raw filter	Off
Elliptical filter	Off

Geometry

Multi-slice mode	Interleaved
Series	Interleaved
Special sat.	None

System

Body	Off
HEP	On
HEA	On
SP4	Off
SP2	Off
SP8	Off
SP6	Off
SP3	Off
SP1	Off
SP7	Off
SP5	Off
Positioning mode	FIX
Table position	H
Table position	0 mm
MSMA	S - C - T
Sagittal	R >> L
Coronal	A >> P
Transversal	F >> H
Save uncombined	Off
Coil Combine Mode	Sum of Squares
AutoAlign	---
Auto Coil Select	Default
Shim mode	Standard
Adjust with body coil	Off
Confirm freq. adjustment	Off
Assume Silicone	Off
? Ref. amplitude 1H	0.000 V
Adjustment Tolerance	Auto
Adjust volume	
Position	L4.3 P10.2 H28.4
Orientation	T > S0.2
Rotation	90.00 deg
A >> P	192 mm
R >> L	192 mm
F >> H	135 mm

Sequence

Introduction	On
Dimension	2D
Asymmetric echo	Off
Contrasts	2
Bandwidth	260 Hz/Px
Flow comp.	Yes
RF pulse type	Normal
Gradient mode	Normal
RF spoiling	On

\\USER\FMRIB Limited Release\Adam Thomas\exercise_protocol\t2_fl3d_tra_p2_swi_TE_4.92ms

TA: 3:53 PAT: 2 Voxel size: 1.0×1.0×2.0 mm Rel. SNR: 1.00 SIEMENS: gre

Properties

Prio Recon	Off
Before measurement	
After measurement	
Load to viewer	On
Inline movie	Off
Auto store images	On
Load to stamp segments	Off
Load images to graphic segments	Off
Auto open inline display	Off
Start measurement without further preparation	On
Wait for user to start	Off
Start measurements	single

Routine

Slab group 1	
Slabs	1
Dist. factor	20 %
Position	Isocenter
Orientation	Transversal
Phase enc. dir.	R >> L
Rotation	90.00 deg
Phase oversampling	0 %
Slice oversampling	12.5 %
Slices per slab	64
FoV read	256 mm
FoV phase	75.0 %
Slice thickness	2.00 mm
TR	30 ms
TE 1	4.92 ms
TE 2	24.60 ms
Averages	1
Concatenations	1
Filter	Prescan Normalize
Coil elements	HEA;HEP

Contrast

MTC	Off
Magn. preparation	None
Flip angle	15 deg
Fat suppr.	None
Water suppr.	None
SWI	Off
Averaging mode	Short term
Reconstruction	Magn./Phase
Measurements	1
Multiple series	Each measurement

Resolution

Base resolution	256
Phase resolution	100 %
Slice resolution	100 %
Phase partial Fourier	Off
Slice partial Fourier	Off
Interpolation	Off
PAT mode	GRAPPA
Accel. factor PE	2
Ref. lines PE	24
Accel. factor 3D	1
Matrix Coil Mode	Auto (Triple)
Reference scan mode	Integrated
Image Filter	Off
Distortion Corr.	Off
Unfiltered images	Off
Prescan Normalize	On
Normalize	Off
B1 filter	Off
Raw filter	Off
Elliptical filter	Off

Geometry

Multi-slice mode	Interleaved
Series	Interleaved
Saturation mode	Standard
Special sat.	None
Tim CT mode	Off

System

Body	Off
HEP	On
HEA	On
Positioning mode	REF
Table position	H
Table position	0 mm
MSMA	S - C - T
Sagittal	R >> L
Coronal	A >> P
Transversal	F >> H
Save uncombined	Off
Coil Combine Mode	Adaptive Combine
AutoAlign	---
Auto Coil Select	Default
Shim mode	Standard
Adjust with body coil	Off
Confirm freq. adjustment	Off
Assume Silicone	Off
? Ref. amplitude 1H	0.000 V
Adjustment Tolerance	Auto
Adjust volume	
Position	Isocenter
Orientation	Transversal
Rotation	90.00 deg
A >> P	256 mm
R >> L	192 mm
F >> H	128 mm

Physio

1st Signal/Mode	None
Segments	1
Dark blood	Off
Resp. control	Off

Inline

Subtract	Off
Liver registration	Off
Std-Dev-Sag	Off
Std-Dev-Cor	Off
Std-Dev-Tra	Off
Std-Dev-Time	Off
MIP-Sag	Off
MIP-Cor	Off
MIP-Tra	Off
MIP-Time	Off

Save original images	On
Wash - In	Off
Wash - Out	Off
TTP	Off
PEI	Off
MIP - time	Off

Sequence

Introduction	On
Dimension	3D
Elliptical scanning	Off
Phase stabilisation	Off
Asymmetric echo	Off
Contrasts	2
Bandwidth 1	200 Hz/Px
Bandwidth 2	200 Hz/Px
Flow comp. 1	No
Flow comp. 2	No
Readout mode	Bipolar
Allowed delay	0 s
RF pulse type	Fast
Gradient mode	Fast
Excitation	Slab-sel.
RF spoiling	On

\\USER\FMRIB Limited Release\Adam Thomas\exercise_protocol\despot1_tr56_fa18

TA: 5:54 Voxel size: 1.7×1.7×1.7 mm Rel. SNR: 1.00 USER: sk_despot1_maxSp

Properties

Prio Recon	Off
Before measurement	
After measurement	
Load to viewer	On
Inline movie	Off
Auto store images	On
Load to stamp segments	Off
Load images to graphic segments	Off
Auto open inline display	Off
Start measurement without further preparation	On
Wait for user to start	On
Start measurements	single

Routine

Slab group 1	
Slabs	1
Dist. factor	20 %
Position	R1.7 P7.4 F10.6
Orientation	Sagittal
Phase enc. dir.	A >> P
Rotation	0.00 deg
Phase oversampling	0 %
Slice oversampling	0.0 %
Slices per slab	96
FoV read	220 mm
FoV phase	100.0 %
Slice thickness	1.70 mm
TR	5.6 ms
TE	2.6 ms
Averages	1
Concatenations	1
Filter	Raw filter
Coil elements	HEA;HEP

Contrast

Flip angle	18 deg
Averaging mode	Short term
Reconstruction	Magnitude
Measurements	8
Pause after meas. 1	0.0 s
Pause after meas. 2	0.0 s
Pause after meas. 3	0.0 s
Pause after meas. 4	0.0 s
Pause after meas. 5	0.0 s
Pause after meas. 6	0.0 s
Pause after meas. 7	0.0 s
Multiple series	Off

Resolution

Base resolution	128
Phase resolution	100 %
Slice resolution	100 %
Phase partial Fourier	6/8
Slice partial Fourier	6/8
Interpolation	Off
Matrix Coil Mode	Auto (CP)
Image Filter	Off
Distortion Corr.	Off
Prescan Normalize	Off
Normalize	Off
B1 filter	Off
Raw filter	On
Intensity	Weak
Slope	25
Elliptical filter	Off

Geometry

Multi-slice mode	Sequential
Series	Ascending

System

Body	Off
HEP	On
HEA	On
SP4	Off
SP2	Off
SP8	Off
SP6	Off
SP3	Off
SP1	Off
SP7	Off
SP5	Off
Positioning mode	FIX
Table position	H
Table position	0 mm
MSMA	S - C - T
Sagittal	R >> L
Coronal	A >> P
Transversal	F >> H
Save uncombined	Off
Coil Combine Mode	Adaptive Combine
AutoAlign	---
Auto Coil Select	Default
Shim mode	Standard
Adjust with body coil	Off
Confirm freq. adjustment	Off
Assume Silicone	Off
? Ref. amplitude 1H	0.000 V
Adjustment Tolerance	Auto
Adjust volume	
! Position	R4.5 P6.2 F19.1
! Orientation	Sagittal
! Rotation	0.00 deg
! F >> H	190 mm
! A >> P	46 mm
! R >> L	75 mm

Physio

1st Signal/Mode	None

Inline

Subtract	Off
Std-Dev-Sag	Off
Std-Dev-Cor	Off
Std-Dev-Tra	Off
Std-Dev-Time	Off
MIP-Sag	Off
MIP-Cor	Off
MIP-Tra	Off
MIP-Time	Off
Save original images	On

Sequence

Introduction	Off
Dimension	3D

Elliptical scanning	Off
Contrasts	1
Bandwidth	400 Hz/Px
RF pulse type	Low SAR
Gradient mode	Fast*
RF spoiling	On
IR Mode	Off
Dummy pulses	1000
Incremented FA Mode	On
mcDESPOT FA Mode	On
Number of FA Increments	8
RF pulse duration	1.1 ms
RF pulse TBW	2.7
RF Spoil Increment	36.7 deg
Duration of Spoiler Gradient X	2070
Duration of Spoiler Gradient Y	340
Duration of Spoiler Gradient Z	330
Scale factor	2.0
Baby Mode	Off

\\USER\FMRIB Limited Release\Adam Thomas\exercise_protocol\irdespot1_tr56_fa5_TI450_fr

TA: 1:18 Voxel size: 1.7×1.7×3.4 mm Rel. SNR: 1.00 USER: sk_despot1_maxSp

Properties

Prio Recon	Off
Before measurement	
After measurement	
Load to viewer	On
Inline movie	Off
Auto store images	On
Load to stamp segments	Off
Load images to graphic segments	Off
Auto open inline display	Off
Start measurement without further preparation	Off
Wait for user to start	Off
Start measurements	single

Routine

Slab group 1	
Slabs	1
Dist. factor	20 %
Position	R1.7 P7.4 F10.6
Orientation	Sagittal
Phase enc. dir.	A >> P
Rotation	0.00 deg
Phase oversampling	0 %
Slice oversampling	0.0 %
Slices per slab	48
FoV read	220 mm
FoV phase	100.0 %
Slice thickness	3.40 mm
TR	5.6 ms
TE	2.6 ms
Averages	1
Concatenations	1
Filter	Raw filter
Coil elements	HEA;HEP

Contrast

Flip angle	5 deg
Averaging mode	Short term
Reconstruction	Magnitude
Measurements	1
Multiple series	Off

Resolution

Base resolution	128
Phase resolution	100 %
Slice resolution	100 %
Phase partial Fourier	Off
Slice partial Fourier	Off
Interpolation	Off
Matrix Coil Mode	Auto (CP)
Image Filter	Off
Distortion Corr.	Off
Prescan Normalize	Off
Normalize	Off
B1 filter	Off
Raw filter	On
Intensity	Weak
Slope	25
Elliptical filter	Off

Geometry

Multi-slice mode	Sequential
Series	Ascending

System

Body	Off
HEP	On
HEA	On
SP4	Off
SP2	Off
SP8	Off
SP6	Off
SP3	Off
SP1	Off
SP7	Off
SP5	Off
Positioning mode	FIX
Table position	H
Table position	0 mm
MSMA	S - C - T
Sagittal	R >> L
Coronal	A >> P
Transversal	F >> H
Save uncombined	Off
Coil Combine Mode	Adaptive Combine
AutoAlign	---
Auto Coil Select	Default
Shim mode	Standard
Adjust with body coil	Off
Confirm freq. adjustment	Off
Assume Silicone	Off
? Ref. amplitude 1H	0.000 V
Adjustment Tolerance	Auto
Adjust volume	
Position	R1.7 P7.4 F10.6
Orientation	Sagittal
Rotation	0.00 deg
F >> H	220 mm
A >> P	220 mm
R >> L	164 mm

Physio

1st Signal/Mode	None

Inline

Subtract	Off
Std-Dev-Sag	Off
Std-Dev-Cor	Off
Std-Dev-Tra	Off
Std-Dev-Time	Off
MIP-Sag	Off
MIP-Cor	Off
MIP-Tra	Off
MIP-Time	Off
Save original images	On

Sequence

Introduction	Off
Dimension	3D
Elliptical scanning	Off
Contrasts	1
Bandwidth	400 Hz/Px
RF pulse type	Low SAR
Gradient mode	Fast*
RF spoiling	On
IR Mode	On

Inversion time	450 ms
RF pulse duration	1.1 ms
RF pulse TBW	2.7
RF Spoil Increment	36.7 deg
Duration of Spoiler Gradient X	2070
Duration of Spoiler Gradient Y	340
Duration of Spoiler Gradient Z	330
Scale factor	2.0
Baby Mode	Off

\\USER\FMRIB Limited Release\Adam Thomas\exercise_protocol\irdespot1_tr56_fa5_TI450_fr

TA: 1:18 Voxel size: 1.7×1.7×3.4 mm Rel. SNR: 1.00 USER: sk_despot1_maxSp

Properties

Prio Recon	Off
Before measurement	
After measurement	
Load to viewer	On
Inline movie	Off
Auto store images	On
Load to stamp segments	Off
Load images to graphic segments	Off
Auto open inline display	Off
Start measurement without further preparation	Off
Wait for user to start	Off
Start measurements	single

Routine

Slab group 1	
Slabs	1
Dist. factor	20 %
Position	R1.7 P7.4 F10.6
Orientation	Sagittal
Phase enc. dir.	A >> P
Rotation	0.00 deg
Phase oversampling	0 %
Slice oversampling	0.0 %
Slices per slab	48
FoV read	220 mm
FoV phase	100.0 %
Slice thickness	3.40 mm
TR	5.6 ms
TE	2.6 ms
Averages	1
Concatenations	1
Filter	Raw filter
Coil elements	HEA;HEP

Contrast

Flip angle	5 deg
Averaging mode	Short term
Reconstruction	Magnitude
Measurements	1
Multiple series	Off

Resolution

Base resolution	128
Phase resolution	100 %
Slice resolution	100 %
Phase partial Fourier	Off
Slice partial Fourier	Off
Interpolation	Off
Matrix Coil Mode	Auto (CP)
Image Filter	Off
Distortion Corr.	Off
Prescan Normalize	Off
Normalize	Off
B1 filter	Off
Raw filter	On
Intensity	Weak
Slope	25
Elliptical filter	Off

Geometry

Multi-slice mode	Sequential
Series	Ascending

System

Body	Off
HEP	On
HEA	On
SP4	Off
SP2	Off
SP8	Off
SP6	Off
SP3	Off
SP1	Off
SP7	Off
SP5	Off
Positioning mode	FIX
Table position	H
Table position	0 mm
MSMA	S - C - T
Sagittal	R >> L
Coronal	A >> P
Transversal	F >> H
Save uncombined	Off
Coil Combine Mode	Adaptive Combine
AutoAlign	---
Auto Coil Select	Default
Shim mode	Standard
Adjust with body coil	Off
Confirm freq. adjustment	Off
Assume Silicone	Off
? Ref. amplitude 1H	0.000 V
Adjustment Tolerance	Auto
Adjust volume	
Position	R1.7 P7.4 F10.6
Orientation	Sagittal
Rotation	0.00 deg
F >> H	220 mm
A >> P	220 mm
R >> L	164 mm

Physio

1st Signal/Mode	None

Inline

Subtract	Off
Std-Dev-Sag	Off
Std-Dev-Cor	Off
Std-Dev-Tra	Off
Std-Dev-Time	Off
MIP-Sag	Off
MIP-Cor	Off
MIP-Tra	Off
MIP-Time	Off
Save original images	On

Sequence

Introduction	Off
Dimension	3D
Elliptical scanning	Off
Contrasts	1
Bandwidth	400 Hz/Px
RF pulse type	Low SAR
Gradient mode	Fast*
RF spoiling	On
IR Mode	On

Inversion time	450 ms
RF pulse duration	1.1 ms
RF pulse TBW	2.7
RF Spoil Increment	36.7 deg
Duration of Spoiler Gradient X	2070
Duration of Spoiler Gradient Y	340
Duration of Spoiler Gradient Z	330
Scale factor	2.0
Baby Mode	Off

\\USER\FMRIB Limited Release\Adam Thomas\exercise_protocol\despot2_TR46_FA59_phase180

TA: 3:33 Voxel size: 1.7×1.7×1.7 mm Rel. SNR: 1.00 USER: sk_despot2_v19

Properties

Prio Recon	Off
Before measurement	
After measurement	
Load to viewer	On
Inline movie	Off
Auto store images	On
Load to stamp segments	Off
Load images to graphic segments	Off
Auto open inline display	Off
Start measurement without further preparation	Off
Wait for user to start	Off
Start measurements	single

Routine

Slab group 1	
Slabs	1
Dist. factor	20 %
Position	R1.7 P7.4 F10.6
Orientation	Sagittal
Phase enc. dir.	A >> P
Rotation	0.00 deg
Phase oversampling	0 %
Slice oversampling	0.0 %
Slices per slab	96
FoV read	220 mm
FoV phase	100.0 %
Slice thickness	1.70 mm
TR	4.6 ms
TE	2.3 ms
Averages	1
Concatenations	1
Filter	Raw filter
Coil elements	HEA;HEP

Contrast

Flip angle	59 deg
Averaging mode	Short term
Reconstruction	Magnitude
Measurements	8
Pause after meas. 1	0.0 s
Pause after meas. 2	0.0 s
Pause after meas. 3	0.0 s
Pause after meas. 4	0.0 s
Pause after meas. 5	0.0 s
Pause after meas. 6	0.0 s
Pause after meas. 7	0.0 s
Multiple series	Off

Resolution

Base resolution	128
Phase resolution	100 %
Slice resolution	100 %
Phase partial Fourier	5/8
Slice partial Fourier	5/8
Interpolation	Off
Matrix Coil Mode	Auto (CP)
Image Filter	Off
Distortion Corr.	Off
Prescan Normalize	Off
Normalize	Off
B1 filter	Off
Raw filter	On
Intensity	Weak
Slope	25
Elliptical filter	Off

Geometry

Multi-slice mode	Sequential
Series	Ascending

System

Body	Off
HEP	On
HEA	On
SP4	Off
SP2	Off
SP8	Off
SP6	Off
SP3	Off
SP1	Off
SP7	Off
SP5	Off
Positioning mode	FIX
Table position	H
Table position	0 mm
MSMA	S - C - T
Sagittal	R >> L
Coronal	A >> P
Transversal	F >> H
Save uncombined	Off
Coil Combine Mode	Adaptive Combine
AutoAlign	---
Auto Coil Select	Default
Shim mode	Tune up
Adjust with body coil	Off
Confirm freq. adjustment	Off
Assume Silicone	Off
? Ref. amplitude 1H	0.000 V
Adjustment Tolerance	Auto
Adjust volume	
Position	Isocenter
Orientation	Transversal
Rotation	0.00 deg
R >> L	350 mm
A >> P	263 mm
F >> H	350 mm

Physio

1st Signal/Mode	None

Inline

Subtract	Off
Std-Dev-Sag	Off
Std-Dev-Cor	Off
Std-Dev-Tra	Off
Std-Dev-Time	Off
MIP-Sag	Off
MIP-Cor	Off
MIP-Tra	Off
MIP-Time	Off
Save original images	On

Sequence

Introduction	Off
Dimension	3D

Elliptical scanning	Off
Contrasts	1
Bandwidth	560 Hz/Px
RF pulse type	Low SAR
Gradient mode	Fast*
RF spoiling	Off
IR Mode	Off
Dummy pulses	1000
Incremented FA Mode	On
mcDESPOT FA Mode	On
Number of FA Increments	8
RF pulse duration	1.1 ms
RF pulse TBW	2.7
RF Phase Increment	180 deg
Baby Mode	Off
Scale factor	2.0

\\USER\FMRIB Limited Release\Adam Thomas\exercise_protocol\despot2_TR46_FA59_phase0

TA: 3:33 Voxel size: 1.7×1.7×1.7 mm Rel. SNR: 1.00 USER: sk_despot2_v19

Properties

Prio Recon	Off
Before measurement	
After measurement	
Load to viewer	On
Inline movie	Off
Auto store images	On
Load to stamp segments	Off
Load images to graphic segments	Off
Auto open inline display	Off
Start measurement without further preparation	Off
Wait for user to start	Off
Start measurements	single

Routine

Slab group 1	
Slabs	1
Dist. factor	20 %
Position	R1.7 P7.4 F10.6
Orientation	Sagittal
Phase enc. dir.	A >> P
Rotation	0.00 deg
Phase oversampling	0 %
Slice oversampling	0.0 %
Slices per slab	96
FoV read	220 mm
FoV phase	100.0 %
Slice thickness	1.70 mm
TR	4.6 ms
TE	2.3 ms
Averages	1
Concatenations	1
Filter	Raw filter
Coil elements	HEA;HEP

Contrast

Flip angle	59 deg
Averaging mode	Short term
Reconstruction	Magnitude
Measurements	8
Pause after meas. 1	0.0 s
Pause after meas. 2	0.0 s
Pause after meas. 3	0.0 s
Pause after meas. 4	0.0 s
Pause after meas. 5	0.0 s
Pause after meas. 6	0.0 s
Pause after meas. 7	0.0 s
Multiple series	Off

Resolution

Base resolution	128
Phase resolution	100 %
Slice resolution	100 %
Phase partial Fourier	5/8
Slice partial Fourier	5/8
Interpolation	Off
Matrix Coil Mode	Auto (CP)
Image Filter	Off
Distortion Corr.	Off
Prescan Normalize	Off
Normalize	Off
B1 filter	Off
Raw filter	On
Intensity	Weak
Slope	25
Elliptical filter	Off

Geometry

Multi-slice mode	Sequential
Series	Ascending

System

Body	Off
HEP	On
HEA	On
SP4	Off
SP2	Off
SP8	Off
SP6	Off
SP3	Off
SP1	Off
SP7	Off
SP5	Off
Positioning mode	FIX
Table position	H
Table position	0 mm
MSMA	S - C - T
Sagittal	R >> L
Coronal	A >> P
Transversal	F >> H
Save uncombined	Off
Coil Combine Mode	Adaptive Combine
AutoAlign	---
Auto Coil Select	Default
Shim mode	Tune up
Adjust with body coil	Off
Confirm freq. adjustment	Off
Assume Silicone	Off
? Ref. amplitude 1H	0.000 V
Adjustment Tolerance	Auto
Adjust volume	
Position	Isocenter
Orientation	Transversal
Rotation	0.00 deg
R >> L	350 mm
A >> P	263 mm
F >> H	350 mm

Physio

1st Signal/Mode	None

Inline

Subtract	Off
Std-Dev-Sag	Off
Std-Dev-Cor	Off
Std-Dev-Tra	Off
Std-Dev-Time	Off
MIP-Sag	Off
MIP-Cor	Off
MIP-Tra	Off
MIP-Time	Off
Save original images	On

Sequence

Introduction	Off
Dimension	3D

Elliptical scanning	Off
Contrasts	1
Bandwidth	560 Hz/Px
RF pulse type	Low SAR
Gradient mode	Fast*
RF spoiling	Off
IR Mode	Off
Dummy pulses	1000
Incremented FA Mode	On
mcDESPOT FA Mode	On
Number of FA Increments	8
RF pulse duration	1.1 ms
RF pulse TBW	2.7
RF Phase Increment	0 deg
Baby Mode	Off
Scale factor	2.0

SIEMENS MAGNETOM Verio syngo MR B17

\\USER\FMRIB Limited Release\Adam Thomas\exercise_protocol\dti_21dir_te87_tr9600_GRAPPA2

TA: 3:50 PAT: 2 Voxel size: 2.0×2.0×2.0 mm Rel. SNR: 1.00 USER: ep2d_advdiff_511

Properties

Prio Recon	Off
Before measurement	
After measurement	
Load to viewer	On
Inline movie	Off
Auto store images	On
Load to stamp segments	Off
Load images to graphic segments	Off
Auto open inline display	Off
Start measurement without further preparation	On
Wait for user to start	Off
Start measurements	single

Routine

Slice group 1	
Slices	65
Dist. factor	0 %
Position	Isocenter
Orientation	Transversal
Phase enc. dir.	A >> P
Rotation	0.00 deg
Phase oversampling	0 %
FoV read	190 mm
FoV phase	100.0 %
Slice thickness	2.0 mm
TR	9600 ms
TE	87 ms
Averages	1
Concatenations	1
Filter	None
Coil elements	HEA;HEP

Contrast

MTC	Off
Magn. preparation	None
Fat suppr.	Fat sat.
Extra Fat Suppr.	on
Saturation Mode	standard
Averaging mode	Long term
Reconstruction	Magnitude
Delay in TR	0 ms
Multiple series	Off

Resolution

Base resolution	96
Phase resolution	100 %
Phase partial Fourier	6/8
Interpolation	Off
PAT mode	GRAPPA
Accel. factor PE	2
Ref. lines PE	24
Matrix Coil Mode	Auto (Triple)
Reference scan mode	Separate
Distortion Corr.	Off
Prescan Normalize	Off
Raw filter	On
Elliptical filter	Off
Hamming	Off

Geometry

Multi-slice mode	Interleaved
Series	Interleaved
Special sat.	None

System

Body	Off
HEP	On
HEA	On
SP4	Off
SP2	Off
SP8	Off
SP6	Off
SP3	Off
SP1	Off
SP7	Off
SP5	Off
Positioning mode	FIX
Table position	H
Table position	0 mm
MSMA	S - C - T
Sagittal	R >> L
Coronal	A >> P
Transversal	F >> H
Coil Combine Mode	Adaptive Combine
AutoAlign	---
Auto Coil Select	Default
Shim mode	Standard
Adjust with body coil	Off
Confirm freq. adjustment	Off
Assume Silicone	Off
? Ref. amplitude 1H	0.000 V
Adjustment Tolerance	Auto
Adjust volume	
Position	Isocenter
Orientation	Transversal
Rotation	0.00 deg
R >> L	190 mm
A >> P	190 mm
F >> H	130 mm

Physio

1st Signal/Mode	None
Resp. control	Off

Diff

Diffusion mode	Free
Diff. weightings	1
b-value	1000 s/mm²
Diff. weighted images	On
Trace weighted images	Off
Average ADC maps	Off
Individual ADC maps	Off
FA maps	Off
Mosaic	On
Tensor	Off
Noise level	40
Diff. directions	21

Sequence

Introduction	Off
Bandwidth	1628 Hz/Px
Optimization	None
Free echo spacing	Off
Echo spacing	0.7 ms

EPI factor	96
RF pulse type	Normal
Gradient mode	Fast

\\USER\FMRIB Limited Release\Adam Thomas\exercise_protocol\dti_22dir_te87_tr9600_GRAPPA2

TA: 4:00 PAT: 2 Voxel size: 2.0×2.0×2.0 mm Rel. SNR: 1.00 USER: ep2d_advdiff_511

Properties

Prio Recon	Off
Before measurement	
After measurement	
Load to viewer	On
Inline movie	Off
Auto store images	On
Load to stamp segments	Off
Load images to graphic segments	Off
Auto open inline display	Off
Start measurement without further preparation	On
Wait for user to start	Off
Start measurements	single

Routine

Slice group 1	
Slices	65
Dist. factor	0 %
Position	Isocenter
Orientation	Transversal
Phase enc. dir.	A >> P
Rotation	0.00 deg
Phase oversampling	0 %
FoV read	190 mm
FoV phase	100.0 %
Slice thickness	2.0 mm
TR	9600 ms
TE	87 ms
Averages	1
Concatenations	1
Filter	None
Coil elements	HEA;HEP

Contrast

MTC	Off
Magn. preparation	None
Fat suppr.	Fat sat.
Extra Fat Suppr.	on
Saturation Mode	standard
Averaging mode	Long term
Reconstruction	Magnitude
Delay in TR	0 ms
Multiple series	Off

Resolution

Base resolution	96
Phase resolution	100 %
Phase partial Fourier	6/8
Interpolation	Off
PAT mode	GRAPPA
Accel. factor PE	2
Ref. lines PE	24
Matrix Coil Mode	Auto (Triple)
Reference scan mode	Separate
Distortion Corr.	Off
Prescan Normalize	Off
Raw filter	On
Elliptical filter	Off
Hamming	Off

Geometry

Multi-slice mode	Interleaved
Series	Interleaved
Special sat.	None

System

Body	Off
HEP	On
HEA	On
SP4	Off
SP2	Off
SP8	Off
SP6	Off
SP3	Off
SP1	Off
SP7	Off
SP5	Off
Positioning mode	FIX
Table position	H
Table position	0 mm
MSMA	S - C - T
Sagittal	R >> L
Coronal	A >> P
Transversal	F >> H
Coil Combine Mode	Adaptive Combine
AutoAlign	---
Auto Coil Select	Default
Shim mode	Standard
Adjust with body coil	Off
Confirm freq. adjustment	Off
Assume Silicone	Off
? Ref. amplitude 1H	0.000 V
Adjustment Tolerance	Auto
Adjust volume	
Position	Isocenter
Orientation	Transversal
Rotation	0.00 deg
R >> L	190 mm
A >> P	190 mm
F >> H	130 mm

Physio

1st Signal/Mode	None
Resp. control	Off

Diff

Diffusion mode	Free
Diff. weightings	1
b-value	1000 s/mm²
Diff. weighted images	On
Trace weighted images	Off
Average ADC maps	Off
Individual ADC maps	Off
FA maps	Off
Mosaic	On
Tensor	Off
Noise level	40
Diff. directions	22

Sequence

Introduction	Off
Bandwidth	1628 Hz/Px
Optimization	None
Free echo spacing	Off
Echo spacing	0.7 ms

EPI factor	96
RF pulse type	Normal
Gradient mode	Fast

SIEMENS MAGNETOM Verio syngo MR B17

\\USER\FMRIB Limited Release\Adam Thomas\exercise_protocol\dti_25dir_te87_tr9600_GRAPPA2

TA: 4:29 PAT: 2 Voxel size: 2.0×2.0×2.0 mm Rel. SNR: 1.00 USER: ep2d_advdiff_511

Properties

Prio Recon	Off
Before measurement	
After measurement	
Load to viewer	On
Inline movie	Off
Auto store images	On
Load to stamp segments	Off
Load images to graphic segments	Off
Auto open inline display	Off
Start measurement without further preparation	On
Wait for user to start	Off
Start measurements	single

Routine

Slice group 1	
Slices	65
Dist. factor	0 %
Position	Isocenter
Orientation	Transversal
Phase enc. dir.	A >> P
Rotation	0.00 deg
Phase oversampling	0 %
FoV read	190 mm
FoV phase	100.0 %
Slice thickness	2.0 mm
TR	9600 ms
TE	87 ms
Averages	1
Concatenations	1
Filter	None
Coil elements	HEA;HEP

Contrast

MTC	Off
Magn. preparation	None
Fat suppr.	Fat sat.
Extra Fat Suppr.	on
Saturation Mode	standard
Averaging mode	Long term
Reconstruction	Magnitude
Delay in TR	0 ms
Multiple series	Off

Resolution

Base resolution	96
Phase resolution	100 %
Phase partial Fourier	6/8
Interpolation	Off
PAT mode	GRAPPA
Accel. factor PE	2
Ref. lines PE	24
Matrix Coil Mode	Auto (Triple)
Reference scan mode	Separate
Distortion Corr.	Off
Prescan Normalize	Off
Raw filter	On
Elliptical filter	Off
Hamming	Off

Geometry

Multi-slice mode	Interleaved
Series	Interleaved
Special sat.	None

System

Body	Off
HEP	On
HEA	On
SP4	Off
SP2	Off
SP8	Off
SP6	Off
SP3	Off
SP1	Off
SP7	Off
SP5	Off
Positioning mode	FIX
Table position	H
Table position	0 mm
MSMA	S - C - T
Sagittal	R >> L
Coronal	A >> P
Transversal	F >> H
Coil Combine Mode	Adaptive Combine
AutoAlign	---
Auto Coil Select	Default
Shim mode	Standard
Adjust with body coil	Off
Confirm freq. adjustment	Off
Assume Silicone	Off
? Ref. amplitude 1H	0.000 V
Adjustment Tolerance	Auto
Adjust volume	
Position	Isocenter
Orientation	Transversal
Rotation	0.00 deg
R >> L	190 mm
A >> P	190 mm
F >> H	130 mm

Physio

1st Signal/Mode	None
Resp. control	Off

Diff

Diffusion mode	Free
Diff. weightings	1
b-value	1000 s/mm²
Diff. weighted images	On
Trace weighted images	Off
Average ADC maps	Off
Individual ADC maps	Off
FA maps	Off
Mosaic	On
Tensor	Off
Noise level	40
Diff. directions	25

Sequence

Introduction	Off
Bandwidth	1628 Hz/Px
Optimization	None
Free echo spacing	Off
Echo spacing	0.7 ms

EPI factor	96
RF pulse type	Normal
Gradient mode	Fast

\\USER\FMRIB Limited Release\Adam Thomas\exercise_protocol\MEMPRAGE_4TE_pre_gad

TA: 6:03 PAT: 2 Voxel size: 1.0×1.0×1.0 mm Rel. SNR: 1.00 USER: tfl_mgh_multiecho

Properties

Prio Recon	Off
Before measurement	
After measurement	
Load to viewer	On
Inline movie	Off
Auto store images	On
Load to stamp segments	Off
Load images to graphic segments	Off
Auto open inline display	Off
Start measurement without further preparation	On
Wait for user to start	Off
Start measurements	single

Routine

Slab group 1	
Slabs	1
Dist. factor	50 %
Position	L10.3 P25.4 F14.5
Orientation	Sagittal
Phase enc. dir.	A >> P
Rotation	0.00 deg
Phase oversampling	0 %
Slice oversampling	0.0 %
Slices per slab	176
FoV read	256 mm
FoV phase	100.0 %
Slice thickness	1.00 mm
TR	2530 ms
TE 1	1.69 ms
TE 2	3.55 ms
TE 3	5.41 ms
TE 4	7.27 ms
Averages	1
Concatenations	1
Filter	Prescan Normalize
Coil elements	HEA;HEP

Contrast

Magn. preparation	Non-sel. IR
TI	1200 ms
Flip angle	7.0 deg
Fat suppr.	None
Water suppr.	None
Averaging mode	Long term
Reconstruction	Magnitude
Measurements	1
Multiple series	Each measurement

Resolution

Base resolution	256
Phase resolution	100 %
Slice resolution	100 %
Phase partial Fourier	Off
Slice partial Fourier	Off
Interpolation	Off
PAT mode	GRAPPA
Accel. factor PE	2
Ref. lines PE	32
Accel. factor 3D	1
Matrix Coil Mode	Auto (Triple)
Reference scan mode	Integrated
Image Filter	Off
Distortion Corr.	Off
Unfiltered images	Off
Prescan Normalize	On
Normalize	Off
B1 filter	Off
Raw filter	Off
Elliptical filter	Off

Geometry

Multi-slice mode	Single shot
Series	Interleaved

System

Body	Off
HEP	On
HEA	On
SP4	Off
SP2	Off
SP8	Off
SP6	Off
SP3	Off
SP1	Off
SP7	Off
SP5	Off
Positioning mode	REF
Table position	H
Table position	0 mm
MSMA	S - C - T
Sagittal	R >> L
Coronal	A >> P
Transversal	F >> H
Save uncombined	Off
Coil Combine Mode	Adaptive Combine
AutoAlign	Head > Brain
Auto Coil Select	Default
Shim mode	Standard
Adjust with body coil	Off
Confirm freq. adjustment	Off
Assume Silicone	Off
? Ref. amplitude 1H	0.000 V
Adjustment Tolerance	Auto
Adjust volume	
Position	L10.3 P25.4 F14.5
Orientation	Sagittal
Rotation	0.00 deg
F >> H	256 mm
A >> P	256 mm
R >> L	176 mm

Physio

1st Signal/Mode	None
Dark blood	Off

Inline

Subtract	Off
Std-Dev-Sag	Off
Std-Dev-Cor	Off
Std-Dev-Tra	Off
Std-Dev-Time	Off
MIP-Sag	Off
MIP-Cor	Off
MIP-Tra	Off
MIP-Time	Off

Save original images	On

Sequence

Introduction	On
Dimension	3D
Elliptical scanning	Off
Asymmetric echo	Off
Contrasts	4
Bandwidth 1	651 Hz/Px
Bandwidth 2	651 Hz/Px
Bandwidth 3	651 Hz/Px
Bandwidth 4	651 Hz/Px
Flow comp. 1	No
Flow comp. 2	No
Flow comp. 3	No
Flow comp. 4	No
Echo spacing	10.7 ms
RF pulse type	Fast
Gradient mode	Fast
Excitation	Non-sel.
RF spoiling	On
Readout polarity	Positive
Readout trajectory	Bipolar
Add. scale factor	8.0
Gradient spoiling	Integral
Gradient moment factor	3.0
Siemens reconstruction	On
Save raw k-space data	Off
Averaging	RMS

\\USER\FMRIB Limited Release\Adam Thomas\exercise_protocol\MEMPRAGE_4TE_post_gad

TA: 6:03 PAT: 2 Voxel size: 1.0×1.0×1.0 mm Rel. SNR: 1.00 USER: tfl_mgh_multiecho

Properties

Prio Recon	Off
Before measurement	
After measurement	
Load to viewer	On
Inline movie	Off
Auto store images	On
Load to stamp segments	Off
Load images to graphic segments	Off
Auto open inline display	Off
Start measurement without further preparation	On
Wait for user to start	On
Start measurements	single

Routine

Slab group 1	
Slabs	1
Dist. factor	50 %
Position	L10.3 P25.4 F14.5
Orientation	Sagittal
Phase enc. dir.	A >> P
Rotation	0.00 deg
Phase oversampling	0 %
Slice oversampling	0.0 %
Slices per slab	176
FoV read	256 mm
FoV phase	100.0 %
Slice thickness	1.00 mm
TR	2530 ms
TE 1	1.69 ms
TE 2	3.55 ms
TE 3	5.41 ms
TE 4	7.27 ms
Averages	1
Concatenations	1
Filter	Prescan Normalize
Coil elements	HEA;HEP

Contrast

Magn. preparation	Non-sel. IR
TI	1200 ms
Flip angle	7.0 deg
Fat suppr.	None
Water suppr.	None
Averaging mode	Long term
Reconstruction	Magnitude
Measurements	1
Multiple series	Each measurement

Resolution

Base resolution	256
Phase resolution	100 %
Slice resolution	100 %
Phase partial Fourier	Off
Slice partial Fourier	Off
Interpolation	Off
PAT mode	GRAPPA
Accel. factor PE	2
Ref. lines PE	32
Accel. factor 3D	1
Matrix Coil Mode	Auto (Triple)
Reference scan mode	Integrated

Image Filter	Off
Distortion Corr.	Off
Unfiltered images	Off
Prescan Normalize	On
Normalize	Off
B1 filter	Off
Raw filter	Off
Elliptical filter	Off

Geometry

Multi-slice mode	Single shot
Series	Interleaved

System

Body	Off
HEP	On
HEA	On
SP4	Off
SP2	Off
SP8	Off
SP6	Off
SP3	Off
SP1	Off
SP7	Off
SP5	Off
Positioning mode	REF
Table position	H
Table position	0 mm
MSMA	S - C - T
Sagittal	R >> L
Coronal	A >> P
Transversal	F >> H
Save uncombined	Off
Coil Combine Mode	Adaptive Combine
AutoAlign	Head > Brain
Auto Coil Select	Default
Shim mode	Standard
Adjust with body coil	Off
Confirm freq. adjustment	Off
Assume Silicone	Off
? Ref. amplitude 1H	0.000 V
Adjustment Tolerance	Auto
Adjust volume	
Position	L10.3 P25.4 F14.5
Orientation	Sagittal
Rotation	0.00 deg
F >> H	256 mm
A >> P	256 mm
R >> L	176 mm

Physio

1st Signal/Mode	None
Dark blood	Off

Inline

Subtract	Off
Std-Dev-Sag	Off
Std-Dev-Cor	Off
Std-Dev-Tra	Off
Std-Dev-Time	Off
MIP-Sag	Off
MIP-Cor	Off
MIP-Tra	Off
MIP-Time	Off

Save original images	On

Sequence

Introduction	On
Dimension	3D
Elliptical scanning	Off
Asymmetric echo	Off
Contrasts	4
Bandwidth 1	651 Hz/Px
Bandwidth 2	651 Hz/Px
Bandwidth 3	651 Hz/Px
Bandwidth 4	651 Hz/Px
Flow comp. 1	No
Flow comp. 2	No
Flow comp. 3	No
Flow comp. 4	No
Echo spacing	10.7 ms
RF pulse type	Fast
Gradient mode	Fast
Excitation	Non-sel.
RF spoiling	On
Readout polarity	Positive
Readout trajectory	Bipolar
Add. scale factor	8.0
Gradient spoiling	Integral
Gradient moment factor	3.0
Siemens reconstruction	On
Save raw k-space data	Off
Averaging	RMS

B.2 7 Tesla Magnetom Sequences

1. Localiser
2. Transmit calibration
3. T1-weighted MPRAGE
4. Gradient echo field map
5. DTI (two sequences)
6. T2*-weighted, partial FOV (for hippocampus)
7. Occipital spectroscopy (SPECIAL, with and without water suppression)
8. EPI BOLD (resting state)

SIEMENS MAGNETOM Investigational_Device_7T syngo MR B17

\\USER\FMRIB User\2013_07 Exercise\HighResHippo\localizer_200V

TA: 0:14 PAT: 2 Voxel size: 1.2×1.1×3.0 mm Rel. SNR: 1.00 SIEMENS: gre

Properties

Prio Recon	Off
Before measurement	
After measurement	
Load to viewer	On
Inline movie	Off
Auto store images	On
Load to stamp segments	Off
Load images to graphic segments	Off
Auto open inline display	Off
Start measurement without further preparation	Off
Wait for user to start	Off
Start measurements	single

Routine

Slice group 1	
Slices	5
Dist. factor	20 %
Position	Isocenter
Orientation	Sagittal
Phase enc. dir.	A >> P
Rotation	0.00 deg
Slice group 2	
Slices	5
Dist. factor	20 %
Position	Isocenter
Orientation	Coronal
Phase enc. dir.	R >> L
Rotation	0.00 deg
Slice group 3	
Slices	5
Dist. factor	20 %
Position	Isocenter
Orientation	Transversal
Phase enc. dir.	A >> P
Rotation	0.00 deg
Phase oversampling	0 %
FoV read	280 mm
FoV phase	100.0 %
Slice thickness	3.0 mm
TR	8.6 ms
TE	3.00 ms
Averages	1
Concatenations	15
Filter	None
Coil elements	A32

Contrast

TD	0 ms
MTC	Off
Magn. preparation	None
Flip angle	20 deg
Fat suppr.	None
Water suppr.	None
SWI	Off
Averaging mode	Short term
Reconstruction	Magnitude
Measurements	1
Multiple series	Each measurement

Resolution

Base resolution	256
Phase resolution	90 %
Phase partial Fourier	6/8
Interpolation	On
PAT mode	GRAPPA
Accel. factor PE	2
Ref. lines PE	24
Reference scan mode	Integrated
Image Filter	Off
Distortion Corr.	Off
Prescan Normalize	Off
Normalize	Off
B1 filter	Off
Raw filter	Off
Elliptical filter	Off

Geometry

Multi-slice mode	Sequential
Series	Interleaved
Saturation mode	Standard
Special sat.	None
Table position	H
Table position	0 mm
Inline Composing	Off
Tim CT mode	Off

System

A32	On
V32	Off
Positioning mode	REF
MSMA	S - C - T
Sagittal	R >> L
Coronal	A >> P
Transversal	F >> H
Save uncombined	Off
Coil Combine Mode	Adaptive Combine
AutoAlign	---
Auto Coil Select	Off
Shim mode	Tune up
Adjust with body coil	Off
Confirm freq. adjustment	Off
Assume Silicone	Off
! Ref. amplitude 1H	250.000 V
Adjustment Tolerance	Auto
Adjust volume	
Position	Isocenter
Orientation	Transversal
Rotation	0.00 deg
R >> L	350 mm
A >> P	263 mm
F >> H	350 mm

Physio

1st Signal/Mode	None
Segments	1
Tagging	None
Dark blood	Off
Resp. control	Off

Inline

Subtract	Off
Liver registration	Off

Std-Dev-Sag	Off
Std-Dev-Cor	Off
Std-Dev-Tra	Off
Std-Dev-Time	Off
MIP-Sag	Off
MIP-Cor	Off
MIP-Tra	Off
MIP-Time	Off
Save original images	On
Wash - In	Off
Wash - Out	Off
TTP	Off
PEI	Off
MIP - time	Off
MapIt	None
Contrasts	1

Sequence

Introduction	On
Dimension	2D
Phase stabilisation	Off
Asymmetric echo	Allowed
Bandwidth	320 Hz/Px
Flow comp.	No
RF pulse type	Normal
Gradient mode	Normal
Excitation	Slice-sel.
RF spoiling	On

\\USER\FMRIB User\2013_07 Exercise\HighResHippo\Quick_Tx_calib_200V_centre_brain

TA: 0:11 Voxel size: 3.9×3.9×5.0 mm Rel. SNR: 1.00 USER: b1map_658

Properties

Prio Recon	Off
Before measurement	
After measurement	
Load to viewer	On
Inline movie	Off
Auto store images	On
Load to stamp segments	Off
Load images to graphic segments	Off
Auto open inline display	Off
Start measurement without further preparation	On
Wait for user to start	Off
Start measurements	single

Routine

Slice group 1	
Slices	1
Dist. factor	150 %
Position	L0.0 A10.8 F37.1
Orientation	Transversal
Phase enc. dir.	A >> P
Rotation	0.00 deg
FoV read	250 mm
FoV phase	100.0 %
Slice thickness	5 mm
TR	100 ms
TE 1	14 ms
TE 2	14 ms
Averages	1
Filter	None
Coil elements	A32

Contrast

Flip angle 1	90 deg
Flip angle 2	120 deg
Flip angle 3	60 deg
Flip angle 4	135 deg
Flip angle 5	45 deg
Measurements	1

Resolution

Base resolution	64
Phase resolution	100 %
Raw filter	Off

Geometry

Series	Interleaved
Navigator 1	
Position	L0.0 A17.5 F35.1
Orientation	Transversal
Rotation	0.08 deg
Base size phase	50 mm
Base size read	50 mm
Thickness	50 mm
Table position	H
Table position	0 mm
Inline Composing	Off

System

A32	On
V32	Off
Positioning mode	FIX
MSMA	S - C - T
Sagittal	R >> L
Coronal	A >> P
Transversal	F >> H
Save uncombined	Off
Coil Combine Mode	Adaptive Combine
AutoAlign	Head > Brain
Auto Coil Select	Default
Shim mode	Tune up
Adjust with body coil	Off
Confirm freq. adjustment	Off
Assume Silicone	Off
! Ref. amplitude 1H	200.000 V
Adjustment Tolerance	Auto
Adjust volume	
Position	Isocenter
Orientation	Transversal
Rotation	0.00 deg
R >> L	350 mm
A >> P	263 mm
F >> H	350 mm

Composing

Sequence

Contrasts	2
Bandwidth	260.416667 Hz/Px
T1 Compensation	Mean T1
Mean T1	500.0 ms
Angles	1
Amplitude Weighting	Linear
Scale Bar	Enabled
Raw Data	Disabled

\\USER\FMRIB User\2013_07 Exercise\HighResHippo\t1_mprage_0.7iso_sag_PAT2

TA: 6:35 PAT: 2 Voxel size: 0.7×0.7×0.7 mm Rel. SNR: 1.00 SIEMENS: tfl

Properties

Prio Recon	Off
Before measurement	
After measurement	
Load to viewer	On
Inline movie	Off
Auto store images	On
Load to stamp segments	Off
Load images to graphic segments	Off
Auto open inline display	Off
Start measurement without further preparation	On
Wait for user to start	On
Start measurements	single

Routine

Slab group 1	
Slabs	1
Dist. factor	50 %
Position	L0.7 A18.3 F49.8
Orientation	Sagittal
Phase enc. dir.	A >> P
Rotation	0.00 deg
Phase oversampling	0 %
Slice oversampling	0.0 %
Slices per slab	256
FoV read	224 mm
FoV phase	100.0 %
Slice thickness	0.70 mm
TR	2200 ms
TE	2.96 ms
Averages	1
Concatenations	1
Filter	None
Coil elements	A32

Contrast

Magn. preparation	Non-sel. IR
TI	1050 ms
Flip angle	7 deg
Fat suppr.	Water excit. fast
Water suppr.	None
Averaging mode	Long term
Reconstruction	Magnitude
Measurements	1
Multiple series	Each measurement

Resolution

Base resolution	320
Phase resolution	100 %
Slice resolution	100 %
Phase partial Fourier	Off
Slice partial Fourier	Off
Interpolation	Off
PAT mode	GRAPPA
Accel. factor PE	2
Ref. lines PE	40
Accel. factor 3D	1
Reference scan mode	Integrated
Image Filter	Off
Distortion Corr.	Off
Prescan Normalize	Off
Normalize	Off
B1 filter	Off
Raw filter	Off
Elliptical filter	Off

Geometry

Multi-slice mode	Single shot
Series	Ascending
Table position	H
Table position	0 mm
Inline Composing	Off

System

A32	On
V32	Off
Positioning mode	FIX
MSMA	S - C - T
Sagittal	R >> L
Coronal	A >> P
Transversal	F >> H
Save uncombined	Off
Coil Combine Mode	Adaptive Combine
AutoAlign	Head > Brain
Auto Coil Select	Default
Shim mode	Standard
Adjust with body coil	Off
Confirm freq. adjustment	On
Assume Silicone	Off
? Ref. amplitude 1H	0.000 V
Adjustment Tolerance	Auto
Adjust volume	
Position	L0.7 A18.3 F49.8
Orientation	Sagittal
Rotation	0.00 deg
F >> H	224 mm
A >> P	224 mm
R >> L	180 mm

Physio

1st Signal/Mode	None
Dark blood	Off
Resp. control	Off

Inline

Subtract	Off
Std-Dev-Sag	Off
Std-Dev-Cor	Off
Std-Dev-Tra	Off
Std-Dev-Time	Off
MIP-Sag	Off
MIP-Cor	Off
MIP-Tra	Off
MIP-Time	Off
Save original images	On

Sequence

Introduction	On
Dimension	3D
Elliptical scanning	Off
Asymmetric echo	Off
Bandwidth	240 Hz/Px
Flow comp.	No

Echo spacing	7.4 ms
RF pulse type	Normal
Gradient mode	Fast
Excitation	Non-sel.
RF spoiling	On

\\USER\FMRIB User\2013_07 Exercise\HighResHippo\gre_field_mapping_2mm

TA: 2:02 Voxel size: 2.0×2.0×2.0 mm Rel. SNR: 1.00 SIEMENS: gre_field_mapping

Properties

Prio Recon	Off
Before measurement	
After measurement	
Load to viewer	On
Inline movie	Off
Auto store images	On
Load to stamp segments	Off
Load images to graphic segments	Off
Auto open inline display	Off
Start measurement without further preparation	On
Wait for user to start	Off
Start measurements	single

Routine

Slice group 1	
Slices	85
Dist. factor	0 %
Position	L0.0 A19.0 F19.1
Orientation	Transversal
Phase enc. dir.	A >> P
Rotation	0.00 deg
Phase oversampling	0 %
FoV read	192 mm
FoV phase	100.0 %
Slice thickness	2.0 mm
TR	620.0 ms
TE 1	4.08 ms
TE 2	5.1 ms
Averages	1
Concatenations	1
Filter	None
Coil elements	A32

Contrast

MTC	Off
Flip angle	39 deg
Fat suppr.	None
Averaging mode	Long term
Reconstruction	Magn./Phase
Measurements	1
Multiple series	Off

Resolution

Base resolution	96
Phase resolution	100 %
Phase partial Fourier	Off
Interpolation	Off
Image Filter	Off
Distortion Corr.	Off
Prescan Normalize	Off
Normalize	Off
B1 filter	Off
Raw filter	Off
Elliptical filter	Off

Geometry

Multi-slice mode	Interleaved
Series	Interleaved
Special sat.	None
Table position	H
Table position	0 mm
Inline Composing	Off

System

A32	On
V32	Off
Positioning mode	FIX
MSMA	S - C - T
Sagittal	R >> L
Coronal	A >> P
Transversal	F >> H
Save uncombined	Off
Coil Combine Mode	Sum of Squares
AutoAlign	---
Auto Coil Select	Off
Shim mode	Standard
Adjust with body coil	Off
Confirm freq. adjustment	Off
Assume Silicone	Off
? Ref. amplitude 1H	0.000 V
Adjustment Tolerance	Auto
Adjust volume	
Position	L0.0 A19.0 F19.1
Orientation	Transversal
Rotation	0.00 deg
R >> L	192 mm
A >> P	192 mm
F >> H	170 mm

Composing

Sequence

Introduction	On
Dimension	2D
Asymmetric echo	Off
Contrasts	2
Bandwidth	734 Hz/Px
Flow comp.	Yes
RF pulse type	Normal
Gradient mode	Whisper
RF spoiling	On

\\USER\FMRIB User\2013_07 Exercise\HighResHippo\ep2d_diff_sine_671a_AP_1.5mm_b1500

TA: 11:10 PAT: 2 Voxel size: 1.5×1.5×1.5 mm Rel. SNR: 1.00 USER: ep2d_diff_sine_671a

Properties

Prio Recon	Off
Before measurement	
After measurement	
Load to viewer	On
Inline movie	Off
Auto store images	On
Load to stamp segments	Off
Load images to graphic segments	Off
Auto open inline display	Off
Start measurement without further preparation	On
Wait for user to start	On
Start measurements	single

Routine

Slice group 1	
Slices	80
Dist. factor	0 %
Position	L0.0 A19.9 F34.5
Orientation	Transversal
Phase enc. dir.	A >> P
Rotation	0.00 deg
Phase oversampling	0 %
FoV read	192 mm
FoV phase	100.0 %
Slice thickness	1.5 mm
TR	10000 ms
TE	64 ms
Averages	1
Concatenations	1
Filter	Raw filter
Coil elements	A32

Contrast

MTC	Off
Magn. preparation	None
Fat suppr.	Fat sat.
Extra Fat Suppr.	off
Saturation Mode	standard
Averaging mode	Long term
Reconstruction	Magnitude
Delay in TR	0 ms
Multiple series	Off

Resolution

Base resolution	128
Phase resolution	100 %
Phase partial Fourier	6/8
Interpolation	Off
PAT mode	GRAPPA
Accel. factor PE	2
Ref. lines PE	38
Reference scan mode	Separate
Distortion Corr.	Off
Prescan Normalize	Off
Raw filter	On
Intensity	Weak
Slope	25
Elliptical filter	Off
Hamming	Off

Geometry

Multi-slice mode	Interleaved
Series	Interleaved
Special sat.	None
Table position	H
Table position	0 mm
Inline Composing	Off

System

A32	On
V32	Off
Positioning mode	REF
MSMA	S - C - T
Sagittal	R >> L
Coronal	A >> P
Transversal	F >> H
Coil Combine Mode	Adaptive Combine
AutoAlign	---
Auto Coil Select	Default
Shim mode	Standard
Adjust with body coil	Off
Confirm freq. adjustment	Off
Assume Silicone	Off
? Ref. amplitude 1H	0.000 V
Adjustment Tolerance	Auto
Adjust volume	
Position	L0.0 A19.9 F34.5
Orientation	Transversal
Rotation	0.00 deg
R >> L	192 mm
A >> P	192 mm
F >> H	120 mm

Physio

1st Signal/Mode	None
PMU Recording	off
Resp. control	Off

Diff

Diffusion mode	Free
Diff. weightings	1
b-value	1500 s/mm²
Diff. weighted images	On
Trace weighted images	Off
Average ADC maps	Off
Individual ADC maps	Off
FA maps	Off
Mosaic	On
Tensor	Off
Noise level	40
Diff. directions	64

Sequence

Introduction	Off
Bandwidth	1698 Hz/Px
Optimization	None
Echo spacing	0.67 ms
EPI factor	128
RF pulse type	Normal
Gradient mode	Fast
FatSat flip angle	110 deg
RF pulse type	External

FFT factor	1.00

\\USER\FMRIB User\2013_07 Exercise\HighResHippo\ep2d_diff_sine_671a_PA_1.5mm_b0

TA: 0:40 PAT: 2 Voxel size: 1.5×1.5×1.5 mm Rel. SNR: 1.00 USER: ep2d_diff_sine_671a

Properties

Prio Recon	Off
Before measurement	
After measurement	
Load to viewer	On
Inline movie	Off
Auto store images	On
Load to stamp segments	Off
Load images to graphic segments	Off
Auto open inline display	Off
Start measurement without further preparation	On
Wait for user to start	Off
Start measurements	single

Routine

Slice group 1	
Slices	80
Dist. factor	0 %
Position	L0.0 A19.9 F34.5
Orientation	Transversal
Phase enc. dir.	A >> P
Rotation	0.00 deg
Phase oversampling	0 %
FoV read	192 mm
FoV phase	100.0 %
Slice thickness	1.5 mm
TR	10000 ms
TE	64 ms
Averages	1
Concatenations	1
Filter	Raw filter
Coil elements	A32

Contrast

MTC	Off
Magn. preparation	None
Fat suppr.	Fat sat.
Extra Fat Suppr.	off
Saturation Mode	standard
Averaging mode	Long term
Reconstruction	Magnitude
Delay in TR	0 ms
Multiple series	Off

Resolution

Base resolution	128
Phase resolution	100 %
Phase partial Fourier	6/8
Interpolation	Off
PAT mode	GRAPPA
Accel. factor PE	2
Ref. lines PE	38
Reference scan mode	Separate
Distortion Corr.	Off
Prescan Normalize	Off
Raw filter	On
Intensity	Weak
Slope	25
Elliptical filter	Off
Hamming	Off

Geometry

Multi-slice mode	Interleaved
Series	Interleaved
Special sat.	None
Table position	H
Table position	0 mm
Inline Composing	Off

System

A32	On
V32	Off
Positioning mode	FIX
MSMA	S - C - T
Sagittal	R >> L
Coronal	A >> P
Transversal	F >> H
Coil Combine Mode	Adaptive Combine
AutoAlign	---
Auto Coil Select	Default
Shim mode	Standard
Adjust with body coil	Off
Confirm freq. adjustment	Off
Assume Silicone	Off
? Ref. amplitude 1H	0.000 V
Adjustment Tolerance	Auto
Adjust volume	
Position	L0.0 A19.9 F34.5
Orientation	Transversal
Rotation	0.00 deg
R >> L	192 mm
A >> P	192 mm
F >> H	120 mm

Physio

1st Signal/Mode	None
PMU Recording	off
Resp. control	Off

Diff

Diffusion mode	Free
Diff. weightings	1
b-value	0 s/mm²
Diff. weighted images	On
Trace weighted images	Off
Average ADC maps	Off
Individual ADC maps	Off
FA maps	Off
Mosaic	On
Tensor	Off
Noise level	40
Diff. directions	64

Sequence

Introduction	Off
Bandwidth	1698 Hz/Px
Optimization	None
Echo spacing	0.67 ms
EPI factor	128
RF pulse type	Normal
Gradient mode	Fast
FatSat flip angle	110 deg
RF pulse type	External

FFT factor	1.00

\\USER\FMRIB User\2013_07 Exercise\HighResHippo\Cho T2STAR TE 25.2 0.5mm FlowComp

TA: 7:17 PAT: Off Voxel size: 0.5×0.5×0.5 mm Rel. SNR: 1.00 SIEMENS: gre

Properties

Prio Recon	Off
Before measurement	
After measurement	
Load to viewer	On
Inline movie	Off
Auto store images	On
Load to stamp segments	Off
Load images to graphic segments	Off
Auto open inline display	Off
Start measurement without further preparation	On
Wait for user to start	Off
Start measurements	single

Routine

Slab group 1	
Slabs	1
Dist. factor	20 %
Position	L1.0 P9.3 F15.8
Orientation	T > C29.0
Phase enc. dir.	R >> L
Rotation	90.00 deg
Phase oversampling	0 %
Slice oversampling	0.0 %
Slices per slab	48
FoV read	192 mm
FoV phase	84.4 %
Slice thickness	0.50 mm
TR	50 ms
TE	25.7 ms
Averages	1
Concatenations	1
Filter	None
Coil elements	A32

Contrast

MTC	Off
Magn. preparation	None
Flip angle	10 deg
Fat suppr.	None
Water suppr.	None
SWI	Off
Averaging mode	Short term
Reconstruction	Magn./Phase
Measurements	1
Multiple series	Each measurement

Resolution

Base resolution	384
Phase resolution	100 %
Slice resolution	100 %
Phase partial Fourier	6/8
Slice partial Fourier	6/8
Interpolation	Off
PAT mode	None
Image Filter	Off
Distortion Corr.	Off
Prescan Normalize	Off
Normalize	Off
B1 filter	Off
Raw filter	Off
Elliptical filter	Off

Geometry

Multi-slice mode	Interleaved
Series	Interleaved
Saturation mode	Standard
Special sat.	None
Table position	H
Table position	0 mm
Inline Composing	Off
Tim CT mode	Off

System

A32	On
V32	Off
Positioning mode	REF
MSMA	S - C - T
Sagittal	R >> L
Coronal	A >> P
Transversal	F >> H
Save uncombined	Off
Coil Combine Mode	Sum of Squares
AutoAlign	Head > Brain
Auto Coil Select	Default
Shim mode	Standard
Adjust with body coil	Off
Confirm freq. adjustment	Off
Assume Silicone	Off
? Ref. amplitude 1H	0.000 V
Adjustment Tolerance	Auto
Adjust volume	
Position	L1.0 P9.3 F15.8
Orientation	T > C29.0
Rotation	90.00 deg
A >> P	192 mm
R >> L	162 mm
F >> H	24 mm

Physio

1st Signal/Mode	None
Segments	1
Tagging	None
Dark blood	Off
Resp. control	Off

Inline

Subtract	Off
Liver registration	Off
Std-Dev-Sag	Off
Std-Dev-Cor	Off
Std-Dev-Tra	Off
Std-Dev-Time	Off
MIP-Sag	Off
MIP-Cor	Off
MIP-Tra	Off
MIP-Time	Off
Save original images	On
Wash - In	Off
Wash - Out	Off
TTP	Off
PEI	Off

MIP - time	Off
MapIt	None
Contrasts	1

Sequence

Introduction	Off
Dimension	3D
Elliptical scanning	Off
Phase stabilisation	Off
Asymmetric echo	Off
Bandwidth	30 Hz/Px
Flow comp.	Slice/Read
RF pulse type	Fast
Gradient mode	Fast*
Excitation	Slab-sel.
RF spoiling	On

\\USER\FMRIB User\2013_07 Exercise\HighResHippo\Cho T2STAR TE 25.2 0.5mm FlowComp

TA: 7:17 PAT: Off Voxel size: 0.5×0.5×0.5 mm Rel. SNR: 1.00 SIEMENS: gre

Properties

Prio Recon	Off
Before measurement	
After measurement	
Load to viewer	On
Inline movie	Off
Auto store images	On
Load to stamp segments	Off
Load images to graphic segments	Off
Auto open inline display	Off
Start measurement without further preparation	On
Wait for user to start	Off
Start measurements	single

Routine

Slab group 1	
Slabs	1
Dist. factor	20 %
Position	L1.0 P9.3 F15.8
Orientation	T > C29.0
Phase enc. dir.	R >> L
Rotation	90.00 deg
Phase oversampling	0 %
Slice oversampling	0.0 %
Slices per slab	48
FoV read	192 mm
FoV phase	84.4 %
Slice thickness	0.50 mm
TR	50 ms
TE	25.7 ms
Averages	1
Concatenations	1
Filter	None
Coil elements	A32

Contrast

MTC	Off
Magn. preparation	None
Flip angle	10 deg
Fat suppr.	None
Water suppr.	None
SWI	Off
Averaging mode	Short term
Reconstruction	Magn./Phase
Measurements	1
Multiple series	Each measurement

Resolution

Base resolution	384
Phase resolution	100 %
Slice resolution	100 %
Phase partial Fourier	6/8
Slice partial Fourier	6/8
Interpolation	Off
PAT mode	None
Image Filter	Off
Distortion Corr.	Off
Prescan Normalize	Off
Normalize	Off
B1 filter	Off
Raw filter	Off
Elliptical filter	Off

Geometry

Multi-slice mode	Interleaved
Series	Interleaved
Saturation mode	Standard
Special sat.	None
Table position	H
Table position	0 mm
Inline Composing	Off
Tim CT mode	Off

System

A32	On
V32	Off
Positioning mode	REF
MSMA	S - C - T
Sagittal	R >> L
Coronal	A >> P
Transversal	F >> H
Save uncombined	Off
Coil Combine Mode	Sum of Squares
AutoAlign	Head > Brain
Auto Coil Select	Default
Shim mode	Standard
Adjust with body coil	Off
Confirm freq. adjustment	Off
Assume Silicone	Off
? Ref. amplitude 1H	0.000 V
Adjustment Tolerance	Auto
Adjust volume	
Position	L1.0 P9.3 F15.8
Orientation	T > C29.0
Rotation	90.00 deg
A >> P	192 mm
R >> L	162 mm
F >> H	24 mm

Physio

1st Signal/Mode	None
Segments	1
Tagging	None
Dark blood	Off
Resp. control	Off

Inline

Subtract	Off
Liver registration	Off
Std-Dev-Sag	Off
Std-Dev-Cor	Off
Std-Dev-Tra	Off
Std-Dev-Time	Off
MIP-Sag	Off
MIP-Cor	Off
MIP-Tra	Off
MIP-Time	Off
Save original images	On
Wash - In	Off
Wash - Out	Off
TTP	Off
PEI	Off

MIP - time	Off
MapIt	None
Contrasts	1

Sequence

Introduction	Off
Dimension	3D
Elliptical scanning	Off
Phase stabilisation	Off
Asymmetric echo	Off
Bandwidth	30 Hz/Px
Flow comp.	Slice/Read
RF pulse type	Fast
Gradient mode	Fast*
Excitation	Slab-sel.
RF spoiling	On

\\USER\FMRIB User\2013_07 Exercise\HighResHippo\Cho T2STAR WholeBrain 2mm Iso

TA: 3:06 PAT: Off Voxel size: 2.0×2.0×2.0 mm Rel. SNR: 1.00 SIEMENS: gre

Properties

Prio Recon	Off
Before measurement	
After measurement	
Load to viewer	On
Inline movie	Off
Auto store images	On
Load to stamp segments	Off
Load images to graphic segments	Off
Auto open inline display	Off
Start measurement without further preparation	On
Wait for user to start	Off
Start measurements	single

Routine

Slab group 1	
Slabs	1
Dist. factor	20 %
Position	R1.7 A22.7 F28.2
Orientation	T > C11.3
Phase enc. dir.	A >> P
Rotation	0.00 deg
Phase oversampling	0 %
Slice oversampling	0.0 %
Slices per slab	72
FoV read	256 mm
FoV phase	71.9 %
Slice thickness	2.00 mm
TR	50 ms
TE	30.0 ms
Averages	1
Concatenations	1
Filter	None
Coil elements	A32

Contrast

MTC	Off
Magn. preparation	None
Flip angle	10 deg
Fat suppr.	None
Water suppr.	None
SWI	Off
Averaging mode	Short term
Reconstruction	Magn./Phase
Measurements	1
Multiple series	Each measurement

Resolution

Base resolution	128
Phase resolution	100 %
Slice resolution	100 %
Phase partial Fourier	6/8
Slice partial Fourier	6/8
Interpolation	Off
PAT mode	None
Image Filter	Off
Distortion Corr.	Off
Prescan Normalize	Off
Normalize	Off
B1 filter	Off
Raw filter	Off
Elliptical filter	Off

Geometry

Multi-slice mode	Interleaved
Series	Interleaved
Saturation mode	Standard
Special sat.	None
Table position	H
Table position	0 mm
Inline Composing	Off
Tim CT mode	Off

System

A32	On
V32	Off
Positioning mode	FIX
MSMA	S - C - T
Sagittal	R >> L
Coronal	A >> P
Transversal	F >> H
Save uncombined	Off
Coil Combine Mode	Sum of Squares
AutoAlign	Head > Brain
Auto Coil Select	Default
Shim mode	Standard
Adjust with body coil	Off
Confirm freq. adjustment	Off
Assume Silicone	Off
? Ref. amplitude 1H	0.000 V
Adjustment Tolerance	Auto
Adjust volume	
Position	R1.7 A22.7 F28.2
Orientation	T > C11.3
Rotation	0.00 deg
R >> L	256 mm
A >> P	184 mm
F >> H	144 mm

Physio

1st Signal/Mode	None
Segments	1
Tagging	None
Dark blood	Off
Resp. control	Off

Inline

Subtract	Off
Liver registration	Off
Std-Dev-Sag	Off
Std-Dev-Cor	Off
Std-Dev-Tra	Off
Std-Dev-Time	Off
MIP-Sag	Off
MIP-Cor	Off
MIP-Tra	Off
MIP-Time	Off
Save original images	On
Wash - In	Off
Wash - Out	Off
TTP	Off
PEI	Off

MIP - time	Off
MapIt	None
Contrasts	1

Sequence

Introduction	Off
Dimension	3D
Elliptical scanning	Off
Phase stabilisation	Off
Asymmetric echo	Off
Bandwidth	30 Hz/Px
Flow comp.	Slice/Read
RF pulse type	Fast
Gradient mode	Fast*
Excitation	Slab-sel.
RF spoiling	On

\\USER\FMRIB User\2013_07 Exercise\HighResHippo\jn_svs_special_exc_occipital_w

TA: 0:36 VoI: 20 ×20 ×20 mm Rel. SNR: 1.00 USER: jn_svs_special_exc

Properties

Prio Recon	Off
Before measurement	
After measurement	
Load to viewer	On
Inline movie	Off
Auto store images	On
Load to stamp segments	Off
Load images to graphic segments	Off
Auto open inline display	Off
Start measurement without further preparation	On
Wait for user to start	Off
Start measurements	single

Routine

Position	L0.0 P33.1 F36.4
Orientation	Coronal
Rotation	0.00 deg
VoI R >> L	20 mm
VoI F >> H	20 mm
VoI A >> P	20 mm
TR	4500 ms
TE	8.50 ms
Averages	8
Filter	None
Coil elements	A32

Contrast

Flip angle	90 deg
Water suppr.	None
Spectral suppr.	None
Measurements	1

Resolution

Prescan Normalize	Off
Vector size	2048

Geometry

Sat. region 1	
Thickness	100 mm
Position	R66.1 P0.0 H0.0
Orientation	Sagittal
Sat. delta frequ.	-3.00 ppm
Sat. region 2	
Thickness	100 mm
Position	L65.5 P0.0 H0.0
Orientation	Sagittal
Sat. delta frequ.	-3.00 ppm
Table position	H
Table position	0 mm
Inline Composing	Off

System

A32	On
V32	Off
Positioning mode	REF
MSMA	S - C - T
Sagittal	R >> L
Coronal	A >> P
Transversal	F >> H
Save uncombined	Off
AutoAlign	---
Auto Coil Select	Default
Shim mode	Advanced
Adj. water suppr.	On
Adjust with body coil	Off
Confirm freq. adjustment	Off
Assume Silicone	Off
? Ref. amplitude 1H	0.000 V
Adjustment Tolerance	Auto
Adjust volume	
! Position	L0.0 P33.1 F36.4
! Orientation	Coronal
! Rotation	0.00 deg
! F >> H	30 mm
! R >> L	30 mm
! A >> P	30 mm

Physio

1st Signal/Mode	None

Composing

Sequence

Preparation scans	0
Delta frequency	-2.3 ppm
Phase cycling	Auto
Bandwidth	4000 Hz
Acquisition duration	512 ms
Remove oversampling	On
Adiabatic Inversion	On
Inversion Duration	5000 us
Wait time after Inversion	22425 us
Excitation Duration	1600 us
Asymm Excite Pulse	On
Pi Pulse Duration	5500 us
sp1 amp	20 mT/m
sp1 dur	880 us
Even/Odd Subtraction	On
VAPOR	On
VAPOR PhaseCycle	On
VAPOR Flip Angle	65 degrees
VapTau8	18000 us

\\USER\FMRIB User\2013_07 Exercise\HighResHippo\jn_svs_special_exc_occipital

TA: 4:30 VoI: 20 ×20 ×20 mm Rel. SNR: 1.00 USER: jn_svs_special_exc

Properties

Prio Recon	Off
Before measurement	
After measurement	
Load to viewer	On
Inline movie	Off
Auto store images	On
Load to stamp segments	Off
Load images to graphic segments	Off
Auto open inline display	Off
Start measurement without further preparation	On
Wait for user to start	Off
Start measurements	single

Routine

Position	L0.0 P33.1 F36.4
Orientation	Coronal
Rotation	0.00 deg
VoI R >> L	20 mm
VoI F >> H	20 mm
VoI A >> P	20 mm
TR	4500 ms
TE	8.50 ms
Averages	60
Filter	None
Coil elements	A32

Contrast

Flip angle	90 deg
Water suppr.	Water sat.
Water suppr. BW	45 Hz
Spectral suppr.	None
Measurements	1

Resolution

Prescan Normalize	Off
Vector size	2048

Geometry

Sat. region 1	
Thickness	100 mm
Position	R66.1 P0.0 H0.0
Orientation	Sagittal
Sat. delta frequ.	-3.00 ppm
Sat. region 2	
Thickness	100 mm
Position	L65.5 P0.0 H0.0
Orientation	Sagittal
Sat. delta frequ.	-3.00 ppm
Table position	H
Table position	0 mm
Inline Composing	Off

System

A32	On
V32	Off
Positioning mode	REF
MSMA	S - C - T
Sagittal	R >> L
Coronal	A >> P
Transversal	F >> H
Save uncombined	Off

AutoAlign	---
Auto Coil Select	Default
Shim mode	Advanced
Adj. water suppr.	On
Adjust with body coil	Off
Confirm freq. adjustment	Off
Assume Silicone	Off
? Ref. amplitude 1H	0.000 V
Adjustment Tolerance	Auto
Adjust volume	
! Position	L0.0 P33.1 F36.4
! Orientation	Coronal
! Rotation	0.00 deg
! F >> H	30 mm
! R >> L	30 mm
! A >> P	30 mm

Physio

1st Signal/Mode	None

Composing

Sequence

Preparation scans	0
Delta frequency	-2.3 ppm
Phase cycling	Auto
Bandwidth	4000 Hz
Acquisition duration	512 ms
Remove oversampling	On
Adiabatic Inversion	On
Inversion Duration	5000 us
Wait time after Inversion	22425 us
Excitation Duration	1600 us
Asymm Excite Pulse	On
Pi Pulse Duration	5500 us
sp1 amp	20 mT/m
sp1 dur	880 us
Even/Odd Subtraction	On
VAPOR	On
VAPOR PhaseCycle	On
VAPOR Flip Angle	65 degrees
VapTau8	18000 us

\\USER\FMRIB User\2013_07 Exercise\HighResHippo\ep2d_bold_sine_676b_2mm

TA: 6:15 PAT: 2 Voxel size: 2.0×2.0×2.0 mm Rel. SNR: 1.00 USER: ep2d_bold_sine_676b

Properties

Prio Recon	Off
Before measurement	
After measurement	
Load to viewer	On
Inline movie	Off
Auto store images	On
Load to stamp segments	Off
Load images to graphic segments	Off
Auto open inline display	Off
Start measurement without further preparation	On
Wait for user to start	On
Start measurements	single

Routine

Slice group 1	
Slices	60
Dist. factor	0 %
Position	L0.0 A18.9 F20.0
Orientation	Transversal
Phase enc. dir.	A >> P
Rotation	0.00 deg
Phase oversampling	0 %
FoV read	220 mm
FoV phase	100.0 %
Slice thickness	2.0 mm
TR	3500 ms
TE	25 ms
Averages	1
Concatenations	1
Filter	None
Coil elements	A32

Contrast

MTC	Off
Flip angle	90 deg
Fat suppr.	Fat sat.
Averaging mode	Long term
Reconstruction	Magnitude
Measurements	100
Delay in TR	0 ms
Multiple series	Off

Resolution

Base resolution	110
Phase resolution	100 %
Phase partial Fourier	Off
Interpolation	Off
PAT mode	GRAPPA
Accel. factor PE	2
Ref. lines PE	40
Reference scan mode	Separate
Distortion Corr.	Off
Prescan Normalize	Off
Raw filter	On
Elliptical filter	Off
Hamming	Off

Geometry

Multi-slice mode	Interleaved
Series	Interleaved
Special sat.	None
Table position	H
Table position	0 mm
Inline Composing	Off

System

A32	On
V32	Off
Positioning mode	REF
MSMA	S - C - T
Sagittal	R >> L
Coronal	A >> P
Transversal	F >> H
Coil Combine Mode	Adaptive Combine
AutoAlign	---
Auto Coil Select	Default
Shim mode	Standard
Adjust with body coil	Off
Confirm freq. adjustment	Off
Assume Silicone	Off
? Ref. amplitude 1H	0.000 V
Adjustment Tolerance	Auto
Adjust volume	
Position	L0.0 A18.9 F20.0
Orientation	Transversal
Rotation	0.00 deg
R >> L	220 mm
A >> P	220 mm
F >> H	120 mm

Physio

1st Signal/Mode	None

BOLD

GLM Statistics	Off
Dynamic t-maps	Off
Starting ignore meas	0
Ignore after transition	0
Model transition states	On
Temp. highpass filter	On
Threshold	4.00
Paradigm size	20
Meas[1]	Baseline
Meas[2]	Baseline
Meas[3]	Baseline
Meas[4]	Baseline
Meas[5]	Baseline
Meas[6]	Baseline
Meas[7]	Baseline
Meas[8]	Baseline
Meas[9]	Baseline
Meas[10]	Baseline
Meas[11]	Active
Meas[12]	Active
Meas[13]	Active
Meas[14]	Active
Meas[15]	Active
Meas[16]	Active
Meas[17]	Active
Meas[18]	Active
Meas[19]	Active
Meas[20]	Active
Motion correction	Off
Spatial filter	Off

Sequence

Introduction	Off
Bandwidth	1568 Hz/Px
Echo spacing	0.72 ms
EPI factor	110
RF pulse type	Normal
Gradient mode	Fast
iPAT reference mode	FLASH
iPAT ref. base res.	64
iPAT ref. bandwidth	200 Hz/Px
iPAT ref. TE	5.1 ms
iPAT ref. flip angle	5 deg
Readout type	Sinusoidal
Phase correction	Local
FatSat flip angle	110 deg
RF pulse type	Sinc
Excitation length	3072 us
BW-Time product	5.20
FFT factor	1.00

Bibliography

Aarts, E., Verhage, M., Veenvliet, J. V., Dolan, C. V., & van der Sluis, S. (2014). A solution to dependency: using multilevel analysis to accommodate nested data. Nature neuroscience, 17, 491–496.

Aberg, M. A. I., Pedersen, N. L., Torén, K., Svartengren, M., Bäckstrand, B., Johnsson, T., Cooper-Kuhn, C. M., Aberg, N. D., Nilsson, M., & Kuhn, H. G. (2009). Cardiovascular fitness is associated with cognition in young adulthood. Proceedings of the National Academy of Sciences of the United States of America, 106, 20906–20911.

Adler, D. H., Pluta, J., Kadivar, S., Craige, C., Gee, J. C., Avants, B. B., & Yushkevich, P. A. (2014). Histology-derived volumetric annotation of the human hippocampal subfields in postmortem MRI. NeuroImage, 84, 505–523.

Ainsworth, B. E., Bassett, D. R., Strath, S. J., Swartz, A. M., O'Brien, W. L., Thompson, R. W., Jones, D. A., Macera, C. A., & Kimsey, C. D. (2000). Comparison of three methods for measuring the time spent in physical activity. Medicine and science in sports and exercise, 32, S457–64.

Altman, J. & Das, G. D. (1965). Autoradiographic and histological evidence of postnatal hippocampal neurogenesis in rats. The Journal of comparative neurology, 124, 319–335.

and Sotiropoulos, S. N. S., Savio, A. M. A., Graña, M. M., & Behrens, T. E. J. T. (2012). Model-based analysis of multishell diffusion MR data for tractography: how to get over fitting problems. Magnetic resonance in medicine : official journal of the Society of

Magnetic Resonance in Medicine / Society of Magnetic Resonance in Medicine, 68, 1846–1855.

Anderson, B. J., Li, X., Alcantara, A. A., Isaacs, K. R., Black, J. E., & Greenough, W. T. (1994). Glial hypertrophy is associated with synaptogenesis following motor-skill learning, but not with angiogenesis following exercise. Glia, 11, 73–80.

Anderson-Hanley, C., Arciero, P. J., Brickman, A. M., Nimon, J. P., Okuma, N., Westen, S. C., Merz, M. E., Pence, B. D., Woods, J. A., Kramer, A. F., & Zimmerman, E. A. (2012). Exergaming and older adult cognition a cluster randomized clinical trial. American journal of preventive medicine, 42, 109–119.

Andersson, J. L. (2007a). Non-linear optimisation . Tech. Rep. TR07JA1, FMRIB, University of Oxford, United Kingdom.

Andersson, J. L. (2007b). Non-linear registration aka Spatial normalisation. Tech. Rep. TR07JA2, FMRIB, University of Oxford, United Kingdom.

Andersson, J. L. R. J., Skare, S. S., & Ashburner, J. J. (2003). How to correct susceptibility distortions in spin-echo echo-planar images: application to diffusion tensor imaging. NeuroImage, 20, 19–19.

Andrews-Hanna, J. R., Snyder, A. Z., Vincent, J. L., Lustig, C., Head, D., Raichle, M. E., & Buckner, R. L. (2007). Disruption of large-scale brain systems in advanced aging. Neuron, 56, 924–935.

Angevaren, M., Aufdemkampe, G., Verhaar, H. J. J., Aleman, A., & Vanhees, L. (2008). Physical activity and enhanced fitness to improve cognitive function in older people without known cognitive impairment. Cochrane Database of Systematic Reviews, p. CD005381.

Arnold, S. E. & Rioux, L. (2001). Challenges, status, and opportunities for studying developmental neuropathology in adult schizophrenia. Schizophrenia Bulletin, 27, 395–416.

Ashburner, J. & Friston, K. (2000). Voxel-based morphometry–the methods. NeuroImage, 11, 805–821.

Ashburner, J. & Friston, K. (2004). Morphometry. In Human Brain Function. (Academic Press).

Ashburner, J., Hutton, C., Frackowiak, R., Johnsrude, I., Price, C., & Friston, K. (1998). Identifying global anatomical differences: deformation-based morphometry. Human brain mapping, 6, 348–357.

Åstrand, P.-O., Rodahl, K., Dahl, H. A., & Stromme, S. B. (2003). Textbook of Work Physiology-4th: Physiological Bases of Exercise. (Human Kinetics), 4th edn.

Augustinack, J. C., Magnain, C., Reuter, M., van der Kouwe, A. J. W., Boas, D., & Fischl, B. (2013). MRI parcellation of ex vivo medial temporal lobe. NeuroImage.

Avants, B. B., Tustison, N. J., Song, G., Cook, P. A., Klein, A., & Gee, J. C. (2011). A reproducible evaluation of ANTs similarity metric performance in brain image registration. NeuroImage, 54, 2033–2044.

Avants, B. B., Yushkevich, P., Pluta, J., Minkoff, D., Korczykowski, M., Detre, J., & Gee, J. C. (2010). The optimal template effect in hippocampus studies of diseased populations. NeuroImage, 49, 2457–2466.

Baecke, J. A., Burema, J., & Frijters, J. E. (1982). A short questionnaire for the measurement of habitual physical activity in epidemiological studies. The American journal of clinical nutrition, 36, 936–942.

Barbier, E. L., Lamalle, L., & Décorps, M. (2001). Methodology of brain perfusion imaging. Journal of magnetic resonance imaging : JMRI, 13, 496–520.

Bartzokis, G., Tishler, T. A., Lu, P. H., Villablanca, P., Altshuler, L. L., Carter, M., Huang, D., Edwards, N., & Mintz, J. (2007). Brain ferritin iron may influence age- and gender-related risks of neurodegeneration. Neurobiology of aging, 28, 414–423.

Basser, P. J., Mattiello, J., & LeBihan, D. (1994). MR diffusion tensor spectroscopy and imaging. Biophysical Journal, 66, 259–267.

Basso, M. R., Bornstein, R. A., & Lang, J. M. (1999). Practice effects on commonly used measures of executive function across twelve months. The Clinical Neuropsychologist (Neuropsychology, Development and Cognition: Section D), 13, 283–292.

Battal, B., Kocaoglu, M., Bulakbasi, N., Husmen, G., Tuba Sanal, H., & Tayfun, C. (2011). Cerebrospinal fluid flow imaging by using phase-contrast MR technique. The British journal of radiology, 84, 758–765.

Becker, E. D. (1993). A brief history of nuclear magnetic resonance. Analytical chemistry, 65, 295A–302A.

Behrens, T. E. J. T., Woolrich, M. W. M., Jenkinson, M. M., Johansen-Berg, H. H., Nunes, R. G. R., Clare, S. S., Matthews, P. M. P., Brady, J. M. J., & Smith, S. M. S. (2003). Characterization and propagation of uncertainty in diffusion-weighted MR imaging. Magnetic resonance in medicine : official journal of the Society of Magnetic Resonance in Medicine / Society of Magnetic Resonance in Medicine, 50, 1077–1088.

Benedict, C., Brooks, S. J., Kullberg, J., Nordenskjöld, R., Burgos, J., Le Grevès, M., Kilander, L., Larsson, E.-M., Johansson, L., Ahlström, H., Lind, L., & Schiöth, H. B. (2012). Association between physical activity and brain health in older adults. Neurobiology of aging.

Benes, F. M., Turtle, M., Khan, Y., & Farol, P. (1994). Myelination of a key relay zone in the hippocampal formation occurs in the human brain during childhood, adolescence, and adulthood. Archives of general psychiatry, 51, 477–484.

Bernal-Rusiel, J. L., Greve, D. N., Reuter, M., Fischl, B., & Sabuncu, M. R. (2013a). Statistical analysis of longitudinal neuroimage data with Linear Mixed Effects models. NeuroImage, 66, 249–260.

Bernal-Rusiel, J. L., Reuter, M., Greve, D. N., Fischl, B., Sabuncu, M. R., & Alzheimer's Disease Neuroimaging Initiative (2013b). Spatiotemporal linear mixed effects modeling

for the mass-univariate analysis of longitudinal neuroimage data. NeuroImage, 81, 358–370.

Bigard, A. X., Duforez, F., Portero, P., & Guezennec, C. Y. (1992). Assessment of physical activity by questionnaire: Validity of the Baecke questionnaire | DETERMINATION DE L'ACTIVITE PHYSIQUE PAR QUESTIONNAIRE: VALIDATION DU QUESTIONNAIRE AUTOADMINISTRABLE DE BAECKE. Science and Sports, 7, 215–221.

Bilgic, B., Pfefferbaum, A., Rohlfing, T., Sullivan, E. V., & Adalsteinsson, E. (2012). MRI estimates of brain iron concentration in normal aging using quantitative susceptibility mapping. NeuroImage, 59, 2625–2635.

Black, J., Isaacs, K., Anderson, B., Alcantara, A., & Greenough, W. (1990). Learning causes synaptogenesis, whereas motor activity causes angiogenesis, in cerebellar cortex of adult rats. Proc Natl Acad Sci U S A, 87, 5568–5572.

Blair, S. N., Kohl, H. W., Gordon, N. F., & Paffenbarger, Jr, R. S. (1992). How much physical activity is good for health? Annual Review of Public Health, 13, 99–126.

Bloch, F., Hansen, W. W., & Packard, M. (1946). The nuclear induction experiment. Physical Review, 70, 474–485.

Bloor, C. M. (2005). Angiogenesis during exercise and training. Angiogenesis, 8, 263–271.

Blumenfeld-Katzir, T., Pasternak, O., Dagan, M., & Assaf, Y. (2011). Diffusion MRI of structural brain plasticity induced by a learning and memory task. PLoS ONE, 6, e20678.

Boldrini, M., Underwood, M. D., Hen, R., Rosoklija, G. B., Dwork, A. J., Mann, J. J., & Arango, V. (2009). Antidepressants increase neural progenitor cells in the human hippocampus. Neuropsychopharmacology : official publication of the American College of Neuropsychopharmacology, 34, 2376–2389.

Borg, G. (1970). Perceived exertion as an indicator of somatic stress. Scandinavian journal of rehabilitation medicine, 2, 92–98.

Borkowski, J. & Benton, A. (1967). Word fluency and brain damage. Neuropsychologia.

Bouchard, C. & Rankinen, T. (2001). Individual differences in response to regular physical activity. Medicine and science in sports and exercise, 33, S446–51– discussion S452–3.

Bouchard, C., Sarzynski, M. A., Rice, T. K., Kraus, W. E., Church, T. S., Sung, Y. J., Rao, D. C., & Rankinen, T. (2010). Genomic Predictors of Maximal Oxygen Uptake Response to Standardized Exercise Training Programs. Journal of applied physiology (Bethesda, Md : 1985).

Braitenberg, V. & Schüz, A. (1998). Cortex: Statistics and Geometry of Neuronal Connectivity. (Springer), 2nd edn.

Bryan, A., Hutchison, K. E., Seals, D. R., & Allen, D. L. (2007). A transdisciplinary model integrating genetic, physiological, and psychological correlates of voluntary exercise. Health psychology : official journal of the Division of Health Psychology, American Psychological Association, 26, 30–39.

Bullitt, E., Rahman, F. N., Smith, J. K., Kim, E., Zeng, D., Katz, L. M., & Marks, B. L. (2009). The effect of exercise on the cerebral vasculature of healthy aged subjects as visualized by MR angiography. AJNR American journal of neuroradiology, 30, 1857–1863.

Busse, A., Jacob Filho, W., Magaldi, R., & Coelho, V. (2008). Effects of resistance training exercise on cognitive performance in elderly individuals with memory impairment: results of a controlled trial. Einstein, 6, 402–407.

Butters, M. A., Young, J. B., Lopez, O., Aizenstein, H. J., Mulsant, B. H., Reynolds, C. F., DeKosky, S. T., & Becker, J. T. (2008). Pathways linking late-life depression to persistent cognitive impairment and dementia. Dialogues in clinical neuroscience, 10, 345–357.

Cancela Carral, J. M. & Ayán Pérez, C. (2007). Effects of high-intensity combined training on women over 65. Gerontology, 53, 340–346.

Canu, M.-H., Carnaud, M., Picquet, F., & Goutebroze, L. (2009). Activity-dependent regulation of myelin maintenance in the adult rat. Brain Research, 1252, 45–51.

Carletti, B. & Rossi, F. (2008). Neurogenesis in the cerebellum. The Neuroscientist : a review journal bringing neurobiology, neurology and psychiatry, 14, 91–100.

Carr, H. (1958). Steady-State Free Precession in Nuclear Magnetic Resonance. Physical Review, 112, 1693–1701.

Caspersen, C. J., Powell, K. E., & Christenson, G. M. (1985). Physical activity, exercise, and physical fitness: definitions and distinctions for health-related research. Public health reports (Washington, DC : 1974), 100, 126–131.

Cassilhas, R. C., Viana, V. A. R., Grassmann, V., Santos, R. T., Santos, R. F., Tufik, S., & Mello, M. T. (2007). The impact of resistance exercise on the cognitive function of the elderly. Medicine and science in sports and exercise, 39, 1401–1407.

Cauthen, N. R. (1978). Verbal fluency: normative data. Journal of clinical psychology, 34, 126–129.

Caviness, V. S., Filipek, P. A., & Kennedy, D. N. (1989). Magnetic resonance technology in human brain science: blueprint for a program based upon morphometry. Brain & development, 11, 1–13.

Chaddock, L., Erickson, K. I., Prakash, R. S., Kim, J. S., Voss, M. W., Vanpatter, M., Pontifex, M. B., Raine, L. B., Konkel, A., Hillman, C. H., Cohen, N. J., & Kramer, A. F. (2010). A neuroimaging investigation of the association between aerobic fitness, hippocampal volume, and memory performance in preadolescent children. Brain Research, 1358, 172–183.

Chen, G., Saad, Z. S., Britton, J. C., Pine, D. S., & Cox, R. W. (2013a). Linear mixed-effects modeling approach to FMRI group analysis. NeuroImage, 73, 176–190.

Chen, W. C., Foxley, S., & Miller, K. L. (2013b). Detecting microstructural properties of white matter based on compartmentalization of magnetic susceptibility. NeuroImage, 70, 1–9.

Cheng, K. (2011). Revealing human ocular dominance columns using high-resolution functional magnetic resonance imaging. NeuroImage.

Cherniak, C. (1990). The bounded brain: Toward quantitative neuroanatomy. Journal of Cognitive Neuroscience, 2, 58–68.

Chklovskii, D. B., Schikorski, T., & Stevens, C. F. (2002). Wiring optimization in cortical circuits. Neuron, 34, 341–347.

Cho, Z.-H., Han, J.-Y., Hwang, S.-I., Kim, D.-s., Kim, K.-N., Kim, N.-B., Kim, S. J., Chi, J.-G., Park, C.-W., & Kim, Y.-B. (2010). Quantitative analysis of the hippocampus using images obtained from 7.0 T MRI. NeuroImage, 49, 2134–2140.

Chung, M. K., Worsley, K. J., Paus, T., Cherif, C., Collins, D. L., Giedd, J. N., Rapoport, J. L., & Evans, A. C. (2001). A unified statistical approach to deformation-based morphometry. NeuroImage, 14, 595–606.

Colcombe, S. & Kramer, A. F. (2003). Fitness effects on the cognitive function of older adults: a meta-analytic study. Psychological science : a journal of the American Psychological Society / APS, 14, 125–130.

Colcombe, S. J., Erickson, K. I., Scalf, P. E., Kim, J. S., Prakash, R., McAuley, E., Elavsky, S., Marquez, D. X., Hu, L., & Kramer, A. F. (2006). Aerobic exercise training increases brain volume in aging humans. The journals of gerontology Series A, Biological sciences and medical sciences, 61, 1166–1170.

Colcombe, S. J., Kramer, A. F., Erickson, K. I., Scalf, P., McAuley, E., Cohen, N. J., Webb, A., Jerome, G. J., Marquez, D. X., & Elavsky, S. (2004). Cardiovascular fitness, cortical plasticity, and aging. Proceedings of the National Academy of Sciences of the United States of America, 101, 3316–3321.

Colucci-D'Amato, L. & di Porzio, U. (2008). Neurogenesis in adult CNS: from denial to opportunities and challenges for therapy. BioEssays : news and reviews in molecular, cellular and developmental biology, 30, 135–145.

Connor, J. R. & Menzies, S. L. (1996). Relationship of iron to oligodendrocytes and myelination. Glia, 17, 83–93.

Convertino, V. A. (1991). Blood volume: its adaptation to endurance training. Medicine and science in sports and exercise, 23, 1338–1348.

Convertino, V. A. (2007). Blood volume response to physical activity and inactivity. The American journal of the medical sciences, 334, 72–79.

Corwin, J. & Bylsma, F. W. (1993). Psychological examination of traumatic encephalopathy. Clinical Neuropsychologist, 7, 3–21.

Couillard-Despres, S. & Aigner, L. (2011). In vivo imaging of adult neurogenesis. European Journal of Neuroscience, 33, 1037–1044.

Craig, C. L., Marshall, A. L., Sjöström, M., Bauman, A. E., Booth, M. L., Ainsworth, B. E., Pratt, M., Ekelund, U., Yngve, A., Sallis, J. F., & Oja, P. (2003). International physical activity questionnaire: 12-country reliability and validity. Medicine and science in sports and exercise, 35, 1381–1395.

Dale, A. M., Fischl, B., & Sereno, M. I. (1999). Cortical surface-based analysis. I. Segmentation and surface reconstruction. NeuroImage, 9, 179–194.

Das, S. R., Avants, B. B., Pluta, J., Wang, H., Suh, J. W., Weiner, M. W., Mueller, S. G., & Yushkevich, P. A. (2012). Measuring longitudinal change in the hippocampal formation from in vivo high-resolution T2-weighted MRI. NeuroImage, 60, 1266–1279.

de Lange, F. P., Koers, A., Kalkman, J. S., Bleijenberg, G., Hagoort, P., van der Meer, J. W. M., & Toni, I. (2008). Increase in prefrontal cortical volume following cognitive behavioural therapy in patients with chronic fatigue syndrome. Brain : a journal of neurology, 131, 2172–2180.

Deistung, A., Schäfer, A., Schweser, F., Biedermann, U., Turner, R., & Reichenbach, J. R. (2013). Toward in vivo histology: a comparison of quantitative susceptibility mapping (QSM) with magnitude-, phase-, and R2*-imaging at ultra-high magnetic field strength. NeuroImage, 65, 299–314.

Deoni, S. C. L. (2007). High-resolution T1 mapping of the brain at 3T with driven equilibrium single pulse observation of T1 with high-speed incorporation of RF field inhomogeneities (DESPOT1-HIFI). Journal of magnetic resonance imaging : JMRI, 26, 1106–1111.

Deoni, S. C. L. (2009). Transverse relaxation time (T2) mapping in the brain with off-resonance correction using phase-cycled steady-state free precession imaging. Journal of magnetic resonance imaging : JMRI, 30, 411–417.

Deoni, S. C. L., Matthews, L., & Kolind, S. H. (2013). One component? Two components? Three? The effect of including a nonexchanging "free" water component in multicomponent driven equilibrium single pulse observation of T1 and T2. Magnetic resonance in medicine : official journal of the Society of Magnetic Resonance in Medicine / Society of Magnetic Resonance in Medicine, 70, 147–154.

Deoni, S. C. L., Peters, T. M., & Rutt, B. K. (2004). Quantitative diffusion imaging with steady-state free precession. Magnetic resonance in medicine : official journal of the Society of Magnetic Resonance in Medicine / Society of Magnetic Resonance in Medicine, 51, 428–433.

Deoni, S. C. L., Peters, T. M., & Rutt, B. K. (2005). High-resolution T1 and T2 mapping of the brain in a clinically acceptable time with DESPOT1 and DESPOT2. Magnetic resonance in medicine : official journal of the Society of Magnetic Resonance in Medicine / Society of Magnetic Resonance in Medicine, 53, 237–241.

Deoni, S. C. L., Rutt, B. K., Arun, T., Pierpaoli, C., & Jones, D. K. (2008). Gleaning multicomponent T1 and T2 information from steady-state imaging data. Magnetic resonance in medicine : official journal of the Society of Magnetic Resonance in Medicine / Society of Magnetic Resonance in Medicine, 60, 1372–1387.

Diamond, M., Krech, D., & Rosenzweig, M. R. (1964). THE EFFECTS OF AN ENRICHED ENVIRONMENT ON THE HISTOLOGY OF THE RAT. The Journal of comparative neurology, 123, 111–120.

Dickson, J. M., Weavers, H. M., Mitchell, N., Winter, E. M., Wilkinson, I. D., Van Beek, E. J. R., Wild, J. M., & Griffiths, P. D. (2005). The effects of dehydration on brain volume – preliminary results. International journal of sports medicine, 26, 481–485.

Ding, Y.-H., Li, J., Zhou, Y., Rafols, J. A., Clark, J. C., & Ding, Y. (2006). Cerebral angiogenesis and expression of angiogenic factors in aging rats after exercise. Current neurovascular research, 3, 15–23.

Ding, Y.-H., Young, C. N., Luan, X., Li, J., Rafols, J. A., Clark, J. C., McAllister, J. P., & Ding, Y. (2005). Exercise preconditioning ameliorates inflammatory injury in ischemic rats during reperfusion. Acta neuropathologica, 109, 237–246.

Draganski, B., Gaser, C., Busch, V., Schuierer, G., Bogdahn, U., & May, A. (2004). Neuroplasticity: Changes in grey matter induced by training - Newly honed juggling skills show up as a transient feature on a brain-imaging scan. Nature, 427, 311–312.

Draganski, B., Gaser, C., Kempermann, G., Kuhn, H. G., Winkler, J., Büchel, C., & May, A. (2006). Temporal and spatial dynamics of brain structure changes during extensive learning. The Journal of neuroscience : the official journal of the Society for Neuroscience, 26, 6314–6317.

Drayer, B., Burger, P., Darwin, R., Riederer, S., Herfkens, R., & Johnson, G. A. (1986). MRI of brain iron. AJR American journal of roentgenology, 147, 103–110.

Duvernoy, H. M. (2005). The Human Hippocampus. Functional Anatomy, Vascularization and Serial Sections with MRI. (Springer).

Duyn, J. (2013). MR susceptibility imaging. Journal of magnetic resonance (San Diego, Calif. : 1997), 229, 198–207.

Duyn, J. H., van Gelderen, P., Li, T.-Q., de Zwart, J. A., Koretsky, A. P., & Fukunaga, M. (2007). High-field MRI of brain cortical substructure based on signal phase. Proc Natl Acad Sci U S A, 104, 11796–11801.

Dwyer, D. (2002). Glucose metabolism in the brain. (Amsterdam ; Boston : Academic Press).

Eickhoff, S., Walters, N. B., Schleicher, A., Kril, J., Egan, G. F., Zilles, K., Watson, J. D. G., & Amunts, K. (2005). High-resolution MRI reflects myeloarchitecture and cytoarchitecture of human cerebral cortex. Human brain mapping, 24, 206–215.

El-Sayed, M. S., Ali, N., & El-Sayed Ali, Z. (2005). Haemorheology in exercise and training. Sports medicine (Auckland, N.Z.), 35, 649–670.

Emir, U. E., Auerbach, E. J., van de Moortele, P. F., Marjańska, M., Ugurbil, K., Terpstra, M., Tkáč, I., & Öz, G. (2012). Regional neurochemical profiles in the human brain measured by 1H MRS at 7T using local B 1 shimming. NMR in Biomedicine, 25, 152–160.

Erickson, K. I., Colcombe, S. J., Elavsky, S., McAuley, E., Korol, D. L., Scalf, P. E., & Kramer, A. F. (2007). Interactive effects of fitness and hormone treatment on brain health in postmenopausal women. Neurobiology of aging, 28, 179–185.

Erickson, K. I., Miller, D. L., & Roecklein, K. A. (2012). The aging hippocampus: interactions between exercise, depression, and BDNF. The Neuroscientist : a review journal bringing neurobiology, neurology and psychiatry, 18, 82–97.

Erickson, K. I., Prakash, R. S., Voss, M. W., Chaddock, L., Hu, L., Morris, K. S., White, S. M., Wójcicki, T. R., McAuley, E., & Kramer, A. F. (2009). Aerobic fitness is associated with hippocampal volume in elderly humans. Hippocampus, 19, 1030–1039.

Erickson, K. I., Voss, M. W., Prakash, R. S., Basak, C., Szabo, A., Chaddock, L., Kim, J. S., Heo, S., Alves, H., White, S. M., Wójcicki, T. R., Mailey, E., Vieira, V. J., Martin, S. A., Pence, B. D., Woods, J. A., McAuley, E., & Kramer, A. F. (2011). Exercise training increases size of hippocampus and improves memory. Proceedings of the National Academy of Sciences of the United States of America, 108, 3017–3022.

Ertl, A. C., Diedrich, A., & Raj, S. R. (2007). Techniques used for the determination of blood volume. The American journal of the medical sciences, 334, 32–36.

Farrer, L. A., Cupples, L. A., Haines, J. L., Hyman, B., Kukull, W. A., Mayeux, R., Myers,

R. H., Pericak-Vance, M. A., Risch, N., & van Duijn, C. M. (1997). Effects of age, sex, and ethnicity on the association between apolipoprotein E genotype and Alzheimer disease. A meta-analysis. APOE and Alzheimer Disease Meta Analysis Consortium. JAMA : the journal of the American Medical Association, 278, 1349–1356.

Fennema-Notestine, C., Ozyurt, I. B., Clark, C. P., Morris, S., Bischoff-Grethe, A., Bondi, M. W., Jernigan, T. L., Fischl, B., Segonne, F., Shattuck, D. W., Leahy, R. M., Rex, D. E., Toga, A. W., Zou, K. H., & Brown, G. G. (2006). Quantitative evaluation of automated skull-stripping methods applied to contemporary and legacy images: effects of diagnosis, bias correction, and slice location. Human brain mapping, 27, 99–113.

Fields, R. D. (2010). Change in the Brain's White Matter. Science (New York, NY), 330, 768–769.

Fields, R. D. (2013). Neuroscience: Map the other brain. Nature, 501, 25–27.

Fields, R. D., Araque, A., Johansen-Berg, H., Lim, S.-S., Lynch, G., Nave, K.-A., Nedergaard, M., Perez, R., Sejnowski, T., & Wake, H. (2013). Glial Biology in Learning and Cognition. The Neuroscientist : a review journal bringing neurobiology, neurology and psychiatry.

Fischl, B., Salat, D. H., Busa, E., Albert, M., Dieterich, M., Haselgrove, C., van der Kouwe, A., Killiany, R., Kennedy, D., Klaveness, S., Montillo, A., Makris, N., Rosen, B., & Dale, A. M. (2002). Whole brain segmentation: Automated labeling of neuroanatomical structures in the human brain. Neuron, 33, 341–355.

Fischl, B., Sereno, M. I., & Dale, A. M. (1999). Cortical surface-based analysis. II: Inflation, flattening, and a surface-based coordinate system. NeuroImage, 9, 195–207.

Fischl, B., van der Kouwe, A., Destrieux, C., Halgren, E., Ségonne, F., Salat, D. H., Busa, E., Seidman, L. J., Goldstein, J., Kennedy, D., Caviness, V., Makris, N., Rosen, B., & Dale, A. M. (2004). Automatically Parcellating the Human Cerebral Cortex. Cerebral cortex (New York, NY : 1991), 14, 11–22.

Fitzmaurice, G. M. ., Laird, N. M. ., & Ware, J. H. . (2011). Applied longitudinal analysis. (Hoboken, N.J. : Wiley).

Flöel, A., Ruscheweyh, R., Krüger, K., Willemer, C., Winter, B., Völker, K., Lohmann, H., Zitzmann, M., Mooren, F., Breitenstein, C., & Knecht, S. (2010). Physical activity and memory functions: are neurotrophins and cerebral gray matter volume the missing link? NeuroImage, 49, 2756–2763.

Fox, N. C., Ridgway, G. R., & Schott, J. M. (2011). Algorithms, atrophy and Alzheimer's disease: cautionary tales for clinical trials. NeuroImage, 57, 15–18.

Friston, K. J., Frith, C. D., Dolan, R. J., Price, C. J., Zeki, S., Ashburner, J. T., & Penny, W. D. (2004). Human Brain Function. (Academic Press).

Gauthier, A. P., Lariviere, M., & Young, N. (2009). Psychometric properties of the IPAQ: a validation study in a sample of northern Franco-Ontarians. Journal of physical activity & health, 6 Suppl 1, S54–60.

Glasser, M. F. & Van Essen, D. C. (2011). Mapping human cortical areas in vivo based on myelin content as revealed by T1- and T2-weighted MRI. The Journal of neuroscience : the official journal of the Society for Neuroscience, 31, 11597–11616.

Goldberg, T. E. & Weinberger, D. R. (2004). Genes and the parsing of cognitive processes. Trends in cognitive sciences, 8, 325–335.

Good, C., Johnsrude, I., Ashburner, J., Henson, R., Friston, K., & Frackowiak, R. (2001). A voxel-based morphometric study of ageing in 465 normal adult human brains. NeuroImage, 14, 21–36.

Goodman, L. J., Valverde, J., Lim, F., Geschwind, M. D., Federoff, H. J., Geller, A. I., & Hefti, F. (1996). Regulated release and polarized localization of brain-derived neurotrophic factor in hippocampal neurons. Molecular and cellular neurosciences, 7, 222–238.

Gould, E., Reeves, A. J., Graziano, M. S., & Gross, C. G. (1999). Neurogenesis in the neocortex of adult primates. Science (New York, NY), 286, 548–552.

Green, A. E., Munafò, M. R., DeYoung, C. G., Fossella, J. A., Fan, J., & Gray, J. R. (2008). Using genetic data in cognitive neuroscience: from growing pains to genuine insights. Nature reviews Neuroscience, 9, 710–720.

Greve, D. N. & Fischl, B. (2009). Accurate and robust brain image alignment using boundary-based registration. NeuroImage, 48, 63–72.

Grossman, A. W., Churchill, J. D., Bates, K. E., Kleim, J. A., & Greenough, W. T. (2002). A brain adaptation view of plasticity: is synaptic plasticity an overly limited concept? Progress in brain research, 138, 91–108.

Guillaume, B., Hua, X., Thompson, P. M., Nichols, T. E., Waldorp, L., & Alzheimer's Disease Neuroimaging Initiative (2013). Fast and accurate modelling of longitudinal neuroimaging data: an application to ADNI data. Meeting of the Organization for Human Brain Mapping, pp. 1–1.

Guizzetti, P. (1915). Principali resultati dell'applicazione grossolana a fresco delle reazione istochimiche del ferro sul sistema nervoso centrale dell'uomo e di alcuni mammiferi domestici [Principal results of the application of the histochemical reactions for iron to gross fresh tissue of the central nervous system of man and some domestic animals] . Rivista di Patologia Nervosa e Mentale, 20, 103–117.

Gullans, S. R. & Verbalis, J. G. (1993). Control of brain volume during hyperosmolar and hypoosmolar conditions. Annual review of medicine, 44, 289–301.

Gussew, A., Rzanny, R., Erdtel, M., Scholle, H. C., Kaiser, W. A., Mentzel, H. J., & Reichenbach, J. R. (2010). Time-resolved functional 1H MR spectroscopic detection of glutamate concentration changes in the brain during acute heat pain stimulation. NeuroImage, 49, 1895–1902.

Haacke, E. M. (1999). Magnetic resonance imaging : physical principles and sequence design. (New York : Wiley).

Haacke, E. M., Cheng, N. Y. C., House, M. J., Liu, Q., Neelavalli, J., Ogg, R. J., Khan,

A., Ayaz, M., Kirsch, W., & Obenaus, A. (2005). Imaging iron stores in the brain using magnetic resonance imaging. Magnetic Resonance Imaging, 23, 1–25.

Haacke, E. M., Xu, Y., Cheng, Y.-C. N., & Reichenbach, J. R. (2004). Susceptibility weighted imaging (SWI). Magnetic resonance in medicine : official journal of the Society of Magnetic Resonance in Medicine / Society of Magnetic Resonance in Medicine, 52, 612–618.

Haacke, E. M. & Ye, Y. (2012). The role of susceptibility weighted imaging in functional MRI. NeuroImage, 62, 923–929.

Hallgren, B. B. & Sourander, P. P. (1958). The effect of age on the non-haemin iron in the human brain. Journal of Neurochemistry, 3, 41–51.

Harris, J. M., Whalley, H., Yates, S., Miller, P., Johnstone, E. C., & Lawrie, S. M. (2004). Abnormal cortical folding in high-risk individuals: a predictor of the development of schizophrenia? Biological Psychiatry, 56, 182–189.

Harris, R. K. R. K. & Wasylishen, R. E. (2012). Encyclopedia of NMR. (Chichester, West Sussex, U.K. : John Wiley and Sons).

Haskell, W. L., Lee, I.-M., Pate, R. R., Powell, K. E., Blair, S. N., Franklin, B. A., Macera, C. A., Heath, G. W., Thompson, P. D., & Bauman, A. (2007). Physical activity and public health: updated recommendation for adults from the American College of Sports Medicine and the American Heart Association. Medicine and science in sports and exercise, 39, 1423–1434.

Hawkins, K. A., Dean, D., & Pearlson, G. D. (2004). Alternative forms of the Rey Auditory Verbal Learning Test: a review. Behavioural neurology, 15, 99–107.

Hayasaka, S., Phan, K., Liberzon, I., Worsley, K., & Nichols, T. (2004). Nonstationary cluster-size inference with random field and permutation methods. NeuroImage, 22, 676–687.

Heo, Voss, S., Prakash, M., Erickson, R., Alves, K., Chaddock, H., Szabo, L., Mailey, A., Wojcicki, E., White, T., Gothe, S., McAuley, N., Sutton, E., Kramer, B., & Arthur

(2011). The influence of aerobic fitness on cerebral white matter integrity and cognitive function in older adults: Results of a one-year exercise intervention. UNPUBLISHED - Hum Brain Mapp, pp. 1–52.

Herculano-Houzel, S., Collins, C. E., Wong, P., & Kaas, J. H. (2007). Cellular scaling rules for primate brains. Proceedings of the National Academy of Sciences of the United States of America, 104, 3562–3567.

Hillman, C. H., Erickson, K. I., & Kramer, A. F. (2008). Be smart, exercise your heart: exercise effects on brain and cognition. Nature reviews Neuroscience, 9, 58–65.

Huettel, S. A., Song, A. W., & McCarthy, G. (2008). Functional magnetic resonance imaging. (Sunderland, Mass. : Sinauer Associates).

Iliff, J. J., Wang, M., Liao, Y., Plogg, B. A., Peng, W., Gundersen, G. A., Benveniste, H., Vates, G. E., Deane, R., Goldman, S. A., Nagelhus, E. A., & Nedergaard, M. (2012). A Paravascular Pathway Facilitates CSF Flow Through the Brain Parenchyma and the Clearance of Interstitial Solutes, Including Amyloid β. Science translational medicine, 4, 147ra111–147ra111.

Isaacs, K. R., Anderson, B. J., Alcantara, A. A., Black, J. E., & Greenough, W. T. (1992). Exercise and the brain: angiogenesis in the adult rat cerebellum after vigorous physical activity and motor skill learning. Journal of cerebral blood flow and metabolism : official journal of the International Society of Cerebral Blood Flow and Metabolism, 12, 110–119.

Jackson, A. S., Sui, X., Hébert, J. R., Church, T. S., & Blair, S. N. (2009). Role of lifestyle and aging on the longitudinal change in cardiorespiratory fitness. Archives of internal medicine, 169, 1781–1787.

Jenkinson, M., Bannister, P., Brady, M., & Smith, S. (2002a). Improved optimization for the robust and accurate linear registration and motion correction of brain images. NeuroImage, 17, 825–841.

Jenkinson, M., Beckmann, C. F., Behrens, T. E. J., Woolrich, M. W., & Smith, S. M. (2011). FSL. NeuroImage.

Jenkinson, M. M., Bannister, P. P., Brady, M. M., & Smith, S. S. (2002b). Improved optimization for the robust and accurate linear registration and motion correction of brain images. NeuroImage, 17, 825–841.

Jenkinson, M. M. & Smith, S. S. (2001). A global optimisation method for robust affine registration of brain images. Medical Image Analysis, 5, 143–156.

Johansen-Berg, H. (2010). Behavioural relevance of variation in white matter microstructure. Current Opinion in Neurology, 23, 351–358.

Johansen-Berg, H. (2012). The future of functionally-related structural change assessment. NeuroImage, 62, 1293–1298.

Johansen-Berg, H., Baptista, C. S., & Thomas, A. G. (2012). Human Structural Plasticity at Record Speed. Neuron, 73, 1058–1060.

Johnson, N. F., Kim, C., Clasey, J. L., Bailey, A., & Gold, B. T. (2012). Cardiorespiratory fitness is positively correlated with cerebral white matter integrity in healthy seniors. NeuroImage, 59, 1514–1523.

Jones, A. M. & Carter, H. (2000). The effect of endurance training on parameters of aerobic fitness. Sports medicine (Auckland, N.Z.), 29, 373–386.

Kappers, C. U. A., Huber, G. C., & Crosby, E. C. (1936). The comparative anatomy of the nervous system of vertebrates, including man, Volume 1. (New York, Macmillan).

Karp, A., Paillard-Borg, S., Wang, H.-X., Silverstein, M., Winblad, B., & Fratiglioni, L. (2006). Mental, physical and social components in leisure activities equally contribute to decrease dementia risk. Dementia and Geriatric Cognitive Disorders, 21, 65–73.

Kempermann, G., Fabel, K., Ehninger, D., Babu, H., Leal-Galicia, P., Garthe, A., & Wolf, S. A. (2010). Why and how physical activity promotes experience-induced brain plasticity. Frontiers in neuroscience, 4, 189.

Kempermann, G., Kuhn, H. G., & Gage, F. H. (1997). More hippocampal neurons in adult mice living in an enriched environment. Nature, 386, 493–495.

Kempton, M. J., Ettinger, U., Foster, R., Williams, S. C. R., Calvert, G. A., Hampshire, A., Zelaya, F. O., O'Gorman, R. L., McMorris, T., Owen, A. M., & Smith, M. S. (2011). Dehydration affects brain structure and function in healthy adolescents. Human brain mapping, 32, 71–79.

Kempton, M. J., Ettinger, U., Schmechtig, A., Winter, E. M., Smith, L., McMorris, T., Wilkinson, I. D., Williams, S. C. R., & Smith, M. S. (2009). Effects of acute dehydration on brain morphology in healthy humans. Human brain mapping, 30, 291–298.

Kerchner, G. A., Hess, C. P., Hammond-Rosenbluth, K. E., Xu, D., Rabinovici, G. D., Kelley, D. A. C., Vigneron, D. B., Nelson, S. J., & Miller, B. L. (2010). Hippocampal CA1 apical neuropil atrophy in mild Alzheimer disease visualized with 7-T MRI. Neurology, 75, 1381–1387.

Kim, J. J. & Diamond, D. M. (2002). The stressed hippocampus, synaptic plasticity and lost memories. Nature reviews Neuroscience, 3, 453–462.

Kinney, J. P., Spacek, J., Bartol, T. M., Bajaj, C. L., Harris, K. M., & Sejnowski, T. J. (2013). Extracellular sheets and tunnels modulate glutamate diffusion in hippocampal neuropil. The Journal of comparative neurology, 521, 448–464.

Kirov, I. I., Hardy, C. J., Matsuda, K., Messinger, J., Cankurtaran, C. Z., Warren, M., Wiggins, G. C., Perry, N. N., Babb, J. S., Goetz, R. R., George, A., Malaspina, D., & Gonen, O. (2013). In vivo 7 Tesla imaging of the dentate granule cell layer in schizophrenia. Schizophrenia Research, 147, 362–367.

Kleim, J., Lussnig, E., Schwarz, E., Comery, T., & Greenough, W. (1996). Synaptogenesis and FOS expression in the motor cortex of the adult rat after motor skill learning. Journal of Neuroscience, 16, 4529–4535.

Kleim, J., Markham, J., Vij, K., Freese, J., Ballard, D., & Greenough, W. (2007). Motor

learning induces astrocytic hypertrophy in the cerebellar cortex. Behav Brain Res, 178, 244–249.

Kleim, J. A., Cooper, N. R., & VandenBerg, P. M. (2002). Exercise induces angiogenesis but does not alter movement representations within rat motor cortex. Brain Research, 934, 1–6.

Kleim, J. A., Vij, K., Ballard, D. H., & Greenough, W. T. (1997). Learning-dependent synaptic modifications in the cerebellar cortex of the adult rat persist for at least four weeks. The Journal of neuroscience : the official journal of the Society for Neuroscience, 17, 717–721.

Klein, A., Andersson, J., Ardekani, B. A., Ashburner, J., Avants, B., Chiang, M.-C., Christensen, G. E., Collins, D. L., Gee, J., Hellier, P., Song, J. H., Jenkinson, M., Lepage, C., Rueckert, D., Thompson, P., Vercauteren, T., Woods, R. P., Mann, J. J., & Parsey, R. V. (2009). Evaluation of 14 nonlinear deformation algorithms applied to human brain MRI registration. NeuroImage, 46, 786–802.

Koeppen, A. H. (1995). The history of iron in the brain. Journal of the Neurological Sciences, 134 Suppl, 1–9.

Kramer, A. F. & Erickson, K. I. (2007). Capitalizing on cortical plasticity: influence of physical activity on cognition and brain function. Trends in cognitive sciences, 11, 342–348.

Kronenberg, G., Reuter, K., Steiner, B., Brandt, M. D., Jessberger, S., Yamaguchi, M., & Kempermann, G. (2003). Subpopulations of proliferating cells of the adult hippocampus respond differently to physiologic neurogenic stimuli. The Journal of comparative neurology, 467, 455–463.

Kuhn, H. G., Dickinson-Anson, H., & Gage, F. H. (1996). Neurogenesis in the dentate gyrus of the adult rat: age-related decrease of neuronal progenitor proliferation. Journal of Neuroscience, 16, 2027–2033.

Kuppusamy, K., Lin, W., Cizek, G. R., & Haacke, E. M. (1996). In vivo regional cerebral

blood volume: quantitative assessment with 3D T1-weighted pre- and postcontrast MR imaging. Radiology, 201, 106–112.

Kurtze, N., Rangul, V., & Hustvedt, B.-E. (2008). Reliability and validity of the international physical activity questionnaire in the Nord-Trøndelag health study (HUNT) population of men. BMC medical research methodology, 8, 63.

Kyle, U. G., Bosaeus, I., De Lorenzo, A. D., Deurenberg, P., Elia, M., Gómez, J. M., Heitmann, B. L., Kent-Smith, L., Melchior, J.-C., Pirlich, M., Scharfetter, H., Schols, A. M. W. J., Pichard, C., & Composition of the ESPEN Working Group (2004). Bioelectrical impedance analysis–part I: review of principles and methods. Clinical nutrition (Edinburgh, Scotland), 23, 1226–1243.

Lachman, M. E., Neupert, S. D., Bertrand, R., & Jette, A. M. (2006). The effects of strength training on memory in older adults. Journal of aging and physical activity, 14, 59–73.

Lankford, C. L. & Does, M. D. (2013). On the inherent precision of mcDESPOT. Magnetic resonance in medicine : official journal of the Society of Magnetic Resonance in Medicine / Society of Magnetic Resonance in Medicine, 69, 127–136.

Le Bihan, D. & Johansen-Berg, H. (2012). Diffusion MRI at 25: exploring brain tissue structure and function. NeuroImage, 61, 324–341.

Le Bihan, D. D., Breton, E. E., Lallemand, D. D., Grenier, P. P., Cabanis, E. E., & Laval-Jeantet, M. M. (1986). MR imaging of intravoxel incoherent motions: application to diffusion and perfusion in neurologic disorders. Radiology, 161, 401–407.

Leenders, K. L., Perani, D., Lammertsma, A. A., Heather, J. D., Buckingham, P., Healy, M. J., Gibbs, J. M., Wise, R. J., Hatazawa, J., & Herold, S. (1990). Cerebral blood flow, blood volume and oxygen utilization. Normal values and effect of age. Brain : a journal of neurology, 113 (Pt 1), 27–47.

Lehtinen, M. K., Zappaterra, M. W., Chen, X., Yang, Y. J., Hill, A. D., Lun, M., Maynard, T., Gonzalez, D., Kim, S., Ye, P., D'Ercole, A. J., Wong, E. T., LaMantia, A. S., &

Walsh, C. A. (2011). The cerebrospinal fluid provides a proliferative niche for neural progenitor cells. Neuron, 69, 893–905.

Leow, A. D., Klunder, A. D., Jack, C. R., Toga, A. W., Dale, A. M., Bernstein, M. A., Britson, P. J., Gunter, J. L., Ward, C. P., Whitwell, J. L., Borowski, B. J., Fleisher, A. S., Fox, N. C., Harvey, D., Kornak, J., Schuff, N., Studholme, C., Alexander, G. E., Weiner, M. W., Thompson, P. M., & ADNI Preparatory Phase Study (2006). Longitudinal stability of MRI for mapping brain change using tensor-based morphometry. NeuroImage, 31, 627–640.

Lerch, J. P., Yiu, A. P., Martinez-Canabal, A., Pekar, T., Bohbot, V. D., Frankland, P. W., Henkelman, R. M., Josselyn, S. A., & Sled, J. G. (2011). Maze training in mice induces MRI-detectable brain shape changes specific to the type of learning. NeuroImage, 54, 2086–2095.

Lin, W., Celik, A., & Paczynski, R. (1999). Regional cerebral blood volume: A comparison of the dynamic imaging and the steady state methods. Journal of Magnetic Resonance Imaging, 9, 44–52.

Lin, W., Paczynski, R. P., Kuppusamy, K., Hsu, C. Y., & Haacke, E. M. (1997). Quantitative measurements of regional cerebral blood volume using MRI in rats: effects of arterial carbon dioxide tension and mannitol. Magnetic resonance in medicine : official journal of the Society of Magnetic Resonance in Medicine / Society of Magnetic Resonance in Medicine, 38, 420–428.

Lin, Y., Stephenson, M. C., Xin, L., Napolitano, A., & Morris, P. G. (2012). Investigating the metabolic changes due to visual stimulation using functional proton magnetic resonance spectroscopy at 7âĂĽT. Journal of cerebral blood flow and metabolism : official journal of the International Society of Cerebral Blood Flow and Metabolism.

MacQueen, G. M., Campbell, S., McEwen, B. S., Macdonald, K., Amano, S., Joffe, R. T., Nahmias, C., & Young, L. T. (2003). Course of illness, hippocampal function, and hippocampal volume in major depression. Proc Natl Acad Sci U S A, 100, 1387–1392.

Maguire, E., Gadian, D., Johnsrude, I., Good, C., Ashburner, J., Frackowiak, R., & Frith, C. (2000). Navigation-related structural change in the hippocampi of taxi drivers. Proc Natl Acad Sci U S A, 97, 4398–4403.

Makanya, A. N., Hlushchuk, R., & Djonov, V. G. (2009). Intussusceptive angiogenesis and its role in vascular morphogenesis, patterning, and remodeling. Angiogenesis, 12, 113–123.

Markham, J. & Greenough, W. T. (2004). Experience-driven brain plasticity: beyond the synapse. Neuron glia biology, 1, 351–363.

Martinowich, K. & Lu, B. (2008). Interaction between BDNF and serotonin: role in mood disorders. Neuropsychopharmacology : official publication of the American College of Neuropsychopharmacology, 33, 73–83.

Masland, R. H. (2004). Neuronal cell types. Current biology : CB, 14, R497–500.

Mata, J., Thompson, R. J., & Gotlib, I. H. (2010). BDNF genotype moderates the relation between physical activity and depressive symptoms. Health psychology : official journal of the Division of Health Psychology, American Psychological Association, 29, 130–133.

MATLAB (2013). version 8.1.0 (2013a). (Natick, Massachusetts: The MathWorks Inc.).

Mazziotta, J. C., Toga, A. W., Evans, A., Fox, P., & Lancaster, J. (1995). A Probabilistic Atlas of the Human Brain: Theory and Rationale for Its Development The International Consortium for Brain Mapping (ICBM). NeuroImage, 2, 89–101.

McAllister, A. K., Katz, L. C., & Lo, D. C. (1999). Neurotrophins and synaptic plasticity. Annual review of neuroscience, 22, 295–318.

McClelland, J. L., McNaughton, B. L., & O'Reilly, R. C. (1995). Why there are complementary learning systems in the hippocampus and neocortex: insights from the successes and failures of connectionist models of learning and memory. Psychological review, 102, 419–457.

Meador, K. J., Loring, D. W., Allen, M. E., Zamrini, E. Y., Moore, E. E., Abney, O. L., & King, D. W. (1991). Comparative cognitive effects of carbamazepine and phenytoin in healthy adults. Neurology, 41, 1537–1540.

Meador, K. J., Moore, E. E., Nichols, M. E., Abney, O. L., Taylor, H. S., Zamrini, E. Y., & Loring, D. W. (1993). The role of cholinergic systems in visuospatial processing and memory. Journal of clinical and experimental neuropsychology, 15, 832–842.

Ming, G.-l. & Song, H. (2005). Adult neurogenesis in the mammalian central nervous system. Annual review of neuroscience, 28, 223–250.

Ming, G.-l. & Song, H. (2011). Adult neurogenesis in the mammalian brain: significant answers and significant questions. Neuron, 70, 687–702.

Mokri, B. (2001). The Monro-Kellie hypothesis: applications in CSF volume depletion. Neurology, 56, 1746–1748.

Moonen, C. T. W., Bandettini, P. A., & Aguirre, G. K. (1999). Functional MRI. (Berlin ; New York : Springer).

Moos, T. & Morgan, E. H. (2004). The metabolism of neuronal iron and its pathogenic role in neurological disease: review. Annals of the New York Academy of Sciences, 1012, 14–26.

Moos, T., Rosengren Nielsen, T., Skjørringe, T., & Morgan, E. H. (2007). Iron trafficking inside the brain. Journal of Neurochemistry, 103, 1730–1740.

Mosteller, F. & Fisher, R. A. (1948). Questions and Answers. The American Statistician, 2, 30–31.

Mugler, J. P. & Brookeman, J. R. (1990). Three-dimensional magnetization-prepared rapid gradient-echo imaging (3D MP RAGE). Magnetic resonance in medicine : official journal of the Society of Magnetic Resonance in Medicine / Society of Magnetic Resonance in Medicine, 15, 152–157.

Neves-Pereira, M., Mundo, E., Muglia, P., King, N., Macciardi, F., & Kennedy, J. L.

(2002). The brain-derived neurotrophic factor gene confers susceptibility to bipolar disorder: evidence from a family-based association study. American journal of human genetics, 71, 651–655.

Nichols, T. & Holmes, A. (2002). Nonparametric permutation tests for functional neuroimaging: A primer with examples. Human brain mapping, 15, 1–25.

Nichols, T., Ridgway, G., Webster, M., & Smith, S. (2008). GLM Permutation - Nonparametric Inference for Arbitrary General Linear Models. 14th Annual Human Brain Mapping Meeting.

Olson, A. K., Eadie, B. D., Ernst, C., & Christie, B. R. (2006). Environmental enrichment and voluntary exercise massively increase neurogenesis in the adult hippocampus via dissociable pathways. Hippocampus, 16, 250–260.

Ono, R., Hirata, S., Yamada, M., Nishiyama, T., Kurosaka, M., & Tamura, Y. (2007). Reliability and validity of the Baecke physical activity questionnaire in adult women with hip disorders. BMC Musculoskeletal Disorders, 8.

Overgaard, K. & Meden, P. (2000). Influence of different fixation procedures on the quantification of infarction and oedema in a rat model of stroke. Neuropathology and applied neurobiology, 26, 243–250.

Pajonk, F.-G., Wobrock, T., Gruber, O., Scherk, H., Berner, D., Kaizl, I., Kierer, A., Müller, S., Oest, M., Meyer, T., Backens, M., Schneider-Axmann, T., Thornton, A. E., Honer, W. G., & Falkai, P. (2010). Hippocampal plasticity in response to exercise in schizophrenia. Archives of general psychiatry, 67, 133–143.

Palmer, T. D., Willhoite, A. R., & Gage, F. H. (2000). Vascular niche for adult hippocampal neurogenesis. The Journal of comparative neurology, 425, 479–494.

Patenaude, B., Smith, S. M., Kennedy, D. N., & Jenkinson, M. (2011). A Bayesian model of shape and appearance for subcortical brain segmentation. NeuroImage, 56, 907–922.

Patt, S., Sampaolo, S., Théallier-Jankó, A., Tschairkin, I., & Cervós-Navarro, J. (1997).

Cerebral angiogenesis triggered by severe chronic hypoxia displays regional differences. Journal of cerebral blood flow and metabolism : official journal of the International Society of Cerebral Blood Flow and Metabolism, 17, 801–806.

Pereira, A., Huddleston, D., Brickman, A., Sosunov, A., Hen, R., McKhann, G., Sloan, R., Gage, F., Brown, T., & Small, S. (2007). An in vivo correlate of exercise-induced neurogenesis in the adult dentate gyrus. Proceedings of the National Academy of Sciences of the United States of America, 104, 5638–5643.

Pierpaoli, C., Jezzard, P., Basser, P. J., Barnett, A., & Di Chiro, G. (1996). Diffusion tensor MR imaging of the human brain. Radiology, 201, 637–648.

Pinheiro, J., Bates, D., DebRoy, S., Sarkar, D., & R Core Team (2013). nlme: Linear and Nonlinear Mixed Effects Models, 3rd edn.

Podewils, L. J., Guallar, E., Kuller, L. H., Fried, L. P., Lopez, O. L., Carlson, M., & Lyketsos, C. G. (2005). Physical activity, APOE genotype, and dementia risk: findings from the Cardiovascular Health Cognition Study. American journal of epidemiology, 161, 639–651.

Pollay, M. (2010). The function and structure of the cerebrospinal fluid outflow system. Cerebrospinal fluid research, 7, 9.

Pols, M. A., Peeters, P. H., Bueno-De-Mesquita, H. B., Ocké, M. C., Wentink, C. A., Kemper, H. C., & Collette, H. J. (1995). Validity and repeatability of a modified Baecke questionnaire on physical activity. International journal of epidemiology, 24, 381–388.

Prior, B. M., Yang, H. T., & Terjung, R. L. (2004). What makes vessels grow with exercise training? Journal of applied physiology (Bethesda, Md : 1985), 97, 1119–1128.

Prudent, V., Kumar, A., Liu, S., Wiggins, G., Malaspina, D., & Gonen, O. (2010). Human Hippocampal Subfields in Young Adults at 7.0 T: Feasibility of Imaging. Radiology, 254, 900–906.

Pujol, J., Junqué, C., Vendrell, P., Grau, J. M., Martí-Vilalta, J. L., Olivé, C., & Gili, J. (1992). Biological significance of iron-related magnetic resonance imaging changes in the brain. Archives of Neurology, 49, 711–717.

R Core Team (2013). R: A language and environment for statistical computing. R Foundation for Statistical Computing. R Foundation for Statistical Computing, Vienna, Austria, version 3.0.0 (2013-04-03) – "masked marvel" edn.

Rabi, I. I., Millman, S., Kusch, P., & Zacharias, J. R. (1939). The molecular beam resonance method for measuring nuclear magnetic moments the magnetic moments of Li63, Li73 and F199. Physical Review, 55, 526–535.

Radloff, L. S. (1977). The CES-D Scale: A Self-Report Depression Scale for Research in the General Population. Applied Psychological Measurement, 1, 385–401.

Rakic, P. (1995). A small step for the cell, a giant leap for mankind: a hypothesis of neocortical expansion during evolution. Trends in neurosciences, 18, 383–388.

Rakic, P. (2002). Neurogenesis in adult primate neocortex: an evaluation of the evidence. Nature reviews Neuroscience, 3, 65–71.

Rankinen, T., Sung, Y. J., Sarzynski, M. A., Rice, T. K., Rao, D. C., & Bouchard, C. (2012). Heritability of submaximal exercise heart rate response to exercise training is accounted for by nine SNPs. Journal of applied physiology (Bethesda, Md : 1985), 112, 892–897.

Reichenbach, J. R., Venkatesan, R., Schillinger, D. J., Kido, D. K., & Haacke, E. M. (1997). Small vessels in the human brain: MR venography with deoxyhemoglobin as an intrinsic contrast agent. Radiology, 204, 272–277.

Reuter, M., Rosas, H. D., & Fischl, B. (2010). Highly accurate inverse consistent registration: a robust approach. NeuroImage, 53, 1181–1196.

Reuter, M., Schmansky, N. J., Rosas, H. D., & Fischl, B. (2012). Within-subject template estimation for unbiased longitudinal image analysis. NeuroImage, 61, 1402–1418.

Rey, A. (1941). Psychological Examination of Traumatic Encephalopathy . Archives of Psychology (Archives de psychologie), 28, 286–340.

Reynolds, C. R. (1997). Forward and backward memory span should not be combined for clinical analysis. Archives of Clinical Neuropsychology, 12, 29–40.

Rhyu, I. J., Bytheway, J. A., Kohler, S. J., Lange, H., Lee, K. J., Boklewski, J., McCormick, K., Williams, N. I., Stanton, G. B., Greenough, W. T., & Cameron, J. L. (2010). Effects of aerobic exercise training on cognitive function and cortical vascularity in monkeys. Neuroscience, 167, 1239–1248.

Riboli, E. (1992). Nutrition and cancer: background and rationale of the European Prospective Investigation into Cancer and Nutrition (EPIC). Annals of oncology : official journal of the European Society for Medical Oncology / ESMO, 3, 783–791.

Richardson, J. T. E. J. (2007). Measures of short-term memory: a historical review. Cortex; a journal devoted to the study of the nervous system and behavior, 43, 635–650.

Rodrigue, K. M., Daugherty, A. M., Haacke, E. M., & Raz, N. (2013). The role of hippocampal iron concentration and hippocampal volume in age-related differences in memory. Cerebral cortex (New York, NY : 1991), 23, 1533–1541.

Rovio, S., Kåreholt, I., Helkala, E.-L., Viitanen, M., Winblad, B., Tuomilehto, J., Soininen, H., Nissinen, A., & Kivipelto, M. (2005). Leisure-time physical activity at midlife and the risk of dementia and Alzheimer's disease. Lancet neurology, 4, 705–711.

Ruscheweyh, R., Willemer, C., Krüger, K., Duning, T., Warnecke, T., Sommer, J., Völker, K., Ho, H. V., Mooren, F., Knecht, S., & Flöel, A. (2011). Physical activity and memory functions: an interventional study. Neurobiology of aging, 32, 1304–1319.

Sagi, Y., Tavor, I., Hofstetter, S., Tzur-Moryosef, S., Blumenfeld-Katzir, T., & Assaf, Y. (2012). Learning in the fast lane: new insights into neuroplasticity. Neuron, 73, 1195–1203.

Salimi-Khorshidi, G., Smith, S. M., & Nichols, T. E. (2011). Adjusting the effect of nonstationarity in cluster-based and TFCE inference. NeuroImage, 54, 2006–2019.

Sampaio-Baptista, C., Khrapitchev, A. A., Foxley, S., Schlagheck, T., Scholz, J., Jbabdi, S., Deluca, G. C., Miller, K. L., Taylor, A., Thomas, N., Kleim, J., Sibson, N. R., Bannerman, D., & Johansen-Berg, H. (2013). Motor skill learning induces changes in white matter microstructure and myelination. The Journal of neuroscience : the official journal of the Society for Neuroscience, 33, 19499–19503.

Sandercock, G. R. H., Bromley, P. D., & Brodie, D. A. (2005). Effects of exercise on heart rate variability: inferences from meta-analysis. Medicine and science in sports and exercise, 37, 433–439.

Sarko, D. K., Catania, K. C., Leitch, D. B., Kaas, J. H., & Herculano-Houzel, S. (2009). Cellular scaling rules of insectivore brains. Frontiers in neuroanatomy, 3, 8.

Sawamoto, K., Wichterle, H., Gonzalez-Perez, O., Cholfin, J. A., Yamada, M., Spassky, N., Murcia, N. S., Garcia-Verdugo, J.-M., Marin, O., Rubenstein, J. L. R., Tessier-Lavigne, M., Okano, H., & Alvarez-Buylla, A. (2006). New neurons follow the flow of cerebrospinal fluid in the adult brain. Science (New York, NY), 311, 629–632.

Sawka, M. N., Convertino, V. A., Eichner, E. R., Schnieder, S. M., & Young, A. J. (2000). Blood volume: importance and adaptations to exercise training, environmental stresses, and trauma/sickness. Medicine and science in sports and exercise, 32, 332–348.

Schenck, J. F. (2003). Magnetic resonance imaging of brain iron. Journal of the Neurological Sciences, 207, 99–102.

Schoeller, D. A., van Santen, E., Peterson, D. W., Dietz, W., Jaspan, J., & Klein, P. D. (1980). Total body water measurement in humans with 18O and 2H labeled water. The American journal of clinical nutrition, 33, 2686–2693.

Scholz, J., Klein, M. C., Behrens, T. E. J., & Johansen-Berg, H. (2009). Training induces changes in white-matter architecture. Nature neuroscience, 12, 1370–1371.

Schröder, N., Figueiredo, L. S., & de Lima, M. N. M. (2013). Role of brain iron accu-

mulation in cognitive dysfunction: evidence from animal models and human studies. Journal of Alzheimer's disease : JAD, 34, 797–812.

Schroeder, A., Goldberg, M. S., Kastrup, C., Wang, Y., Jiang, S., Joseph, B. J., Levins, C. G., Kannan, S. T., Langer, R., & Anderson, D. G. (2012). Remotely activated protein-producing nanoparticles. Nano letters, 12, 2685–2689.

Schuit, A. J., Feskens, E. J., Launer, L. J., & Kromhout, D. (2001). Physical activity and cognitive decline, the role of the apolipoprotein e4 allele. Medicine and science in sports and exercise, 33, 772–777.

Schulz, J., Siegert, T., Bazin, P. L., Maclaren, J., Herbst, M., Zaitsev, M., & Turner, R. (2014). Prospective slice-by-slice motion correction reduces false positive activations in fMRI with task-correlated motion. NeuroImage, 84, 124–132.

Shehzad, Z., Kelly, A. M. C., Reiss, P. T., Gee, D. G., Gotimer, K., Uddin, L. Q., Lee, S. H., Margulies, D. S., Roy, A. K., Biswal, B. B., Petkova, E., Castellanos, F. X., & Milham, M. P. (2009). The resting brain: unconstrained yet reliable. Cerebral cortex (New York, NY : 1991), 19, 2209–2229.

Sheline, Y. I. (2000). 3D MRI studies of neuroanatomic changes in unipolar major depression: the role of stress and medical comorbidity. Biological Psychiatry, 48, 791–800.

Shweiki, D., Itin, A., Soffer, D., & Keshet, E. (1992). Vascular endothelial growth factor induced by hypoxia may mediate hypoxia-initiated angiogenesis. Nature, 359, 843–845.

Siconolfi, S. F., Lasater, T. M., Snow, R. C., & Carleton, R. A. (1985). Self-reported physical activity compared with maximal oxygen uptake. American journal of epidemiology, 122, 101–105.

Sirevaag, A. M., Black, J. E., Shafron, D., & Greenough, W. T. (1988). Direct evidence that complex experience increases capillary branching and surface area in visual cortex of young rats. Brain Research, 471, 299–304.

Skinner, J. S., Jaskólski, A., Jaskólska, A., Krasnoff, J., Gagnon, J., Leon, A. S., Rao,

D. C., Wilmore, J. H., Bouchard, C., & HERITAGE Family Study (2001). Age, sex, race, initial fitness, and response to training: the HERITAGE Family Study. Journal of applied physiology (Bethesda, Md : 1985), 90, 1770–1776.

Sklar, P., Gabriel, S. B., McInnis, M. G., Bennett, P., Lim, Y. M., Tsan, G., Schaffner, S., Kirov, G., Jones, I., Owen, M., Craddock, N., DePaulo, J. R., & Lander, E. S. (2002). Family-based association study of 76 candidate genes in bipolar disorder: BDNF is a potential risk locus. Brain-derived neutrophic factor. Molecular Psychiatry, 7, 579–593.

Small, S. A. (2004). Imaging correlates of brain function in monkeys and rats isolates a hippocampal subregion differentially vulnerable to aging. Proceedings of the National Academy of Sciences of the United States of America, 101, 7181–7186.

Small, S. A., Schobel, S. A., Buxton, R. B., Witter, M. P., & Barnes, C. A. (2011). A pathophysiological framework of hippocampal dysfunction in ageing and disease. Nature reviews Neuroscience, 12, 585–601.

Smiley-Oyen, A. L., Lowry, K. A., Francois, S. J., Kohut, M. L., & Ekkekakis, P. (2008). Exercise, fitness, and neurocognitive function in older adults: the "selective improvement" and "cardiovascular fitness" hypotheses. Annals of behavioral medicine : a publication of the Society of Behavioral Medicine, 36, 280–291.

Smith, P. J., Blumenthal, J. A., Hoffman, B. M., Cooper, H., Strauman, T. A., Welsh-Bohmer, K., Browndyke, J. N., & Sherwood, A. (2010). Aerobic Exercise and Neurocognitive Performance: A Meta-Analytic Review of Randomized Controlled Trials. Psychosomatic Medicine, 72, 239–252.

Smith, S., Zhang, Y., Jenkinson, M., Chen, J., Matthews, P., Federico, A., & De Stefano, N. (2002). Accurate, robust, and automated longitudinal and cross-sectional brain change analysis. NeuroImage, 17, 479–489.

Smith, S. M., Jenkinson, M., Johansen-Berg, H., Rueckert, D., Nichols, T. E., Mackay, C. E., Watkins, K. E., Ciccarelli, O., Cader, M. Z., Matthews, P. M., & Behrens, T.

E. J. (2006). Tract-based spatial statistics: voxelwise analysis of multi-subject diffusion data. NeuroImage, 31, 1487–1505.

Smith, S. M., Miller, K. L., Salimi-Khorshidi, G., Webster, M., Beckmann, C. F., Nichols, T. E., Ramsey, J. D., & Woolrich, M. W. (2011). Network modelling methods for FMRI. NeuroImage, 54, 875–891.

Smith, S. M. & Nichols, T. E. (2009). Threshold-free cluster enhancement: Addressing problems of smoothing, threshold dependence and localisation in cluster inference. NeuroImage, 44, 83–98.

Smith, S. M. S., Jenkinson, M. M., Woolrich, M. W. M., Beckmann, C. F. C., Behrens, T. E. J. T., Johansen-Berg, H. H., Bannister, P. R. P., De Luca, M. M., Drobnjak, I. I., Flitney, D. E. D., Niazy, R. K. R., Saunders, J. J., Vickers, J. J., Zhang, Y. Y., De Stefano, N. N., Brady, J. M. J., & Matthews, P. M. P. (2004). Advances in functional and structural MR image analysis and implementation as FSL. NeuroImage, 23 Suppl 1, S208–S219.

Speck, O., Chang, L., Itti, L., Itti, E., & Ernst, T. (1999). Comparison of static and dynamic MRI techniques for the measurement of regional cerebral blood volume. Magnetic resonance in medicine : official journal of the Society of Magnetic Resonance in Medicine / Society of Magnetic Resonance in Medicine, 41, 1264–1268.

Steffens, D. C., Byrum, C. E., McQuoid, D. R., Greenberg, D. L., Payne, M. E., Blitchington, T. F., MacFall, J. R., & Krishnan, K. R. (2000). Hippocampal volume in geriatric depression. Biological Psychiatry, 48, 301–309.

Stejskal, E. O. & Tanner, J. E. (1965). Spin Diffusion Measurements: Spin Echoes in the Presence of a Time-Dependent Field Gradient. The Journal of Chemical Physics, 42, 288.

Stouffer, S. A., Suchman, E. A., DeVinney, L. C., Star, S. A., Williams, R. M., & Jr (1949). Studies in Social Psychology in World War II: The American Soldier. Princeton, Princeton University Press.

Strauss, J., Barr, C. L., George, C. J., Devlin, B., Vetró, A., Kiss, E., Baji, I., King, N., Shaikh, S., Lanktree, M., Kovacs, M., & Kennedy, J. L. (2005). Brain-derived neurotrophic factor variants are associated with childhood-onset mood disorder: confirmation in a Hungarian sample. Molecular Psychiatry, 10, 861–867.

Streitburger, D.-P., Möller, H. E., Tittgemeyer, M., Hund-Georgiadis, M., Schroeter, M. L., & Mueller, K. (2012). Investigating structural brain changes of dehydration using voxel-based morphometry. PLoS ONE, 7, e44195.

Stroth, S., Reinhardt, R. K., Thöne, J., Hille, K., Schneider, M., Härtel, S., Weidemann, W., Bös, K., & Spitzer, M. (2010). Impact of aerobic exercise training on cognitive functions and affect associated to the COMT polymorphism in young adults. Neurobiology of learning and memory, 94, 364–372.

Sullivan, E. V., Adalsteinsson, E., Rohlfing, T., & Pfefferbaum, A. (2009). Relevance of Iron Deposition in Deep Gray Matter Brain Structures to Cognitive and Motor Performance in Healthy Elderly Men and Women: Exploratory Findings. Brain Imaging and Behavior, 3, 167–175.

Swain, R., Harris, A., Wiener, E., Dutka, M., Morris, H., Theien, B., Konda, S., Engberg, K., Lauterbur, P., & Greenough, W. (2003). Prolonged exercise induces angiogenesis and increases cerebral blood volume in primary motor cortex of the rat. Neuroscience, 117, 1037–1046.

Syková, E. (1997). The extracellular space in the CNS: Its regulation, volume and geometry in normal and pathological neuronal function. The Neuroscientist : a review journal bringing neurobiology, neurology and psychiatry, 3, 28–41.

Syková, E. & Nicholson, C. (2008). Diffusion in brain extracellular space. Physiological reviews, 88, 1277–1340.

Thomas, A. G., Dennis, A., Bandettini, P. A., & Johansen-Berg, H. (2012). The effects of aerobic activity on brain structure. Frontiers in psychology, 3, 86.

Thomas, A. G., Marrett, S., Saad, Z. S., Ruff, D. A., Martin, A., & Bandettini, P. A.

(2009). Functional but not structural changes associated with learning: an exploration of longitudinal voxel-based morphometry (VBM). NeuroImage, 48, 117–125.

Thomas, B. P., Welch, E. B., Niederhauser, B. D., Whetsell, W. O., Anderson, A. W., Gore, J. C., Avison, M. J., & Creasy, J. L. (2008). High-resolution 7T MRI of the human hippocampus in vivo. Journal of magnetic resonance imaging : JMRI, 28, 1266–1272.

Thomas, C. & Baker, C. I. (2012). Teaching an adult brain new tricks: A critical review of evidence for training-dependent structural plasticity in humans. NeuroImage.

Thomas, L. O., Boyko, O. B., Anthony, D. C., & Burger, P. C. (1993). MR detection of brain iron. AJNR American journal of neuroradiology, 14, 1043–1048.

Tisdall, M. D., Hess, A. T., Reuter, M., Meintjes, E. M., Fischl, B., & van der Kouwe, A. J. W. (2012). Volumetric navigators for prospective motion correction and selective reacquisition in neuroanatomical MRI. Magnetic resonance in medicine : official journal of the Society of Magnetic Resonance in Medicine / Society of Magnetic Resonance in Medicine, 68, 389–399.

Todorich, B., Pasquini, J. M., Garcia, C. I., Paez, P. M., & Connor, J. R. (2009). Oligodendrocytes and myelination: the role of iron. Glia, 57, 467–478.

Toscano-Silva, M., Gomes da Silva, S., Scorza, F. A., Bonvent, J. J., Cavalheiro, E. A., & Arida, R. M. (2010). Hippocampal mossy fiber sprouting induced by forced and voluntary physical exercise. Physiology & behavior, 101, 302–308.

Tremblay, M.-È., Lowery, R. L., & Majewska, A. K. (2010). Microglial interactions with synapses are modulated by visual experience. PLoS biology, 8, e1000527.

Tseng, B. Y., Gundapuneedi, T., Khan, M. A., Diaz-Arrastia, R., Levine, B. D., Lu, H., Huang, H., & Zhang, R. (2013). White matter integrity in physically fit older adults. NeuroImage, 82, 510–516.

Tudor-Locke, C. E. & Myers, A. M. (2001). Challenges and opportunities for measuring physical activity in sedentary adults. Sports medicine (Auckland, N.Z.), 31, 91–100.

United Kingdom Department of Health (2011). UK Physical Activity Guidelines. Tech. rep., United Kingdom Department of Health.

US Department of Health and Human Services (1998). Physical activity and Health: A Report of the Surgeon General. Tech. rep., US Department of Health and Human Services.

Van der Borght, K., Kóbor-Nyakas, D. E., Klauke, K., Eggen, B. J. L., Nyakas, C., Van der Zee, E. A., & Meerlo, P. (2009). Physical exercise leads to rapid adaptations in hippocampal vasculature: temporal dynamics and relationship to cell proliferation and neurogenesis. Hippocampus, 19, 928–936.

van der Kouwe, A. J. W., Benner, T., Salat, D. H., & Fischl, B. (2008). Brain morphometry with multiecho MPRAGE. NeuroImage, 40, 559–569.

Van Essen, D. C., Dierker, D., Snyder, A. Z., Raichle, M. E., Reiss, A. L., & Korenberg, J. (2006). Symmetry of cortical folding abnormalities in Williams syndrome revealed by surface-based analyses. The Journal of neuroscience : the official journal of the Society for Neuroscience, 26, 5470–5483.

Van Leemput, K., Bakkour, A., Benner, T., Wiggins, G., Wald, L. L., Augustinack, J., Dickerson, B. C., Golland, P., & Fischl, B. (2009). Automated segmentation of hippocampal subfields from ultra-high resolution in vivo MRI. Hippocampus, 19, 549–557.

van Praag, H., Christie, B. R., Sejnowski, T. J., & Gage, F. H. (1999a). Running enhances neurogenesis, learning, and long-term potentiation in mice. Proceedings of the National Academy of Sciences of the United States of America, 96, 13427–13431.

van Praag, H., Kempermann, G., & Gage, F. H. (1999b). Running increases cell proliferation and neurogenesis in the adult mouse dentate gyrus. Nature neuroscience, 2, 266–270.

van Praag, H., Kempermann, G., & Gage, F. H. (2000). Neural consequences of enviromental enrichment. Nature reviews Neuroscience, 1, 191–198.

van Praag, H., Shubert, T., Zhao, C., & Gage, F. H. (2005). Exercise enhances learning and hippocampal neurogenesis in aged mice. The Journal of neuroscience : the official journal of the Society for Neuroscience, 25, 8680–8685.

Ventriglia, M., Zanardini, R., Pedrini, L., Placentino, A., Nielsen, M. G., Gennarelli, M., & Bocchio-Chiavetto, L. (2009). VEGF serum levels in depressed patients during SSRI antidepressant treatment. Progress in neuro-psychopharmacology & biological psychiatry, 33, 146–149.

Verbeke, G. & Molenberghs, G. (2009). Linear mixed models for longitudinal data. (New York : Springer).

Viikki, M., Anttila, S., Kampman, O., Illi, A., Huuhka, M., Setälä-Soikkeli, E., Mononen, N., Lehtimäki, T., & Leinonen, E. (2010). Vascular endothelial growth factor (VEGF) polymorphism is associated with treatment resistant depression. Neuroscience Letters, 477, 105–108.

Voss, M. W., Erickson, K. I., Prakash, R. S., Chaddock, L., Kim, J. S., Alves, H., Szabo, A., Phillips, S. M., Wójcicki, T. R., Mailey, E. L., Olson, E. A., Gothe, N., Vieira-Potter, V. J., Martin, S. A., Pence, B. D., Cook, M. D., Woods, J. A., McAuley, E., & Kramer, A. F. (2013a). Neurobiological markers of exercise-related brain plasticity in older adults. Brain, behavior, and immunity, 28, 90–99.

Voss, M. W., Erickson, K. I., Prakash, R. S., Chaddock, L., Malkowski, E., Alves, H., Kim, J. S., Morris, K. S., White, S. M., Wójcicki, T. R., Hu, L., Szabo, A., Klamm, E., McAuley, E., & Kramer, A. F. (2010). Functional connectivity: a source of variance in the association between cardiorespiratory fitness and cognition? Neuropsychologia, 48, 1394–1406.

Voss, M. W., Heo, S., Prakash, R. S., Erickson, K. I., Alves, H., Chaddock, L., Szabo, A. N., Mailey, E. L., Wójcicki, T. R., White, S. M., Gothe, N., McAuley, E., Sutton, B. P., & Kramer, A. F. (2012). The influence of aerobic fitness on cerebral white matter integrity and cognitive function in older adults: Results of a one-year exercise

intervention. Human brain mapping.

Voss, M. W., Vivar, C., Kramer, A. F., & van Praag, H. (2013b). Bridging animal and human models of exercise-induced brain plasticity. Trends in cognitive sciences, 17, 525–544.

Wake, H., Lee, P. R., & Fields, R. D. (2011). Control of local protein synthesis and initial events in myelination by action potentials. Science (New York, NY), 333, 1647–1651.

Weinstein, A. M., Voss, M. W., Prakash, R. S., Chaddock, L., Szabo, A., White, S. M., Wójcicki, T. R., Mailey, E., McAuley, E., Kramer, A. F., & Erickson, K. I. (2012). The association between aerobic fitness and executive function is mediated by prefrontal cortex volume. Brain, behavior, and immunity, 26, 811–819.

Weissman, M. M., Sholomskas, D., Pottenger, M., Prusoff, B. A., & Locke, B. Z. (1977). Assessing depressive symptoms in five psychiatric populations: a validation study. American journal of epidemiology, 106, 203–214.

Wenz, F., Rempp, K., Brix, G., Knopp, M. V., Gückel, F., Hess, T., & van Kaick, G. (1996). Age dependency of the regional cerebral blood volume (rCBV) measured with dynamic susceptibility contrast MR imaging (DSC). Magnetic Resonance Imaging, 14, 157–162.

Wharton, S. & Bowtell, R. (2010). Whole-brain susceptibility mapping at high field: a comparison of multiple- and single-orientation methods. NeuroImage, 53, 515–525.

Wharton, S. & Bowtell, R. (2012). Fiber orientation-dependent white matter contrast in gradient echo MRI. Proceedings of the National Academy of Sciences of the United States of America, 109, 18559–18564.

Wharton, S., Schäfer, A., & Bowtell, R. (2010). Susceptibility mapping in the human brain using threshold-based k-space division. Magnetic resonance in medicine : official journal of the Society of Magnetic Resonance in Medicine / Society of Magnetic Resonance in Medicine, 63, 1292–1304.

White, N., Roddey, C., Shankaranarayanan, A., Han, E., Rettmann, D., Santos, J.,

Kuperman, J., & Dale, A. (2010). PROMO: Real-time prospective motion correction in MRI using image-based tracking. Magnetic resonance in medicine : official journal of the Society of Magnetic Resonance in Medicine / Society of Magnetic Resonance in Medicine, 63, 91–105.

Whittle, S., Allen, N. B., Fornito, A., Lubman, D. I., Simmons, J. G., Pantelis, C., & Yücel, M. (2009). Variations in cortical folding patterns are related to individual differences in temperament. Psychiatry research, 172, 68–74.

Wilson, R. S., Mendes De Leon, C. F., Barnes, L. L., Schneider, J. A., Bienias, J. L., Evans, D. A., & Bennett, D. A. (2002). Participation in cognitively stimulating activities and risk of incident Alzheimer disease. JAMA : the journal of the American Medical Association, 287, 742–748.

Winter, B., Breitenstein, C., Mooren, F. C., Voelker, K., Fobker, M., Lechtermann, A., Krueger, K., Fromme, A., Korsukewitz, C., Floel, A., & Knecht, S. (2007). High impact running improves learning. Neurobiology of learning and memory, 87, 597–609.

Wisse, L. E. M., Gerritsen, L., Zwanenburg, J. J. M., Kuijf, H. J., Luijten, P. R., Biessels, G. J., & Geerlings, M. I. (2012). Subfields of the hippocampal formation at 7T MRI: In vivo volumetric assessment. NeuroImage, 61, 1043–1049.

Woods, D. L., Kishiyama, M. M., Yund, E. W., Herron, T. J., Edwards, B., Poliva, O., Hink, R. F., & Reed, B. (2010). Improving digit span assessment of short-term verbal memory. Journal of clinical and experimental neuropsychology, pp. 1–11.

Woods, R. P., Grafton, S. T., Holmes, C. J., Cherry, S. R., & Mazziotta, J. C. (1998). Automated image registration: I. General methods and intrasubject, intramodality validation. Journal of computer assisted tomography, 22, 139–152.

Xiao, Y., Bailey, L., Chakravarty, M. M., Beriault, S., Sadikot, A. F., Pike, G. B., & Collins, D. L. (2012). Atlas-based segmentation of the subthalamic nucleus, red nucleus, and substantia nigra for deep brain stimulation by incorporating multiple MRI contrasts.

Xie, L., Kang, H., Xu, Q., Chen, M. J., Liao, Y., Thiyagarajan, M., O'Donnell, J., Christensen, D. J., Nicholson, C., Iliff, J. J., Takano, T., Deane, R., & Nedergaard, M. (2013). Sleep Drives Metabolite Clearance from the Adult Brain. Science (New York, NY), 342, 373–377.

Xu, X., Wang, Q., & Zhang, M. (2008). Age, gender, and hemispheric differences in iron deposition in the human brain: an in vivo MRI study. NeuroImage, 40, 35–42.

Yaffe, K., Barnes, D., Nevitt, M., Lui, L. Y., & Covinsky, K. (2001). A prospective study of physical activity and cognitive decline in elderly women: women who walk. Archives of internal medicine, 161, 1703–1708.

Zatorre, R. J., Fields, R. D., & Johansen-Berg, H. (2012). Plasticity in gray and white: neuroimaging changes in brain structure during learning. Nature neuroscience, 15, 528–536.

Zeng, H., Shen, E. H., Hohmann, J. G., Oh, S. W., Bernard, A., Royall, J. J., Glattfelder, K. J., Sunkin, S. M., Morris, J. A., Guillozet-Bongaarts, A. L., Smith, K. A., Ebbert, A. J., Swanson, B., Kuan, L., Page, D. T., Overly, C. C., Lein, E. S., Hawrylycz, M. J., Hof, P. R., Hyde, T. M., Kleinman, J. E., & Jones, A. R. (2012). Large-scale cellular-resolution gene profiling in human neocortex reveals species-specific molecular signatures. Cell, 149, 483–496.

Zhang, Q. & Haydon, P. G. (2005). Roles for gliotransmission in the nervous system. Journal of neural transmission (Vienna, Austria : 1996), 112, 121–125.

Zhang, Y., Brady, M., & Smith, S. (2001). Segmentation of brain MR images through a hidden Markov random field model and the expectation-maximization algorithm. IEEE transactions on medical imaging, 20, 45–57.

Zhao, C., Deng, W., & Gage, F. H. (2008). Mechanisms and functional implications of adult neurogenesis. Cell, 132, 645–660.